UNIVERSITE D'AIX-MARSEILLE
EDSVS - ED62
IBDM-UMR7288

Thèse présentée pour obtenir le grade universitaire de docteur

Discipline : Biologie
Spécialité : Neurobiologie

Alexandra ANGELOVA

Propriétés moléculaires, morphologiques et physiologiques des neurones glutamatergiques juxtaglomérulaires dans le bulbe olfactif de la souris

Molecular, morphological and physiological properties of glutamatergic juxtaglomerular neurons in the mouse olfactory bulb

Codirigée par : Nathalie Coré et Jean-Claude Platel

Soutenue le 17/12/2018 devant le jury :

Isabelle CAILLÉ	IBPS UMR 8246	Rapportrice
Alan CARLETON	Université de Genève	Rapporteur
Rosa COSSART	INMED-Inserm UMR901	Examinatrice
Sophie CHAUVET	IBDM-AMU/CNRS UMR7288	Examinatrice
Nathalie CORÉ	IBDM-AMU/CNRS UMR7288	Directrice de thèse

Membre invité :

Jean-Claude PLATEL	IBDM-AMU/CNRS UMR7288	Co-directeur de thèse

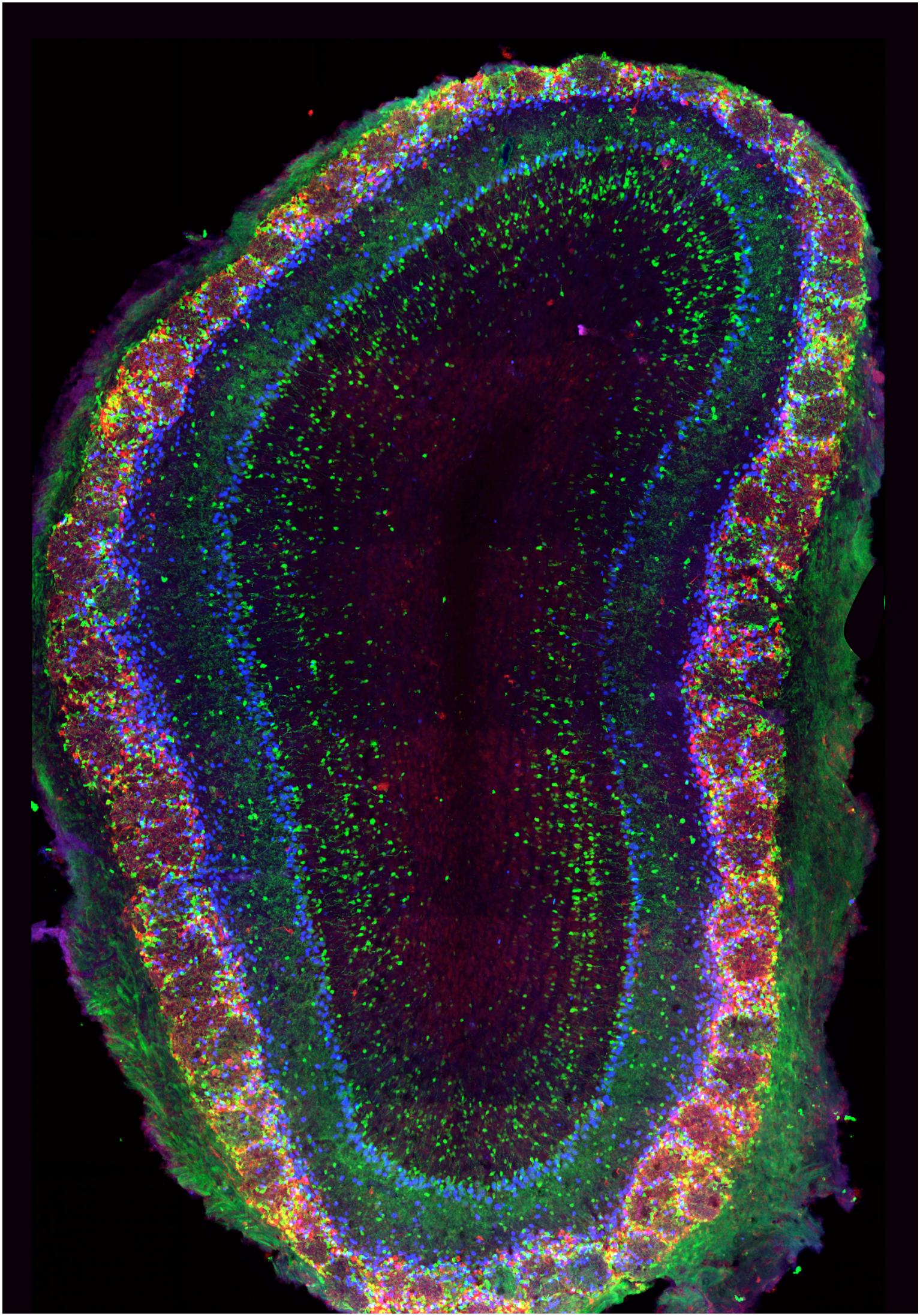

RÉSUMÉ

Le bulbe olfactif (BO) du rongeur est le seul système sensoriel chez les vertébrés qui est sujet à la neurogenèse adulte. Outre l'intérêt évident d'étudier ce système dans le contexte du traitement des odeurs, il représente également un modèle idéal pour étudier comment les réseaux neuronaux sont construits et maintenus par l'interaction entre des programmes génétiques et des stimuli environnementaux.

Au cours de la neurogenèse post-natale, des cellules souches prédéterminées résidant dans la zone ventriculo-subventriculaire génèrent continuellement des progéniteurs qui migrent à travers le flux migratoire rostral, se différencient et s'intègrent dans le bulbe olfactif (BO). Bien que la grande majorité des interneurones ainsi produits soient inhibiteurs, une sous-fraction correspond à des interneurones glutamatergiques qui s'intègrent dans la couche glomérulaire superficielle. Étant donné que ces cellules juxtaglomérulaires (CJGs) excitatrices sont situées à l'entrée même du circuit olfactif, là où les neurones sensoriels de l'épithélium nasal établissent des synapses avec les neurones du cerveau, elles exercent probablement une fonction importante dans ce circuit. J'ai donc entrepris d'étudier plus en détail cette population neuronale.

Dans mon travail de thèse, j'ai démontré que le facteur de transcription bHLH NeuroD6 est spécifiquement et transitoirement exprimé dans le lignage neurogenique dorsal qui génère les CJGs glutamatergiques pour le bulbe. En raison d'une redondance possible avec les facteurs de la même famille, NeuroD2 et NeuroD1, la fonction de NeuroD6 reste difficile à appréhender. Cependant, les lignées de souris transgéniques NeuroD6^{Cre} et NeuroD6^{CreERT2} apparaissent comme des outils puissants pour étudier les CJGs glutamatergiques. Par l'analyse du lignage, combinée à une méthode de transparisation du cerveau, j'ai apporté de nouvelles connaissances sur la période de génération des CJGs glutamatergiques, ainsi que sur leur morphologie et connectivité. Les interneurones glutamatergiques représentant une fraction substantielle de l'ensemble de la population CJG et l'unique source locale d'excitation dans le BO, j'ai cherché à élucider leur rôle dans le circuit neuronal du BO. Dans une première approche, j'ai soumis ces neurones à une privation sensorielle et je les ai suivis au cours du temps, de façon chronique, par imagerie *in vivo*. De façon intéressante, j'ai trouvé que, contrairement aux interneurones GABAergiques du BO, les CJG glutamatergiques survivent dans ces conditions difficiles, suggérant un équilibre homéostatique et dynamique entre excitation et inhibition dans ce système. Dans une deuxième approche, j'ai caractérisé les profils de réponse olfactive des CJG glutamatergiques à l'aide de souris transgéniques

GCaMP6s, qui expriment un indicateur sensible au calcium, pour examiner l'activité neuronale. J'ai découvert que ces neurones présentent un ensemble diversifié de réponses excitatrices, inhibitrices et mixtes avec différents degrés d'homo- et d'hétérogénéité dans les glomérules individuels. Ces résultats représentent les premières données *in vivo* sur la réponse olfactive disponibles pour les CJG glutamatergiques et renforcent l'idée que ces neurones agissent comme amplificateurs du signal sensoriel.

ABSTRACT

The rodent olfactory bulb (OB) is the only sensory system in vertebrates that is subject to adult neurogenesis. Besides the evident interest to study this system in the context of olfactory processing, it also represents an ideal model to study how neuronal networks are built and maintained by the interaction of genetic programs and environmental stimuli.

During postnatal OB neurogenesis, predetermined stem cells residing in the ventricular-subventricular zone continuously generate progenitors that migrate through the rostral migratory stream and integrate into the OB. Although the vast majority of these postnatally generated interneurons are inhibitory, a sub-fraction represents glutamatergic interneurons that integrate into the superficial glomerular layer. Given the fact that these excitatory juxtaglomerular cells (JGCs) are situated at the very entry of the olfactory circuit, where the sensory neurons of the nasal epithelium synapse with the brain, they likely exert an important function within the OB circuit. I have thus set out to study this neuronal population in more detail.

In the following work I demonstrate that the bHLH transcription factor NeuroD6 is specifically and transitorily expressed in the dorsal neurogenic lineage that generates glutamatergic JGCs for the OB. Due to possible redundancy with closely related factors NeuroD2 and NeuroD1, function of NeuroD6 remains elusive. However, NeuroD6^{Cre} and NeuroD6^{CreERT2} lines emerge as powerful tools to study glutamatergic JGCs. Using lineage tracing and whole brain clearing, I provide new insight into timing of generation, morphology and connectivity of glutamatergic JGCs. As glutamatergic interneurons represent a substantial fraction of the overall JGC population and the only local source of excitation within the OB, I sought to elucidate their role in the OB circuit. In a first approach, I subjected these neurons to sensory deprivation and followed them over time using chronic *in vivo* imaging. Interestingly, I found that, contrary to GABAergic OB interneurons, glutamatergic JGCs survive under these challenging conditions, pointing to a possible homeostatic and highly dynamic balance between excitation and inhibition within the OB. In a second approach, I characterized odor-evoked response profiles of glutamatergic JGCs using GCaMP6s mice that genetically encode a calcium sensitive indicator to monitor neuronal activity. I found that these neurons display a diverse set of excitatory, inhibitory and mixed responses with different degrees of homo- and heterogeneity across individual glomeruli. These results represent the first *in vivo* data on odor-response available for glutamatergic JGCs and strengthen the notion that these neurons act as signal amplifiers to gate glomerular output.

REMERCIEMENTS

This moment has really arrived. I am joyful and sad at the same time. I am so grateful to the whole team for the good energy that was always present, the funny moments we shared, the passionate discussions we had, les sorties bar à vin and so many more aspects that made my lab life a joyful, complete and fulfilling experience, in personal and professional ways.

Merci Harold. You were exactly the type of boss I wanted. You gave me the freedom to develop my own way while still being demanding and pushing my limits to make me a better researcher. You easily spotted my strengths and weaknesses and helped me develop and improve. I always felt supported by you. I appreciated this a lot. **Merci Nathalie.** You were always there to support me when the situation got serious. I really appreciated how you can bring order into a mess (on many levels) and I particularly like your global view of things. I was very lucky to have been sous tes ailes. **Merci Jean-Claude.** You were the mentor that gave me scientific bliss, the stuff that makes a researcher. I was incredibly lucky to work with you and I had the best moments of my scientific career with you in front of the microscope. For this type of moments I did a PhD. **Merci Christophe.** You were like a spiritual guide. I so much enjoyed our philosophical discussions and very much appreciated your advice and your positive energy. You are truly Mr. Cool. **Merci Marie-Cath.** You were the person-to-be-with in terms of cultural enlightenment (or maybe we just have the same taste). I very much enjoyed discussionsw with you and your passion about them has always been inspiring. **Merci Stéphane.** You have been a resting pole when my stuff got agitated. I so much appreciated your stoicism and your laid-back attitude. We balanced each other very well. **Merci Andrea.** We had a connection from the beginning. I appreciated a lot your unique way of seeing things and your energy. **Merci Clara.** You have been a constant source of good energy. Like a medical prescription against grumpiness.

Merci Theodora. Having you by my side all along this journey was an essential part of my happiness. **Merci Marwa**. Having you join the PhD clan made me feel like I have a family here. **Merci** to all the other people of the IBDM that have shared unforgettable moments with me.

Merci to my family. Their support has always been unconditional. Merci specifically to my mum, for her love but also for her incredible excel skills that can solve any problem with a button.

TABLE OF CONTENTS

LIST OF ABBREVIATIONS

4OH-TAM	hydroxytamoxifen
AC	amacrine cell
AONpE	anterior olfactory nucleus pars externa
Ascl	achaete-scute complex-like
Atoh	atonal homolog
bHLH	basic helix loop helix
biETC	external bi-tufted cell
BO	bulbe olfactif
BrdU	bromodeoxyuridine
BUT	butanal
CalB	calbindin
CalR	calretinin
CaMKIIα	Ca2+/calmodulin dependent protein kinase IIα
CCK	cholesystokinin
CJG	cellule juxtglomerulaire
CNGA2	cyclic nucleotide gated channel
CNS	central nervous system
ctrl	control
DAT	dopamine transporter
DREADD	designer receptors exclusively activated by designer drugs
E(X)	embryonic day (x)
EPL	external plexiform layer

ET	ethyl tiglate
ETC	external tufted cell
ex-inh	excitation-inhibition
GABA	gamma-aminobutyric acid
GAD 65/67	glutamic acid decarboxylase 65/67
GC	granule cell
GCL	granule cell layer
GL	glomerular layer
GLAST	glutamate aspartate transporter
GOF	gain-of-function
GPCR	G-protein coupled receptor
HET	heterozygous
hm4Di	modified human M4 muscaric receptor
HO	homoygous
IAA	isoamylacetate
IAB	isoamylbutyrate
IAS	intrabulbar association system
inh-ex	inhibition-excitation
IOS	intrinsic optical signal
IPL	inner plexiform layer
ISI	inter stimulation interval
JGC	juxtaglomerular cell
LGE	lateral ganglionic eminence

LOT	lateral olfactory tract
M/T	mitral/tufted cell
MC	mitral cell
MCL	mitral cell layer
MGE	medial ganglionic eminence
ND	NeuroD
NeuroD	neurogenic differentiation
Neurog2	Neurogenin 2
nGnG	non-glycinergic non GAGAergic
OB	olfactory bulb
OCNC1	olfactory cyclic nucleotide-gated channel subunit 1
OMP	olfactory marker protein
OR	olfactory receptor
OSN	olfactory sensory neuron
P(X)	postnatal day (x)
PGC	periglomerular cell
PRO	propanal
PV	parvalbumin
RGC	radial glia cell
RMS	rostral migratory stream
ROI	region of interest
rSVZ	rostral subventricular zone
SAC	short axon cell

secETC	external tufted cell with secondary dendrites
Shh	sonic hedgehog
TAM	tamoxifen
Tbr1/2	T-box brain 1/2
TC	tufted cell
tdTom	tdTomato (cells)
TF	transcription factor
TH	tyrosine hydroxylase
Vglut1/2/3	vesicular glutamate transporter 1/2/3
V-SVZ	ventricular-subventricular zone
VTA	ventral tegmental area
VZ	ventricular zone

LIST OF FIGURES

INTRODUCTION

In the following I will present my scientific work of the last four years which was dedicated to studying the biology of glutamatergic juxtaglomerular neurons, specifically external tufted cells, in the olfactory bulb (OB). To endow the reader with the background necessary to contextualize my work, I will review the current knowledge and some prevailing concepts in various domains of developmental and sensory neuroscience. I will start with a brief excerpt on the history of adult neurogenesis, followed by the current knowledge on how neural stem cells create neuronal diversity for the OB. I will then introduce the most relevant neuronal OB subtypes, followed by a section on their genetic determination, particularly pointing towards NeuroD6, a bHLH transcription factor that I used as a molecular entry point for the current study. Subsequently, I will go on with the current knowledge on how olfactory information is processed by the OB circuit, specifically focusing on the glomerular layer which is where external tufted cells are situated. I will also briefly mention some local circuits formed by external tufted cells. Finally, I will close with a small overview on how changes in sensory information impact the OB network.

1. NEUROGENESIS IN THE OLFACTORY BULB

1.1 Adult neurogenesis: the difficult birth of a concept

For most part in the history of neuroscience, neurogenesis was viewed as a process inextricably linked to embryonic development. Up until the mid-20th century, reports on mitotic figures or immature neuronal morphologies within the adult brain were scarce and generally ignored. One of the main reasons was the lack of a reliable method that could detect cell division and allow the distinction between glia and neurons (Ramón y Cajal, 1928).

However, things started to change when tritiated [^{3}H]- thymidine, a radiolabeled thymidine analogue, appeared. In the 1960ies Joseph Altman published a series of articles, providing the first evidence of newborn neurons that had incorporated [^{3}H]-thymidine in the young and adult rat brain (Altman, 1962, 1969; Altman and Chorover, 1963; Altman and Das, 1965, 1966). Unfortunately, the dogma he fought proved to be tenacious, his work was considered controversial and has subsequently fallen into oblivion.

One decade later, direct support for Altman's work in rats came from studies using electron microscopy, thus proving that the [^{3}H]-thymidine incorporating cells were indeed neurons with dendrites and synapses and not glia (Kaplan and Hinds, 1977). Nevertheless, it took

many more years and the accumulated evidence of independent observations of adult neurogenesis in songbirds (Paton and Nottebohm, 1984), reptiles (Lopez-Garcia et al., 1988) and primates (Gould et al., 1998) to fully convince the scientific community by the late 1990ies.

At present, it is generally acknowledged that adult neurogenesis is an evolutionary conserved process across vertebrates and that sites of neuronal birth and integration are species-specific (Paredes et al., 2016). In rodents, two regions retain their neurogenic capacity into adulthood: the dentate gyrus of the hippocampus and the ventricular-subventricular zone (V-SVZ) of the lateral ventricle that produces neurons for the olfactory bulb (OB).

1.2 From embryo to adult: neurogenesis as a developmental continuum

During embryonic development, neural stem cells called radial glia cells (RGCs), located in the ventricular zone (VZ) of the lateral ventricle proliferate massively to generate neurons for the developing brain. As embryogenesis approaches its end and the major brain structures are generated, most RGCs lose their characteristic apical and basal processes and undergo terminal differentiation into astrocytes and, during the first postnatal week, into multiciliated ependymal cells (Spassky, 2005; Kriegstein and Alvarez-Buylla, 2009). However, a subset of RG-like cells remains in the walls of the lateral ventricle and continues to generate neurons, even into adulthood (**Fig. 1**) (Gage, 2002; Alvarez-Buylla and Lim, 2004).

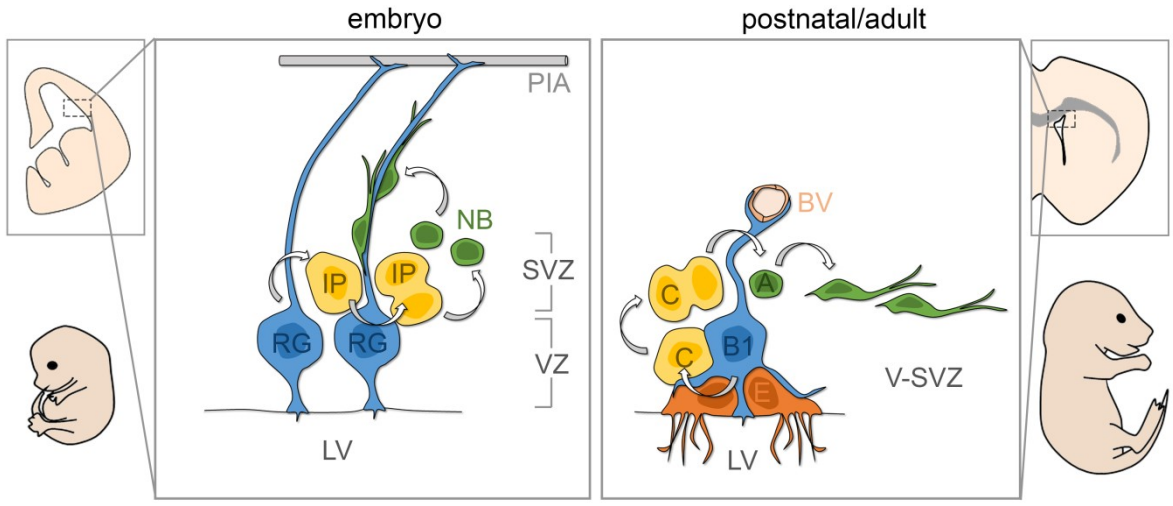

Figure 1. Schematic illustration depicting embryonic (cortical) and postnatal/adult neurogenesis. **Left:** Embryonic radial glia (RG) cells extend an apical process into the lateral ventricle (LV) and a basal process to the pia. Asymmetric division of RG cells gives rise to intermediate progenitors (IP) which rapidly divide to expand the neuroblast (NB) population. NBs migrate radially on RG cell processes towards their layer of destination within the cortex. **Right:** Postnatal/adult B1 cells extend an apical process into the LV and a basal process to blood vessels (BV). Asymmetric division

of B1 cells gives rise to intermediate progenitors (C cells) which rapidly divide to expand the neuroblast (A cells) population. A cells migrate tangentially towards the olfactory bulb. B1 cells terminally differentiate into ependymal (E) cells.

Neural stem cells that remain active into postnatal and adult stages are also called B1 cells (Doetsch et al., 1997). B1 cells derive from embryonic RGCs (Merkle et al., 2004). In fact, a lineage relationship between B1 cells and RGCs that give rise to cortex, striatum and septum can be established as early as E15.5 (Fuentealba et al., 2015). Currently, our understanding of the mechanisms that lead to the division between embryonic RGCs and future B1 cells is still limited. However, one of the important aspects could be cell cycle kinetics: between E13.5 and E15.5 a subset of RGCs that will become future B1 cells, slows down their cell cycle while embryonic RGCs keep on dividing rapidly (Furutachi et al., 2015). More generally, B1 cells and RGCs share some basic properties and morphological features. Both share a common set of stem cell and glial markers (e.g. Nestin, Sox2 and GLAST, respectively) (Kriegstein and Alvarez-Buylla, 2009). Both have an apical process with a primary cilium that connects to the surface of the ventricle. However, instead of connecting the pia with their basal process like RGCs, B1 cells connect to blood vessels (**Fig. 1**) (Mirzadeh et al., 2008). Finally, like in the embryo, B1 cells give rise to a proliferative type of intermediate progenitors (or C cells), which in turn will generate immature neurons, also called neuroblasts (or A cells, **Fig. 1**) (Doetsch et al., 1997). Neuroblasts generated postnatally at the walls of the lateral ventricle will then start to migrate in chains through the rostral migratory stream (RMS) until they reach and eventually integrate into the OB (**Fig. 2**) (Lois, C. & Alvarez-Buylla, 1994; Luskin, 1993).

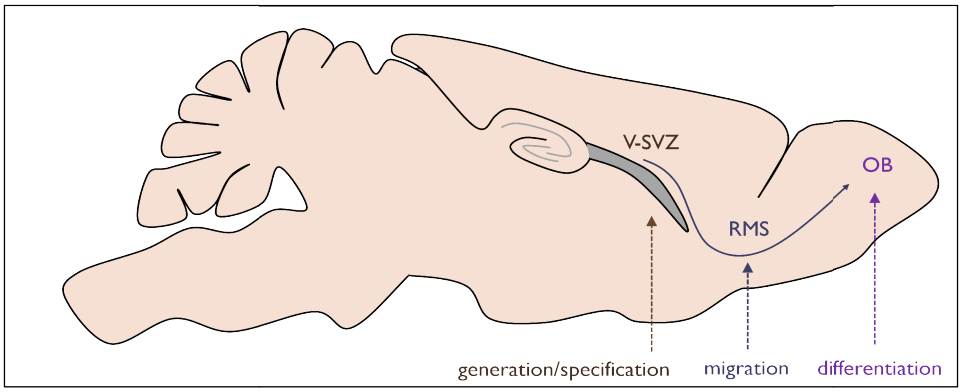

Figure 2. Schematic illustration of a mouse brain depicting the V-SVZ-RMS-OB system. Immature neurons are generated in the ventricular-subventricular zone (V-SVZ) and subsequently migrate in chains through the rostral migratory stream (RMS) before they integrate into the olfactory bulb (OB).

1.3 Positional identity of adult neural stem cells in the V-SVZ

Already during early development, different RGCs located at distinct places along the embryonic VZ are predetermined to produce only certain types of neurons. For instance, cortical excitatory projection neurons are produced only from the dorsal pallium, whereas cortical inhibitory interneurons are issued from the ventrally located subpallium (Puelles et al., 2000; Molyneaux et al., 2007). During the transition from embryogenesis to birth, the neurogenic zone surrounding the lateral ventricle undergoes considerable morphological and molecular remodeling. Pallium and subpallium turn into the dorsal, lateral and medial walls of the lateral ventricle. The recent understanding that the postnatal (and adult) neurogenic niche retains characteristics of both, the embryonic VZ and SVZ, also led to the new term V-SVZ (Lim et al., 2016).

Interestingly, the V-SVZ retains a molecular dorso-ventral and medio-lateral patterning reminiscent of that in the embryo (**Fig. 3**). The positional identity of RG/B1 cells and possibly other early progenitors is defined by an ever growing list of specific niche cues, chromatin remodeling factors and unique transcription factor signatures (Lim et al., 2016; Delgado and Lim, 2017). Inevitably, one might wonder whether or to what extend the properties of stem cells are intrinsic or determined by their environment.

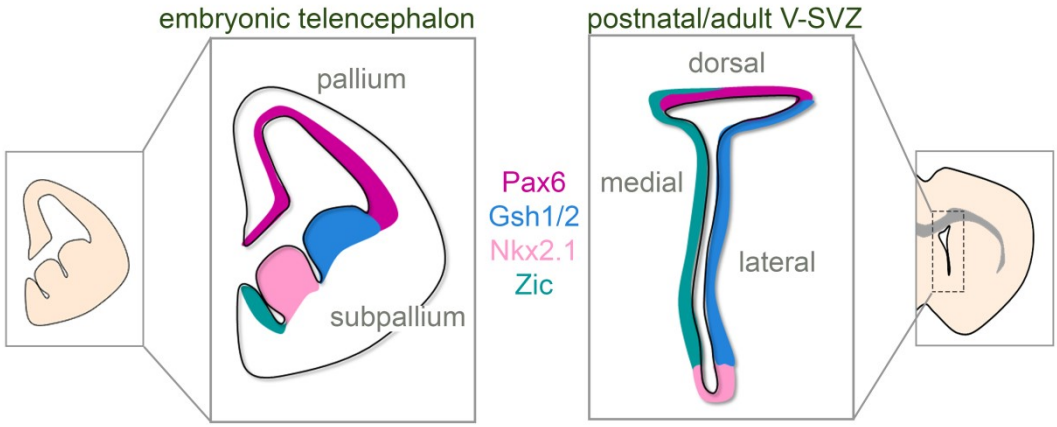

Figure 3. Schematic illustration of molecular patterning in embryonic telencephalon and postnatal/adult V-SVZ. Colors indicate patterning by different transcription factors. The examples Pax6, Gsh1/2, Nkx2.1 and Zic mark different subregions of the neurogenic niche along the lateral ventricle. Although the neurogenic niche undergoes a morphological transition from embryogenesis to postnatal/adult, molecular patterning remains present. V-SVZ: ventricular-subventricular zone.

To address this question, many transplantation studies were carried out in the 1990ies. Expectedly, V-SVZ tissue homotopically grafted into the V-SVZ of another adult animal, was capable of producing new OB neurons (Lois, C. & Alvarez-Buylla, 1994). Even tissue originating from the dentate gyrus and grafted into the RMS could generate OB neurons (reviewed in Gage, 2000). To push the limits even further, in another study multipotent progenitors from the non-neurogenic spinal cord were transplanted into the adult dentate gyrus and produced differentiated putative hippocampal granule cells (Shihabuddin et al., 2000). On the other hand, when V-SVZ tissue was grafted into non-neurogenic regions like the cortex or striatum, astrocytes were the main outcome (Herrera et al., 1999). These are intriguing results which suggest that is indeed the neurogenic niche itself that provides the factors necessary to generate neurons and that it possibly even instructs progenitors from ectopic brain areas to acquire a basic "bulk" identity corresponding to the host niche itself. Unfortunately, the molecular nature of these factors is still poorly understood (Götz et al., 2016).

However, more recent studies set out to investigate the regionalization of the V-SVZ and obtained results pointing towards a strong intrinsic specification of neural stem cells (Kelsch et al., 2007; Merkle et al., 2007). When progenitors from specific V-SVZ locations were put into culture, they produced only specific neuron subtypes, thus recapitulating neurogenesis according to their region of origin. Likewise, when neonatal V-SVZ progenitors were heterotopically grafted into another subdomain of the same niche, they again produced neurons that corresponded to their region of origin rather than their graft location. This was not only true for their characteristic marker expression but also their OB integration site and even dendritic branching pattern (Kelsch et al., 2007; Merkle et al., 2007).

Based on these results, it is reasonable to conclude that the environmental cues from the neurogenic niche itself provide a permissive context necessary for neurogenesis in general. However, given these seemingly opposing results on cell-autonomous properties of precursors guiding neuronal identity, one could imagine two scenarios: (1) The studies from the 1990ies and the studies performed by Merkle et al. and Kelsch et al. did not use the same progenitors, with the later possibly using more committed progenitors while true neuronal stem cells would have displayed more plasticity. (2) Progenitors from different parts of the brain are prone to re-specification when grafted into a different neurogenic niche due to the interference of new niche cues and their intrinsic molecular programs. However, if progenitors are autochthonous to the tissue and share a set of molecular signaling cascades, even when re-

grafted, they could retain their cell-autonomous molecular program to produce only certain types of neurons. More experimental work is necessary to unequivocally resolve this issue. However, it is clear that in their endogenous environment V-SVZ progenitors are strongly regionalized and pre-determined to produce distinct sets of OB neurons.

2. NEURONAL SUBTYPES OF THE MAIN OLFACTORY BULB

Like the cortex, the olfactory bulb is a highly laminated structure where different steps of information processing take place in specialized layers. However, its most striking difference to the adjacent cortex is that the OB is a predominantly inhibitory circuit and its major cell types are diverse sets of locally connecting interneurons rather than excitatory projection neurons (Shepherd, 2004; Parrish-Aungst et al., 2007). This particularity is an inherent property of olfactory information processing.

2.1 The glomerular layer

The glomerular layer (GL) is the outer-most layer of the OB and is composed by the totality of glomeruli. Glomeruli are neuropil-rich spherical structures that contain the axonal projections of olfactory sensory neurons (OSNs) which synapse with the dendritic tufts of the principal output cells and the dendritic processes of diverse types of interneurons, called juxtaglomerular cells (JGCs). JGCs form a distinctive shell of cell bodies around each glomerulus. Therefore, the glomerulus is the first relay station of information processing within the OB.

Classification of neurons is indispensable. However, based on the criteria, classification turns out quite different and does not always help to clarify neuronal complexity within the brain. OB interneurons are a classical example of this problem. Historically, there are three main criteria for neuronal classification within the GL: (1) morphology, (2) connectivity and (3) molecular identity. Based on morphological features, JGCs were classified into periglomerular cells (PGCs), external tufted cells (ETCs) and short axon cells (SACs, **Fig. 4)** (Pinching and Powell, 1971a). Based on OSN-related connectivity, JGCs are classified into type-I JGCs that receive direct (monosynaptic) OSN input or type-II JGCs which receive indirect OSN input (Kosaka et al., 1997; Kasowski et al., 1999). Based on neurochemical expression profile, JGCs are grouped into categories of non-overlapping markers which include GABA/dopaminergic neurons immunoreactive for tyrosine hydroxylase (TH), purely GABAergic neurons immunopositive for calbindin (CalB) and calretinin (CalR) (Parrish-

Aungst et al., 2007) and glutamatergic neurons immunoreactive for T-box transcription factors Tbr1 and Tbr2 (Brill et al., 2009; Winpenny et al., 2011).

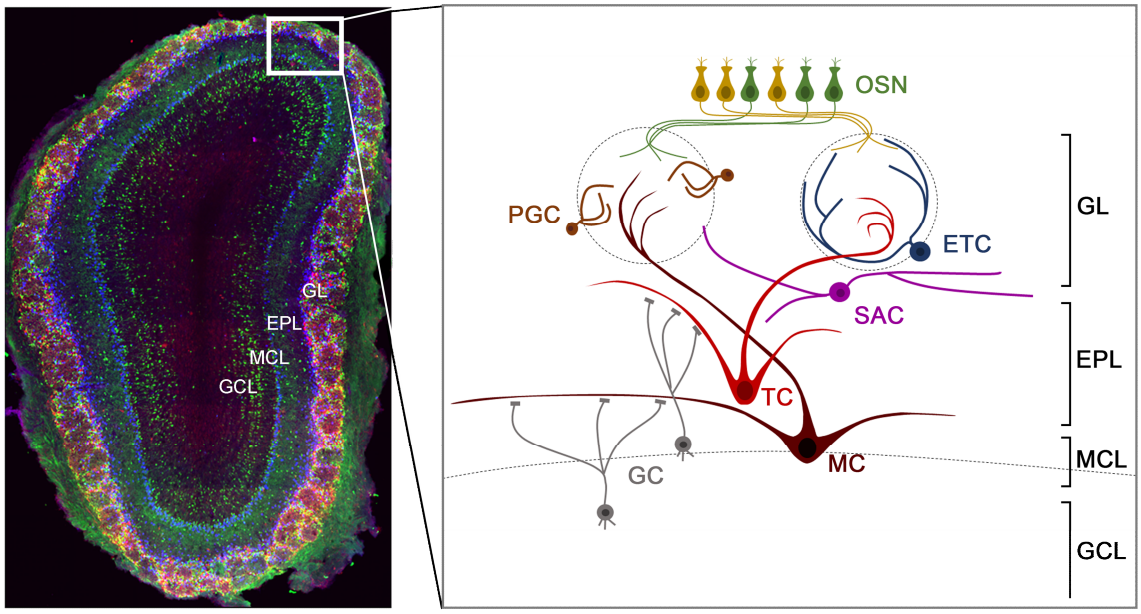

Figure 4. Major types of OB interneurons. **Left:** Coronal section of a mouse OB. Colors indicate different non-overlapping OB subtypes and help visualize OB layers (from inside to outside: GCL, MCL, EPL and GL). **Right:** Schematic illustration of OB subtypes. OSN project into glomeruli (sphere). Glomeruli are innervated by JGCs with intraglomerular (PGCs and ETCs) and interglomerular (SACs) dendritic trees. Apical tufts of MCs and MCs also innervate glomeruli. GCs situated in the GCL extend their dendrites into the EPL. OSN: olfactory sensory neuron; JGC: juxtaglomerular cell; PGC: periglomerular cell; ETC: external tufted cell; SAC: short axon cell; TC: tufted cell; MC: mitral cell; GC: granule cell; GCL: granule cell layer; MCL: mitral cell layer; EPL: external plexiform layer; GL: glomerular layer.

PGCs are the most abundant, have the smallest cell body (5-10 µm) and typically project their dendrite into one glomerulus where they occupy only a fraction of the glomerular space (**Fig. 4**) (Nagayama et al., 2014). There are axon-bearing as well as axon-less types (Kosaka and Kosaka, 2011). On a molecular level PGCs are immunoreactive for either glutamic acid decarboxylase (GAD) 65 or GAD67 and are thus inhibitory neurons. Additionally, roughly 50% of PGCs are also immunoreactive for some mutually exclusive markers which thus each define different PGC subtypes. PGCs subtypes include tyrosine hydroxylase (TH), calretinin (CalR) and calbindin (CalB) positive neurons. Regarding connectivity, TH+ PGCs are type-I while CalR+ and CalB+ PGCs are type-II connected (Kosaka and Kosaka, 2007a).

SACs have slightly larger somata (8-12 µm). Their overall occurrence is estimated to be small but no clear quantifications have been done so far. Their dendrites connect to several

glomeruli and ramify into the interglomerular space (**Fig. 4**) (Nagayama et al., 2014). Although their name suggests otherwise, these cells have axons that can connect up to 25 glomeruli (Kiyokage et al., 2010). SACs do not receive monosynaptic input from OSNs and are thus type-II JGCs (Hayar et al., 2004). Although these cells were once reported as glutamatergic (Aungst et al., 2003), later studies from the same group have identified them as TH+/GAD67+ (Kiyokage et al., 2010). However, since these cells do not fully correspond to the original classification of SACs (Pinching and Powell, 1971b; a) it seems likely that there are more than one SAC type. Indeed, glutamatergic SACs positive for vesicular glutamate transporter 2 (Vglut2) have been reported (Brill et al., 2009; Winpenny et al., 2011) although the morphology or connectivity of these cells has not been further studied.

ETCs have the largest somata (10-15 µm). They are often situated at the lower part of a glomerulus or at the border between the GL and the subjacent external plexiform layer (EPL, **Fig. 4**). They usually ramify into one glomerulus although also a small proportion represents bi-tufted cells connecting two glomeruli (Hayar, 2004). ETC dendrites usually occupy the majority of the glomerular space. So far, two types of ETCs have been described: (1) a group that exclusively bears an apical dendritic tuft without secondary dendrites and (2) a second group that has an apical dendritic tuft and also secondary dendrites that branch into the EPL. ETCs, in contrary to other JGCs display rhythmical theta bursts (6-7 Hz) (Hayar, 2004; Hayar et al., 2004). However, other studies observed these bursts only in ETCs without secondary dendrites (Antal et al., 2006; Takahashi et al., 2016). The majority of these cells seem to have axons, some of which stay within the GL and others diving deep into GCL (Hayar, 2004). ETCs receive monosynaptic input from OSNs (Hayar et al., 2004). ETCs are classically seen as excitatory neurons, however a recent study (Tatti et al., 2014) has found that ETCs can be divided into two molecularly different groups: (1) ETCs that express vesicular glutamate transporter 2 (Vglut2) being purely excitatory and (2) ETCs that express another type, Vglut3, some of which are purely GABAergic. The majority (60%) of these GABAergic ETCs also express CalB and to a much lesser extend CalR and TH (Tatti et al., 2014). Furthermore, some ETCs express the neuropeptides cholecytokinin (CCK) (Liu et al., 1994) or vasopressin (Tobin et al., 2010). However, to what extend these peptides mark the whole ETC population or just a fraction is unknown. Finally, a study that investigated glutamatergic OB interneurons found that T-box transcription factor Tbr2 marks JGCs with ETC features born up to postnatal day 0 (P0) (Winpenny et al., 2011).

2.2 The external plexiform and mitral cell layer

Just beneath the GL and its associated cells lies the EPL, a layer which is characterized by the high density of neuronal processes and low density of cell bodies. The interneurons found here are GABAergic cells mostly immunoreactive for parvalbumin (PV). However, PV+ neurons form a very heterogeneous group including different types of short axon and multipolar cells, and thus cannot be regarded as a single neuronal subtype (Kosaka et al., 1994; Nagayama et al., 2014).

Additionally, the EPL harbors the tufted cells (TCs), one of the two excitatory principal cell types of the OB. TCs have bigger cell bodies (15-20 µm), project a single apical tuft into one glomerulus and extend their secondary dendrites laterally into the EPL (**Fig. 4**). According to the location of their soma within the EPL, TCs are typically classified into external (sometimes referred to as superficial), middle and internal (or deep) TCs (Nagayama et al., 2014).

When it comes to TCs and ETCs, neuronal nomenclature is somewhat confusing. In fact, the previously described ETCs have been often included into the projection neuron category of TCs. This confusion lies in the similarity of their morphology and the expression of some common markers. However their connectivity and thus function seems to be highly heterogeneous. Indeed, using retrograde tracers some superficially located TCs have been shown to project to the most rostral olfactory cortical area, the anterior olfactory nucleus pars externa (AONpE). However, a substantial part of ETCs have only intrabulbar projections (Schoenfeld et al., 1984). Thus, in the current study I will refer to ETCs as interneurons in contrast to TCs, which are classical projection neurons.

It is noteworthy that a recent study tried to unify morphological categories with physiological properties and connectivity of JGCs (Tavakoli et al., 2018). Using a computational approach the authors could obtain 7 clusters from which 4 corresponded to the prevailing JGC concepts whereas 3 did not. Interestingly two out of these three new categories appeared to be new forms of superficial tufted cells, further pointing towards the heterogeneity of this neuronal class.

The inner border of the EPL is delineated by a thin layer mainly composed of the second type of OB projection neurons, the mitral cells (MCs). MCs have the biggest somata (>20 µm) and share with TCs their distinct morphology, i.e. a single apical tuft branching into one glomerulus and basal dendrites that extent laterally into the EPL (**Fig. 4**). Each glomerulus is

innervated by approximately 20 mitral and tufted (M/T) cells that are located in close proximity to each other and to the glomerulus in question (Buonviso et al., 1991; Nagayama et al., 2014)

The aforementioned dense neuropil within the EPL is mainly composed of dendrites from M/T cells that form dendro-dendritic synapses from inhibitory granule cells that reside below the mitral cell layer. When a signal received by the glomerular tuft M/T cells arrives to the cell body, it is subsequently back-propagated to the lateral dendrites in the EPL. If strong enough, the signal will excite a granule cell which in turn will inhibit another neighboring M/T cell (Xiong and Chen, 2002). This process is called lateral inhibition and believed to be one of the major strategies to inhibit the activity of other M/T cells and thus increase the signal-to-noise ratio of a sensory stimulus.

Axons of M/T cells converge into the latero-ventrally located lateral olfactory tract (LOT) to relay olfactory information into cortical areas. TCs and MCs differ also in their projection patterns. While TCs connect to the more rostral cortical areas like the olfactory peduncle, olfactory tubercle and the anterior part of the piriform cortex, MCs connect throughout the entire olfactory cortex (Nagayama et al., 2010; Igarashi et al., 2012).

2.3 The granule cell layer

The granule cell layer (GCL) is almost entirely occupied with inhibitory interneurons called granule cells (GCs). GCs are the most numerous neuronal subtype in the OB. They have a small cell body (6-8 μm), a characteristic apical dendritic tree with pronounced spines that extends into the EPL and no axon (Price and Powell, 1970). Thus, GC output relies solely on dendro-dendritic synapses that they typically form with the lateral dendrites of M/T cells in the EPL (**Fig. 4**). Classically, GCs are placed into two main categories: (1) GCs located in the deep GCL which extend dendrites into the deep EPL and (2) GCs located in the superficial GCL which extend dendrites into the superficial EPL (Mori et al., 1983; Orona et al., 1983). A recent study showed that rare additional GC types with specific branching patterns exist, pointing towards a more complex view of this seemingly uniform cell type (Merkle et al., 2014). Molecular markers are scarce for GCs. However, GCs that are intermingled into the MCL express the leucine-rich-repeat transmembrane protein 5T4 and a subpopulation of GCs in the superficial GCL express CalR (Nagayama et al., 2014). Additionally to these topographic markers, a recent study has found that Ca2+/calmodulin dependent protein kinase IIα (CaMKIIα) can reliably distinguish GCs involved in different functional circuits (Malvaut et al., 2017).

2.4 Temporal origin of OB neurons

The formation of the OB is achieved by the sequential generation of different neuron subtypes. The first OB cells to be born are the mitral cells which are issued from the rostral-most pallial VZ between E10.5 and E13.5 and form the MCL by E14.5 (Hinds, 1968; Blanchart et al., 2006; Imamura et al., 2011). Tufted cells are born shortly after MCs, between E13.5 and E16.5 (Hinds, 1968; Imamura et al., 2011). At E14.5, OSN axons also start to invade the OB and first protoglomeruli form by E15.5 (De Carlos et al., 1995; Blanchart et al., 2006). MCs seem to establish their first OSN contact by E16.5 (Blanchart et al., 2006).

In the subpallium, in particular the lateral ganglionic eminence (LGE) OB interneurons start to be produced from E12.5 on (Wichterle et al., 1999; Weinandy et al., 2011). However, while some neuronal subtypes are mainly produced in the embryo, others are preferentially generated after birth or even in adult. In fact, overall OB interneuron production peaks not until the first postnatal week. TH+ JGCs can be found among the very first born interneurons. Their peak of generation lies at E12.5 and production declines steadily although still some TH+ neurons are born in postnatal animals (Batista-Brito et al., 2008). Glutamatergic Tbr1/Tbr2+ JGCs too seem be early born. They can be detected as early as E13.5 and most likely have their generation peak around birth with a rapid decline afterwards (Brill et al., 2009; Weinandy et al., 2011; Winpenny et al., 2011). PV+ neurons are also mostly generated in the embryo starting from E15.5 up until P10. Similarly, CalB+ neuron production peaks early (E15.5-E17.5) but some neurons are also produced postnatally. On the other hand, CalR+ JGC production starts at E12.5 but steadily increases until P30. Likewise, GCs start to be generated from E12.5 on but are continuously produced into adult stages. In fact, GCs represent the most abundant adult-generated neuronal subtype in the OB (Batista-Brito et al., 2008).

In a system like the OB that continuously generates different types of neurons, it is natural to assume that neuronal birth date correlates with neuronal function within the circuit. Unfortunately, current knowledge about the specific function of each neuronal subtype is still incomplete and has not yet allowed us to put meaning into their temporal generation pattern.

3. GENETIC PROGRAMS GOVERNING OB NEURON PRODUCTION

The origin of neuronal diversity within the OB is to be found in the molecular patterning of the neurogenic niche surrounding the lateral ventricle. Fate mapping with Cre recombinase under the control of pallial- and subpallial-specific transcription factor (TF) promoters has

demonstrated that the postnatal V-SVZ is derived from its earlier embryonic counterpart (reviewed in Fiorelli et al., 2015). Moreover, the possibility to label a defined subset of neural stem cells by lineage tracing (Kohwi, 2005; Young et al., 2007), viral labeling (Merkle et al., 2007, 2014) and targeted electroporation (Fernández et al., 2011; de Chevigny et al., 2012b; Azim et al., 2015; Tiveron et al., 2017) substantially contributed to our understanding of stem cell regionalization and allowed to directly test the implication of candidate genes underlying this patterning.

3.1 Genetic programs involved in GABAergic OB neuron production

The lateral V-SVZ, derived from the LGE, is the neurogenic region that gives rise to most OB interneurons (Alvarez-Buylla et al., 2008). The most abundant cell type produced from this region are deep GCs (>90%, **Fig. 5**) and to a lesser extend TH+ and CalB+ interneurons (Fernández et al., 2011; de Chevigny et al., 2012b). Indeed, the lateral V-SVZ can be further divided into the dorso-lateral, purely lateral and ventro-lateral sub-domains. One interesting example is the homeobox gene Gsh2 which is expressed in the dorso-lateral tip of the lateral V-SVZ also marked by Er81 (Stenman et al., 2003; Lopez-Juarez et al., 2013). Deletion of Gsh2 leads to severe OB defects and dramatically reduces the Er81+ GC and JGC population, demonstrating that it is a major player in the generation for these OB neurons (Toresson and Campbell, 2001; Stenman et al., 2003; Lopez-Juarez et al., 2013).

On the other hand, CalB+ JGCs and specific subtypes of superficial GCs originate rather from the ventro-lateral tip of the lateral V-SVZ (**Fig. 5**) that derives from the medial ganglionic eminescence (MGE) (Merkle et al., 2007, 2014). B1 cells of this region express Nkx2.1 which is under the control of the morphogen sonic hedgehog (Shh). Importantly, adult deletion of Shh reduces the number of ventrally-derived neurons in the OB (Ihrie et al., 2011) pointing towards a major role in maintaining ventral B1 cell identity.

The medial V-SVZ, derived from the embryonic septum, is the only sub-domain that produces almost exclusively JGCs (Merkle et al., 2007). CalR+ JGCs are among the most represented subtype generated from this region (**Fig. 5**) (Merkle et al., 2007; Fernández et al., 2011). The medial wall is patterned by TFs like Zic1/2, Sp8, Gsh2 and, towards the medio-dorsal tip, Emx1 (Alvarez-Buylla et al., 2008; Merkle et al., 2014). Conditional deletion of Sp8 in the ventral embryonic telencephalon results in increased cell death, abnormal migration patterns of neuroblasts and reduced numbers of CalR+ JGCs (Waclaw et al., 2006).

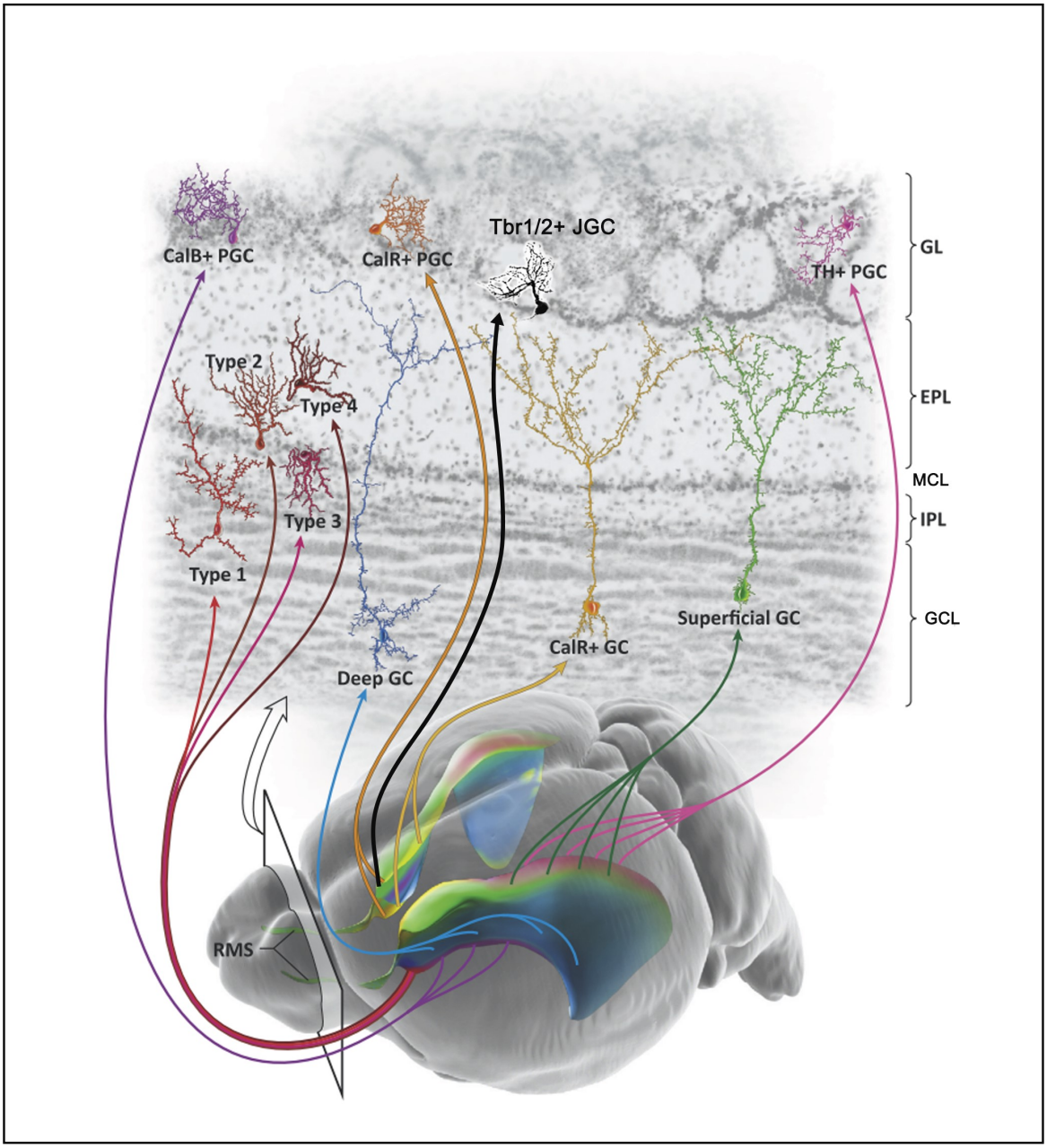

Figure 5. Regionalization of ventricular-subventricular zone (V-SVZ) progenitors. Mouse brain (bottom) with color-coded neurogenic niche surrounding the lateral ventricle. Cells originating from different subregions of the V-SVZ migrate through the rostral migratory stream (RMS) to integrate in different layers of the OB. Examples depict CalR+, CalB+ and TH+ PGCs, Tbr1/2+ JGCs, and different types of GCs (CalR+, deep, superficial, type 1-4). GL: glomerular layer, EPL: external plexiform layer; MCL: mitral cell layer; IPL: inner plexiform layer; GCL: granule cell layer; CalB: calbindin; CalR: calretinin; TH: tyrosine hydroxylase; PGC: periglomerular cell, JGC: juxtaglomerular cell; GC: granule cell. Illustration adopted from (Lim and Alvarez-Buylla, 2014).

The dorsal V-SVZ, of pallial origin, undergoes most likely the profoundest molecular rearrangement from embryo to postnatal/adult. It switches from producing embryonic

projection neurons to production of almost exclusively GABAergic neurons (TH+ and CalR+ JGCs and superficial GCs, **Fig. 5**) in postnatal/adult. In fact, this switch is not only accompanied by the expression of novel transcription factors like Zic proteins (Tiveron et al., 2017, see **Appendix I**) but is also likely associated with more upstream regulators like chromatin remodeling factors (reviewed in Angelova et al., 2018, see **Appendix II**) that possibly modulate the function of TFs already present in the system. Pallial-associated genes Emx1 and Pax6 would make good candidates for such a scenario. Indeed, while the Emx1 territory is associated exclusively with pyramidal neuron production during embryogenesis, postnatal Emx1-derived progeny is composed of GABAergic CalR+ and TH+ JGCs, as well as superficial GCs (Kohwi et al., 2007). Likewise, Pax6 deletion strongly reduces superficial GC and TH+ JGC production (Hack et al., 2005; Kohwi, 2005), indicating that this TF constitutes a major fate-determinant of these GABAergic neuron populations. Numerous TFs contribute to the patterning and fate-determination within the V-SVZ. However, regulation of this zone likely includes control mechanisms on various molecular levels. Indeed, the dorso-ventral gradient of Pax6 was recently found to be counteracted by the microRNA mir-7a. Mir-7a is expressed in an opposed gradient along the lateral V-SVZ and prevents Pax6-mediated dopaminergic fate acquisition of lateral neurons (de Chevigny et al., 2012a). Thus, post-transcriptional regulation is yet another important mechanism to restrain TF territory and directly contributes to patterning of the V-SVZ.

3.2 Genetic programs involved in glutamatergic OB neuron production

Although glutamatergic OB neurons were studied by physiologists for quite some time, it was not until recently that glutamatergic JGC production beyond embryogenesis was demonstrated (Brill et al., 2009; Winpenny et al., 2011). Using Neurogenin2- (Neurog2) mediated lineage tracing, the authors identified a progenitor pool residing in the dorsal V-SVZ co-expressing a set of TFs (Tbr2 and Tbr1) associated with glutamatergic fate (**Fig. 5**). Indeed, these progenitors gave rise to glutamatergic OB interneurons, as shown by co-localization of Neurog2-derived cells with Tbr1, Tbr2 and Vglut2, while no overlap with known GABAergic OB markers (GAD67, GAD65, TH, CalR, CalB) was observed (Brill et al., 2009; Winpenny et al., 2011). Molecularly, early-born (E13.5 – E17.5) JGCs were Tbr2+/Tbr1- while P0-born JGCs were Tbr2+/Tbr1+ (Winpenny et al., 2011). Adult-born JGCs, although passing through transient Tbr2 and Tbr1 expression, downregulate Tbr2 (no information for Tbr1 provided) before integrating in the GL (Brill et al., 2009). In addition, early-born JGCs seem to preferentially adopt ETC morphology while late-born JGCs show rather SAC morphology. Whether there is a functional difference between early- and late-born

neurons (of the same JGC category) and to what extend this molecular heterogeneity might contribute to it, has not yet been investigated.

However, general transcriptional cascades leading to glutamatergic neuron production are fairly well known and surprisingly conserved across the brain. Indeed, progenitors giving rise to the cortical projection neurons, hippocampal granule cells and glutamatergic OB neurons seem to follow a specific sequence which includes Pax6 → Neurogenin2 → Tbr2 → NeuroD1 → Tbr1 (Englund et al., 2005; Hodge et al., 2008; Roybon et al., 2009; Winpenny et al., 2011). Although the TF sequence is shared, these regions produce significantly different neurons. Therefore, it seems likely that other downstream mechanisms are put into place to further specify neuronal subtypes.

3.3 Genes that specify neuronal differentiation: NeuroD proteins

The evolutionary conserved basic helix-loop-helix (bHLH) protein super-family plays a vital role in cell determination and differentiation across many cell lineages of different species. BHLH transcription factors specific to the nervous system were first discovered in *Drosophila* in the 1980ies based on their ability to induce neuronal identity on ectodermal cells (Huang et al., 2014). Vertebrate homologues of neuronal bHLH genes can be distinguished according to sequence similarity and form the sub-families Atoh (Atonal homolog), Ascl (Achaete-Scute complex-like), Neurogenin, NeuroD (Neurogenic differentiation) and Olig whose members act during neurogenesis, neuronal differentiation and/or gliogenesis. Throughout evolution, these different categories arose most likely through gene duplication. Interestingly, in more complex organisms, more members of these genes are found, raising the possibility that they might contribute to neuronal diversity (Baker and Brown, 2018).

3.3.1 NeuroD proteins in neural development

The NeuroD (ND) family comprises four members NeuroD1/2/4 and 6, with ND1/2 and 6 sharing over 90% sequence similarity (McCormick et al., 1996). Studies on the function of NeuroD proteins in the mouse brain focus mostly on the three members ND1/2/6 since ND4 is only weakly expressed in this region (Bormuth, 2016). In the developing CNS, ND1/2/6 show highly overlapping but not identical expression patterns. Expression is most pronounced in the developing telencephalon and in adult neocortex, hippocampus and cerebellum. On a cellular level, all three members are expressed in postmitotic neurons in agreement with their role in later steps of neuronal differentiation (Schwab et al., 1998).

A recent study in the cortex pinpointed the cooperative action of ND2 in ND6 in commissural formation (Bormuth et al., 2013). While in a single ND6 mutant background no detectable phenotype was observed, deletion of both genes impeded callosal axons from successfully crossing the midline and axons defasciculated in the V-SVZ instead. As a consequence, no corpus callosum and no anterior commissure were formed. These defects were accompanied by deregulation of downstream targets implicated in axonal signaling like the lack of the cell adhesion molecule Contactin-2 and an ectopic expression of Robo1. On a physiological level, recordings of spontaneous EPSCs by patch-clamp showed that cultured double mutant cells almost completely lost their spontaneous burst activity. Moreover, Vglut1 immunoreactivity strongly decreased in tissue sections, further indicating that the overall network activity was compromised in double mutants. However, the later effects of ND2/ND6 double mutants could not be further investigated due to postnatal lethality caused by early respiratory failure (Goebbels et al., 2006; Bormuth et al., 2013).

NeuroD6 seems to be particularly dispensable for cortical development due to high functional redundancy with NeuroD2. However, in other brain regions like the retina, this protein acts alone as a fate determinant of an amacrine cell (AC) type (Kay et al., 2011). In this system, the transient expression of ND6 defines a glycinergic AC subtype while prolonged ND6 expression promotes the fate of a “non-glycinergic non-GABAergic” (nGnG) AC subtype which is specifically lost after ND6 deletion (Kay et al., 2011). The midbrain is another area where NeuroD6 alone seems to play a role. While in the embryo survival of excitatory VTA dopaminergic neurons depends on the joint function of ND6 and ND1, a subset (30%) of these neurons depend on ND6 alone for postnatal survival (Khan et al., 2017).

These studies highlight the diverse functions that NeuroD proteins can employ. The combinatorial expression among different family members and also modification of the time window of expression likely contribute to the recruitment of diverse sets of downstream targets adapted to their respective developmental contexts.

3.3.2 NeuroD proteins in the olfactory bulb

To date, function and expression patterns of NeuroD proteins in the OB system remain poorly understood. NeuroD2-positive cells have been detected in the V-SVZ and RMS (Roybon et al., 2009) but their identity or lineage relationship was not further studied. Lineage tracing with NeuroD6$^{cre/LacZ}$ (Goebbels et al., 2006) indicates delimited OB cell populations located in the MCL and GL, but again, these cells were not further characterized. Expression of NeuroD1 in the OB has been better studied. ND1 forms part of a transcriptional cascade that

involves factors Pax6, Neurog2 and Tbr2 and Tbr1 within the V-SVZ (Roybon et al., 2009). Within the OB, expression is either transient or stable and confined to a subpopulation of MCs and glutamatergic JGCs (Roybon et al., 2015). Functional data for NeuroD proteins is rather fragmentary and only available for ND1. Forced expression of ND1 by postnatal (Boutin et al., 2010) or *in utero* electroporation (Roybon et al., 2015) induces ectopic differentiation of OB neurons. In conclusion, NeuroD proteins are present in the OB system and could likely function in neuronal maturation, however, more work is needed to further elucidate their specific role.

4. ODOR PROCESSING IN THE OB CIRCUITRY

In order to understand olfactory processing one must wonder about the ultimate goals of the olfactory system. To this end, one could imagine several crucial elements: (1) an odor has to be rapidly identified and compared to known odors (odor recognition and memory); (2) the odor source has to be located but also recognized across a wide concentration range (concentration-invariant recognition); (3) the odor has to be isolated from a sensory noisy background (segmentation of sensory or neural noise); (4) the animal has to make a fast decision (Uchida et al., 2014). According to the "efficient coding hypothesis" sensory systems should encode a maximum amount of relevant information with a minimum amount of spikes (Barlow, 1961). Conveniently, computational ability of principal cells can be increased by interneuron diversity (Buzsáki and Chrobak, 1995; Roux and Buzsáki, 2015). The glomerular layer harbors the highest degree of interneuron diversity within the OB which makes it particularly attractive to study processing mechanisms of olfactory input.

In the following, I will review (non-exhaustively) the current knowledge on odor processing specifically focusing on the glomerular layer, which is where external tufted cells are situated. I will not mention downstream processing mechanisms like processing in GCs or further processing in the piriform cortex which are out of scope of this work. Finally, I will briefly, review two local circuits formed by ETCs and their possible functional implications.

4.1 Odor detection in the olfactory epithelium

The detection of odorants is achieved by the binding of odorant molecules to olfactory receptors (ORs). The discovery that ORs underlie the molecular basis of smell was a milestone for the field. In the 1980ies a series of biochemical experiments indicated that ORs are G-protein coupled receptors (GPCRs) with seven transmembrane domains (reviewed in Malnic et al., 2010). Simultaneously, the polymerase chain reaction (PCR) technique was

developed (Saiki et al., 1988) and expanded tremendously the experimental possibilities in molecular biology. Given the sequence similarity of GPCRs, it was reasoned that degenerate primers used on rat olfactory epithelium should identify OR genes specific to this tissue. Indeed, in 1991, Linda Buck and Richard Axel managed to clone the first OR (Buck and Axel, 1991) and thus paved the way for the discovery of the OR gene family which includes 1000 OR genes (Axel, 1995; Buck, 1996). For this finding Buck and Axel were awarded the Nobel Prize in Physiology or Medicine in 2004.

ORs are located in the cilia of dendrites of olfactory sensory neurons (OSNs) which reside in the olfactory epithelium situated in the nasal cavity (**Fig. 6**). Each OSN expresses only one type of OR (Mombaerts et al., 1996; Malnic et al., 1999). OSNs that express the same OR, form axonal bundles which converge in a topographical manner into two glomeruli, located medio-laterally in the OB (Ressler et al., 1994; Vassar et al., 1994; Mombaerts et al., 1996). In the mouse OB there are approximately 1800 glomeruli (Mori et al., 1999). Interestingly, OSNs that express specific sets of ORs are topographically organized in a dorso-ventral manner within the olfactory epithelium and form a stereotyped glomerular odor map in the OB (**Fig. 6**) (Ressler et al., 1993; Vassar et al., 1993; Miyamichi et al., 2005).

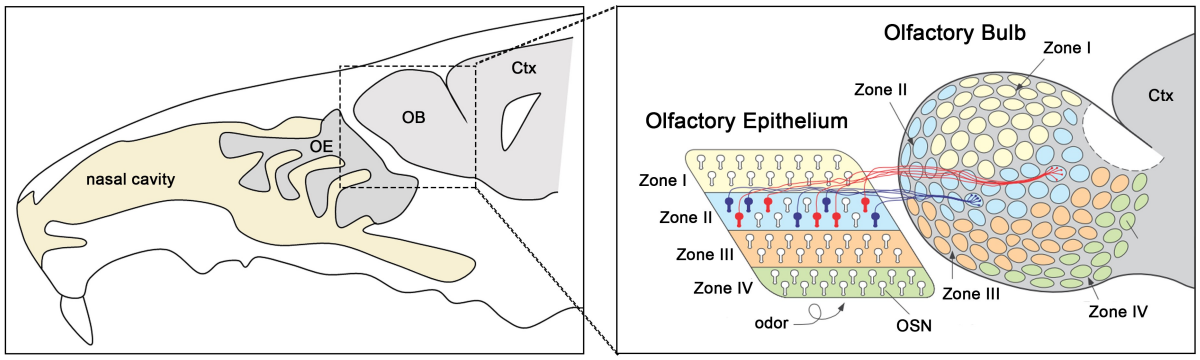

Figure 6. Schematic view of the topographic organization of OSN axons from the olfactory epithelium (OE) to the OB. **Left:** Macroscopic view of the nasal cavity, the OE and the brain. **Right:** Detailed view of axonal connectivity between OE and OB. OSN are divided into four zones depending on OR expression but different OSNs of a given zone are intermingled (blue and red) within the respective zone. OSNs of a given zone project to a topographically defined region within the OB. OSNs that express the same OR project into one glomerulus. OSN: olfactory sensory neurons; OB: olfactory bulb; Ctx: cortex. Illustration adapted from (Mori et al., 1999).

OSN activation leads to combinatorial patterns of activated glomeruli which are transformed by OB interneurons into M/T cell output for cortical and subcortical areas. This multistep

computation yields to an interpretation of OSN activation patterns which underlies the perception of smell and eventually produces behavior. Although behavioral output is species-specific, the organization of the olfactory pathway (from OR protein structure to OB wiring circuitry) is remarkably well preserved across species and even phyla (Ache and Young, 2005). This high degree of functional conservation indicates the exquisite accuracy and optimization of olfactory computation in odor discrimination. A property, even more fascinating when considering that there is a near-infinite source of input molecules (Imai et al., 2010).

4.2 The glomerulus: the functional unit that determines the odor map

The spectrum of odor response of a glomerulus is defined by the ligand-binding properties of the OR. An OR can respond to a range of molecules with different affinities. Subsequently, an odor is capable of activating different ORs with different efficacies (Mori et al., 1999; Araneda et al., 2000; Saito et al., 2009). Thus, the combination of activated glomeruli and the level of their activation carry the primary information about odorant identity (Wachowiak and Shipley, 2006). Another important principle in the organization of glomerular topology is the fact that glomeruli activated by structurally similar molecules are in close proximity and form clusters or domains within the glomerular map (**Fig. 6**) (Mori, 2006; Johnson and Leon, 2007; Matsumoto et al., 2010). However, clustering is rather loose and even in these domains, glomeruli can be activated by very dissimilar odorants (Rubin and Katz, 1999; Bozza et al., 2004; McGann et al., 2005).

Finally, glomerular activity maps do not only code for absolute odorant identity but also change in a concentration-dependent manner. Increased odorant concentration recruits more ORs and thus activates more glomeruli (Wachowiak and Cohen, 2001; Bozza et al., 2004; Wachowiak and Shipley, 2006). Often these additionally recruited “low affinity” glomeruli can be distributed widely across the OB (Wachowiak and Cohen, 2001). Interestingly though, significantly different glomerular odor maps caused by different concentrations, still result in a fairly stable M/T cell output, indicating that input-output transformations are put into place to convey stable odor identity (Storace and Cohen, 2017; but see also Economo et al., 2016).

4.3 Temporal dynamics of odorant input and output encode odor information

There is a considerable amount of evidence that supports the idea that not only spatial but also temporal encoding conveys odor information (reviewed in Nunez-Parra et al., 2014). There

are two sources of temporal dynamics in the OB: (1) OSN onset latency caused by receptor accessibility or ligand-receptor binding kinetics and (2) the respiration cycle of the animal.

Evidence for the first was observed in a study, using calcium-sensitive dyes in OSN terminals of anesthetized mice, which showed that different odorants evoke different temporal activation patterns in glomeruli with possible implications for odor coding (Spors et al., 2006; Wachowiak and Shipley, 2006). However, the strongest source of temporal modulation in glomerular dynamics is the sampling behavior itself (Spors and Grinvald, 2002; Spors et al., 2006).

The resting respiration cycle (3-5 Hz in mice) is the principal sensorimotor process that drives spontaneous activity within the OB circuit (Verhagen et al., 2007). In fact, it is mechanosensation of air-driven OSN inputs that evokes spontaneous M/T cell spiking. This is shown in CNGA2 mutants (cyclic nucleotide gated channel, a major compound of OSN signal transduction), where spontaneous respiration-coupled M/T cell activity is eliminated (Grosmaitre et al., 2007). Different M/T cells also show preference for spiking at a particular latency from inhalation onset, thus "tiling" the entire respiration (sniff) cycle (Shusterman et al., 2011; Fukunaga et al., 2012). M/T cells that innervate the same glomerulus (sister M/T cells) show similar latencies compared with M/T cells that innervate different glomeruli (Dhawale et al., 2010). Interestingly, TCs consistently fire earlier than MCs within the sniff cycle and while concentration-related changes induce firing rate modulation in TCs, MCs show a rate change but also a phase-advance (Fukunaga et al., 2012). Thus, the prevailing hypothesis states that the respiration/sniff cycle serves as a base for spike distributions and thus sets a limit to the time window for integrating odor information (Schaefer and Margrie, 2007; Nunez-Parra et al., 2014).

Changes in sniffing frequency, from respiratory frequency to investigative sampling (6-12 Hz in mice) can dramatically alter temporal patterns of OSN activation. Interestingly though, mere odor detection can be achieved within a single sniff only (Goldberg and Moulton, 1987; Uchida and Mainen, 2003; Wesson et al., 2008). However, later aspects of odor representations cause persistent responses of MCs and are related to behavioral responses (Doucette and Restrepo, 2008; Doucette et al., 2011; Patterson et al., 2013). This was further corroborated by a recent study that investigated different sniffing strategies and found that they robustly correlate with odor response changes in M/T cells in the behavioral context of learning (Jordan et al., 2018).

4.4 Postsynaptic processing by juxtaglomerular neurons

Spatially and temporally encoded odor input (generated by sniffing strategies as well as OSN properties and their wiring) is processed within the glomerulus to become a refined output pattern of M/T cells (**Fig. 7A**). As described earlier, the glomerulus is the initial site of synaptic integration where OSN axons meet processes of different classes of JGCs as well as the dendrites of M/T cells. "Monoglomerular" ETCs are the only source of local excitation. In turn, inhibition is conveyed by "monoglomerular" PGCs and "oligoglomerular" SACs which engage a wider network of a few surrounding glomeruli.

4.4.1 The role of local inhibition through PGCs and SACs

A number of transformation mechanisms within the OB have been attributed to inhibitory circuits: (1) pattern separation/decorrelation of odor representation (i.e. separation of the representation of stimuli that have overlapping features); (2) gain control (i.e. adjustment of the relationship between input and output due to changing environment); (3) filtering of weak inputs; (4) shaping the pattern of M/T cell response and synchronization of their activity (Economo et al., 2016). Of note, most data stems from slice experiments which in turn have inspired a whole domain of theoretical modeling in the field. To date, *in vivo* data clearly demonstrating these claims remain fragmentary.

PGCs display broader odor tuning (i.e. they are significantly less selective in odor responsiveness) than M/T cells *in vivo* (Tan et al., 2010; Wachowiak et al., 2013; Adam et al., 2014) and can mediate feedforward inhibition to the glomerular circuit (**Fig. 7B**) (Najac et al., 2011, 2015). Thus, PGCs could convey intraglomerular "self-inhibition" by preventing activation of glomeruli by weak inputs. This is one proposed mechanism to generate pattern separation and ultimately sharpen M/T tuning (Gire and Schoppa, 2009; Cleland, 2010; Tan et al., 2010). Indeed, *in vivo* data shows that interglomerular inhibition can successfully suppress excitatory MC responses (Economo et al., 2016) and pharmacological blocking of GABAergic transmission increases in strength of MC responses to "non-optimal" stimuli (Yokoi et al., 1995; Tan et al., 2010). Although these data represent evidence for pattern separation through selective glomerular inhibition, it remains to be defined whether the main actors in this process are PGCs, SACs or GCs.

SACs are the sparsest population among JGCs but can have a strong impact on glomerular output. Optogenetic activation of SACs results in suppression of spontaneous and odor-evoked M/T cell activity (Banerjee et al., 2015; Liu et al., 2016). Interestingly, the main target of SACS are ETCs (**Fig. 7B**) (Banerjee et al., 2015). Another interesting feature of SACs is

that their activity scales in a concentration-dependent manner. Diphtheria-toxin mediated ablation of DAT+ (dopamine transporter) SACs significantly altered concentration-dependent responses in MCs: M/T population responses became denser and more correlated across odors; In addition, M/T cell responses scaled with stimulus intensity and showed reduced onset latency (Banerjee et al., 2015). These data provide evidence that dopaminergic SACs mediate gain-control of concentration-dependent input but also pattern separation by sparsening M/T cell responses. Unfortunately, it is still unknown how or whether these two mechanisms relate to SAC morphology. SACs with widely distributed axons across the OB would likely promote gain control, while SACs which target specific subsets of glomeruli could rather mediate contrast enhancement (Cleland and Sethupathy, 2006; Burton, 2017).

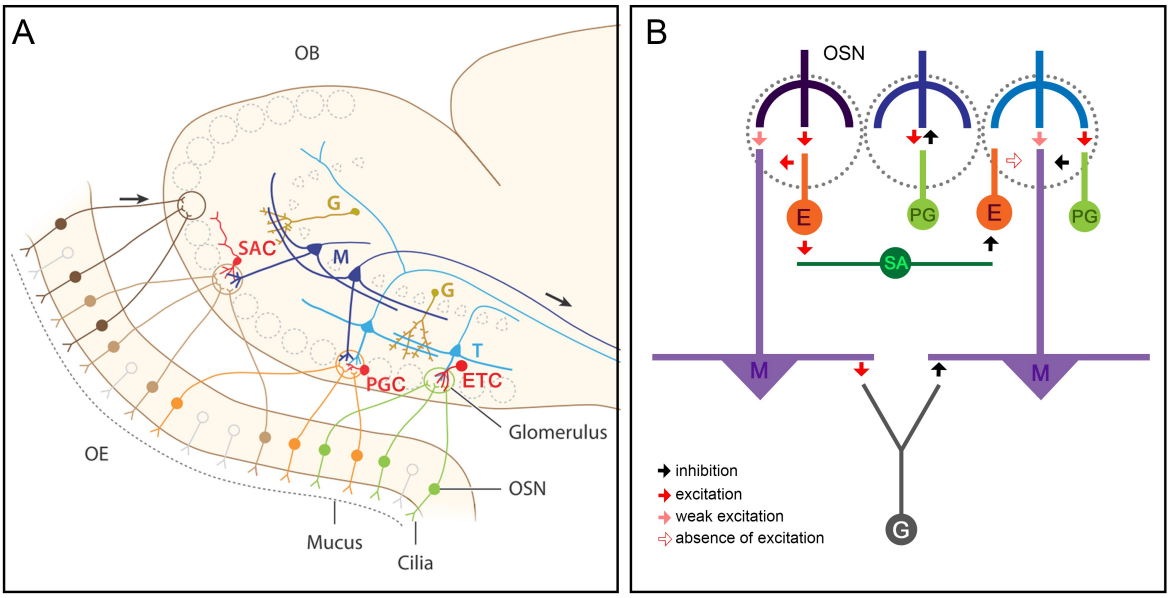

Figure 7. Schematic view of the olfactory pathway (A) and hypothetical model of olfactory processing within the glomerular layer (B). **(A)** OSNs project into defined glomeruli surrounded by different types of JGCs (SACs, PGCs and ETCs). Information is processed by JGCs and relayed to M/T cells. Granule cells (G) exert lateral inhibition onto M/T cells. OB output from M/T cells is relayed to cortical areas (not seen). OSN: olfactory sensory neuron; SAC: short axon cell; PGC: periglomerular cell; ETC: external tufted cell; M: mitral cell; T: tufted cell; OE: olfactory epithelium; OB: olfactory bulb. Illustration adapted from (Uchida et al., 2014). **(B)** Hypothetical and minimalist model of odor processing in the glomerular layer. OSN input is too weak (pink arrow) to directly excite mitral cells (M) but robustly activates ETCs (red arrow) which in turn excite M cells. ETCs can excite short axon cells (SA) which inhibit (black arrow) heterotypic ETCs. Due to the lack of ETC activation (hollow arrow), M cells of this glomerulus are not excited. Periglomerular cells (PG) can be excited by OSN input and can monosynaptically inhibit M cells but also exert presynaptic inhibition onto OSNs. G cells can be excited by M cells and inhibit heterotypic M cells (lateral inhibition). Illustration adapted from (Hayar et al., 2004).

4.4.1 The role of local excitation through ETCs

OSNs are monosynaptically connected to MCs (Najac et al., 2011; Gire et al., 2012; Bourne and Schoppa, 2017). However, slice experiments show that OSNs input evokes only weak or no MC spiking but reliable activates ETCs instead (**Fig. 7B**) (Hayar et al., 2004; Gire and Schoppa, 2009; Gire et al., 2012). In turn, MCs can be readily activated by ETCs (De Saint Jan et al., 2009; Najac et al., 2011; Gire et al., 2012). *In vivo* data is scarce but points to the same direction. Whole cell recordings in anesthetized mice showed that within the respiratory cycle ET/TCs consistently fired earlier than MCs and late onset of MC response was due to local inhibitory circuits (Fukunaga et al., 2012). Another indirect hint comes from the previously mentioned study that manipulated SACs using DAT-Cre and observed that upon optogenetic DAT+ cell activation, odor-evoked spiking in M/T cells was strongly suppressed despite a lack of a direct connection between DAT+ cells and M/T cells (Banerjee et al., 2015). Given that ETCs are the main target of DAT+ SACs, the authors infer that the observed effect was indirectly mediated by ETCs. Taken together, the data available on ETCs supports the idea that they could act as gatekeepers of odor signals. Furthermore, a central role of ETCs within the OB circuit is supported by a vast body of research which shows that OSNs are monosynaptically connected to only 30% of PGCs and 30% of SACs while the remaining 70% of both populations receive their input from ETCs (Kosaka et al., 1997, 2001, Toida et al., 1998, 2000; Hayar et al., 2004; Murphy et al., 2004, 2005, Kosaka and Kosaka, 2007a; b; Shao et al., 2009; Kiyokage et al., 2010; Burton, 2017).

To sum up, the current model supports the idea that MCs are activated by OSNs in a multistep process where ETCs provide a strong excitatory drive through feedforward excitation. Inhibition within the GL, mediated by PGCs and SACs, acts on but is also driven by excitatory ETCs (**Fig. 7B**). Ultimately, this intra- and interglomerular inhibition provides the basis of neuronal computations like gain-control and pattern separation which are necessary for meaningful M/T cell output.

However, direct proof for the role of ETCs in this model is still missing. To date, the only *in vivo* recordings of ETCs have been done on a subpopulation of inhibitory Vglut3+ which specifically synapse on TCs but not MCs (Tatti et al., 2014). Additionally, only in recent years did calcium-sensitive dyes become sensitive enough to reveal that not only excitation but also inhibition represents an important part of MC computations (Economo et al., 2016; Yamada et al., 2017). These conclusions open the following questions: (1) Do excitatory

ETCs generally respond to odors? (2) Could inhibition of ETCs determine MC inhibition? (3) Does MC activation require ETC activation *in vivo*?

4.5 Short- and midrange circuits established by ETCs

4.5.1 Intrabulbar circuits

In most vertebrate sensory systems there is clear sector-to-sector topographic representation of sensory stimuli through several orders of synaptic connections. Although not fully clear, topographic maps seem to represent an efficient manner to interconnect appropriate sets of neurons and thus facilitate spatiotemporal computation which is also related to perception (Kaas, 1997; Thivierge and Marcus, 2007). The olfactory bulb differs from other sensory systems insofar as there is a topographic organization from the olfactory epithelium to the OB, however, there is no such representation in bulbofugal projections to the olfactory cortex (Ghosh et al., 2011; Miyamichi et al., 2011; Sosulski et al., 2011). In fact, most M/T cells participate in broad interactions within and outside of the OB without any evident spatial organization. Interestingly, ETCs located at the GL/EPL border exhibit a highly topographic axonal projection pattern between opposed glomeruli along the medio-lateral axis of the OB (Macrides et al., 1985; Schoenfeld et al., 1985). This intrabulbar circuit is called intrabulbar associational system (IAS).

The IAS is a reciprocal network formed by ETCs immunoreactive for the neuropeptide CCK (Liu et al., 1994). They project medio-laterally across the OB and terminate in a narrow neuropil-rich layer between MCL and GCL, the inner plexiform layer (IPL). Within the IPL, ETC axons synapse with GCs located under the glomerulus activated by the same OR, the so-called mirror glomerulus (Liu et al., 1994; Belluscio et al., 2002). Experiments with genetically engineered mice where a ventrally expressed OR (rI7) was substituted into a dorsally expressed receptor locus (M71), showed that a functional IAS still forms, even if the glomerulus in question is situated in an ectopic location. This result suggests that this circuitry is instructed by the ORs themselves (Belluscio et al., 2002). Interestingly, the IAS is also present in anosmic OCNC1 (olfactory cyclic nucleotide-gated channel subunit 1, required for OSN signal transduction) knockout mice, suggesting that it is not sensory stimuli *per se* that drive its formation. However, without sensory input IAS projections remain broad and imprecise, resembling their immature state which indicates that IAS refinement is dependent on sensory activity (Marks et al., 2006). The IAS can be detected as early as P7 in mice (Marks et al., 2006). Because the IAS is topographic and reciprocal it is believed that its

function is to modulate glomerular output most likely through inhibition since ETCs synapse on GABAergic GCs. However, the functional consequence of the IAS is still unknown.

4.5.2 Interbulbar circuits

Additionally to the IAS, another topographically organized projection system between the two olfactory bulbs was discovered (Schoenfeld et al., 1984). Like the IAS, this system is supported by ETCs at the GL/EPL border. However, tracing experiments using double injections within and outside of the OB suggest that the intra- and interbulbar connections are not mediated by the same ETCs (Schoenfeld et al., 1985).

ETCs that participate in this circuit send their axons through the superficial GCL (just below the IPL) ventro-laterally until they reach a cortical area called the anterior olfactory nucleus (AON) (Schoenfeld et al., 1984). Although the AON was first termed nucleus (Herrick, 1924) it represents a laminated structure that contains pyramidal cells (Haberly and Price, 1978) and is thus considered a cortical structure. Within the AON, ETC axons terminate in a discrete architectonic subdivision, the *pars externa* (AONpE) where they synapse with neurons that exclusively project through the anterior commissure to the contralateral bulb (Schoenfeld et al., 1984; Scott et al., 1985; Reyher et al., 1988). These interbulbar projections connect isofunctional mirror glomeruli in a topographic manner (Schoenfeld et al., 1984).

The functional importance of this interbulbar connection has only recently been addressed. Using M71-GFP mice a study showed that upon odor stimulation of one nostril only, the contralateral isofunctional glomeruli could be specifically activated via the AONpE (Yan et al., 2008). Then, the authors asked whether the AONpE could also convey olfactory memory. Therefore, Yan et al. used an olfactory conditioning approach with one open and one closed (contralateral) nostril in mice with intact and lesioned AONpE. When examining the performance of the contralateral (reopened) OB, they found that mice could only remember the conditioning when the AONpE was intact. On the contrary, mice with lesions specific to the AONpE performed like naïve subjects. These series of intriguing experiments indicates that the interbulbar circuit is not only implicated in cross activation but also participates in conveying olfactory memories locally stored in each OB.

Another function of this circuit seems to be the spatial localization of odors. A study performing extracellular recordings in AONpE neurons, demonstrated that these neurons responded preferentially to stimuli presented ispilaterally and less to contralateral stimuli

(Kikuta et al., 2010). Thus, the interbulbar circuit could likely be implicated in the "stereo" perception of smell.

5. IMPACT OF SENSORY DEPRIVATION ON THE OB CIRCUITRY

The beauty of studying a sensory system lies in the fact of dealing with a brain area which is in direct contact with the outside world. Therefore, sensory systems are particularly suitable to investigate environmental effects and how they interact with the intrinsic programs of the brain circuitry. From an experimental point of view, sensory systems have drawn the attention of neuroanatomists from very early on because a few simple manipulations would allow to precisely control the interaction between the brain and its environment. This is how the paradigm of sensory deprivation was born, a powerful approach to study brain function, development and plasticity. Olfactory deprivation through unilateral naris occlusion has been first described by B. Gudden more than 100 years ago (Gudden, 1870) and has since been extensively studied. Accordingly, the basic phenomenology of naris occlusion is fairly well described.

Within a few weeks of occlusion, a drastic 25-30% volume decrease is observed in the occluded compared to non-occluded OB (Brunjes, 1994). Histological analysis shows that this decrease is due to reduction in all OB layers: glomeruli become smaller and the EPL and GCL are reduced (Frazier and Brunjes, 1988; Cummings and Belluscio, 2010). Analyses with thymidine analogs like [^{3}H]-thymidine or bromodeoxyuridine (BrdU) have shown that this drastic volume reduction is due to reduced cell survival in the OB and not decreased neurogenesis (Frazier-Cierpial and Brunjes, 1989; Saghatelyan et al., 2005). On a neurochemical level, a strong decrease of TH immunoreactivity becomes evident within one week of occlusion (Baker, 1990; Baker et al., 1993). Although, rarely addressed experimentally, these changes are assumed to be the direct result of stimulus deprivation. This assumption is supported by the fact that OMP- (olfactory marker protein, marks OSN fibers) positive fibers remain unchanged under occlusion, indicating that OSNs remain in place (Baker et al., 1993).

Indeed, deprivation-induced cell death in the OB has received much attention and many studies have investigated the effect on different OB subtypes. However, while the community agrees on the presence of deprivation-induced cell death across all OB layers (Najbauer and Leon, 1995; Mandairon et al., 2006), results for specific neuronal subtypes are not as clear-cut and sometimes contradictory. In particular, it has been claimed that TH neurons die (Bastien-

Dionne et al., 2010; Sawada et al., 2011; but see also Baker et al., 1990, 1993) while CalR neurons are not affected (Bastien-Dionne et al., 2010; Philpot et al., 1997; Sawada et al., 2011 but see also Kato et al., 2012) during occlusion.

However, these studies have all used very different and mostly indirect ways to study cell survival under occlusion (BrdU pulse-chase, histological markers but recently also *in vivo* imaging). In a recent study from our team we demonstrate that cell survival can only be reliably monitored by direct observation like *in vivo* imaging and that indirect observations are particularly error-prone in a system with ongoing neurogenesis like the OB (Platel et al., 2018, under revision, see **Appendix III**).

Finally, the effect on sensory deprivation in the OB has only been studied on GABAergic interneurons. Given the role of glutamatergic JGCs at the initial phase of sensory processing, it would be of great interest to know how these neurons are affected by sensory deprivation.

AIM OF THE STUDY

Although the olfactory bulb has been studied for decades, little knowledge is available about the specific roles of different neuronal subtypes. Being the only source of local excitation in the otherwise inhibitory interneuron network of the OB, there is considerable interest in studying glutamatergic JGCs. However, genetic markers that allow to specifically mark the whole population are still scarce and little explored. Therefore, one main focus of the current study was to find and establish a new tool to study glutamatergic JGCs in the OB. For this purpose, I chose the bHLH transcription factor NeuroD6 as a molecular entry point. Consequently, I dedicated a considerable amount of my thesis to characterize the expression pattern of NeuroD6 and to elucidate the function of NeuroD6 within the V-SVZ-RMS-OB system.

Once I established a tool that allowed me to specifically mark glutamatergic JGC, I set out to study the postnatal generation, morphology and connectivity, but also physiology of glutamatergic JGCs. Given the fact that glutamatergic JGCs are situated at the initial site of odor processing, I studied how their survival was affected by sensory deprivation using a chronic *in vivo* imaging approach. Lastly, I started to test some prevailing concepts about the role of glutamatergic JGCs in odorant processing using *in vivo* calcium imaging. Particularly, I addressed whether these cells were responsive to odors, how their activity was related to the glomerular network and whether they could act as signal gatekeepers.

RESULTS

1. Characterization of perinatally born glutamatergic interneurons of the mouse olfactory bulb based on NeuroD6 expression reveals their resistance to sensory deprivation

First part in from of submitted manuscript: Angelova et al., 2018, *Journal of Comparative Neurology*

Characterization of perinatally born glutamatergic interneurons of the mouse olfactory bulb based on NeuroD6 expression reveals their resistance to sensory deprivation

Running title: ND6 glutamatergic olfactory interneurons

Alexandra Angelova, Jean-Claude Platel, Christophe Béclin, Harold Cremer† and Nathalie Coré†

Aix Marseille Univ, CNRS UMR 7288, Developmental Biology Institute of Marseille (IBDM), Parc scientifique de Luminy, 13009, Marseille, France

HC and NC should be considered joint senior author

Correspondence to HC

Authors contributions

AA, JCP, HC and NC developed the concept and designed the experiments. AA acquired and analyzed the data with the help of JCP. CB designed, conducted and

analyzed the qRTPCR experiment. AA made the figures. AA, HC and NC wrote the manuscript.

Conflict of interest

The authors declare no sources of interest

Acknowledgements

We thank Sandra Goebbels and Markus Schwab for NeuroD6^{Cre} and NeuroD6^{CreERT2} animals, and Yuchio Yanagawa for Gad67^{GFP} mice. We are particularly grateful to the local PiCSL-FBI core facility (IBDM, AMU-Marseille) supported by the French National Research Agency through the « Investments for the Future" program (France-BioImaging, ANR-10-INBS-04) as well as the IBDM animal facilities. This work was supported by fellowships from the Biotrail program and the Fondation pour la Recherche Medicale (FRM) to A. Angelova. H. Cremer was supported by Agence National pour la Recherche (grant ANR- 13-BSV4-0013), Fondation pour la Recherche Médicale (FRM) grants ING20150532361 and FDT20160435597, Fondation de France (FDF) grant FDF70959 and the Association France Parkinson.

Abstract

During postnatal OB neurogenesis, predetermined stem cells residing in the ventricular-subventricular zone continuously generate progenitors that migrate in the rostral migratory stream and integrate into the OB. Although the vast majority of these postnatally generated interneurons are inhibitory, a sub-fraction represents glutamatergic interneurons that integrate into the superficial glomerular layer. In the present work we demonstrate that the bHLH transcription factor NeuroD6 is specifically and transitorily expressed in the dorsal neurogenic lineage that generates glutamatergic JGCs for the OB. Using lineage tracing combined with whole brain clearing, we provide new insight into timing of generation, morphology and connectivity of glutamatergic JGCs. Specifically, we show that all glutamatergic interneurons send complex axons with varying projection patterns into different layers

of the OB. Moreover, we find that, contrary to GABAergic OB interneurons, glutamatergic JGCs survive under sensory deprivation, indicating that inhibitory and excitatory populations are differentially susceptible to environmental stimulation.

Keywords

Post-natal neurogenesis, olfactory bulb, glutamatergic interneurons, NeuroD6 bHLH transcription factor, sensory deprivation, RRID_2749806RRID: AB_2068336, RRID:AB_2619904, RRID: AB_393778, RRID: AB_1587367, RRID: AB_828390, RRID: AB_2336063, RRID: AB_2200219, RRID: AB_778267, RRID: AB_10013440, RRID: AB_887877, RRID: AB_2187539, RRID: MGI:5308867, RRID: MGI:4429523, RRID: MGI:5510844, RRID: IMSR_JAX:007914, RRID: SCR_002285, RRID: SCR_007370, RRID: SCR_013672, RRID: SCR_001905

1 INTRODUCTION

Postnatal and adult stem cell populations lining the lateral ventricles permanently generate neuronal precursors that migrate into the olfactory bub where they integrate into the granule and glomerular layers. The vast majority of these postnatal- and adult-born interneurons are inhibitory, using GABA and in part additionally dopamine as their neurotransmitters (Parrish-Aungst et al., 2007). However, more recent work demonstrated that also excitatory glutamatergic interneurons are produced during postnatal and in some cases adult stages (Brill et al., 2009; Winpenny et al., 2011). In addition to such heterogeneity at the neurotransmitter level, OB neurons can be sub-grouped by the expression of specific markers like calretinin (CalR) or calbindin (CalB), their final position in the OB and their connectivity (Whitman and Greer, 2009; Weinandy et al., 2011; Fiorelli et al., 2015).

This diversity among OB interneurons reflects the regionalization of neural stem cell (NSC) pools around the lateral ventricle. Indeed, the position of NSCs in the ventricular-subventricular zone (V-SVZ) determines the above-described phenotypic features of the resulting interneurons (Merkle et al., 2007). For example, purely GABAergic granule neurons are generated from NSCs located in the lateral subventricular zone. In contrast CalB-positive neurons are derived from the ventro-

lateral progenitor domain, while CalR-positive and dopaminergic (TH+) juxtaglomerular cells (JGC) are generated in medial and dorsal domains of the ventricular wall (Fuentealba et al., 2015).

Over the past decades the generation, morphology and function of postnatal and adult born inhibitory OB interneurons have been extensively characterized (Whitman and Greer, 2007). However, while there is substantial data concerning the structure and physiology of OB excitatory JGCs in general (Aungst et al., 2003; Hayar et al., 2004a; Antal et al., 2006), information concerning specifically the postnatal- and adult-born fraction is far more fragmentary. Lineage analyses based on the expression of the transcription factor Neurogenin2 (Neurog2) (Winpenny et al., 2011) provided insight into the sequence of generation and basic morphology/connectivity of these cells. Indeed, they are generated from the dorsal wall of the lateral ventricles and integrate after their migration into juxtaglomerular positions of the OB. Two major classes of Neurog2-derived JGCs have been defined so far. First, external tufted cells that extend complex primary dendrites inside a single glomerulus. Second, neurons with more extended dendritic arborizations, that were categorized as short axon cells (Winpenny et al., 2011). However, timing of their generation and the respective proportion that these two sub-populations represent in the postnatal OB is not well characterized. Also, while glutamatergic interneurons in general have been shown to bear axons (Hayar et al., 2004a), specific information about the postnatally generated fraction is sparse.

A striking feature of the OB concerns its sensitivity to sensory deprivation, making it a model of choice to study the impact of experience in the generation, maintenance and renewal of brain circuitry. Indeed, a considerable number of studies, using naris closure as an experimental paradigm, demonstrated a size reduction of the OB associated with cell loss of defined subsets of OB inhibitory interneurons including the tyrosine hydroxylase (TH) expressing and the CalR and CalB positive subtypes (Bovetti et al., 2009; Bastien-Dionne et al., 2010; Parrish-Aungst et al., 2011; Sawada et al., 2011; Kato et al., 2012). Information about the behavior of glutamatergic OB interneurons under sensory deprivation is so far not available despite the key role of glutamatergic neurotransmission in olfactory processing.

We show here that the bHLH transcription factor NeuroD6 is specifically and transitorily expressed in the dorsal neurogenic lineage that generate glutamatergic

JGCs for the olfactory bulb. We find that ND6^{CreERT2} mice allow the analysis of this cell type at high temporal and spatial resolution. Using this tool, we further characterize the timing of their generation and combine it with 2-photon imaging of cleared brain to provide new insight of their morphology and connectivity. Finally, we combine ND6 lineage tracing with 2-photon in vivo imaging to demonstrate that glutamatergic OB interneurons, unlike the inhibitory populations, survive even under conditions of sensory deprivation.

2 MATERIALS AND METHODS

2.1 Animals

In this study, NeuroD6^{Cre} (ND6^{Cre}) knock-in mice(Goebbels et al., 2006), NeuroD6^{CreERT2} (ND6^{CreERT2}) knock-in mice (Agarwal et al., 2012), Rosa26^{tdTomato} reporter mice (Ai14, Jackson Laboratories, RRID: IMSR_JAX:007914) and GAD67^{GFP} knock-in mice (Tamamaki et al., 2003) (RRID: MGI:5510844), of both sexes were used. Mouse lines were kept on a pure C57BL/6 genetic background unless they were crossed to Rosa26^{tdTomato} reporter mice, which were maintained on an outbred CD 1 (Charles-River, Lyon, France) background. Mice were kept on a 12h day/night cycle and had access to food and water *ad libidum*. All animal experiments were carried out in accordance to the European Communities Council Directive 2010/63/EU and approved by French ethical committees (Comité d'Ethique pour l'expérimentation animale n°14; permission numbers: 00967.03; 2017112111116881v2).

2.2 Tamoxifen induction of Cre-mediated recombination

For induction of Cre mouse lines, tamoxifen (TAM, T5648-1G, SIGMA) was injected subcutaneously for pups and intraperitoneally for juvenile and adult mice, respectively, at a dose of 100 mg/kg. Typically, neonatal (P0-P6) ND6^{CreERT2} mice were injected for 2 days with one subcutaneous TAM injection/day. ND6^{CreERT2} mice at P15 and P45 were injected 3 and 5 times with TAM respectively, using 1 injection/day.

For intraventricular injection, the metabolically active component (Z)-4-Hydroxytamoxifen (4OH-TAM) was used. 4OH-TAM powder (H7904, SIGMA) was

dissolved in 96% EtOH to obtain a 20 mM stock solution. Typically, 2 µl of 500µM 4OH-TAM in sterile PBS were injected into neonatal (P0 or P1) ND6^{CreERT2} mice.

2.3 Postnatal electroporation

Postnatal electroporation was performed as described previously (Boutin et al., 2008). The pCAG-Cre and pCAG-EGFP plasmids (Morin et al., 2007) were purified using NucleoBond Xtra Maxiprep DNA extraction kit (Macherey-Nagel) following the manufacturer's protocol and resuspended in sterile PBS. Briefly, neonatal pups (P0-P1) were anesthetized by hypothermia. Approximately 2 µl of 5 µg/µl plasmid DNA combined with 0.1% Fast Green were injected into the lateral ventricle by expiratory pressure using an aspirator tube assembly (Drummond) connected to a pulled glass capillary (30-0057, Harvard Apparatus). For electroporation, injected pups were subjected to 5x 95 V electrical pulses (50 ms, separated by 950 ms intervals) using an CUY21 edit device (Nepagene, Chiba, Japan) and 10 mm tweezer electrodes (CUY650P10, Nepagene) coated with conductive gel (Control Graphique Medical, France). Orientation of the electrodes determined whether the dorsal or lateral portion of the V-SVZ (ventricular-subventricular zone) was transfected. Pups were then reanimated in a 37°C incubator before returned to the mother.

2.4 Quantitative real-time PCR (qRT-PCR)

RNA extraction was performed using RNeasy Mini Kit (Qiagen) following the manufacturer's protocol. cDNAs were produced using Superscript III Reverse Transcriptase (Thermo Fisher Scientific). QPCRs were performed on a Bio-Rad CFX system using SYBR-GreenER qPCR Super-Mix (Thermo Fisher Scientific), with □-actin as a reference gene. Primers used for mRNA detection were: β-actin-FOR_CTAAGGCCAACCGTGAAAAG and β-actin-REV_ACCAGAGGCATACAGGGACA ; ND6-FOR_GTTGATGCATGAATGCTGGT and ND6-REV_GTGACATTGATGCCAACTGC.

2.5 Primary antibody characterization

The anti-Ankyrin G antibody is used to label axonal initial segment (AIS) of neurons. This antibody specifically stains AIS of neurons in the mouse olfactory bulb similarly as it was described in a previous study (Kosaka and Kosaka, 2011).

With the anti-calretinin and anti-calbindin antibodies, we stained two specific sub-populations of mature neurons within the glomerular layer of the olfactory bulb with a similar pattern as obtained in previous studies (de Chevigny et al., 2012; Tiveron et al., 2017).

The anti-Ki67 antibody recognizes a nuclear antigen exclusively expressed in proliferating cells. We observed extensive nuclear staining in the ventricular-subventricular zone of the forebrain where proliferating progenitors reside. The antibody stained very few cells in brain area such as the corpus callosum or the olfactory bulb where few cells are supposed to divide.

The anti-Pax6 antibody labeled the nucleus of progenitor cells expressing the transcription factor Pax6 within the ventricular zone from the dorsal aspect of the lateral ventricle. This pattern is similar as it was observed in previous studies (de Chevigny et al., 2012a; b).

The anti-RFP antibodies were used to amplify the signal emitted by tdTomato fluorescent protein, derivative of DsRed. This antibody only labeled cells that were recombined in the forebrain of ND6-Cre mice, with a similar pattern that was described for these mice (Goebbels et al., 2006; Agarwal et al., 2012).

The anti-Tbr1 and anti-Tbr2 antibodies specifically stained the nucleus of mature neurons expressing the transcription factors Tbr1 and Tbr2, in the glomerular layer of the olfactory bulb and progenitor cells in the subventricular zone from the dorsal aspect of the lateral ventricle, similarly as it was obtained in previous studies (Brill et al., 2009; Winpenny et al., 2011).

The anti-TH antibody recognized the tyrosine hydroxylase which is specifically expressed in dopaminergic neurons. This antibody stained a sub-population of mature neurons in the glomerular layer of the olfactory bulb in a pattern similar that has been observed in previous studies (de Chevigny et al., 2012; Qin et al., 2017; Tiveron et al., 2017).

The anti-Vglut1 and anti-Vglut2 antibodies recognized vesicular glutamate transporters and revealed the nerve terminals of glutamatergic neurons in the olfactory bulb. We observed punctate staining in all layers where glutamatergic neurons project, including the mitral cell layer, the external plexiform layer and the glomerular layer. These staining were similarly obtained in previous works (Brill et al., 2009; Winpenny et al., 2011; Roybon et al., 2015).

2.6 Immunohistochemistry

For histological analysis, mice were intracardially perfused with 4% paraformaldehyde (PFA) using a peristaltic pump. Brains were subsequently dissected and postfixed in 4% PFA overnight at 4°C. The next day, brains were either subjected to cryoprotection in 30% sucrose or placed in PBS azide 0.01% for long term storage at 4°C. Typically, brains were sectioned in 50 µm slices using a microtome (Microm, HM 450).

Standard immunostaining protocols were used, unless stated otherwise. Briefly, coronal free floating sections were rinsed in PBS and, if necessary, antigen retrieval was performed using a sodium citrate buffer (10 mM sodim citrate, 0.05% Tween20, pH 6.0) for 20 min at 90°C. Then, brain sections were incubated in blocking buffer (10% fetal bovine serum (FBS), 0.3% Triton X-100 in PBS) for one hour. Subsequently, sections were incubated in primary antibody solution (5% FBS, 0.1% Triton X-100 in PBS (PBST) and primary antibody) overnight at 4°C. The following day, sections were rinsed 3 times in PBS and incubated with species-appropriate secondary antibody in PBST for 2h at RT using gentle rocking. Alexa Fluor-conjugated secondary antibodies were from Jackson ImmunoResearch. Nuclear counterstain HOECHST (Invitrogen, 1:2000) was added before sections were washed in PBS and mounted on glass slides using Mowiol as a mounting medium.
Images were acquired with laser scanning confocal microscopes (LSM780 or LSM880, Zeiss, Germany) using Plan-Apochromat 20x/0.8 NA and oil-immersion Plan-Apochromat 40x/1.4 NA objectives. Images were acquired with Zen software (Zeiss, RRID: SCR_013672) and processing was performed using Fiji software (RRID: SCR_002285,(Schindelin et al., 2012)).

2.7 Tissue clearing and Lightsheet microscopy

For whole brain clearing the advanced Cubic protocol (Susaki et al., 2015) was used. Briefly, brains were incubated in Cubic1 solution (250g/L Urea, 250g/L Quadrol, 150g/L Triton X-100) until they appeared transparent. For neonatal brains this was typically 2-3 days while adult brains incubated for 7-10 days. For subsequent immunostaining, brains were washed in PBS for 1-2h and incubated in blocking solution (5% FBS, 0.1% Triton X-100, 0.1% Tween-20 and 0.01% sodium azide, in PBS) for 1 day. Then, brains were submerged in 2.5 ml blocking solution containing the primary antibody for 4 days. Antibody concentration was sometimes doubled as compared to classical immunostaining protocols to obtain a better signal-to-noise

ratio. The samples were then washed 2-3 times for one day with washing solution (0.01% Tween-20, 0.01% sodium azide, in PBS) and subsequently incubated for 3 days in 2.5 ml washing solution containing the Alexa Fluor-conjugated secondary antibodies and TOPRO-3 (1/1000) nuclear stain. Finally, the samples were washed again and incubated in Cubic1 for 2h, then in Cubic2 (25g/L Urea, 50g/L sucrose, 10g/L Triethanolamine) for 1-2 days before imaging. All procedures were performed in a water bath at 37°C under gentle agitation.

Whole tissue 3-D images were acquired using a Lightsheet Z.1 microscope (Zeiss, Germany) equipped with a 5x/0.16 NA objective (RI 1.45). The sample was glued caudally to the sample holder which was subsequently submerged in a chamber containing Cubic2 solution. Images were processed using ImageJ (NIH, https://imagej.nih.gov/ij/, RRID: SCR_003070) and Imaris (Bitplane, Zurich, Switzerland, RRID: SCR_007370) softwares.

For reconstruction of axonal processes, neonatal ND6$^{CreERT2/tdTom}$ mice were induced by intraventricular injection of 4OH-TAM to obtain very sparse labeling which allowed for following single processes. Mice were sacrificed at 6 wpi (weeks post induction) and brains subjected to the Cubic tissue clearing protocol, with the difference that brains were imaged in Cubic1 instead of Cubic2 solution. Therefore, the incubation step with Cubic2 was skipped. Images were acquired with a 7MP two-photon microscope (Zeiss, Germany) using a 20x/1.0 NA objective. Neurons were traced using Simple Neurite Tracer plugin of ImageJ (NIH). Reconstructions were represented using NeuTube (Feng et al., 2015) software.

2.8 Stereotaxic injection and retrograde tracing

For retrograde tracing of axonal processes, 6 weeks old ND6$^{Cre/tdTom}$ mice were anesthetized with intra-peritoneal injection (i.p.) of ketamine/xylazine (125 and 12.5 mg/kg, respectively). Before surgery started, mice received subcutaneous injections of Carprofen (5 mg/kg), Dexamethasone (0.2 mg/kg) and Buprenorphine (0.3 mg/kg). Mice were placed in a stereotaxic apparatus (Harvard Apparatus); the skin over both OBs was incised with a scalpel and gently moved aside for better access to the skull. Injection point was identified (AP: +5 mm, ML: +1.1 mm, DV: 200-300µm) using Bregma coordinates and a small hole was drilled into the skull to allow subsequent injection. Mice received 500 nl of 2 mg/ml CTB (cholera toxin subunit B, Thermo

Fisher Scientific) conjugated with Alexa Fluor 488 using a Hamilton syringe. One week after CTB injections, mice were intracardially perfused with 4% PFA.

2.9 Thinned skull technique for chronic in vivo observation of neuronal survival

To visualize glutamatergic OB neurons and follow their survival, neonatal ND6$^{CreERT2/tdTom}$ mice were given two subcutaneous TAM injections (one injection per day). To visualize GABAergic neurons, pCAG-Cre plasmid was dorsally electroporated into neonatal Rosa26^{tdTom} mice. Mice were subjected to surgery when 4 weeks old. The thinned-skull technique (Yang et al., 2010; Shih et al., 2012) was used to allow in vivo observation of neuronal populations over time. Briefly, mice were anesthetized with ketamine/xylazine. Additional subcutaneous injections of Carprofen (5 mg/kg), Dexamethasone (0.2 mg/kg) and Buprenorphine (0.3 mg/kg) were performed before surgery. Skin over both OBs was incised with a surgical scalpel blade and gently pushed aside to expose the skull. Surface of the skull was scrubbed with the scalpel and cleaned with 10% citric acid to ensure adhesion. A custom-made metal bar was then fixed caudally to the OBs using first superglue and then dental cement (Super-Bond C&B). Subsequently, the mouse was attached to a stereotaxic apparatus, using the metal bar. The skull was then gently thinned using a surgical scalpel blade until a thickness of approximately 15 µm was reached over the desired area. During this procedure great care was taken not to exert excessive pressure and to avoid bleeding or drying of the skull. Once the desired thickness was reached, a 3 mm cover slip was placed with the aid of a drop of superglue over the thinned area and sealed with dental cement. The preparation was left to dry for 1-2 min before imaging. If desired, unilateral nasal occlusion was performed (see section for details). Fluorescently labeled neurons of alive mice were then imaged with a 7MP two-photon microscope (Zeiss, Germany) using a water-immersion 20x/1.0 NA objective. Images were acquired at 970 nm wavelength with a XY resolution of 0.6 µm, Z step of 3 µm. Images were analyzed and processed with ImageJ (NIH) software.

2.10 Unilateral nasal occlusion

For olfactory deprivation, mice were subjected to unilateral nasal occlusion (UNO) as previously described (Cummings et al., 1997). UNO was performed on the right OB. Briefly mice were anesthetized with ketamine/xylazine. Then, 2% lidocaine was

applied locally onto the nostril. A polyethylene tubing (BD Intramedic, PE50) that was previously sealed with superglue was inserted in the nostril using Vaseline to facilitate the insertion. If necessary, an additional drop of superglue was applied on the outside to seal the nostril completely. UNO was verified weekly. Only animals with successful UNO were analyzed. UNO was maintained for 4 weeks.

2.11 Statistical analysis

Statistical analyses were performed using R software (RRID: SCR_001905) and R Commander Package (https://CRAN.R-project.org/package=Rcmdr). Data are presented as mean ± SEM. Two tailed Mann Whitney U test was performed for Figure 6 and Figure 7. Probability assignment: $p > 0.05$ (not significant, ns), $0.01 < p < 0.05$ (*), $0.001 < p < 0.01$ (**) and $p < 0.001$ (***).

3 RESULTS

3.1 ND6 is specific to the glutamatergic lineage in the OB

In order to identify molecular markers and determinants of OB neurons we expressed GFP in the dorsal and lateral stem cell pools surrounding the lateral ventricles using targeted in vivo electroporation (Boutin et al., 2008). Subsequent microdissection and Fluorescent Activated Cell Sorting of labelled cohorts at different time points post-electroporation was followed by microarray analysis. This approach led to a high resolution picture of gene expression in the two lineages (Tiveron et al., 2017). Investigation of differentially expressed genes between both lineages showed that the bHLH transcription factor NeuroD6 (ND6) was strongly induced in the dorsal lineage between 1 and 4 days post electroporation (dpe) but absent from lateral isolates (Fig. 1A). We validated this expression for postnatal stages by qRT-PCR of micro-dissected dorsal or lateral V-SVZ as well as OB tissue. ND6 expression was undetectable when adult tissues were used (Fig. 1B).

We aimed at characterizing the expression of ND6 in more spatial and temporal detail. In the absence of reliable antibodies against the transcription factor we used constitutive $ND6^{Cre}$ (Goebbels et al., 2006) and inducible $ND6^{CreERT2}$ mice ((Agarwal et al., 2012); Schemes in Fig. 1C) bred to a Cre-inducible $Rosa26^{tdTomato(tdTom)}$ reporter line (Madisen et al., 2010). In a constitutive $ND6^{Cre}$

background at P1, strong tdTom expression was observed in callosal axons, in agreement with the early expression of the TF in cortico-cortical projection neurons (Fig. 1D; (Goebbels et al., 2006)). Moreover, axon bundles in the striatum (Fig. 1D, arrow heads), likely representing cortico-striatal connections, as well as individual cells in the septal region were tdTom positive. ND6 was generally absent from V-SVZ surrounding the lateral ventricles, except for a sparse cell population located in the dorsal aspect (Fig. 1D'). In the OB of ND6$^{Cre/tdTom}$ mice at P21 (Fig. 1E), mitral and tufted cells were tdTom+, in agreement with previous observations (Goebbels et al., 2006). In addition, juxtaglomerular cells (JGCs) in the glomerular layer (GL) were labelled with tdTom. Quantification of these neurons demonstrated that ND6-derived cells represented 17.95% ± 2.34% among all cells (n=3, 885 cells) within the GL.

Then we aimed at identifying the neurotransmitter phenotype of these ND6-derived JGCs. In ND6$^{Cre/tdTom}$ mice at P21, tdTom+ neurons never co-expressed GFP in a GAD67^{GFP} transgenic background nor were immunopositive for GAD65 staining (Fig. 2A, B) indicating that they are not GABAergic. There was also no overlap with markers for specific GABAergic subtypes like calretinin (CalR) or calbindin (CalB, Fig. 2C, D). Moreover, ND6 lineage cells also never expressed tyrosine hydroxylase (TH, Fig. 2E), indicating that they are not dopaminergic.

Next we used markers for glutamatergic neurons. In a constitutive ND6$^{Cre/tdTom}$ background 4.9% ± 1.3% of JGCs at P21 expressed Tbr1 (n=3, 225 cells) and 71.3% ± 6.9% were Tbr2 positive (n=3, 386 cells, Fig. 2F, G, J). Moreover, the vesicular glutamate transporters Vglut1 and Vglut2 were expressed in 66.7% ± 2.9 and 42% ± 6.5% of tdTom+ JGCs, respectively (n=3, 108 and 146 cells, Fig. 2H, I, J). When exclusively perinatally born tdTom+ neurons were analyzed in ND6$^{CreERT2/tdTom}$ mice induced at P0, significantly more neurons were Tbr1 and Tbr2 positive (Tbr1 26.8% ± 8.2%, n=3, 194 cells; Tbr2 98.8% ± 1.2%, n=3, 195 cells) and the ratio of Vglut1 to Vglut2 positive cells was inverted (Vglut1 37.3% ± 1.8% and Vglut2 63% ± 2.9%, n=3, 241 and 123 cells, respectively) (Fig. 2J). Thus, ND6^{Cre} labels embryonically and perinatally born glutamatergic neurons of the olfactory bulb.

To specifically analyze the generation and properties of perinatally born glutamatergic OB neurons, we used inducible ND6$^{CreERT2/tdTom}$ mice. When mice were injected with tamoxifen at P1 and analyzed 1 day post induction (dpi), most of the corpus callosum, striatum and septum were devoid of tdTom staining (Fig. 1F), thus facilitating the identification of individual tdTom+ cells. However, a small cell

population located in the dorsal V-SVZ strongly expressed tdTom (Fig. 1F'), comparable to the label in constitutive ND6^{Cre} mice (Fig. 1D, D'). Immunostaining experiments revealed that all ND6-expressing V-SVZ cells co-expressed Tbr1 confirming that ND6 is specifically expressed in glutamatergic precursors (Fig. 3A). However, ND6-tdTom+ V-SVZ cells never expressed the early marker Pax6 and were very rarely positive for Ki67+ (0.5 ± 0.4%), showing that ND6 is confined to post-mitotic precursors (Fig.3B).

In the OB, at 21 dpi, most mitral and tufted cells were tdTom-negative after induction (Fig. 1G), indicating that ND6 is no longer expressed in these cells after birth. This result is also in agreement with the embryonic origin of OB projection neurons. In contrast, JGCs within the glomerular layer were tdTom+, like in constitutive ND6$^{Cre/tdTom}$ mice (Fig. 1G).

Next we investigated the dynamics and potential lineage relation of the postnatal ND6 expressing populations in the dorsal V-SVZ, the RMS and the OB. To this aim we induced ND6$^{CreERT2/tdTom}$ mice with tamoxifen at P0 and analyzed the tdTom+ cell pool at 1, 7 and 21 dpi at different rostro-caudal levels within the forebrain (Fig. 4A). Induction at P0 and analysis at 1 dpi led to the detection of labelled cells in the dorsal V-SVZ (Fig. 4B, see also Fig. 1F), in dorsal aspects of the developing RMS as well as in the center of the OB (Fig. 4B). Moreover, individual radial oriented cells in the GCL showed tdTom expression (Fig. 4B, arrow head). These cells had generally the spindle like morphology of migratory neurons. At 7 dpi the thinning dorsal V-SVZ was devoid of tdTom positive cells and fluorescent cells in the mid-RMS were observed only sporadically (Fig. 4B). However, many cells were still found in the rostral RMS, within the OB, and in the GCL. At this time point cells with neuronal morphology appeared in the peripheral layers of the OB, the mitral cell layer, the EPL and the GL. When P0 induced brains were analyzed at 21 dpi, the V-SVZ, the RMS and the GCL were devoid of tdTom positive cells, while many cells with mature neuronal morphology were now observed in the peripheral layers of the OB (Fig. 4B). We interpret that ND6 is expressed in lineage related progenitors and migratory neuroblasts in the V-SVZ and RMS that eventually settle in the GL.

Altogether the combined use of gene expression analyses and Cre-loxP based lineage tracing leads to the conclusion that NeuroD6 is specifically but transitorily expressed in a subpopulation of perinatally generated neuronal precursors that

migrate from the dorsal aspect of the V-SVZ to peripheral layers of the OB to differentiate into glutamatergic interneurons.

3.2 Glutamatergic OB neurons are generated early after birth

Morphological characterization of labeled JGCs in ND6$^{CreERT2/tdTom}$ mice 21 days after induction at P0 identified three main categories. First, external tufted cells (ETCs) that extend complex branched dendrite trees into a single glomerulus. Second, external bi-tufted cells (biETCs), residing within the GL and sending branched dendrites into two or more glomeruli. Third, ETCs that in addition to their complex primary tuft, extend a sparsely branched secondary dendrite into the EPL (Fig. 5A). Rarely, we also observed cells found in juxtaglomerular positions that extend sparsely branched dendrites into the interglomerular space resembling short axon cells (SACs, Fig. 5C) as well as some small-soma sized cells that reside in the MCL. This classification was in general agreement with previous works (Macrides and Schneider, 1982; Hayar et al., 2004a; Brill et al., 2009; Winpenny et al., 2011).

To gain insight into the temporal generation dynamics of these postnatal generated types we induced Cre expression from the NeuroD6 locus by tamoxifen injection at different time points and analyzed the morphology of the induced cohorts 21 days later, after their arrival and integration in the OB (Fig. 5B). When induced at P0, we typically observed about 7 fluorescent neurons per glomerulus. Over all analyzed glomeruli this population consisted of about 61% ETCs, 9% biETCs, 26% secETCs and 4% SACs (Fig. 5C, D). After induction at P6, generation of ETCs dropped relative to the other cell types leading to a relatively even distribution of the cell types. After induction at P15, production of all three subtypes decreased considerably (Fig. 5C, D) and secETC processes in the EPL became most prominent (Fig. 5D, arrow head). After induction at P45 only very few cells (9 cells in 4 animals) with lateral dendrites that extend into the EPL were identified (Fig. 5D), showing that the adult generation of glutamatergic OB cells represents a rare exception.

3.3 Glutamatergic JGCs project axons across the OB.

Perinatally generated ND6-derived JGCs displayed along with their dendritic trees also thin axon-like processes (arrows in Fig. 5A). Using the axonal initial segment marker Ankyrin G, we doubtlessly confirmed axonal identity (Fig. 6A). Indeed, all ND6-derived neurons had axons. Next, we aimed at describing the axonal projection

pattern of the different perinatally generated glutamatergic cell populations in detail. To this end, we performed intraventricular Hydroxytamoxifen (4OH-TAM) injection in P0 ND6$^{CreERT2/tdTom}$ mice. This approach allowed the local recombination of glutamatergic progenitors lining the lateral ventricle in the absence of contaminating centrifugal cortical projections into the OB. Animals were perfused 6 weeks post induction (wpi) when neurons had fully integrated into their target layer within the OB. As complex axons can hardly be observed in standard tissue sections, we performed tissue clearing of entire brains using the CUBIC protocol (Susaki et al., 2015) and imaged transparent brains with 2-photon microscopy (for experimental setup see Fig. 6B). Tracing of axons of individual external tufted and bi-tufted neurons revealed the existence of two distinguishable subgroups based on their projection pattern (Fig. 6C). First, we observed type-1 axonal projections of ETCs and biETCs that extend only within superficial layers (GL and EPL). These represent 57% and 80% of the total population, respectively (Fig. 6E, n=3, 38 cells traced). Second, type-2 projecting ETCs and biETCs, in addition to superficial axons, send projections into the deep layers including the GCL (43% and 20%, respectively; Fig. 6C, E). Type-1 axonal projections cover a significantly wider array of glomeruli than type-2 axons (Fig. 6D). Finally, secETCs always had deep (type-2) projections that branched extensively in the IPL and GCL (n=3, 4 cells, Fig. 6C, E).

Then, we aimed at investigating the projection site of the axonal processes of glutamatergic JGCs. However, despite the use of clearing protocols and 2-photon microscopy, tracing of individual tdTom positive axons was limited due to high density of axons within the GCL. Therefore, we performed a retrograde labelling approach. The retrograde tracer cholera toxin subunit B (CTB) was locally injected into the lateral aspect of the OB of 6 weeks old ND6$^{Cre/tdTom}$ animals (n=3, Fig. 6F). One week later CTB/tdTom double positive cells were systematically found in proximity of the injection side, indicating the presence of type-1 JGCs with superficially branching axons (Fig. 6F''). In addition, double positive cells (approximately 60 cells per animal within a Z-depth of 150 µm) were identified within the GL opposite to the injection site, i.e. on the medial aspect of the ipsilateral OB (Fig. 6F'). We conclude that glutamatergic JGCs project complex axonal projections, often over considerable distances, throughout the OB.

3.4 Glutamatergic JGCs survive sensory deprivation

Several studies demonstrated sensitivity of GABAergic and dopaminergic JGCs to environmental stimuli (Baker, 1990; Mandairon et al., 2003; Sawada et al., 2011; Kato et al., 2012). Indeed, sensory deprivation by naris closure leads to extensive neuronal death among neonatal and adult born inhibitory interneurons of the OB GCL and GL. Excitatory interneurons have not been studied in this context. We used chronic in vivo brain imaging of ND6$^{CreERT2/tdTom}$ mice to study the long-term survival of glutamatergic JGCs under normal conditions and under sensory deprivation. To induce a control cohort of mostly GABAergic JGCs, for which deprivation-sensitivity has been demonstrated, we performed postnatal (P0) electroporation of a Cre expressing DNA plasmid into the dorsal ventricular wall of Rosa26^{tdTomato} mice. This approach labelled a mixed population of GABAergic and GABA/dopaminergic JGCs but only scarcely glutamatergic JGCs (Tiveron et al., 2017). In parallel, we induced postnatally born cohorts of tdTom expressing glutamatergic JGCs by TAM injection in ND6$^{CreERT2/tdTom}$ mice at P0. Four weeks after induction or electroporation, thin-skull surgery (Yang et al., 2010; Shih et al., 2012) was performed above the relevant OB. A field of view containing large amounts of fluorescent neurons was chosen and a volume of 600 x 600 µm in XY and 200 µm in Z was imaged at high resolution with a 2-photon microscope (Fig. 7A). Regular imaging over 4 weeks allowed the in vivo observation of neurons under both labelling schemes at high resolution (Fig. 7B). Neurons were individually identified, numbered and revisited several times (Fig. 7B-D). These data demonstrated that under normal conditions cells labeled by both CRE induction protocols, postnatal dorsal electroporation or injection of ND6$^{CreERT2/tdTom}$ mice, were extremely stable over time and neuronal loss was quasi absent (Fig. 7B-E).

Next, we performed the same labelling approaches, but combined with unilateral naris occlusion to cause sensory deprivation (Fig. 7F for experimental setup). As previously reported (Sawada et al., 2011), the occluded OB side significantly shrunk (Fig. 7G) and lost a considerable amount of TH immunoreactivity as a consequence of successful naris occlusion (Fig. 7H). GABA- and dopaminergic JGCs labelled by dorsal electroporation showed a significant cell loss of 13% (279 cells in 6 animals, Fig. 7I, J, L). In contrast, among the 403 glutamatergic JGCs followed over the 4 weeks deprivation period, only 13 cells were not clearly identifiable in subsequent imaging sessions and therefore labelled as “dead”. Thus

survival of glutamatergic neurons was unaffected as compared to the control condition (Fig. 7K, L).

Thus, while a considerable sub-fraction of perinatally born GABA- and dopaminergic JGCs are sensitive to sensory deprivation, perinatally born glutamatergic JGCs are resistant and survive even in the absence of environmental stimulation.

4 DISCUSSION

In the present study we show that the bHLH transcription factor NeuroD6 represents a novel and reliable marker for glutamatergic neurons in the OB. We therefore exploited $ND6^{Cre}$ and $ND6^{CreERT2}$ mice as genetic tools to study this elusive cell population. We found that ND6 expression in the V-SVZ-RMS-OB system is transient and confined to immature progenitors. Induction of $ND6^{CreERT2}$ labels therefore a well-defined and timed cohort. Next we demonstrated that glutamatergic JGCs are not only heterogeneous in dendritic arborization but also in axonal projection patterns. Lastly, we showed that other than inhibitory JGCs, glutamatergic JGCs resist sensory deprivation.

4.1 ND6 expression is transient and confined to glutamatergic OB progenitors

ND6 expression has been described for a multitude of brain areas including the neocortex, hippocampus, as well as some mid- and hindbrain structures (Goebbels et al., 2006). Interestingly, while studies that have investigated ND6 expression in detail agree upon the fact that promoter activity starts at the level of postmitotic progenitors, expression maintenance varies greatly according to brain area and possibly protein function (Wu et al., 2005; Goebbels et al., 2006; Kay et al., 2011). Using a battery of markers in the V-SVZ we found no colocalization of tdTom with the stem cell marker Pax6, rare co-localization with intermediate progenitor marker Ki67, and full overlap with postmitotic marker Tbr1. This indicates that also in the postnatal V-SVZ, ND6 is expressed in postmitotic progenitors (Brill et al., 2009). These results are further corroborated by our observations from lineage tracing experiments with $ND6^{CreERT2/tdTom}$ mice where we obtain a defined cohort of recombined neurons after induction. Moreover, the lack of recombined cells within the VZ with radial glia-like or

ependymal cell morphology argues against the possibility that ND6 is expressed in RGCs at their last round of division before becoming ependymal cells. Finally, the absence of fluorescent neurons within the GL at 1 dpi indicates that ND6 promoter is not active once neuroblasts reached their target layer. Altogether, these data show that ND6 is transiently expressed starting from postmitotic progenitors and stopping before final neuronal integration.

4.2 Glutamatergic JGCs are morphologically heterogeneous and project axons across the OB

The OB is dominated by inhibitory transmission, with the vast majority of neurons being GABAergic (Parrish-Aungst et al., 2007; Burton, 2017). However, locally connecting excitatory OB neurons like short axon cells (Aungst et al., 2003) and external tufted and bi-tufted cells(Hayar et al., 2004a; Hayar et al., 2004b) constitute an important part of the OB circuitry. With the emergence of lineage tracing in mouse mutants two studies have shown that these JGCs are also produced postnatally (Winpenny et al., 2011) and to a lesser extent even in adult (Brill et al., 2009). In agreement, we show that short axon cells as well as external tufted and bi-tufted cells are indeed generated at perinatal stages. Moreover, we show that the majority of glutamatergic perinatally born JGCs are ETCs and that the overall neuron production drops drastically and rapidly after birth.

In addition, we provide evidence for two types of axonal projections in perinatally born JGCs; type-1 projections that remain within the glomerular layer and type-2 projections that contact less glomeruli and dive deep into the core of the OB. Moreover, our retrograde tracing shows that some glutamatergic JGCs project even across the medio-lateral aspects of the OB. This finding suggests that type-2 projections belong to the intrabulbar associated system (Liu and Shipley, 1994) or mirror-symmetric isofunctional odor columns (Grobman et al., 2018). This intrabulbar circuit typically connects two glomeruli that express the same odorant receptor in a medio-lateral manner and is mediated by ETCs that project through the GCL and synapse with GCs situated just underneath its associated glomerulus on the other side of the OB (Liu and Shipley, 1994).

4.3 Perinatally born glutamatergic JGCs resist sensory deprivation

How does environmental information impact glutamatergic JGCs? Sensory deprivation by unilateral naris occlusion is a powerful approach to investigate this question within the OB brain circuitry. There is a well-established body of literature that shows how olfactory sensory deprivation causes cell death throughout all OB layers (Najbauer and Leon, 1995; Mandairon et al., 2006) thereby emphasizing the importance of sensory input for survival of OB interneurons (Petreanu and Alvarez-Buylla, 2002; Rochefort et al., 2002; Yamaguchi and Mori, 2005). We use a chronic in vivo imaging approach to directly monitor the survival of a to-date unexplored OB interneuron population, glutamatergic JGCs. In the first imaging session, we identify individual fluorescently labeled GABAergic and glutamatergic neurons and follow them over time in control situation and under occlusion. We demonstrate that while a significant fraction of GABAergic JGCs disappear, the vast majority of glutamatergic JGCs remain in place under unilateral naris occlusion. Many studies have demonstrated that a fraction of GABAergic cells undergo cell death under occlusion (Bovetti et al., 2009; Bastien-Dionne et al., 2010; Parrish-Aungst et al., 2011; Sawada et al., 2011; Kato et al., 2012). But why does this apparently general phenomenon not apply to glutamatergic JGCs? The most obvious difference between these two cell types clearly is reflected in their neurotransmitter phenotype and thus their function in the OB as either excitatory or inhibitory circuit elements. It is intriguing to view the OB system as an intricate homeostatic balance between excitation and inhibition, finely tuned by the environmental challenges imposed to the system. In this scenario, the decreased environmental excitation has to be compensated by an overall decrease in bulbar inhibition, allowing the system to still confer information to higher order brain areas. Since adult neurogenesis provides the OB continuously with inhibitory interneurons, directed apoptosis could be a feasible mechanism to fine-tune inhibitory elements of the OB system. In the meantime, excitatory elements have to adjust their excitability too. However, given that adult neurogenesis does not supply the OB with a significant amount of glutamatergic neurons at later ages, it seems unlikely that apoptosis could be a regulative mechanism for adjustment of excitation.

Further experiments will be needed to elucidate why cell death occurs selectively to some elements of the OB circuit and not to others. However, our results represent a first step towards a more differentiated view of the OB network where

both, local excitation and as well as inhibition are provided and adjusted by the interplay of an intricately complex network with its environment.

REFERENCES

Agarwal, A., Dibaj, P., Kassmann, C. M., Goebbels, S., Nave, K. A., & Schwab, M. H. (2012). In vivo imaging and noninvasive ablation of pyramidal neurons in adult NEX-CreERT2 mice. *Cereb Cortex, 22*(7), 1473-1486.

Antal, M., Eyre, M., Finklea, B., & Nusser, Z. (2006). External tufted cells in the main olfactory bulb form two distinct subpopulations. *Eur J Neurosci, 24*(4), 1124-1136.

Aungst, J. L., Heyward, P. M., Puche, A. C., Karnup, S. V., Hayar, A., Szabo, G., & Shipley, M. T. (2003). Centre-surround inhibition among olfactory bulb glomeruli.. *Nature, 426*(6967), 623-629.

Baker, H. (1990). Unilateral, neonatal olfactory deprivation alters tyrosine hydroxylase expression but not aromatic amino acid decarboxylase or GABA immunoreactivity.. *Neuroscience, 36*(3), 761-771.

Bastien-Dionne, P. O., David, L. S., Parent, A., & Saghatelyan, A. (2010). Role of sensory activity on chemospecific populations of interneurons in the adult olfactory bulb.. *J Comp Neurol, 518*(10), 1847-1861.

Boutin, C., Diestel, S., Desoeuvre, A., Tiveron, M. C., & Cremer, H. (2008). Efficient in vivo electroporation of the postnatal rodent forebrain. *PLoS ONE, 3*(4), e1883.

Bovetti, S., Veyrac, A., Peretto, P., Fasolo, A., & De Marchis, S. (2009). Olfactory enrichment influences adult neurogenesis modulating GAD67 and plasticity-related molecules expression in newborn cells of the olfactory bulb. *PLoS One, 4*(7), e6359.

Brill, M. S., Ninkovic, J., Winpenny, E., Hodge, R. D., Ozen, I., Yang, R., . . . Gotz, M. (2009). Adult generation of glutamatergic olfactory bulb interneurons. *Nat Neurosci, 12*(12), 1524-1533.

Burton, S. D. (2017). Inhibitory circuits of the mammalian main olfactory bulb. *J Neurophysiol, 118*(4), 2034-2051.

Cummings, D. M., Henning, H. E., & Brunjes, P. C. (1997). Olfactory bulb recovery after early sensory deprivation. *J Neurosci, 17*(19), 7433-7440.

de Chevigny, A., Core, N., Follert, P., Gaudin, M., Barbry, P., Beclin, C., & Cremer, H. (2012). miR-7a regulation of Pax6 controls spatial origin of forebrain dopaminergic neurons. *Nat Neurosci, 15*(8), 1120-1126.

Feng, L., Zhao, T., & Kim, J. (2015). neuTube 1.0: A New Design for Efficient Neuron Reconstruction Software Based on the SWC Format. *eNeuro, 2*(1).

Fiorelli, R., Azim, K., Fischer, B., & Raineteau, O. (2015). Adding a spatial dimension to postnatal ventricular-subventricular zone neurogenesis. *Development, 142*(12), 2109-2120.

Fuentealba, L. C., Rompani, S. B., Parraguez, J. I., Obernier, K., Romero, R., Cepko, C. L., & Alvarez-Buylla, A. (2015). Embryonic Origin of Postnatal Neural Stem Cells. *Cell, 161*(7), 1644-1655.

Goebbels, S., Bormuth, I., Bode, U., Hermanson, O., Schwab, M. H., & Nave, K. A. (2006). Genetic targeting of principal neurons in neocortex and hippocampus of NEX-Cre mice. *Genesis, 44*(12), 611-621.

Grobman, M., Dalal, T., Lavian, H., Shmuel, R., Belelovsky, K., Xu, F., . . . Haddad, R. (2018). A Mirror-Symmetric Excitatory Link Coordinates Odor Maps across Olfactory Bulbs and Enables Odor Perceptual Unity. *Neuron, 99*(4), 800-813.

Hayar, A., Karnup, S., Ennis, M., & Shipley, M. T. (2004). External tufted cells: a major excitatory element that coordinates glomerular activity. *J Neurosci, 24*(30), 6676-6685.

Hayar, A., Karnup, S., Shipley, M. T., & Ennis, M. (2004). Olfactory bulb glomeruli: external tufted cells intrinsically burst at theta frequency and are entrained by patterned olfactory input. *J Neurosci, 24*(5), 1190-1199.

Kato, Y., Kaneko, N., Sawada, M., Ito, K., Arakawa, S., Murakami, S., & Sawamoto, K. (2012). A subtype-specific critical period for neurogenesis in the postnatal development of mouse olfactory glomeruli. *PLoS One, 7*(11), e48431.

Kay, J. N., Voinescu, P. E., Chu, M. W., & Sanes, J. R. (2011). Neurod6 expression defines new retinal amacrine cell subtypes and regulates their fate. *Nat Neurosci, 14*(8), 965-972.

Kosaka, T., & Kosaka, K. (2011). "Interneurons" in the olfactory bulb revisited. *Neurosci Res, 69*(2), 93-99.

Liu, W. L., & Shipley, M. T. (1994). Intrabulbar associational system in the rat olfactory bulb comprises cholecystokinin-containing tufted cells that synapse onto the dendrites of GABAergic granule cells. *J Comp Neurol, 346*(4), 541-558.

Macrides, F., & Schneider, S. P. (1982). Laminar organization of mitral and tufted cells in the main olfactory bulb of the adult hamster. *J Comp Neurol, 208*(4), 419-430.

Madisen, L., Zwingman, T. A., Sunkin, S. M., Oh, S. W., Zariwala, H. A., Gu, H., . . . Zeng, H. (2010). A robust and high-throughput Cre reporting and characterization system for the whole mouse brain. *Nat Neurosci, 13*(1), 133-140.

Mandairon, N., Jourdan, F., & Didier, A. (2003). Deprivation of sensory inputs to the olfactory bulb up-regulates cell death and proliferation in the subventricular zone of adult mice. *Neuroscience, 119*(2), 507-516.

Mandairon, N., Sacquet, J., Jourdan, F., & Didier, A. (2006). Long-term fate and distribution of newborn cells in the adult mouse olfactory bulb: Influences of olfactory deprivation. *Neuroscience, 141*(1), 443-451.

Merkle, F. T., Mirzadeh, Z., & Alvarez-Buylla, A. (2007). Mosaic organization of neural stem cells in the adult brain. *Science, 317*(5836), 381-384.

Morin, X., Jaouen, F., & Durbec, P. (2007). Control of planar divisions by the G-protein regulator LGN maintains progenitors in the chick neuroepithelium. *Nat Neurosci, 10*(11), 1440-1448.

Najbauer, J., & Leon, M. (1995). Olfactory experience modulated apoptosis in the developing olfactory bulb. *Brain Res, 674*(2), 245-251.

Parrish-Aungst, S., Kiyokage, E., Szabo, G., Yanagawa, Y., Shipley, M. T., & Puche, A. C. (2011). Sensory experience selectively regulates transmitter synthesis enzymes in interglomerular circuits. *Brain Res, 1382*, 70-76.

Parrish-Aungst, S., Shipley, M. T., Erdelyi, F., Szabo, G., & Puche, A. C. (2007). Quantitative analysis of neuronal diversity in the mouse olfactory bulb. *J Comp Neurol, 501*(6), 825-836.

Petreanu, L., & Alvarez-Buylla, A. (2002). Maturation and death of adult-born olfactory bulb granule neurons: role of olfaction. *J Neurosci, 22*(14), 6106-6113.

Qin, S., Ware, S. M., Waclaw, R. R., & Campbell, K. (2017). Septal contributions to olfactory bulb interneuron diversity in the embryonic mouse telencephalon: role of the homeobox gene Gsx2. *Neural Dev, 12*(1), 13.

Rochefort, C., Gheusi, G., Vincent, J. D., & Lledo, P. M. (2002). Enriched odor exposure increases the number of newborn neurons in the adult olfactory bulb and improves odor memory. *J Neurosci, 22*(7), 2679-2689.

Roybon, L., Mastracci, T. L., Li, J., Stott, S. R., Leiter, A. B., Sussel, L., . . . Li, J. Y. (2015). The Origin, Development and Molecular Diversity of Rodent Olfactory Bulb Glutamatergic Neurons Distinguished by Expression of Transcription Factor NeuroD1. *PLoS One, 10*(6), e0128035.

Sawada, M., Kaneko, N., Inada, H., Wake, H., Kato, Y., Yanagawa, Y., . . . Sawamoto, K. (2011). Sensory input regulates spatial and subtype-specific patterns of neuronal turnover in the adult olfactory bulb. *J Neurosci, 31*(32), 11587-11596.

Schindelin, J., Arganda-Carreras, I., Frise, E., Kaynig, V., Longair, M., Pietzsch, T., . . . Cardona, A. (2012). Fiji: an open-source platform for biological-image analysis. *Nat Methods, 9*(7), 676-682.

Shih, A. Y., Mateo, C., Drew, P. J., Tsai, P. S., & Kleinfeld, D. (2012). A polished and reinforced thinned-skull window for long-term imaging of the mouse brain. *J Vis Exp*(61). e3742

Susaki, E. A., Tainaka, K., Perrin, D., Yukinaga, H., Kuno, A., & Ueda, H. R. (2015). Advanced CUBIC protocols for whole-brain and whole-body clearing and imaging. *Nat Protoc, 10*(11), 1709-1727.

Tamamaki, N., Yanagawa, Y., Tomioka, R., Miyazaki, J., Obata, K., & Kaneko, T. (2003). Green fluorescent protein expression and colocalization with calretinin, parvalbumin, and somatostatin in the GAD67-GFP knock-in mouse. *J Comp Neurol, 467*(1), 60-79.

Tiveron, M. C., Beclin, C., Murgan, S., Wild, S., Angelova, A., Marc, J., . . . Cremer, H. (2017). Zic-Proteins Are Repressors of Dopaminergic Forebrain Fate in Mice and C. elegans. *J Neurosci, 37*(44), 10611-10623.

Weinandy, F., Ninkovic, J., & Gotz, M. (2011). Restrictions in time and space--new insights into generation of specific neuronal subtypes in the adult mammalian brain. *Eur J Neurosci, 33*(6), 1045-1054.

Whitman, M. C., & Greer, C. A. (2007). Adult-generated neurons exhibit diverse developmental fates. *Dev Neurobiol, 67*(8), 1079-1093.

Whitman, M. C., & Greer, C. A. (2009). Adult neurogenesis and the olfactory system. *Prog Neurobiol, 89*(2), 162-175.

Winpenny, E., Lebel-Potter, M., Fernandez, M. E., Brill, M. S., Gotz, M., Guillemot, F., & Raineteau, O. (2011). Sequential generation of olfactory bulb glutamatergic neurons by Neurog2-expressing precursor cells. *Neural Dev, 6*, 12.

Wu, S. X., Goebbels, S., Nakamura, K., Kometani, K., Minato, N., Kaneko, T., . . . Tamamaki, N. (2005). Pyramidal neurons of upper cortical layers generated by NEX-positive progenitor cells in the subventricular zone. *Proc Natl Acad Sci U S A, 102*(47), 17172-17177.

Yamaguchi, M., & Mori, K. (2005). Critical period for sensory experience-dependent survival of newly generated granule cells in the adult mouse olfactory bulb. *Proc Natl Acad Sci U S A, 102*(27), 9697-9702.

Yang, G., Pan, F., Parkhurst, C. N., Grutzendler, J., & Gan, W. B. (2010). Thinned-skull cranial window technique for long-term imaging of the cortex in live mice. *Nat Protoc, 5*(2), 201-208.

Table 1. Primary antibodies used in this study

Antigen	Manufacturer, Catalog#, RRID	Immunogen	Host/clone	Dilution
Ankyrin-G	Millipore, #MABN466, RRID_2749806	Recombinant protein corresponding to human Ankyrin-G	Rat (monoclonal), IgG_{1k}, clone N106/36	1:2000
Calbindin D-28K	Millipore, #AB1778, AB_2068336	Recombinant mouse Calbindin	Rabbit (polyclonal)	1:1000
Calretinin	Synaptic System, #214 111, AB_2619904	Recombinant full length mouse Calretinin	Mouse (monoclonal), IgG1, clone 37C9	
Ki-67	BD Biosciences, #550609, AB_393778	Human Ki-67	Mouse (monoclonal), IgG_{1k}, clone B56	1:200
Pax6	Millipore, #AB2237, AB_1587367	KLH conjugated synthetic peptide corresponding to the C-terminal region of PAX6	Rabbit (polyclonal)	1:1000
RFP	Rockland, #600-401-379,	Full length RFP protein	Rabbit	1:500

	AB_828390	from the mushroom polyp coral Discosoma	(polyclonal)	
RFP	Chromotek, #5F8, AB_2336063	Full length RFP protein from the mushroom polyp coral Discosoma	Rat (monoclonal), IgG_{2A}, clone 5F8	1:500
Tbr1	Abcam, #ab31940, AB_2200219	Synthetic peptide conjugated to KLH derived from within residues 50-150 of mouse TBR1	Rabbit (polyclonal)	1:1000
Tbr2	Abcam, # ab23345, AB_778267	Synthetic peptide conjugated to KLH derived from within residues 650 to C-terminus of mouse TBR2	Rabbit (polyclonal)	1:1000
TH (tyrosine hydroxylase)	Avès Labs, #TYH, AB_10013440	Cocktail of 2 synthetic peptide conjugated to KLH	Chicken (polyclonal), IgY	1:1000

		corresponding to different regions of the Tyrosine Hydroxylase protein shared between Human and Mouse sequences		
VGLUT1	Synaptic System, #135 302 AB_887877	Recombinant protein corresponding to AA 456 to 560 from Rat VGLUT1	Rabbit (polyclonal)	1:2000
VGLUT2	Synaptic System, #135 402, AB_2187539	Recombinant protein corresponding to AA 510 to 582 from Rat VGLUT2	Rabbit (polyclonal)	1:2000

FIGURES LEGENDS

Figure 1. NeuroD6 marks a progenitor pool situated in the dorsal V-SVZ. **A**, Relative expression ratio of NeuroD6 (ND6) in sorted cells of dorsal versus lateral neurogenic lineages at different time points of the neurogenic progression. Data originates from micro-array-based screen published by (Tiveron et al., 2017). Ratios show that dorsal expression is predominant. **B**, Confirmation of ND6 expression data with quantitative RT-PCR on micro-dissected tissue originating from dorsal (d-SVZ) and lateral (l-SVZ) V-SVZ, as well as OB tissue from neonatal and adult animals, respectively. Expression levels are highest in d-SVZ sample. RQ: Relative Quantification. **C**,

Schematic representation of Cre recombinase knock-in in ND6^{Cre} and ND6^{CreERT2} lines crossed to Rosa26^{tdTomato} (tdTom) reporter line. **D**, V-SVZ of neonatal (P1) ND6$^{Cre/tdTom}$ mice. Note that recombined tdTomato (tdTom) cells are present in the dorsal sub-portion of the V-SVZ (**D'**). **E**, OB of juvenile (P21) ND6$^{Cre/tdTom}$ mice. Note that recombined cells are present in the mitral cell layer (MCL) and in the glomerular layer (GL). **F**, V-SVZ of induced (1 dpi) neonatal ND6$^{CreERT2/tdTom}$ mice after induction with tamoxifen (Tam) at P0. Note that again recombined cells are present in the dorsal sub-portion of the V-SVZ (**F'**). **G**, OB of induced (21 dpi) juvenile ND6$^{Cre/tdTom}$ mice after TAM induction at P0. Note that recombined cells are almost absent from the MCL and less cells are present in the GL as compared to (**E**). Nuclei are stained in blue with Hoechst. White contour lines in the OB (**E, G**) delineate glomeruli. hpe: hours post electroporation, dpe: days post electroporation, dpi: days post induction. CC: corpus callosum, GCL: granule cell layer, LV: lateral ventricle, OB: olfactory bulb, Sep: Septum, Str: Striatum, V-SVZ: ventricular-subventricular zone. Scale bars: **D**, 200 µm; **E**, 100µm

Figure 2. ND6-derived OB neurons display a glutamatergic phenotype. No co-localization between known GABAergic OB markers (in green) GAD67-GFP (**A**), GAD65 (**B**), Calbindin (**C**), Calretinin (**D**), Tyrosin Hydroxylase (TH, **E**), and tdTom+ cells in constitutively Cre-expressing line (ND6^{Cre}). **B**, tdTom+ cells co-localize (arrow heads) with glutamatergic markers (in green) Tbr1 (**F**), Tbr2 (**G**), Vglut1 (**H**) and Vglut2 (**I**). **J**, Quantification of co-localization of glutamatergic markers with tdTom+ neurons in both ND6 mouse lines. Proportion of double positive cells varies dependent on the labelling strategy (constitutively expressed ND6^{Cre} which marks all glutamatergic neurons vs. inducible ND6^{CreERT2} line which marks a subpopulation of neurons born around P0). Scale bars: **A**, **F**, 20 µm. Error bars indicate SEM.

Figure 3. NeuroD6 is expressed in postmitotic neurons. **A**, Colocalization analysis of tdTom+ cells with specific markers in dorsal V-SVZ of neonatal NeuroD6$^{cre/tdTom}$ mice. No colocalization with tdTom cells and stem cell marker Pax6 or proliferative marker Ki67. Full colocalization with tdtTom cells and postmitotic marker Tbr1. **B,** Schematic representation of transcriptional cascade of glutamatergic neuron generation in the OB. Note that adult-born glutamatergic JGCs do not express Tbr2 (unknown for Tbr1) in mature stage. Scale bars: **A,** 20 µm.

Figure 4. TAM induction in neonatal ND6^{CreERT2} mice recombines neuronal progenitors along the V-SVZ-RMS-OB axis. **A**, Schematic representation of TAM-induced pulse-chase experiments. Pups were induced at P0 and brains were harvested 1, 7 and 21 days post induction (dpi), respectively. Dotted lines on sagittal representation indicate the level of slice analysis from V-SVZ to OB. **B**, Presence of recombined red cells along the V-SVZ-RMS-OB axis at different time points after TAM induction. At 1 dpi neuronal progenitors are found in the dorsal V-SVZ, in the RMS and in the deeper OB layers. Most cells display a migratory morphology (arrow head). At 7 dpi recombined cells are found mainly within the OB. Cells with more complex morphology start to appear in the GL. At 21 dpi cells are found almost exclusively within the GL and have acquired a mature neuronal morphology. Some cells are found close to the mitral cell layer (MCL, arrow head). RMS, rostral migratory stream. Scale bars: **C**, left to right: 100 µm, 40 µm, 100 µm.

Figure 5. Glutamatergic juxtaglomerular cells (JGCs) are morphologically heterogeneous and can be classified into three main categories. **A**, Schematic representation (above) and real examples (below) of three main interneuron categories based on their dendritic branching pattern into one glomerulus (external tufted cells, ETCs), more than one glomerulus (bitufted ETCs, biETCs) or the presence of an additional secondary dendrite extending into the EPL (secETCs). All categories display a fine protrusion, resembling an axon (indicated in red on scheme and with red arrows on real cells). **B**, Schematic representation of induction protocol used in **C** and **D**. ND6$^{CreERT2/tdTom}$ mice are induced with TAM at P0, P6, P15 and P45 respectively and brains collected 21 dpi. **C**, Quantification of categories of recombined glutamatergic JGCs when induction is performed at different time points. Note that a fourth category, short axon cells (SAC), is also detected. However, given that this cell type is seldom observed and that dendritic morphology does not correspond to the classical description, we did not further quantify these cells. **D**, Representative confocal images of animals induced at different time points showing enlarged view of the GL and EPL. The amount of recombined red cells declines progressively as induction is performed in older animals. Scale bars: **A**, 20 µm, **D**, 100 µm

Figure 6. Glutamatergic JGCs project axons across all layers of the olfactory bulb. **A**, tdTom+ cells display thin protrusions which are immunoreactive for axonal initial

segment marker Ankyrin G (AnkG). Detail of colocalization shown in **A'**. **B**, Schematic representation of experimental setup to induce sparse labelling and follow axonal projections. Intraventricular Hydroxytamoxifen (4OH-TAM) injection in neonatal $ND6^{CreERT2/tdTom}$ mice. 6 weeks post injection (wpi) brains are harvested and cleared using the Cubic protocol. To obtain as complete axonal reconstructions as possible, entire transparent brains were imaged using 2-photon microscopy. **C**, Partial axonal reconstructions of the different postnatal generated glutamatergic JGCs. Axonal projections (red) either remain within the glomerular layer (type-1 superficial axons) or dive into the GCL (type-2 deep axons) where they cannot be traced anymore due to high density of projections. Deep axons are frequently observed to specifically branch within the inner plexiform layer (IPL). **D**, Type-1 axons contact significantly more glomeruli than type-2 axons ($p = 0.0098$, $^{**}p < 0.01$, two-tailed Mann Whitney U test, $n_{(superficial/deep)} = 25/17$ cells, 3 animals). **E**, Relative occurrence of axonal types on glutamatergic JGC categories. Type-1 and type-2 axons appear on external tufted (ETCs) and bitufted cells (biETCs). All traced external tufted cells with secondary dendrites (secETCs) displayed type-2 axons ($n_{(ETC/biETC/secETC)} = 28/10/4$ cells, 3 animals). **F**, Retrograde labeling of tdTom+ cells (medial) after localized CTB injection (lateral) suggests that type-2 axons connect to the opposite side within the same OB. **F'**, Double labeled CTB+ tdTom+ cells are systematically found on OB side opposite to the injection site (59 cells, 3 animals) but also adjacent (**F''**) to the injection site. Scale bars **A**, 20 µm; **F**, 1 mm; **F'**, 20 µm. Error bars indicate SEM.

Figure 7. Glutamatergic JGCs are resistant to sensory deprivation. **A,** Schematic representation of experimental procedure carried out to study in vivo survival of glutamatergic and GABAergic cells. To mark GABAergic JGCs, Cre recombinase plasmid was electroporated (elpo) into P0 tdTom reporter mice. To mark glutamatergic JGCs $ND6^{creERT2/tdTom}$ was induced at P0. 4 weeks after elpo or induction, thin-skull surgery was performed. Mice were imaged for 4 weeks using a 2-photon microscope. Their brains were subsequently fixed and processed for histological analysis. **B**, Image of the same region for GABAergic cells (above) and glutamatergic JGCs (below), short after tdTom recombination (week0) and 4 weeks later (week4). Each cell is numbered and identified based on their relative position to other cells and distinctive dendritic branching pattern (whenever possible). **C**, Number of GABAergic JGCs followed in individual animals (black lines) in the course

of 4 weeks. **D**, Number of glutamatergic neurons followed in individual animals (red lines) in the course of 4 weeks. **E**, Percentage of GABA- and glutamatergic JGCs that survived under control condition in the course of 4 weeks as compared to week0. **F**, Schematic representation of experimental setup conducted for sensory deprivation using unilateral naris occlusion. The scheme recapitulates essentially the protocol depicted in (**A**) with the difference that in a group of animals, unilateral naris occlusion was additionally performed at the moment of the surgery. **G**, Loss of approximately 30% of OB volume in occluded (occl) OB as compared to control OB (ctrl). **H**, Strong decrease in TH immunoreactivity further confirms successful occlusion. **I**, Image before (week0) and 4 weeks after (week4) occlusion of the same region for GABAergic cells (above) and glutamatergic JGCs (below). Note that under occlusion, a fraction of GABAergic cells disappears (circle). **J**, Number of GABAergic JGCs followed in individual animals (black lines) during 4 weeks of occlusion. **K**, Number of glutamatergic neurons followed in individual animals (red lines) during 4 weeks of occlusion. **L**, Percentage of GABA- and glutamatergic JGCs that survived under occlusion in the course of 4 weeks as compared to week0. While a significant decrease in GABAergic cell number is observed ($p = 0.00804$ for $GABA_{ctrl}$ vs $GABA_{occl}$, $p = 0.0018$ for $GABA_{occl}$ vs $gluta_{occl}$, $^{**}p < 0.01$, two-tailed Mann Whitney U test, $n_{GABA(ctrl/occl)}$ = 214/279 cells, 5/6 animals respectively), glutamatergic cell number remains stable ($n_{Gluta(ctrl/occl)}$ = 365/403 cells, 5/9 animals respectively). Scale bars: **B**, 20 µm; **H**, 1 mm; **I**, 20 µm. Error bars indicate SEM.

Figure 1.

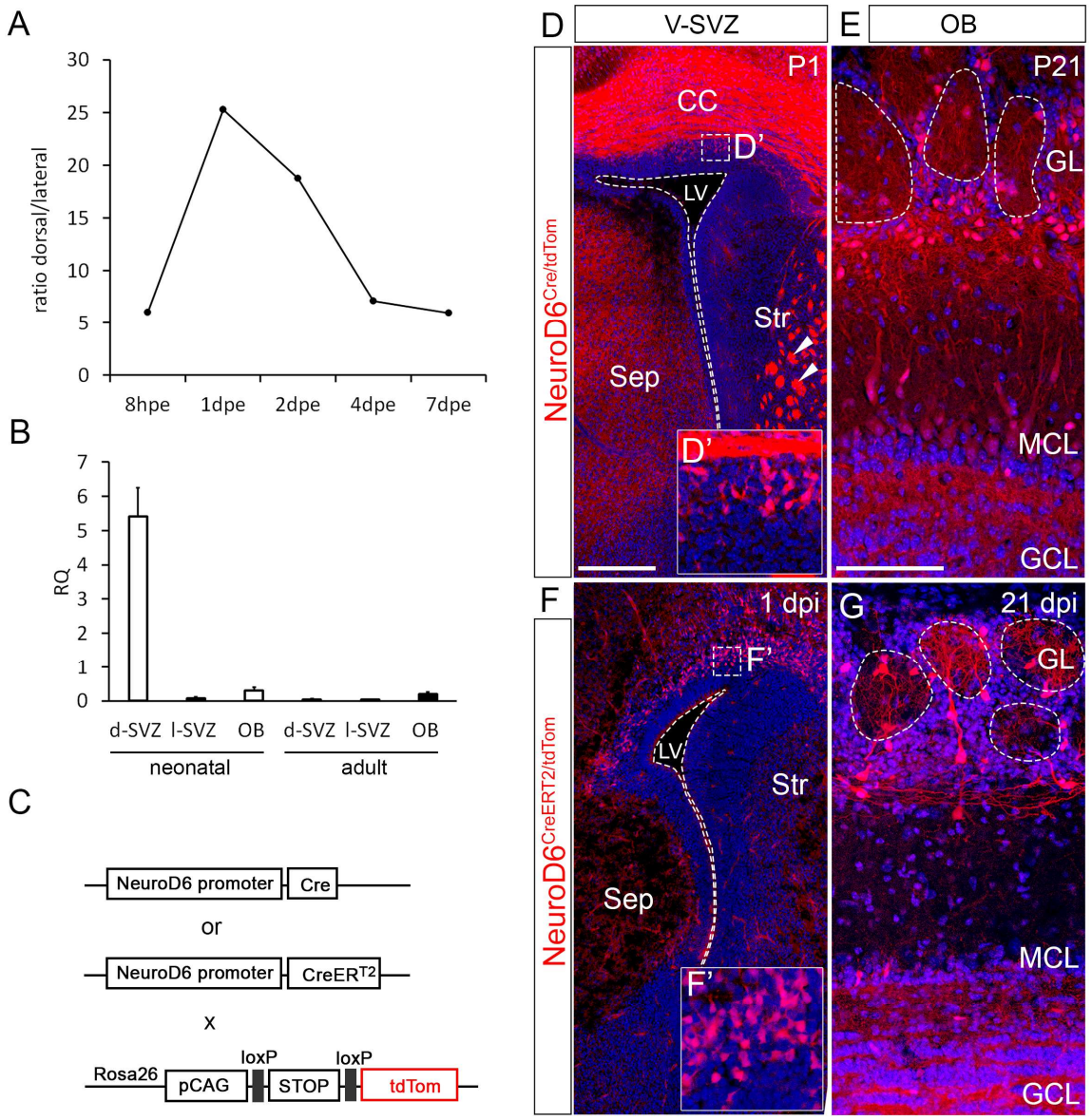
A
ratio dorsal/lateral
30
25
20
15
10
5
0
8hpe
1dpe
2dpe
4dpe
7dpe
B
RQ
7
6
5
4
3
2
1
0
d-SVZ
l-SVZ
OB
d-SVZ
l-SVZ
OB
neonatal
adult
C
NeuroD6 promoter
Cre
or
NeuroD6 promoter
CreER^{T2}
x
Rosa26
pCAG
loxP
STOP
loxP
tdTom
D
V-SVZ
E
OB
NeuroD6$^{Cre/tdTom}$
P1
CC
D'
LV
Str
Sep
D'
P21
GL
MCL
GCL
F
1 dpi
G
21 dpi
NeuroD6$^{CreERT2/tdTom}$
F'
LV
Str
Sep
F'
GL
MCL
GCL

Figure 2.

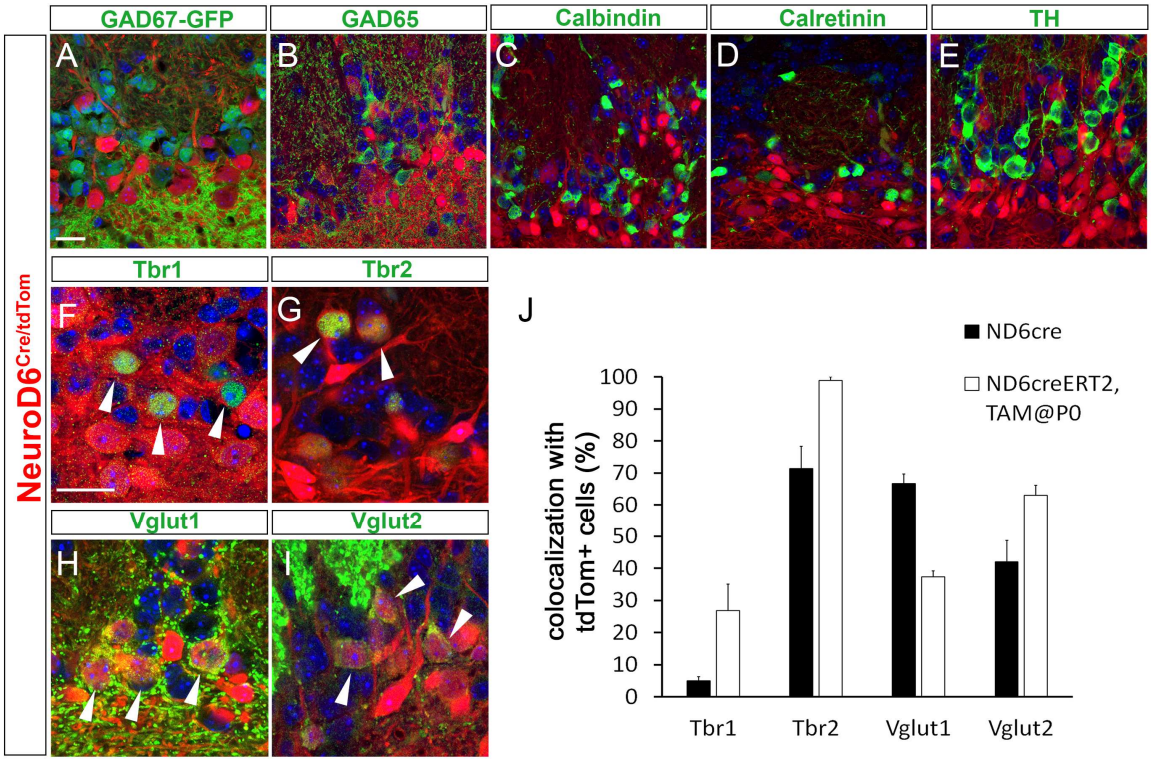
GAD67-GFP
GAD65
Calbindin
Calretinin
TH
A
B
C
D
E
NeuroD6Cre/tdTom
Tbr1
Tbr2
F
G
Vglut1
Vglut2
H
I
J
ND6cre
ND6creERT2, TAM@P0
colocalization with tdTom+ cells (%)
100
90
80
70
60
50
40
30
20
10
0
Tbr1
Tbr2
Vglut1
Vglut2

Figure 3.

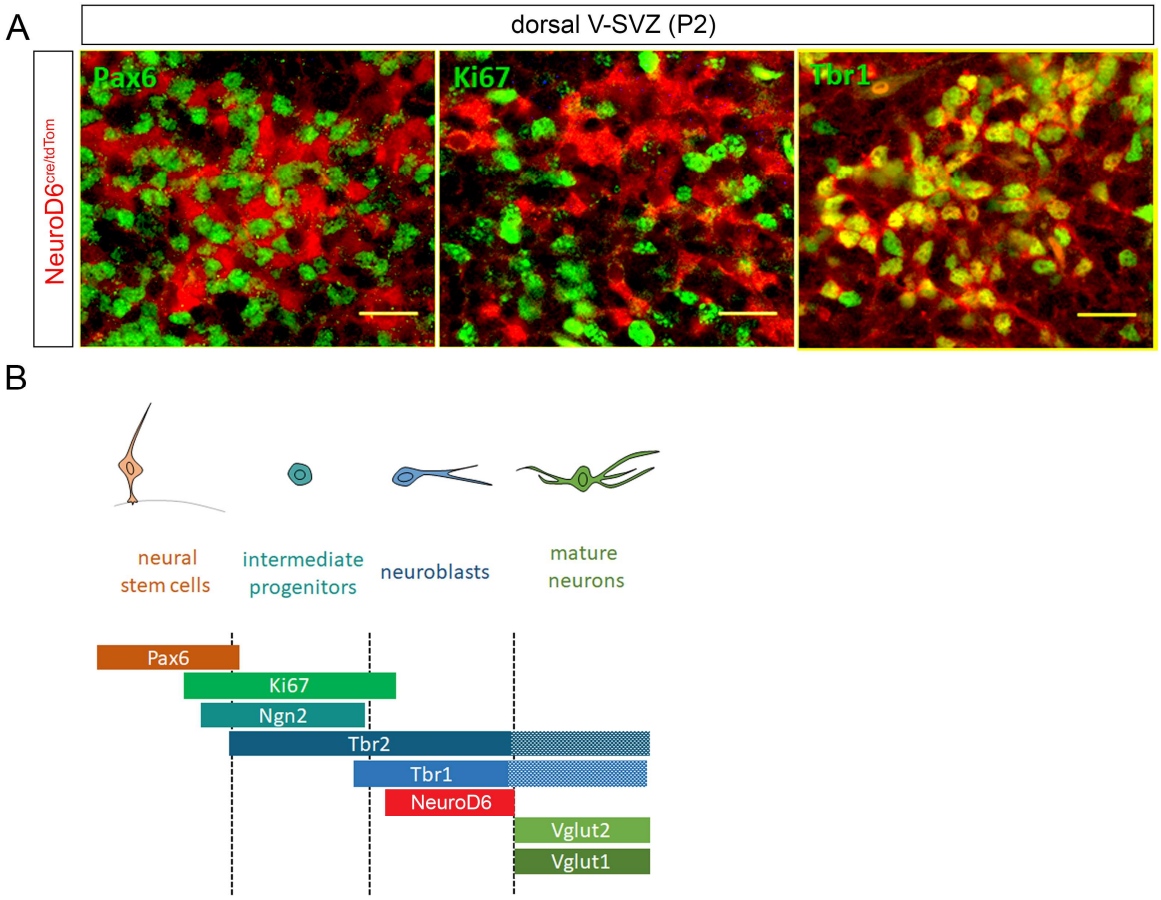
A
dorsal V-SVZ (P2)
NeuroD6cre/tdTom
Pax6
Ki67
Tbr1
B
neural stem cells
intermediate progenitors
neuroblasts
mature neurons
Pax6
Ki67
Ngn2
Tbr2
Tbr1
NeuroD6
Vglut2
Vglut1

Figure 4.

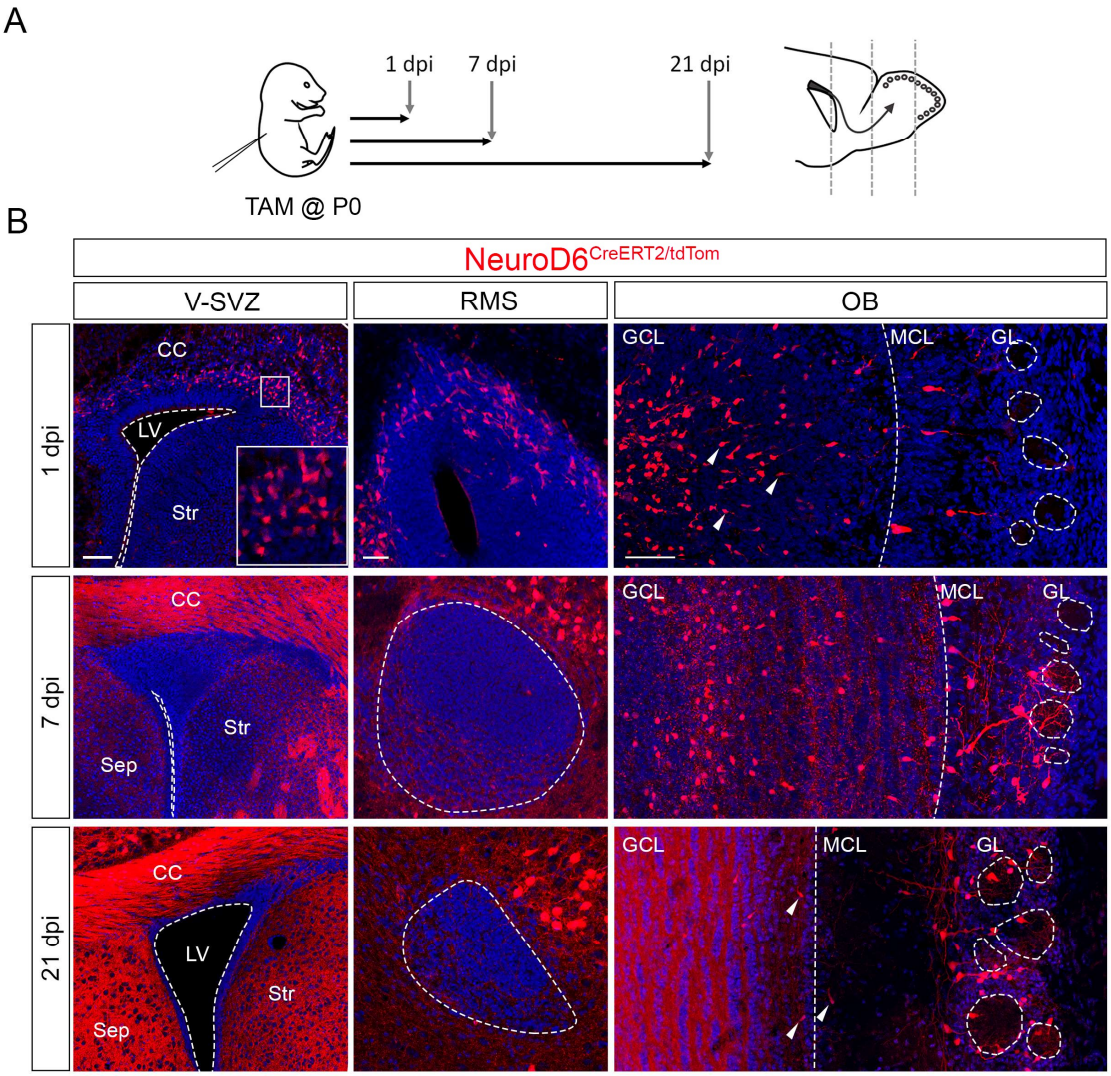
A
1 dpi
7 dpi
21 dpi
TAM @ P0
B
NeuroD6CreERT2/tdTom
V-SVZ
RMS
OB
1 dpi
7 dpi
21 dpi
CC
LV
Str
Sep
GCL
MCL
GL

Figure 5.

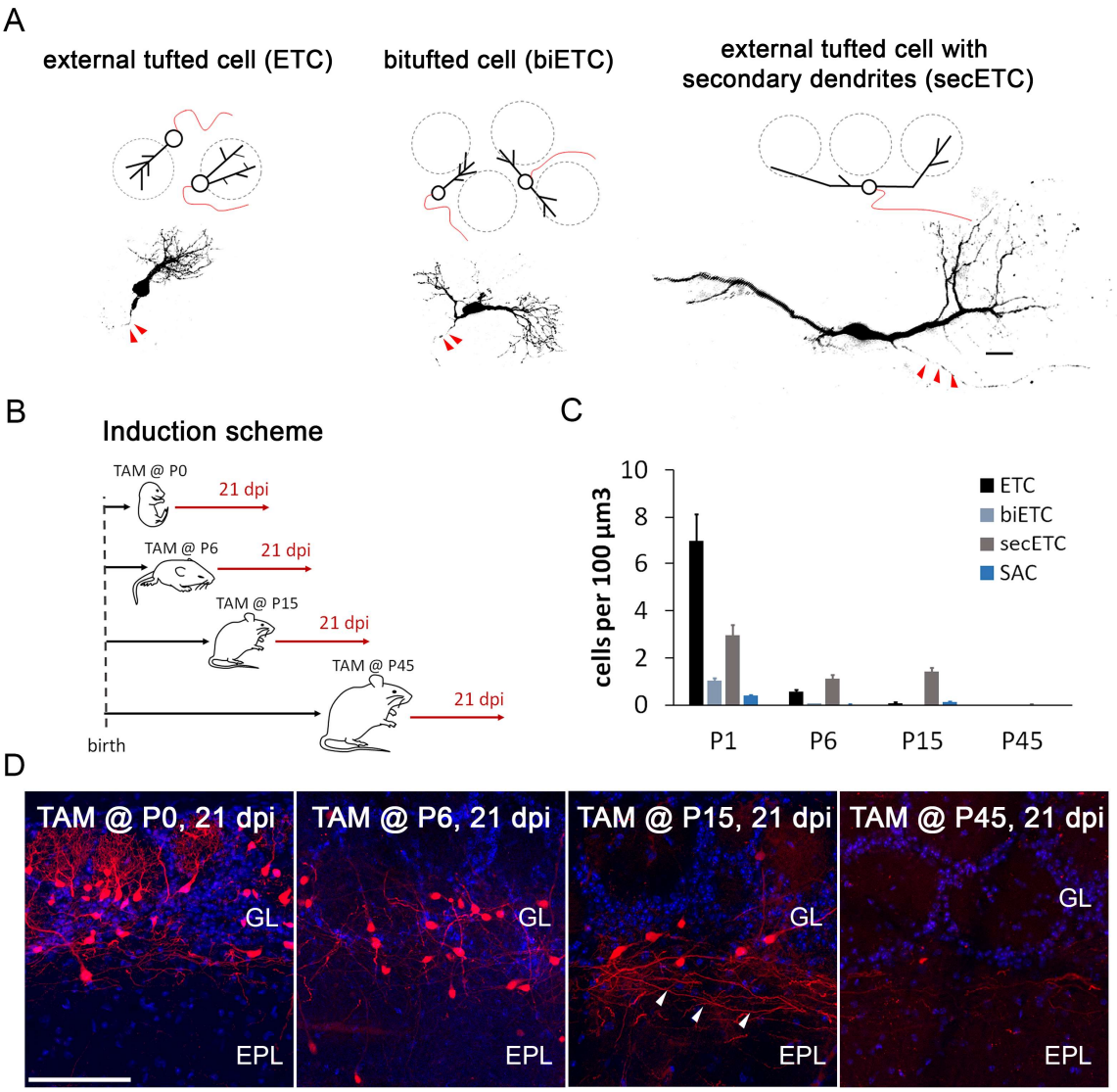
A
external tufted cell (ETC)
bitufted cell (biETC)
external tufted cell with secondary dendrites (secETC)
B
Induction scheme
TAM @ P0
21 dpi
TAM @ P6
21 dpi
TAM @ P15
21 dpi
TAM @ P45
21 dpi
birth
C
cells per 100 µm3
10
8
6
4
2
0
P1
P6
P15
P45
ETC
biETC
secETC
SAC
D
TAM @ P0, 21 dpi
TAM @ P6, 21 dpi
TAM @ P15, 21 dpi
TAM @ P45, 21 dpi
GL
EPL

Figure 6.

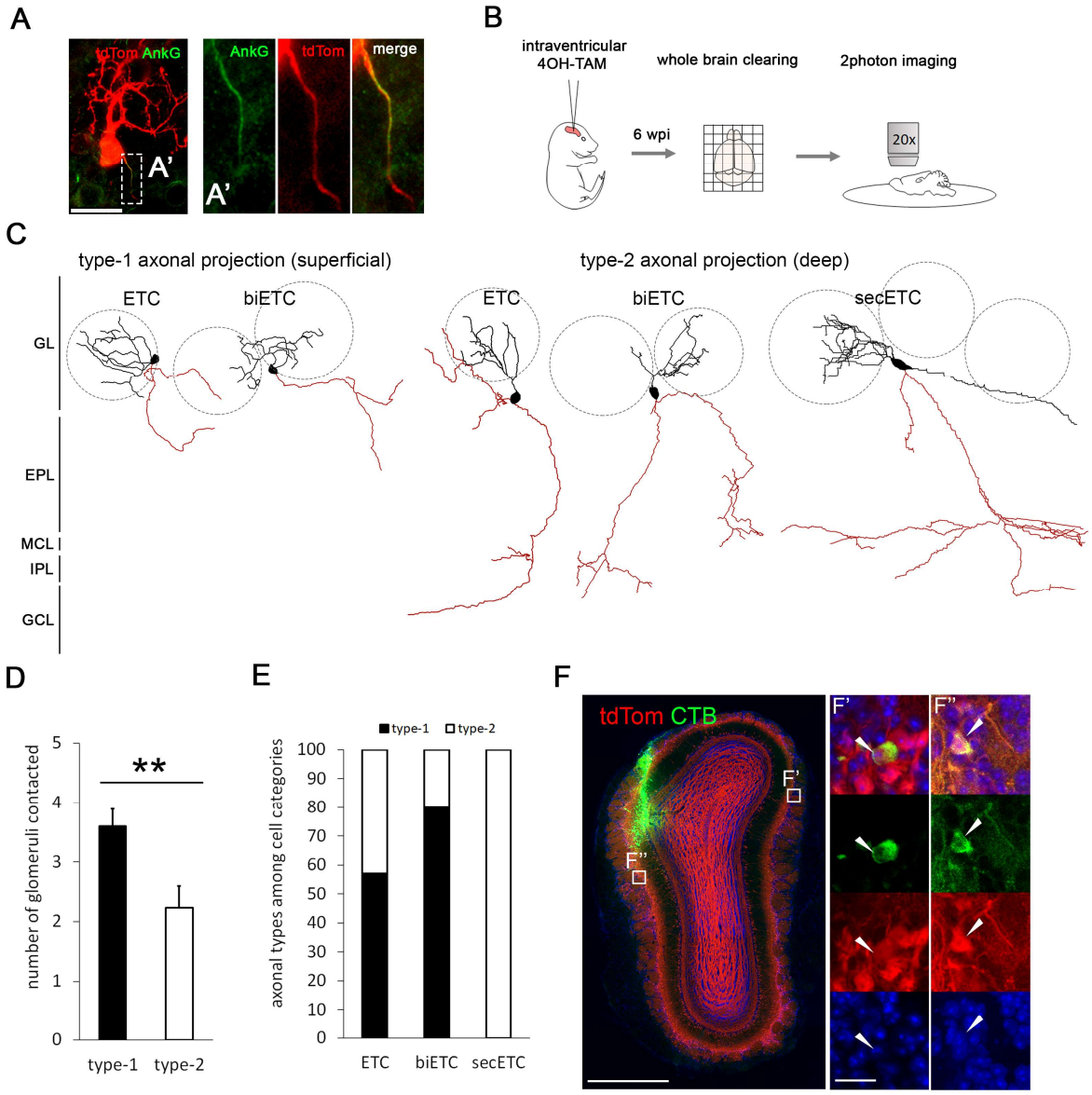
A
tdTom AnkG
A'
AnkG
tdTom
merge
A'
B
intraventricular
4OH-TAM
whole brain clearing
2photon imaging
6 wpi
20x
C
type-1 axonal projection (superficial)
type-2 axonal projection (deep)
ETC
biETC
ETC
biETC
secETC
GL
EPL
MCL
IPL
GCL
D
number of glomeruli contacted
**
type-1
type-2
E
type-1
type-2
axonal types among cell categories
ETC
biETC
secETC
F
tdTom CTB
F'
F''
F'
F''

Figure 7.

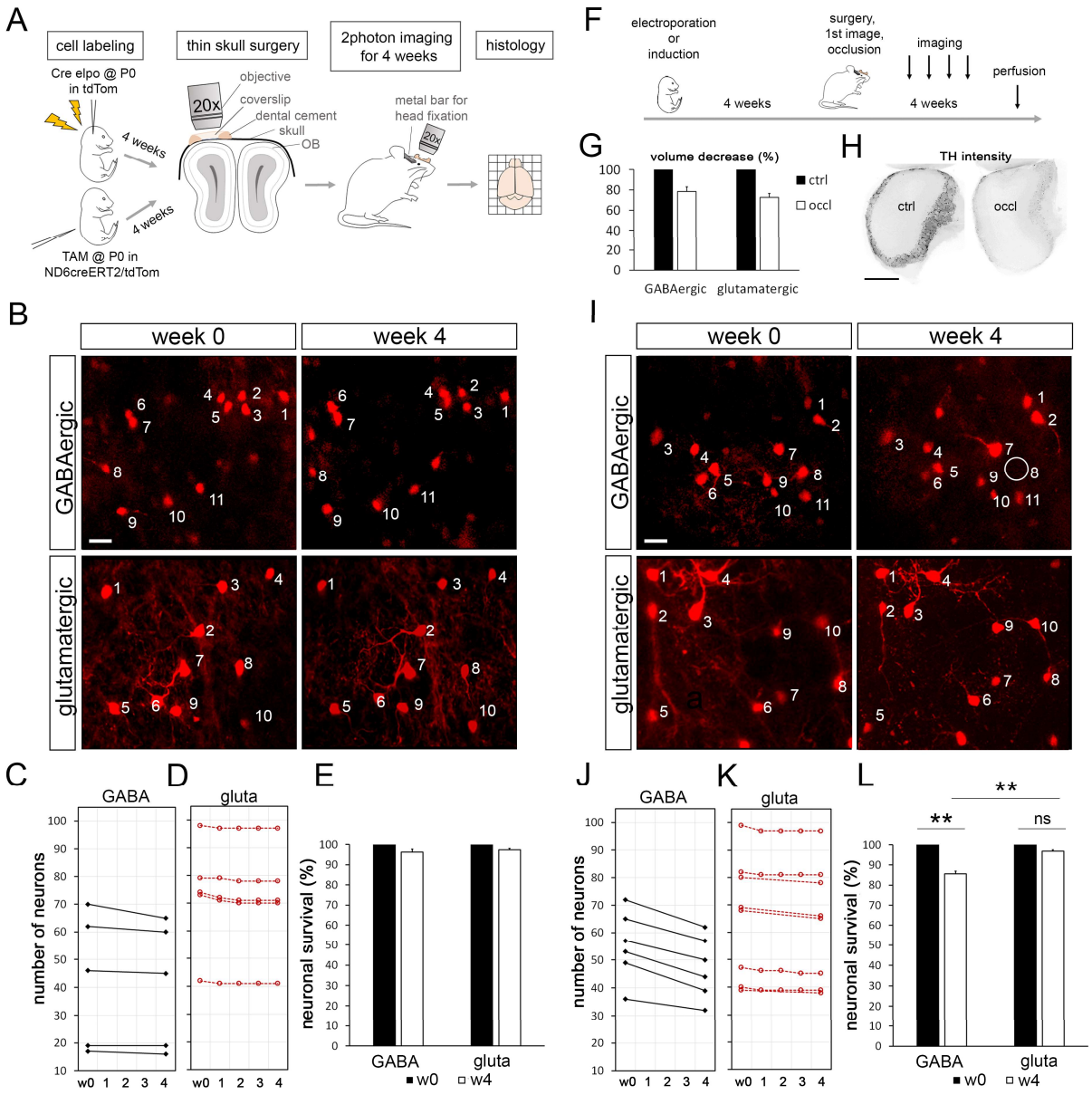
A
cell labeling
thin skull surgery
2photon imaging for 4 weeks
histology
Cre elpo @ P0 in tdTom
4 weeks
4 weeks
TAM @ P0 in ND6creERT2/tdTom
objective
coverslip
dental cement
skull
OB
20x
metal bar for head fixation
F
electroporation or induction
4 weeks
surgery, 1st image, occlusion
4 weeks
imaging
perfusion
G
volume decrease (%)
ctrl
occl
GABAergic
glutamatergic
H
TH intensity
ctrl
occl
B
week 0
week 4
GABAergic
glutamatergic
I
week 0
week 4
GABAergic
glutamatergic
C
GABA
number of neurons
D
gluta
E
neuronal survival (%)
GABA
gluta
w0
w4
J
GABA
number of neurons
K
gluta
L
**
**
ns
neuronal survival (%)
GABA
gluta
w0
w4

2. Function of NeuroD6 in the OB

Previously I have demonstrated that NeuroD6 is transiently and specifically expressed in glutamatergic progenitors of the OB. Functional studies from different brain areas have reported an implication of NeuroD6 in corpus callosum formation (Bormuth et al., 2013), cell fate determination (Kay et al., 2011) and cell survival (Khan et al., 2017). Moreover, ND1, a sister protein, has been implicated in neuronal maturation in the OB. Therefore, I set out to study NeuroD6 function in the OB using loss-of-function and gain-of-function approaches.

2.1 Materials and Methods

Mice. For this study, NeuroD6^{Cre} (ND6^{Cre}) knock-in mice (Goebbels et al., 2006), NeuroD6^{CreERT2} knock-in mice (Agarwal et al., 2012), NeuroD2^{flox} mice (obtained from Antoine de Chevigny, unpublished), Rosa26^{tdTomato} reporter mice (Ai14, Jackson Laboratories, stock-number 007914) and outbred CD1 mice (Charles-River, Lyon, France) of both sexes were used. For tamoxifen induction protocol, see Results part I. NeuroD2 conditional mice were generated as followed: targeted embryonic stem cells with the reporter-tagged conditional construct were injected in blastocysts at the Knock-Out/Knock-In (KO-KI) Booster platform, CIPHE, Marseille (http://www.celphedia.eu/en/centers/ciphe). Generated mice (Neurod2tm1a(KOMP)Wtsi) were then bred with mice constitutively expressing the FLP flippase (ACTB:FLPe B6;SJL, Jackson Laboratories, stock-number 003800). This breeding allowed the removal of the lacZ/neo cassette by recombination of the FRT sites. In NeuroD2$^{fl/fl}$ mice, Cre-mediated recombination of the loxP sites leads to the removal of the main exon of the NeuroD2 gene (i.e. second exon).

DNA plasmids. The pCAG-GFP and pCAG-ND6 vectors were derived from pCAG-MCS2 (Morin et al., 2007). For subsequent electroporation, plasmids were used at a concentration of 5 µg/µl in PBS and 0.1% Fast Green. For electroporation protocol see Results part I.

Histology and immunohistochemistry for NeuroD2 antibody. Rabbit anti-NeuroD2 antibody (Abcam) stained efficiently cortical neurons under standard conditions. However, using these conditions staining within the OB was never observed. Therefore, I specifically developed a "low-fixation" protocol to reveal ND2 immunostaining in the V-SVZ-OB system. Mice were intracardially perfused with PBS using a peristaltic pump. Brains were subsequently dissected and postfixed for 2 hours in in 4% PFA at 4°C. Immediately after, brains were sectioned (50 µm) using a HM 450 Sliding Microtome (Thermo Fisher Scientific) and dry ice and subjected to a standard immunostaining protocol (see Results part I) using

rabbit anti-ND2 at 1/1000 dilution. Attention was paid not to exceed 0.1% Triton-X in the buffers because of fragility of tissue. The specificity of ND2 antibody was validated on cortex tissue from ND2 knock-out mice. Immunostaining with other makers (Tbr1/2, Vglut1/2) is described in Results part I.

Statistical analysis. Statistical analyses were performed using R software (RRID: SCR_001905) and R Commander Package (https://CRAN.R-project.org/package=Rcmdr). Data are presented as mean ± SEM. Two tailed Mann Whitney U test was performed for Figure 9 and Figure 10. Probability assignment: $p > 0.05$ (not significant, ns), $0.01 < p < 0.05$ (*), $0.001 < p < 0.01$ (**) and $p < 0.001$ (***).

2.1 Loss-of-function of NeuroD6 in the OB

In order to elucidate NeuroD6 function in the V-SVZ-OB system, I took advantage of the targeting strategy that was used to generate $ND6^{Cre}$ knock-in mice (Goebbels et al., 2006). In this mouse line, most of the coding region is replaced by Cre recombinase. This feature makes homozygous (HO) $ND6^{Cre/Cre}$ mice constitutive functional knockouts which I will compare in the following with hererozygous (HET) $ND6^{Cre/+}$ mice with one functional copy of ND6. Although I cannot be certain that HET animals do not display an altered phenotype, I chose this initial strategy which allowed me to visualize $ND6^{Cre}$ recombined cells using a $Rosa26^{tdTomato\ (tdTom)}$ reporter mouse line. Altered phenotype has so far not been reported for heterozygous $ND6^{Cre/+}$ animals.

At a macroscopic scale HET and HO mice could not be distinguished and showed normal behavior. The first question I addressed was whether the total number of ND6-derived JGCs was changed in HET and HO mice. I analyzed littermates of HET and HO $ND6^{Cre/tdTom}$ mice at P21. Counting of tdTom+ cells among all cells stained with the nuclear marker DAPI within the glomerular layer revealed no obvious difference in relative cell number between HET and HO mice (**Fig. 8A**, 17.95 ± 3.78% for HET and 22.66 ± 5.24% for HO, $n_{(HET/HO)}$ = 885/891 cells, 3/3 animals). Thus, deletion of ND6 does not seem to alter total number of glutamatergic JGCs.

In the retina, ND6 acts as a fate determinant of an amacrine cell type (Kay et al., 2011). Therefore, I wondered whether this could be also the case within the OB. I used the glutamatergic markers Tbr1, Tbr2, Vglut1 and Vglut2 to determine if the glutamatergic identity of ND6-derived JGCs in the OB was affected in absence of Neurod6. Comparison of HET and HO $ND6^{Cre/tdTom}$ littermates (at P21 for Tbr1, Vglut1 and Vglut2; P15 for Tbr2)

showed no difference in glutamatergic marker expression of tdTom+ cells (**Fig. 8B,** Tbr1: 5.54 ± 0.48% for HET and 5.76 ± 1.86% for HO; Tbr2: 96.14 ± 0.59% for HET and 90.43 ± 2.8% for HO; Vglut1: 62.98 ± 4.4% for HET and 55.34 ± 5.76% in HO; Vglut2: 34.75 ± 4.59% for HET and 40.57 ± 2.48% for HO). Thus, ND6 does not seem to alter glutamatergic identity in JGCs.

In agreement with the above results, gross morphology of JGCs in HO mice seemed indistinguishable from morphology in HET mice and was not further analyzed. All three major JGC types (ETC, biETC and secETC) were also present in HO mice (data not shown). Although the analysis of Neurod6 knock-out mice has not been extensively conducted on a large amount of animals, it seems likely that this gene is not necessary for the proper generation of glutamatergic JGCs in the OB.

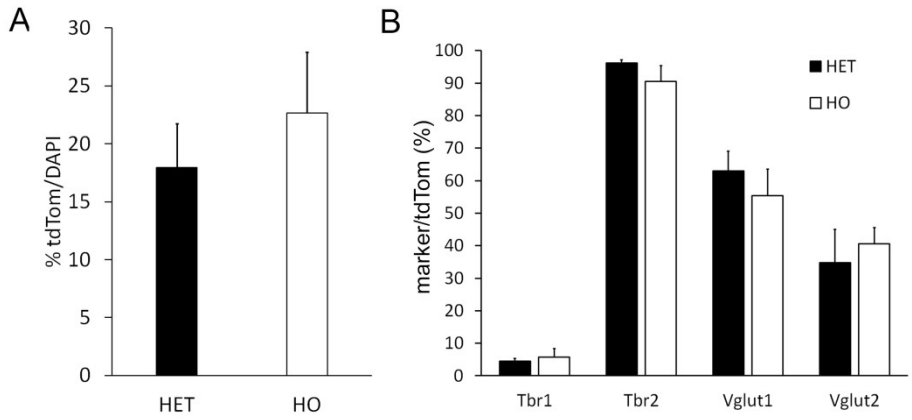

Figure 8. Loss-of-function of NeuroD6 does neither change total number of glutamatergic JGCs nor their molecular identity. **(A)** Percentage of recombined tdTom+ cells among DAPI cells within the GL of heterozygous (HET) versus homozygous (HO) $ND6^{cre/tdTom}$ mice at P21 ($n_{(HET/HO)}$ = 885/891 cells, 3/3 animals). No obvious change in amount of cells between HET and HO. **(B)** Glutamatergic marker colocalization with tdTom+ cells in HET and HO $ND6^{cre/tdTom}$ mice at P25 (P15 for Tbr2) (n-$Tbr1_{(HET/HO)}$ = 1924/1799 cells; 3/3 animals, n-$Tbr2_{(HET/HO)}$ = 2021/1252 cells, 3/3 animals; n-$Vglut1_{(HET/HO)}$ = 307/270 cells, 2/2 animals; n-$Vglut2_{(HET/HO)}$ = 1527/2848 cells, 3/4 animals). No obvious difference of marker colocalization with tdTom+ cells between HET and HO animals. Error bars indicate SEM.

2.2 Gain-of-function of NeuroD6 in the OB

Another way to approach ND6 function was to ask whether ectopic expression in progenitor cells is sufficient to modify cell fate. Therefore, I performed dorsal postnatal electroporation of CD1 wild-type mice at P0 using either a pCAG-GFP expressing plasmid as a control or a ND6 gain-of-function (GOF) construct (pCAG-ND6 with pCAG-GFP in a ratio of 3:1). Mice

were sacrificed 7 days post electroporation (dpe), a time point at which the majority of cells has arrived to the OB. Given the fact that over-expression of ND1, a close member of the NeuroD family, causes ectopic cell differentiation (Boutin et al., 2010; Roybon et al., 2015), I wondered whether ND6 over-expression could have a similar effect. Indeed, analysis of rostro-caudal cell repartition in control (ctrl) and GOF animals revealed that a significant fraction of cells electroporated with the GOF construct remained within the V-SVZ, whereas most cells in control animals had arrived in the OB (**Fig. 9A**, p = 0.00952, **p < 0.01, two-tailed Mann Whitney U test, $n_{(ctrl/GOF)}$ = 4/6 animals).

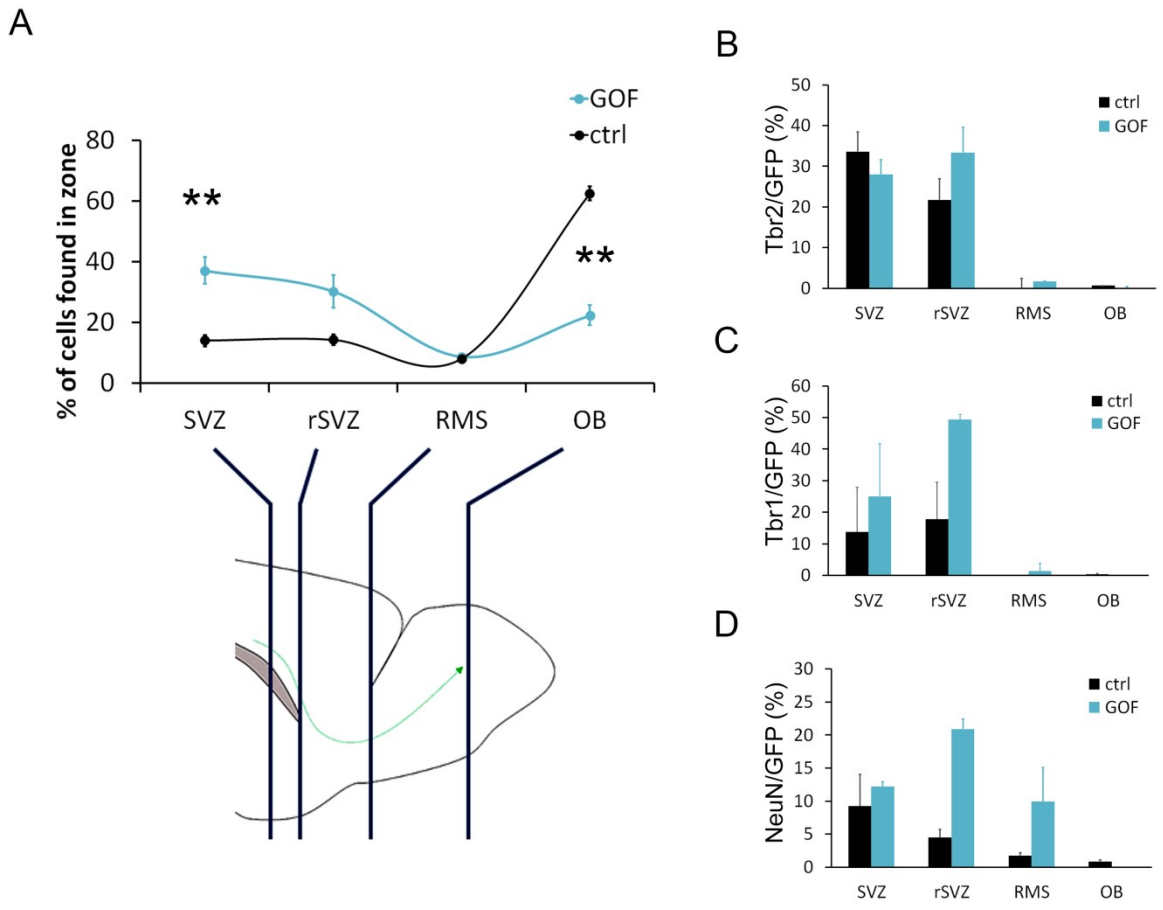

Figure 9. Gain-of-function of NeuroD6 causes cell retention in the V-SVZ possibly due to precocious neuronal maturation. **(A)** Distribution of control (ctrl) cells electroporated with GFP and ND6 gain-of-function (GOF) construct at 7 days post electroporation (dpe). Scheme below indicates rostro-caudal level of slice analysis. GOF causes significant cell retention within the V-SVZ which results in significantly less cells in the OB (p = 0.00952, **p < 0.01, two-tailed Mann Whitney U test, $n_{(ctrl/GOF)}$ = 4/6 animals). **(B)** Colocalization of GFP+ cells with Tbr2 ($n_{(ctrl/GOF)}$ = 3/3 animals) at the previously described rostro-caudal levels at 7 dpe. **(C)** Colocalization of GFP+ cells with Tbr1 ($n_{(ctrl/GOF)}$ = 4/3 animals). There is tendency of increased Tbr1 expression in GOF cells at the rostral V-SVZ level. **(D)** Colocalization of GFP+ cells with NeuN ($n_{(ctrl/GOF)}$ = 3/3 animals). There is a strong tendency of increased NeuN expression in GOF cells at the rostral V-SVZ and RMS level. SVZ: subventricular zone. rSVZ: rostral subventricular zone. RMS: rostral migratory stream. OB: olfactory bulb. Error bars indicate SEM.

Next, I wanted to know whether ND6 was capable of inducing glutamatergic phenotype in GOF electroporated cells. Therefore, I used the markers Tbr1 and Tbr2 which are well-described markers for glutamatergic progenitors in the V-SVZ (Brill et al., 2009; Winpenny et al., 2011). Analysis of Tbr1/2 expression in ctrl and GOF cells in different rostro-caudal levels showed that Tbr2 expression remained unchanged in GOF compared to control (**Fig. 9B**, $n_{(ctrl/GOF)}$ = 3/3 animals). However, Tbr1 showed a strong tendency of up-regulation specifically within the rostral portion of the V-SVZ (**Fig. 9C**, rSVZ, $n_{(ctrl/GOF)}$ = 4/3 animals). Finally, I asked whether cells retained within the V-SVZ corresponded to precociously mature neurons. Therefore, I analyzed NeuN (a marker of mature neurons) immunoreactivity in control and GOF animals. Interestingly, GOF cells in the rostral part of the V-SVZ as well as within the RMS displayed a strong tendency of increased NeuN immunoreactivity **(Fig. 9D**, rSVZ and RMS, $n_{(ctrl/GOF)}$ = 3/3 animals). To sum up, constitutive over-expression of ND6 causes significant cell retention within the V-SVZ. An increased number of cells seem to express NeuN which points towards ectopic differentiation as the cause of this cell retention. In addition, some cells seem to ectopically express Tbr1, raising the possibility that ND6 could be sufficient to induce glutamatergic fate. Unfortunately, the sample size for this experiment was insufficient to conclude about the statistical significance of these results.

2.3 Concomitant loss-of-function of NeuroD6 and NeuroD2 in the OB

Loss-of-function of ND6 alone did not cause any major defect within the OB. Therefore, I wondered whether the lack of phenotype could be due to a possible redundancy with other NeuroD proteins. ND2 can be detected within the V-SVZ (Roybon et al., 2009). Moreover, ND2 and ND6 together have been shown to act in corpus callosum formation in the cortex (Bormuth et al., 2013). In a first approach I therefore sought to confirm the presence of ND2 in the V-SVZ-OB system. I used ND2 antibody on neonatal (P2) OB tissue of $ND6^{Cre/tdTom}$ mice and found that ND2 immunoreactivity specifically colocalized with tdTom+ cells in the OB (**Fig. 10A**). Moreover, the staining was only present in putatively migrating cells situated within the GCL and not in cells that had arrived at their final location within the GL (**Fig. 10A**, right). This expression pattern is highly reminiscent of the expression of ND6 itself, further pointing towards the possibility of functional redundancy between these two proteins.

Unfortunately, constitutive double knockouts, as used in the study by Bormuth et al., (2013) are lethal at birth, which makes it impossible to study postnatally generated neurons. However, Antoine de Chevigny, a former member of our lab, has generated a conditional ND2 mutant where most of the coding region is flanked by loxP sites. Thus, I bred $ND2^{flox}$

mice to the inducible ND6$^{CreERT2/tdTom}$ line (ND2/ND6) to study the effect of the deletion of both genes within the glutamatergic JGC population.

In a first attempt, given the fact that previous analysis of ND6 HO animals did not show an obvious defect, I considered ND6 single mutants (sHO) as controls and compared them to ND2/ND6 double mutants (dHO). Unfortunately, subcutaneous injection of TAM into P0 dHO pups frequently led to death. The high lethality in double mutants induced at birth could be explained by respiratory failure, also observed in constitutive double mutants (Bormuth et al., 2013). Indeed, at P0 the nucleus of the solitary tract (a part or the pre-Bötzinger complex that controls respiration) expressed ND2 and ND6 (Olson et al., 2001; Lin et al., 2004; Goebbels et al., 2006). Systemic induction with TAM could cause a deleterious effect in these cells and cause postnatal lethality. I therefore changed the induction strategy and induced ND2/ND6 pups with intraventricular injection of the metabolically active component Hydroxytamoxifen (4OH-TAM). I adjusted 4OH-TAM concentration to 500 µM, which allowed for only local recombination of V-SVZ residing progenitors that, after migration through the RMS, settle in the OB. I validated this induction approach by staining the OB of dHO animals with ND2 antibody at 7 days post induction (dpi), a time point were most cells have arrived to the deeper layers of the OB and where ND2 immunoreactivity can be readily quantified. Indeed, quantification showed that 89% of tdTom cells express ND2 in sHO, whereas only 21% of tdTom cells expressed ND2 in dHO animals (n = 2 animals).

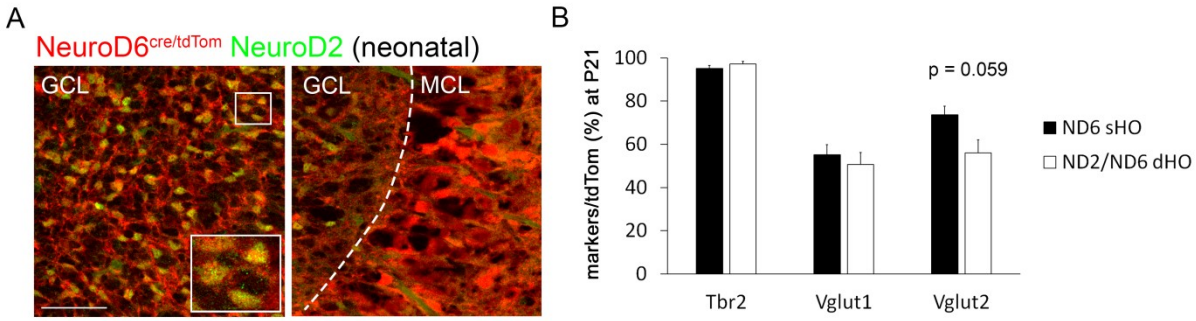

Figure 10. Loss-of-function of ND2 and ND6 does not alter molecular identity of glutamatergic JGCs. **(A)** Coronal OB section of neonatal (P2) ND6$^{cre/tdTom}$ mouse. At this time point many tdTom+ cells are found within the GCL (see Results part I, Figure 4). TdTom+ cells located within the GCL show immunoreactivity for NeuroD2 while no colocalization is found in tdTom+ cells that have crossed the MCL. Presence of ND2 in tdTom+ cells is confirmed.**(B)** Colocalization of glutamatergic markers with tdTom+ cells in single homozygous ND6 (sHO) and double homozygous (dHO) ND2/ND6 mutant at P21. There is a tendency towards less Vglut2 expression in dHO compared to sHO ($p = 0.0059$, not significant $p > 0.05$, two-tailed Mann Whitney U test, $n_{(sHO/dHO)}$ = 273/252 cells, 9/6 animals). Error bars indicate SEM. GCL: granule cell layer. MCL: mitral cell layer. Scale bar: (A) 50 µm.

Finally, I set out to study the phenotype of ND2/ND6 double mutant cells from animals induced by intraventricular 4OH-TAM injection. Quantification of Tbr2, Vglut1 and Vglut2 at 21 dpi showed no significant difference in any of these markers between the sHO and dHO animals (**Fig. 10B,** Tbr2: 95.17 ± 01.36% for sHO and 97.11 ± 1.35% for dHO; Vglut1: 55.17 ± 4.63% for sHO and 50.71 ± 5.56% for dHO; Vglut2: 73.65 ± 3.98% for sHO and 55.97 ± 6.18% in dHO). Tbr1 could not be quantified due to experimental problems with a new antibody lot. Gross morphology of the cells seemed unchanged and all three JGC types were present. Thin axonal projections were also visible in most cells and showed immunoreactivity with axonal initial segment marker AnkG (data not shown). Therefore, these morphological features were not further analyzed.

In conclusion from these initial experiments, single ND6 or double ND2/ ND6 deletion in glutamatergic JGCs did not cause changes in their molecular identity nor in their gross morphology pointing towards the possibility of a more subtle, physiological effect with implications on synaptic transmission or integration for example. Alternatively, redundancy with the third NeuroD family member, ND1, which is also expressed in a sub-fraction of glutamatergic JGCs seems also plausible (Roybon et al., 2015).

3. Two-photon calcium imaging of odor-evoked neuronal activity in ND6^{Cre} mice

Although olfactory processing has long been a subject of intensive study, only recently has the emergence of ultra-sensitive calcium indicators and state-of-the-art microscopy allowed addressing these concepts by direct *in vivo* recordings. Within the processing circuit of the glomerular layer, ETCs are thought of taking a crucial role as signal gatekeepers to M/T cells. However, no study has addressed whether and how excitatory ETCs actually respond to odor stimulation *in vivo* and whether they really gate odor information.

In this study, I will start to address these questions. Moreover, I will use a to date unprecedented approach of analyzing not only single ETCs, but analyze their odor-evoked activity in the context of circuit-related cell ensembles affiliated to the same glomerulus.

3.1 Matherials and Methods

Mice. For this study, NeuroD6^{Cre} (ND6^{Cre}) knock-in mice (Goebbels et al., 2006) were bred with Rosa6^{tdTomato} reporter mice (Ai14, Jackson Laboratories, stock-number 007914) and GCaMP6s mice (Jackson Laboratories, stock-number 007914). Mice of both sexes were used.

Implantation of cranial window. When mice reached 4 weeks of age, I surgically implanted a cranial window above the right OB. The cranial window allowed for better visibility than a thin-skull preparation which also resulted in less laser power needed for successful imaging of fluorescent changes in glutamatergic JGCs. Briefly, mice were anesthetized i.p. with ketamine/xylazine (125 and 12.5 mg/kg, respectively). Additional subcutaneous injections of Carprofen (5 mg/kg), Dexamethasone (0.2 mg/kg) and Buprenorphine (0.3 mg/kg) where performed at the beginning of the surgery. Skin over both OBs was incised with a surgical scalpel blade (No. 24, Swann-Morton Ltd) and gently pushed aside to expose the skull. Surface of the skull was scrubbed with the scalpel and cleaned with 10% citric acid to ensure adhesion. A custom-made metal bar was then fixed caudally to the OBs using first superglue and then dental cement (Super-Bond C&B). Subsequently, the mouse was attached to a stereotaxic apparatus (Harvard Apparatus), using the metal bar. The skull was then gently thinned using a surgical scalpel blade (No. 15, Swann-Morton Ltd) until a thickness of approximately 20-30 was reached over the desired area. During this procedure great care was taken not to exert excessive pressure and to avoid bleeding or drying of the skull. Finally, using a sharp surgical scalpel blade (No. 11, Swann-Morton Ltd), a small rectangular area was incised very carefully without damaging the *dura mater*. The rectangular piece of skull was carefully removed with forceps. A small drop of translucent silicone (Kwil-Sil low toxicity Silicone Adhesive, WPI) was placed over the window and a 3 mm cover slip quickly placed on top. The cover slip was sealed to the skull using a drop of superglue and dental cement. The preparation was left to dry for 1-2 min. The animals were allowed to recover from surgery for one week before the imaging session started to avoid any inflammation-related artifacts in neuronal activity.

Calcium imaging. For imaging, mice were anesthetized i.p. with ketamine/xylazine (125 and 12.5 mg/kg, respectively) and a clear field of view (600 x 600 µm) was chosen using a 20x/1.0 NA objective on a 7MP two-photon microscope (Zeiss). Before the protocol for odorant stimulation started, a Z-stack of the entire field of view of a depth of approximately 250 µm (2 µm step in the Z dimension and 0.6 µm lateral resolution) was acquired. Using this approach, I was able to identify the focal plane used for calcium imaging within the Z-stack, reliably reconstruct and assign JGCs to their affiliated glomeruli and identify their morphological subtype. Subsequent calcium imaging was performed at three different dorso-ventral levels of the GL, each 20 µm apart. This approach allowed for more complete sampling of JGCs affiliated to each given glomerulus, as well as to assess the degree of response homogeneity within the glomerulus. Images were analyzed and processed with

ImageJ (NIH) software. Calcium transients were analyzed using a custom made Matlab-based interface (Platel et al., 2007). Data was normalized to the resting level of flourescence and threshold of calcium transients was fixed at for increase and decrease at 20% dF/F0. Peaks were automatically detected but manually curated.

Olfactometry. Odors were delivered using a 6-valve liquid dilution olfactometer (Knosys Olfactometers). Commercially available odorant molecules were diluted in mineral oil to obtain either 0.1% or 1% odorant dilutions. Odors used in this study were aldehydes (propanal, butanal) and esters (isoamyl acetate, isoamyl butyrate, ethyl tiglate) known to activate dorsal glomeruli (Adam et al., 2014). All odors were purchased at the highest possible degree of purity (> 98%) from Sigma-Aldrich. The experimental protocol included 8 seconds of delivery exhaust, 3s (5s in rare cases) odor stimulation and 25s of inter-stimulation-intervals (ISI). At the beginning of each session, animals were stimulated with clean air as a control. Rare cases of glomeruli that responded to clean-air stimulation were not analyzed. All stimulations were repeated once. Images were acquired at a 2 Hz rate.

3.2 Characterization of odor-evoked responses in glomeruli of anesthetized ND6^{Cre} mice

In a first approach I focused on fluorescent changes within the neuropil of glomeruli. Given the fact that in ND6^{Cre} mice, JGCs but also M/T cells are recombined (**Fig. 11A**, left), I took great care to exclude the cell body and the main arborization of ETCs from the ROI of the glomerulus (**Fig. 11A**, right). Therefore, it seems conceivable that the glomerular fluorescent signals I measured, represent mainly apical M/T cell dendrites. It is nevertheless possible that this signal is slightly polluted by fluorescence coming from fine dendritic ETC processes. OSN axonal projections are not recombined in ND6^{Cre} mice (**Fig. 11A**, left, nerve layer is tdTom negative). Imaging at low magnification allowed for the visualization of GCaMP signals from approximately 20 glomeruli simultaneously (**Fig. 11A**, right). Resting GCaMP fluorescence levels were variable and some glomeruli displayed spontaneous fluorescence transients. However, amplitude of spontaneous activity was always weak and occurred rarely.

Odorant presentation evoked different types of responses: increase and decrease in GCaMP fluorescence as well as mixed profiles containing both elements mapped to individual glomeruli (**Fig. 11A** right**, B**). Odor responses varied in onset latency, signal rise and decay time, amplitude, duration and shape. However, for the current analysis these parameters were not considered. Instead, I grouped odor-evoked responses into discrete categories which I labeled (1) plateau (prolonged excitation), (2) peak (acute excitation), (3) excitation followed

by inhibition (ex-inh), (4) inhibition followed by excitation (inh-ex), (5) pure inhibition and (6) no response (no) (**Fig. 11B**). Although this categorization does not take into account the heterogeneity and thus full complexity of the odor response, this reductionist approach allows for simplification and more global assessment of odor-evoked profiles.

Among 5 different monomolecular odors used in this study, ethyl tiglate (ET) and butyrate (BUT) were capable of evoking responses in more than 60% and 80% of glomeruli, respectively, while the remaining three odors (propanal (PRO), isoamylbutyrate (IAB) and isoamylacetate (IAA)), evoked responses in only 30% of the glomeruli within the field of view (**Fig. 11C**). In 59 analyzed glomeruli, 81% responded to at least one of the presented odors. Across all glomerulus-odor pairs, 47% showed an odor response, while 53% did not. Among responding glomeruli, excitatory responses were most frequently observed (5% plateau and 69.5% peak), followed by composed responses (13% ex-inh and 1.5% inh-ex). Pure inhibitory responses were least frequently observed in only 11% of responding glomerulus-odor pairs (**Fig. 11C,** n = 436 glomerulus-odor pairs in 5 animals).

In general, glomeruli displayed coherence of odor-responses in at least two of three dorso-ventral levels. However, a fraction of glomeruli displayed some degree of modulation: for example a peak response could become an ex-inh response in the next focal plane but change in response sign (from excitation to inhibition) was not observed. For the current analysis, I compared two approaches of data analysis: (1) when all three planes were considered as one glomerulus and (2) considering all planes separately. Both quantifications yielded a highly similar result but the approach considering all planes separately yielded a more diversified picture of response profiles which is why for the current analysis I chose to represent the results using this latter approach.

The ability to directly visualize OB glomeruli allows for the characterization of functional organization of activation and inhibition within the glomerular map *in vivo*. Glomerular response profiles were odor-specific and spatially intermingled (**Fig. 11D**). Excited glomeruli were situated next to inhibited or not responding glomeruli and this map changed upon presentation of a new odor. Time courses (traces) of different glomeruli stimulated with different odors reveal that glomeruli are able to change nearly all aspects of their response like onset latency, amplitude and duration depending on the odor presented (**Fig. 11E**).

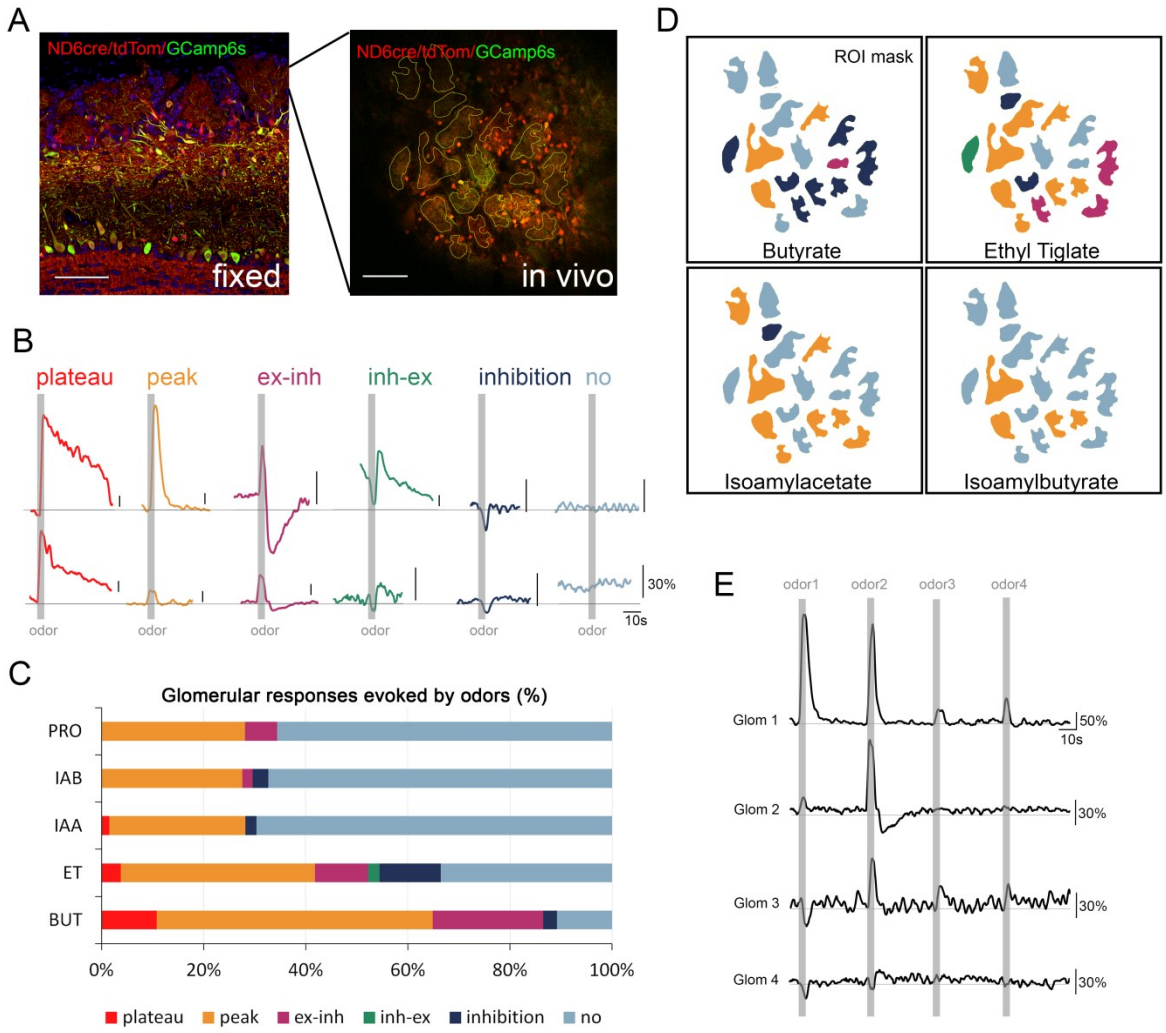

Figure 11. Odor-evoked excitation and suppression in OB glomeruli of anesthetized ND6^{cre}/tdTom/GCaMP6s mice. **(A)** Left: representative image of GCaMP6s expression in glutamatergic JGCs and M/T cells of ND6$^{Cre/tdTom}$ mice. Right: Two-photon image of GCaMP expression in dorsal glomeruli *in vivo*. Fluorescent changes in glomeruli were interpreted as signals mainly from M/T cells. Blue stain represents nuclear marker Hoechst. Scale bar: 100 µm. **(B)** Two examples of categories of fluorescent changes (dF/F) in dorsal glomeruli upon odor presentation (grey). Response profiles were classified into plateau (prolonged excitation, red), peak (acute excitation, orange), excitation followed by inhibition (ex-inh, magenta), inhibition followed by excitation (inh-ex, green), pure inhibition (dark blue) and no response (no, grey) relative to baseline fluorescence. All scale bars (bottom right) represent 30% dF/F. **(C)** Relative occurrence of odor-evoked glomerular response profiles (n = 436 glomerulus-odor pairs in 5 animals) according to odors: propanal (PRO), isoamylbutyrate (IAB), iasoamylacetate (IAA), ethyl tiglate (ET) and butantal (BUT). **(D)** Pseudocolored glomerular activation maps evoked by four different odors. For color code, see (B). Note that the same glomeruli respond differently with changing odors. **(E)** Four examples of diverse odor-specific glomerular (Glom) response profiles upon presentation of four different odors. Note that not only sign of response can change but nearly all aspects of signal onset and shape as well. Scale bars (bottom left) represent either 30% or 50% dF/F0.

3.3 Concentration-dependent changes of glomerular response profiles

Next, I asked whether and how concentration-dependent changes of odorants impact glomerular response profiles. To this end, I exposed animals to the same odor at two concentrations (0.1% and 1%) and quantified the amount of activated glomeruli, as well as their sign of response (n = 638 glomerulus-odor pairs in 4 animals). Interestingly, increased odor concentrations did not only engage more glomeruli into a response, but also increased heterogeneity in response signs: on average, excitatory responses (plateau and peak) increased 16.85 ± 1.32%, composed responses (ex-inh and inh-ex) increased 9.81 ± 5.72%, inhibitory responses increased 2.04 ± 0.86% and the null-responses decreased 38.78 ± 24.5% across the three odors used at two concentrations (**Fig. 12A**). Some glomeruli did not exhibit detectable changes in response to both concentrations (**Fig. 12B,** first two traces), while others showed variable degrees of response modulation (following three traces) and yet other glomeruli showed reversal of response sign (last trace). This data, although still fragmentary, indicates that concentration-dependent changes are glomerulus and odor-specific. However, it opens the intriguing question to what extend these changes are also reflected in response profiles of JGCs. This analysis is still under progress.

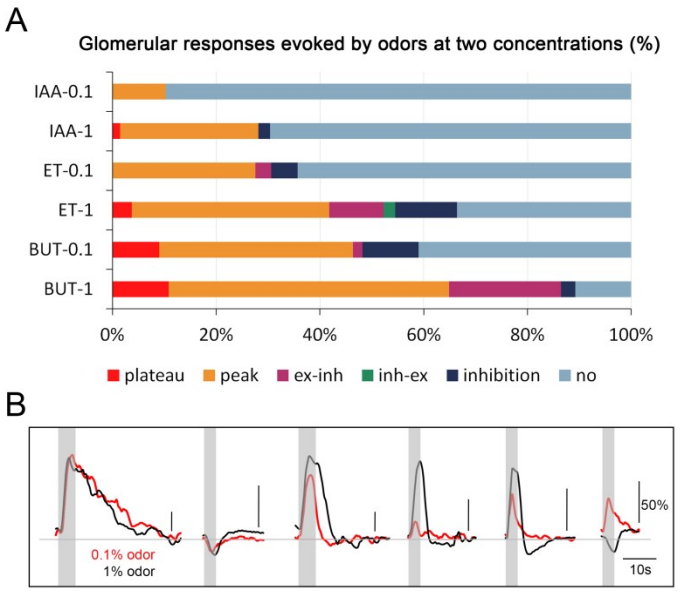

Figure 12. Higher odor concentrations recruit more activated glomeruli and more diverse response-profiles (A) Relative occurrence of odor-evoked glomerular response profiles (n = 638 glomerulus-odor pairs in 4 animals) for three odors (IAA, ET, BUT) at two different concentrations (0.1% and 1%). Note that with increasing odor concentration, more glomeruli show an odor-evoked response and response profiles become more diverse. **(B)** Examples of traces (dF/F) of selected glomeruli elicited upon odor stimulation (grey) at different concentrations. Note how some response profiles do not change significantly at the two different concentrations (first two traces), some become modulated with changing

concentration (following three traces) and some can change sign of response (last). Scale bars (bottom left) represent 50% dF/F0.

3.4 Relating JGC response to glomerular response profile

Finally, I wanted to relate the previously characterized odor-evoked glomerular response profiles to the response profiles of JGCs affiliated to these glomeruli. For this analysis I chose a few glomeruli in each field of view which showed a strong odor-evoked response of any sign. Then I identified all cells in close proximity of the glomerulus of interest (**Fig. 13D,** left). Using the Z-stack obtained at the beginning of the imaging session, I was able to unequivocally assign the cells to their respective glomeruli based on the location of their dendritic branching. I took advantage of the high quality of the preparation and opted for an even more detailed morphological analysis, assigning all identified cells to the three previously described classes of external tufted cells: external tufted cells without secondary dendrites (ETC), bitufted ETCs (biETC), ETCs with secondary dendrites (secETC, **Fig. 13A**). Whenever morphological identification was not possible, I assigned these cells to the category "unknown". When considering all three planes of one glomerulus as a whole, I could assign on average 19 cells per glomerulus in a total of 38 glomeruli successfully sampled at these three levels (n = 5 animals). Within these 38 glomeruli, I found on average 52% ETCs, 9% biETCs, 13% secETCs and 26% unknown cells (**Fig. 13B**). Next, I wanted to know whether a particular cell type was biased towards a certain response profile. The analysis of 565 cell-odor pairs (n = 5 animals) revealed that the relative occurrence of response profiles was similar among all cell types (**Fig. 13C**). Among these cell-odor pairs, I observed that 67% of the cells also showed a response while in 33% of cells no odor-evoked response was detected. Among responding cells, I found that excitatory responses were the most prevalent (22% plateau and 62% peak responses), followed by composed responses (10% ex-inh and 2% inh-ex). Particularly interesting was the observation that indeed ETCs can also be inhibited which corresponded to 5% of active cells.

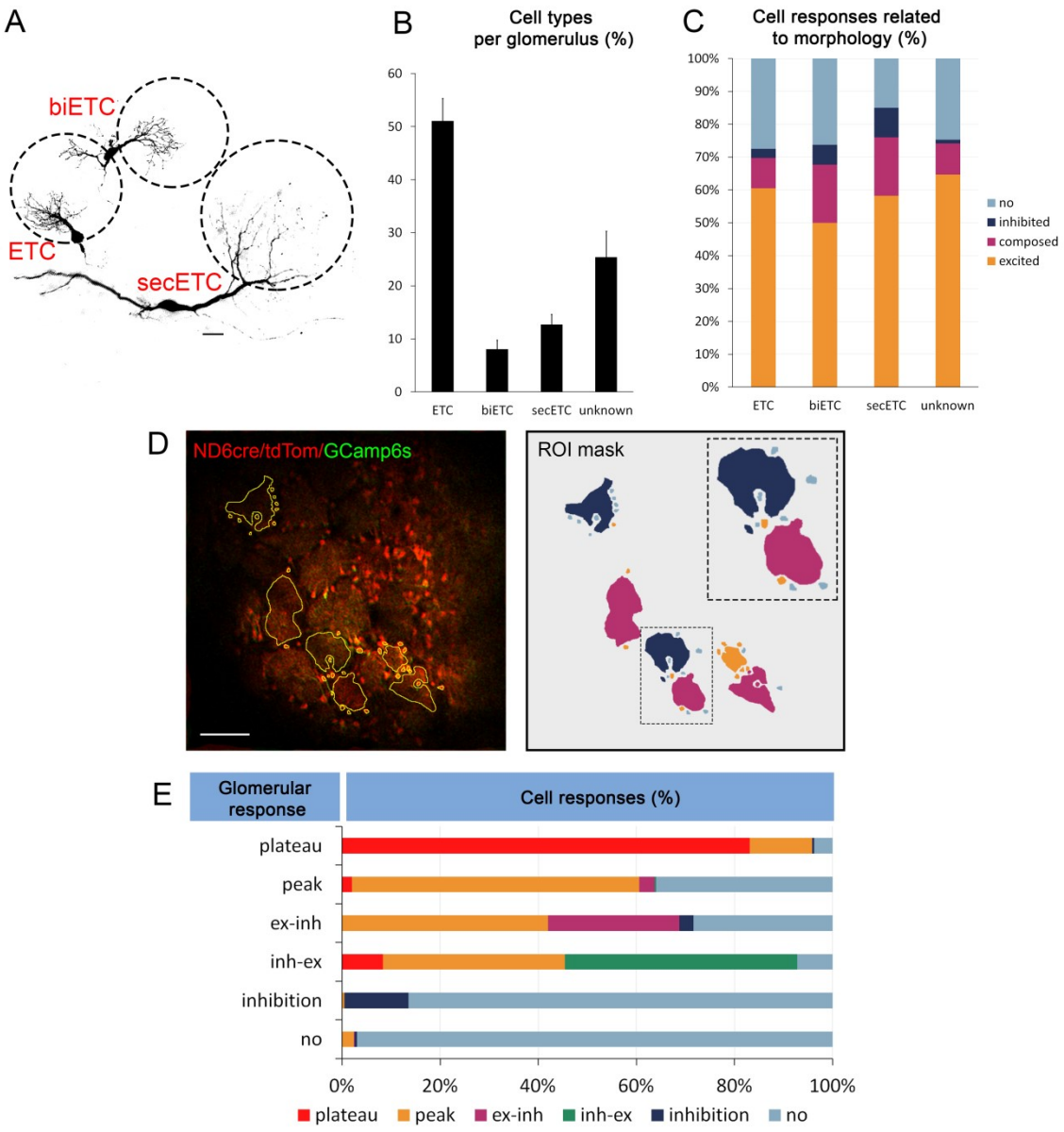

Figure 13. Relating odor-evoked response profiles of JGCs to glomerular response. **(A)** Three morphological cell types clearly innervate glomeruli in ND6$^{Cre/tdTom}$;GCaMP6s mice: external tufted cells (ETC); bitufted external tufted cells (biETC); external tufted cells with secondary dendrites (secETC). For more information on these cell types see Results part I, Figure 5. Morphology of neurons was identified based on a Z-stack taken from the *in vivo* field of view. Scar bar: 10 µm. **(B)** Mean composition of cell types identified for analysed glomeruli. Note that whenever morphology could not be assigned unequivocally, the cell was labeled "unknown". (n = 389 cells in 5 animals). Error bars indicate SEM. **(C)** Relative occurrence of odor-evoked response profiles according to cell type using a battery of 5 different odors (n = 565 cell-odor pairs in 5 animals). Note that for easier depiction response, the profiles plateau and peak were pooled (excitatory), as well as ex-inh and inh-ex (composed). **(D)** Right: Two-photon *in vivo* image of GCaMP expression in dorsal glomeruli. Several glomeruli that displayed odor-evoked responses were chosen. ROIs (yellow) were placed on glomeruli and somata of neurons which belonged to the respective glomerulus (identified by Z-stack). Great care was taken to exclude any cell bodies on top of the glomerular ROI. Left: Pseudocolored ROI mask of chosen glomeruli and neurons using the before established color code. Note that cell responses are heterogeneous in respect to glomerular responses (inlay). Scale bar: 100 µm. **(E)** Relative composition of response profiles in cells affiliated to a glomerulus with a given response. (n = 305 glomerulus-odor pairs with 1789 affiliated cell-odor pairs in 5 animals). Note that although the glomerular response profile is always represented

among cellular responses, there is also a high degree of heterogeneity in cell response profiles affiliated to the same glomerulus.

Having established that response profiles of glutamatergic JGCs occur independently of cell morphology, I went on to relating these cellular responses to the response profile of their affiliated glomerulus (**Fig. 13D,** left). I observed in glomeruli that showed excited or composed response profiles that approximately 60-90% of the affiliated JGCs were engaged in a response (96.25% JGCs active in glomerular plateau-response, 64.06% JGCs active in peak-response, 71.63% JGCs active in ex-inh-response, 92.8% JGCs active in inh-ex-response). The majority of these cells showed responses of the same sign. However, while the latter is also true for the "responsive" fraction of JGCs in inhibited glomeruli, most JGCs did not show any detectable response (only 13.55% JGCs active in null-responding glomeruli). A small fraction of JGCs (3.02%) also showed responses when no response was detected at the glomerular level (**Fig. 13E**). Nevertheless, when comparing cell response profiles to glomerular response profiles I could observe a certain degree of heterogeneity in cellular responses within the same glomerulus (**Fig. 13D,** right (inlay), **E**). This was true when each plane was considered separately as well as when glomeruli across all three planes where considered as a whole. Overall, this result also validates that the glomeruli recordings reflect indeed M/T cell activity. To sum up, the presented data indicates that all three ETC types engage equally into all response profiles. Moreover, majority of ETCs affiliated to the same glomerulus show responses of the same sign as the glomerular response. The heterogeneity of responses possibly indicates the existence of sub-circuits within one glomerulus.

DISCUSSION

4.1 NeuroD6 expression is transient and confined to glutamatergic OB progenitors

ND6 expression has been described for a multitude of brain areas including the neocortex, hippocampus, as well as some mid- and hindbrain structures (Goebbels et al., 2006). Interestingly, while studies that have investigated ND6 expression in detail agree upon the fact that promoter activity starts at the level of postmitotic progenitors, expression maintenance varies greatly according to brain area and possibly protein function (Wu et al., 2005; Goebbels et al., 2006; Kay et al., 2011). Using a battery of markers in the V-SVZ I found no colocalization of tdTom with the stem cell marker Pax6, rare co-localization with intermediate progenitor marker Ki67, and full overlap with postmitotic marker Tbr1. This indicates that also in the postnatal V-SVZ, ND6 is expressed in postmitotic progenitors(Brill et al., 2009). These results are further corroborated by my observations from lineage tracing experiments with ND6$^{CreERT2/tdTom}$ mice where I obtain a defined cohort of recombined neurons after induction. Moreover, the lack of recombined cells within the VZ with radial glia-like or ependymal cell morphology argues against the possibility that ND6 is expressed in RGCs at their last round of division before becoming ependymal cells. Finally, the absence of fluorescent neurons within the GL at 1 dpi indicates that ND6 promoter is not active once neuroblasts reached their target layer. Altogether, these data show that ND6 is transiently expressed starting from postmitotic progenitors and stopping before final neuronal integration.

4.2 Glutamatergic JGCs are morphologically heterogeneous and project axons across the OB

The OB is dominated by inhibitory transmission, with the vast majority of neurons being GABAergic (Parrish-Aungst et al., 2007; Burton, 2017). However, locally connecting excitatory OB neurons like short axon cells (Brill et al., 2009) and external tufted and bi-tufted cells (Hayar et al., 2004a; Hayar et al., 2004b) constitute an important part of the OB circuitry. With the emergence of lineage tracing in mouse mutants two studies have shown that these JGCs are also produced postnatally (Winpenny et al., 2011) and to a lesser extent even in adult (Brill et al., 2009). In agreement, I show that few short axon cells (SACs) as well as well as external tufted and bi-tufted cells (ETCs) are indeed generated at perinatal stages. However, glutamatergic SACs were extremely rare and thus, it was difficult to assess to what extend their morphology really corresponded to the classical description for

GABAergic SACs (Pinching and Powell, 1971a; Kiyokage et al., 2010) or the rather anecdotic population of adult born glutamatergic SACs (Brill et al., 2009). The morphological classification of SACs is particularly delicate since some studies define SACs as purely interglomerular cells while others include cells that display an intraglomerular tuft-like dendritic branching (Hayar et al., 2004; Kiyokage et al., 2010). This difference would have important functional implications for their circuit function. Interestingly, external tufted cells with secondary dendrites (secETCs) could very well correspond to this second type of SAC. Moreover, the fact that there is also a subfraction of inhibitory Vglut3+ ETCs, some of which have secondary dendrites (Tatti et al., 2014), raises the possibility that the confusion around SACs and secETCs is more of a semantic issue than a biologically relevant one. To conclude, in this study I show that the majority of glutamatergic perinatally born JGCs are ETCs. Moreover, the overall neuron production drops drastically and rapidly after birth.

In addition, I provide evidence for two types of axonal projections in perinatally born JGCs; type-1 projections that remain within the glomerular layer and type-2 projections that contact less glomeruli and dive deep into the core of the OB. It is unlikely that type-1 projections represent truncated type-2 projections because frequently along the thin axon, thick swollen axonal boutons were visible. Generally, type-1 axons terminated in a clearly visible bouton indicating the true end of the axon. This also reflects the strength of the experimental approach, using cleared whole brains rather than sections. Subsequent retrograde tracing shows that some glutamatergic JGCs project even across the medio-lateral aspects of the OB. This finding suggests that type-2 projections belong to the intrabulbar associated system, also called mirror-symmetric isofunctional odor columns and connect medio-laterally located homotypic glomeruli (Liu et al., 1994; Grobman et al., 2018). The existence of two different axonal projection patterns suggests that type-1 and type-2 projecting ETCs form two functionally different circuits. Type-1 projecting ETCs could be implicated in odor processing mechanisms of nearby glomeruli while type-2 projecting ETCs connect homotypic glomeruli activated by the same odor stimulus. It would be very interesting to know the postsynaptic target of type-1 projecting ETCs. Dependent on whether they project to GABAergic PGCs/SACs or excitatory ETCs of close-by glomeruli, they could mediate either interglomerular inhibition or activation, respectively. This is intriguing insofar, as the current model of odor-processing within the GL, only SACs have been attributed a function in interglomerular inhibition (Burton, 2017). Moreover, one could also imagine that selective interglomerular excitation could contribute to the odor code.

4.3 Perinatally born glutamatergic JGCs resist sensory deprivation

How does environmental information impact glutamatergic JGCs? Sensory deprivation by unilateral naris occlusion is a powerful approach to investigate this question within the OB brain circuitry. There is a well-established body of literature that shows how olfactory sensory deprivation causes cell death throughout all OB layers (Najbauer and Leon, 1995; Mandairon et al., 2006) thereby emphasizing the importance of sensory input for survival of OB interneurons (Petreanu and Alvarez-Buylla, 2002; Rochefort et al., 2002; Yamaguchi and Mori, 2005). However, when it comes to the specific effect of naris occlusion on neuronal subtypes, studies yield contradicting results. For example, while the seminal works of H. Baker (Baker, 1990; Baker et al., 1993) suggested that dopaminergic interneurons loose TH expression but do not die, more recent studies (Bastien-Dionne et al., 2010; Sawada et al., 2011) suggest that indeed these neurons undergo apoptosis. Likewise, while Kato and colleagues (Kato et al., 2012) found that CalR JGCs die under occlusion, other studies have suggested the contrary (Philpot et al., 1997; Bastien-Dionne et al., 2010; Sawada et al., 2011). These conflicting results are probably due to different approaches on how cell survival is monitored (BrdU pulse-chase, histological markers, *in vivo* imaging) and respective model systems (rats and mice, different mouse strains).

I used a chronic *in vivo* imaging approach to directly monitor the survival of a to-date unexplored OB interneuron population, glutamatergic JGCs. In addition, I compared these neurons to a population of GABAergic JGCs which include TH+, CalR+ and purely GAD65/67+ neurons. In the first imaging session, I identified individual fluorescently labeled GABAergic and glutamatergic neurons and follow them over a few weeks in control situation and under occlusion. I demonstrate that while a small but significant fraction of GABAergic JGCs disappear, the vast majority of glutamatergic JGCs remain in place under unilateral naris occlusion.

This result bears two implications. First, GABAergic cell death induced by sensory deprivation is present but not as extensive as previously assumed (in some cases up to 50% of cells). The majority of studies that have demonstrated extensive GABAergic cell death under occlusion did so by using the thymidine analog BrdU (Mandairon et al., 2006; Bovetti et al., 2009; Bastien-Dionne et al., 2010; Kato et al., 2012). However, in a seminal study from our team, we demonstrated that at the most commonly used concentration of 50 mg/kg, BrdU itself causes neuronal death (Platel et al., 2018, under revision, see **Appendix III**). In fact, the only other study that has investigated the effect of sensory deprivation using a direct chronic

in vivo approach has obtained a comparable amount of roughly 12% of GABAergic cell death using VGAT- (vesicular GABA transporter) Venus reporter mice (Sawada et al., 2011). Therefore, given the many pitfalls of indirect observation, it seems that the method-of-choice to study neuronal survival has to be direct, like for example *in vivo* imaging. Moreover, it will be of great interest to perform *in vivo* imaging using mouse mutants that allow the "online" identification of OB subtypes and to understand the possibly differential impact of sensory deprivation on these neurons.

Second, the fact that some GABAergic but not glutamatergic JGCs die upon occlusion, shows unequivocally that the OB does not fall into a state of general apoptosis under sensory deprivation. Rather, one could view the OB system as an intricate homeostatic balance between excitation and inhibition, finely tuned by the environmental challenges imposed to the system. Although the importance of a balance between excitation and inhibition has been demonstrated in many sub-systems of the brain (Dehghani et al., 2016; Spitzer, 2017; Mongillo et al., 2018), a prevailing concept of neuronal survival states that no activation means cell death (Pfisterer and Khodosevich, 2017) However, if we move away from this single-cell view (no activity equals cell death) towards a more network-based view (homeostasis), one could imagine that a sudden local excitation-inhibition misbalance caused by sensory deprivation could lead to excessive increase of inhibition in the network. In this scenario, the decreased environmental excitation has to be counter-acted by an overall decrease in bulbar inhibition, allowing the system to still confer information to higher order brain areas. Since adult neurogenesis provides the OB continuously with inhibitory interneurons, directed apoptosis of some of these cells could be a feasible mechanism to fine-tune inhibitory elements of the OB system. Accordingly, one could also imagine that excitability in excitatory OB neurons increases to further facilitate signal transmission. Moreover, apoptosis is likely not the main adaptation of the OB to deprivation as can be seen by the drastic shrinkage in OB volume (up to 30%) upon occlusion which most likely represents loss of neurite complexity instead of cell death.

Conceivable approaches to address this homeostasis hypothesis could be to perform calcium imaging of odor-evoked activity in glutamatergic JGCs just after reopening of an occlusion. Increased excitability of these neurons would support the proposed hypothesis. An even more direct way to test for the presence of an excitation-inhibition imbalance that could cause GABAergic cell death in the OB, is to decrease inhibition provided by GABAergic neurons, chemogenetically (by e.g. electroporation of a hm4Di DREADD construct) while under

occlusion (using chronic *in vivo* observation). If the proposed hypothesis is correct, we should expect inhibited GABAergic neurons to survive under sensory deprivation.

Further experiments are clearly needed to elucidate why cell death occurs selectively to some elements of the OB circuit and not to others. More neuronal subtypes need to be studied and more parameters, other than cellular survival need to be examined. However, the results of this study represent a first step towards a more differentiated view of the OB network where both, local excitation as well as inhibition are provided and adjusted by the interplay of an intricately complex network with its environment.

4.4 Function of NeuroD6 in the olfactory bulb

NeuroD proteins are an intriguing transcription factor family. They have highly overlapping but distinct expression patterns across the central nervous system (Schwab et al., 1998). They exhibit a high degree of redundancy when co-expressed within a particular cell-type but exert completely different functions within different brain sub-systems, like cell survival (Khan et al., 2017), cell fate determination (Kay et al., 2011) or axonal guidance (Bormuth et al., 2013). The only common denominator of these studies is that NeuroD proteins are expressed post-mitotically and their preferential presence in excitatory cells. Both aspects point towards a role in early maturation stages, specific to excitatory cells. Therefore, I set out to study the function of NeuroD6 in glutamatergic JGCs of the OB.

4.4.1 ND6 is dispensable for the generation of glutamatergic JGCs

To study loss-of-function of ND6 in glutamatergic JGCs, I used heterozygous (HET) and homozygous (HO) $ND6^{Cre}$ knock-in mice where Cre-recombinase substitutes most of the ND6 coding region. Comparison of total cell number present in the GL at P21 showed no obvious difference between HET and HO mice. However, the sample size is small and the values quite variable. Therefore it would be of interest to repeat this analysis and unequivocally confirm this result.

Using a battery of markers (Tbr1, Tbr2, Vglut1, Vglut2) I asked whether the glutamatergic identity of HO cells was compromised. However, I found no change in the expression of these markers in tdTom cells, pointing towards no role in glutamatergic fate determination of NeuroD6 in the OB system. Also gross morphology seemed unchanged and all JGC subtypes were present, further excluding a role in dendritic maturation or JGC subtype specification.

The lack of phenotype in $ND6^{Cre}$ mutants raised the possibility of redundancy with other NeuroD proteins. Since ND1 was present only in a subpopulation of glutamatergic JGCs (Roybon et al., 2015), I turned to ND2 as a candidate. Using immunostaining, I confirmed the presence of ND2 in the OB. Strikingly, ND2 was strictly confined to tdTom cells and only during their immature migratory phase; an expression pattern highly reminiscent of ND6. This finding indeed suggested possible redundancy between ND2 and ND6 and so I set out to study ND2/ND6 double mutants.

Constitutive ND2/ND6 mutants die after birth due to respiratory failure (Bormuth et al., 2013). Therefore, I used conditional $ND2^{flox}$ mice which I bred to inducible $ND6^{CreERT2}$ mice. I analyzed expression of the markers Tbr2, Vglut1 and Vglut2 in tdTom cells of ND2/ND6 double homozygous (dHO) mice which I compared to homozygous ND6 single mutants (sHO) at P21. No significant difference was found in colocalization of these markers with tdTom cells in dHO and sHO animals. However, there was a tendency towards decrease in Vglut2 immunoreactivity in dHO compared to sHO. Two inevitable flaws of the approach could contribute to masking a potential effect in dHO animals: (1) quantification of efficiency of recombination using 4OH-TAM showed that an average of 21% of cells did not recombine the floxed ND2 allele while the tdTom allele recombined; this could easily dilute any observable effect; (2) the sparse induction protocol typically yields very few cells which enormously increases the variability between animals and makes a high number of animals indispensable. However, a possible decrease in Vglut2 could mean that synaptic transmission in dHO animals is indeed impeded. This is an intriguing possibility, since ND2 has been linked to synaptic transmission and synaptogenesis in cortex and hippocampus (Wilke et al., 2012; Chen et al., 2016). A possible downstream target to investigate could be the synaptic protein GAP-43 which was shown to be directly regulated ND2 (McCormick et al., 1996; Ince-Dunn et al., 2006). However, unequivocal demonstration of a defect in synaptic transmission of ND2/ND6 mutants could only be confirmed by electrophysiological recordings.

Morphological aspects like dendritic morphology and presence of axons seemed unchanged between sHO and dHO animals, making it unlikely that ND2/ND6 deficiency acts on these aspects of neuronal maturation. Given the fact that axonal guidance is the main defect the cortex of ND2/ND6 mutants it is natural to wonder if axonal targeting in dHO mutants could be affected. However, type-1 projections are too variable for quantification of changes in axonal length or branching and type-2 projections cannot be reliably tracked across the bulb.

In addition, CTB injections would be unfeasible due to too sparse labeling of JGCs in dHO cells. One feasible alternative to approach ND2/ND6 function in glutamatergic JGCs could be to study late embryonic OBs, however, in this context physiological parameters can be very difficultly assessed. Lastly, I cannot exclude additional redundancy with the third member of the NeuroD family, ND1.

4.4.2 Ectopic over-expression of ND6 points towards a role in neuronal maturation

In search of the function of ND6 in glutamatergic JGCs of the OB, I over-expressed a ND6 gain-of-function (GOF) construct by dorsal electroporation in P0 wild-type CD1 pups and sacrificed animals 7 dpe. At this time point the majority of cells typically have arrived to the deep layers of the OB in control situation (GFP electroporation). Analysis of the cell repartition at different rostro-caudal levels of the V-SVZ-RMS-OB system allows for robust assessment of defects in cell migration. Indeed, when I compared ND6 GOF to GFP electroporated cells, I found that the majority of GOF cells were retained within the V-SVZ while the majority of control cells were situated in the OB. Moreover, a substantial fraction of these cells in the rostral V-SVZ were positive for the marker NeuN, a marker typically expressed by mature cells. The increased colocalization of NeuN with GOF cells points towards the possibility that cell retention is caused by precocious maturation. Although morphology of GOF cells was not analyzed in detail, GOF cells did display rather variable neurite morphology than the typical bipolar morphology of migrating neuroblasts. No change in Tbr2 expression was observed between GOF and control cells. This is not surprising since this transcription factor marks intermediate progenitors and is situated upstream of ND6. More interestingly, an increased fraction of retained GOF cells in the rostral V-SVZ showed expression of the glutamatergic marker Tbr1. This result indicates that ND6 alone could be sufficient to induce (at least partially) a genetic program specific to glutamatergic neurons and indicates that these two genes are tightly linked in their genetic cascade. Indeed, a study that investigated the regulatory networks of bHLH proteins including ND6 found that Tbr1 was present in this module (Li et al., 2007). However, the hierarchical relationship between these two transcription factors is still not clear. It would be interesting to analyze later markers of glutamatergic neurons like Vglut1/2 to investigate whether ectopic Tbr1+ neurons could show features of functionality. However, the over-expression contruct is driven by a strong pCAG promoter which leads to an unnaturally high gene dosage in GOF cells. From induction experiments with the $ND6^{CreERT2/tdTom}$ line I have observed that recombination occurs much more efficiently in cortical pyramidal neurons than in V-SVZ progenitors. This observation

indicates that the ND6 promoter is much less active in V-SVZ progenitors and possibly bears functional implications. Therefore, I cannot exclude that strong ND6 over-expression reflects a general induction of a "generic" glutamatergic neuronal cascade, rather than one specific to OB JGCs. This concern is further corroborated by the fact that ND6 is actually expressed in migratory neuroblasts while GOF leads to migratory arrest and possibly precocious maturation.

To conclude, there are strong indications for functional redundancy between ND2 and ND6 in the OB. Over-expression shows that ND6 is strongly tied to the glutamatergic program involving Tbr1. Interestingly, in cortex, Tbr1 and also ND2 defects have been associated with synaptogenesis and excitability (Wilke et al., 2012; Chen et al., 2016; Fazel Darbandi et al., 2018). Slight decrease in Vglut2 upon ND2/ND6 deletion indicates that ND2 and ND6 could also have a role in synaptic transmission in the OB.

4.5. Odor-evoked responses of M/T cells and ETCs in anesthetized ND6^{Cre} mice

The perception of smell depends on the efficient decoding and interpretation of OSN activation patterns. For this purpose, the OB harbors a network of different types of interneurons which are engaged in postsynaptic processing of OSN inputs before the signal reaches OB output cells (Wachowiak and Shipley, 2006). Within the glomerular layer, PGCs and SACs mediate intra- and interglomerular inhibition while local excitation is provided by ETCs (Burton, 2017). ETCs have been proposed to exert a role as signal gatekeepers within the odor processing cascade (De Saint Jan et al., 2009; Banerjee et al., 2015). However, direct *in vivo* evidence for this role of ETCs is still missing. In the present study I have started to address this question by imaging odor-evoked responses of apical M/T cell tufts in glomeruli and also surrounding ETCs in young adult ND6^{Cre}/tdTom/GCaMP6s mice.

4.5.1 Glomeruli display activation, suppression and mixed responses

In ND6^{Cre} mice the glomerular neuropil is a mixture between dendritic processes from M/T cells and glutamatergic JGC processes. I took advantage of this fact and used it as a possibility to monitor both, M/T cell and ETC odor-evoked responses. In order to observe M/T cell responses, I took great care to exclude any ETC cell bodies or prominent ETC processes from the glomerular ROI. Observation of GCaMP fluorescent changes in discrete glomeruli therefore allowed me to study odor-evoked activation and suppression of M/T cells. Analysis of odor-evoked glomerular activity showed that glomeruli can be excited, inhibited

and show composed responses. I grouped response signals in discrete categories of (1) excitation, including prolonged excitation (plateau) and acute excitation (peak); (2) inhibition; (3) composed responses, including excitation followed by inhibition (ex-inh) and *vice versa* (inh-ex); and (4) no response (no). Excited responses were most frequently seen, followed by composed and inhibited responses. Glomerular responses were also glomerulus and odor-specific, as nearly all aspects of glomerular response signals (shape, duration, amplitude, etc.) could be modified by application of different odors. Moreover, excited, inhibited and composed responses were spatially intermingled in the glomerular layer. Finally, sampling glomerular fluorescent changes at three different dorso-ventral levels showed that glomeruli mostly yielded uniform responses which further supported the validity of the current approach.

The current data points towards several conclusions. First, putative M/T cell responses are entirely shaped by the surrounding circuit. The variety in M/T cell responses also raises the question to what extend different aspects of the signal (onset latency, duration, amplitude, shape, etc.) convey information which is subsequently interpreted by cortical circuits. Second, the observations in this study fall into line with two other very recent studies that, for the first time, could observe inhibition in M/T cells using calcium imaging (Economo et al., 2016; Yamada et al., 2017). The lack of sensitivity of older generations of calcium probes and the difficulty to record the generally smaller changes in fluorescence have not allowed for successful observations of inhibition. This also shows to what extend our conceptual understanding of OB processing is dependent on the technical possibilities. Third, the high degree of spatial intermingling of excitatory, inhibitory and mixed responses in M/T cells suggests that inhibition is rather selective and does not support the long standing idea of centre-surround inhibition, where an activated M/T cell causes inhibition of surrounding M/T cells to improve the signal-to-noise level of a given input (Aungst et al., 2003; Vučinić et al., 2006; Cleland and Linster, 2012). This important conclusion has already been made by Economo et al. (2016) and is supported by the current work.

4.5.2 Glomerular responses show different degrees of concentration-dependent modulation

It is still not well understood how concentration changes are coded for in the OB. Odor intensities have to be readily distinguished because they are indicative of the distance from the odor source. However, odors have also to be perceived as the same across different concentration ranges. Multiple lines of research indicate that higher odor concentrations

engage more glomeruli and thus JGCs in an odor response (Wachowiak and Cohen, 2001; Bozza et al., 2004; Wachowiak and Shipley, 2006). Recently dopaminergic SACs have been identified as important player in mediation of concentration related information to M/T cells (Banerjee et al., 2015). However, although on a global scale M/T cell output is highly filtered and remains fairly stable (Storace and Cohen, 2017), close analysis on individual glomeruli shows that MCs can respond very differently to changes in concentration (Economo et al., 2016). I asked how ETCs respond to concentration-dependent changes in odorant stimulation. To do so, in a first step I characterized glomerular response changes. I found that increasing concentrations not only increased the number of responding glomeruli but also modulated the response sign. Interestingly, while some glomeruli did not detectably change any aspect of their response with increasing concentration, other glomeruli showed various degrees of response modulation as well as inversion of response sign (from excitation to inhibition). Similar observations have also been made by Economo et al. (2016) who studied concentration-dependent responses of MCs. In a next step I wanted to analyze how these glomerular response changes relate to responses in surrounding ETCs. However, at this time point this analysis is still under progress and this data is still not available.

4.5.3 All three ETC subtypes can be activated but also readily suppressed

After having analyzed putative M/T cell responses, I deepened my analysis and extended it to include response profiles of ETCs affiliated to glomeruli. Previous studies that have combined glomerular responses to JGC response profiles, have mostly used intrinsic optical signal (IOS) imaging (Luo and Katz, 2001; Adam et al., 2014). Although IOS imaging is a reliable method that reflects OSN activity (Vincis et al., 2015), its spatial and temporal resolution is inferior to analyses with calcium sensitive indicators. Moreover, studies that investigate cell ensembles connected to the same glomerulus, rarely rely on more information than the focal plane of imaging (Adam et al., 2014). Therefore, these analyses are intrinsically error-prone because an adjacent cell does not necessarily connect to a glomerulus just because of proximity. To avoid this bias, I tracked and unequivocally assigned all analyzed cells with the help of a Z-stack, taken at the beginning of the imaging session. Therefore, the approach of the current study involved a to-date unprecedented level of precision in the analysis of cell ensembles affiliated to the same glomerulus.

In a first level of analysis, I set out to identify the morphological subtype of cells affiliated to glomeruli. I could readily identify the morphology of an average of 74% of cells per

glomerulus and assign them to the categories ETC, biETC and secETC. Next, I asked whether differed ETC subtypes could be biased towards certain response types. Quantification of response profiles revealed that all ETC types could display all response types with a similar distribution. However, the current criterion for response profiles does not take into account any other aspect than response sign. One could very well imagine differences in responses such as onset latency, response strength or response threshold among different ETCs subtypes depending on their respective sub-circuit. Type-1 and type-2 projecting ETCs could be good candidates due to their different projection patterns and probably their participation in different sub-circuits. Previous data suggests that secETCs project to homotypic mirror glomeruli (Antal et al., 2006) which is also in agreement with my observations that secETCs have type-2 projections. Therefore, analyzing secETCs compared to other ETC types in more detail could be a feasible approach to address this question. Another so far unexplored aspect of the dataset is the response of biETCs. This rare ETC type extends dendritic branches into typically two glomeruli. It will be very interesting to analyze the response sign of these cells when both glomeruli display divergent responses.

In a second level of analysis, I wanted to relate the glomerular response profile to responses in affiliated ETCs. I found that excitatory M/T responses were correlated with responses in more than 60% (for peak) and 90% (for plateau) of affiliated ETC and the majority of these cells showed a response of the same sign (excitation). Similarly, composed responses of M/T cells were correlated with 70% of responding ETCs which included excitation and composed response profiles. Interestingly, when M/T cell response was inhibited, only a minority (approx. 13%) of affiliated ETCs were engaged into a response. However, response sign of ETCs corresponded to M/T cell response sign. Finally, no M/T cell response correlated with absence of response in the majority of all affiliated ETCs (< 5% responses).

There are several implications to these data. First, the fact that I observe heterogeneous responses in ETCs affiliated to one glomerulus but homogeneous responses in glomerular neuropil across several focal planes further strengthens the validity of the current approach to use glomerular neuropil as M/T cell read-out.

Second, there is a strong correlation between responses in ETCs and M/T cells. Indeed, the present data is in agreement with the proposed OSN→ETC→M/T processing pathway. Assuming this model, my observations imply the following hypothesis: to trigger an M/T cell response which includes excitation (peak, plateau or composed response profiles), the majority of homotypic ETCs have to be engaged in a response. Although slice preparations

have shown that current injection in a single ETC could trigger M/T population bursts (De Saint Jan et al., 2009), these experimental conditions were rather artificial and did not correspond to endogenous signal strength. An alternative to this hypothesis could be that if a minimal number of ETCs receive strong excitation, they rapidly engage the majority of homotypic ETCs in a response (possibly mediated) through gap junctions, which in turn leads to M/T cell activation (**Fig. 14**). However, heterogeneity in homotypic ETC responses rather points to the first possibility.

Third, ETCs like M/T cells respond sparsely to odors. This is demonstrated by the almost complete lack of ETC responses in null-responding glomeruli. If ETCs drive M/T cell output that would imply that M/T cell response is sparse due to sparse ETC response (**Fig. 14**).

Forth, this study is the first to show odor-evoked inhibition of ETCs. There are two interesting points to this finding. (1) It is intriguing that what seems to be a rule for excitatory responses (majority of homotypic ETCs act as an ensemble) does not hold true for inhibitory responses where the majority of homotypic ETCs no dot engage into the odor-response. Instead, only a minority of ETCs shows inhibition. Could, these few cells have central positions within the glomerular circuit? Could the lack of excitatory drive "silence" the glomerular circuit? This question directly leads to (2): Could odor-evoked ETC inhibition cause M/T inhibition? In line with the OSN→ETC→M/T model, one could imagine that odor-evoked suppression of spontaneous rhythmic ETC bursts could result in lack of sufficient excitatory drive to M/T cells and therefore lead to suppression of M/T cell activity (**Fig. 14**).

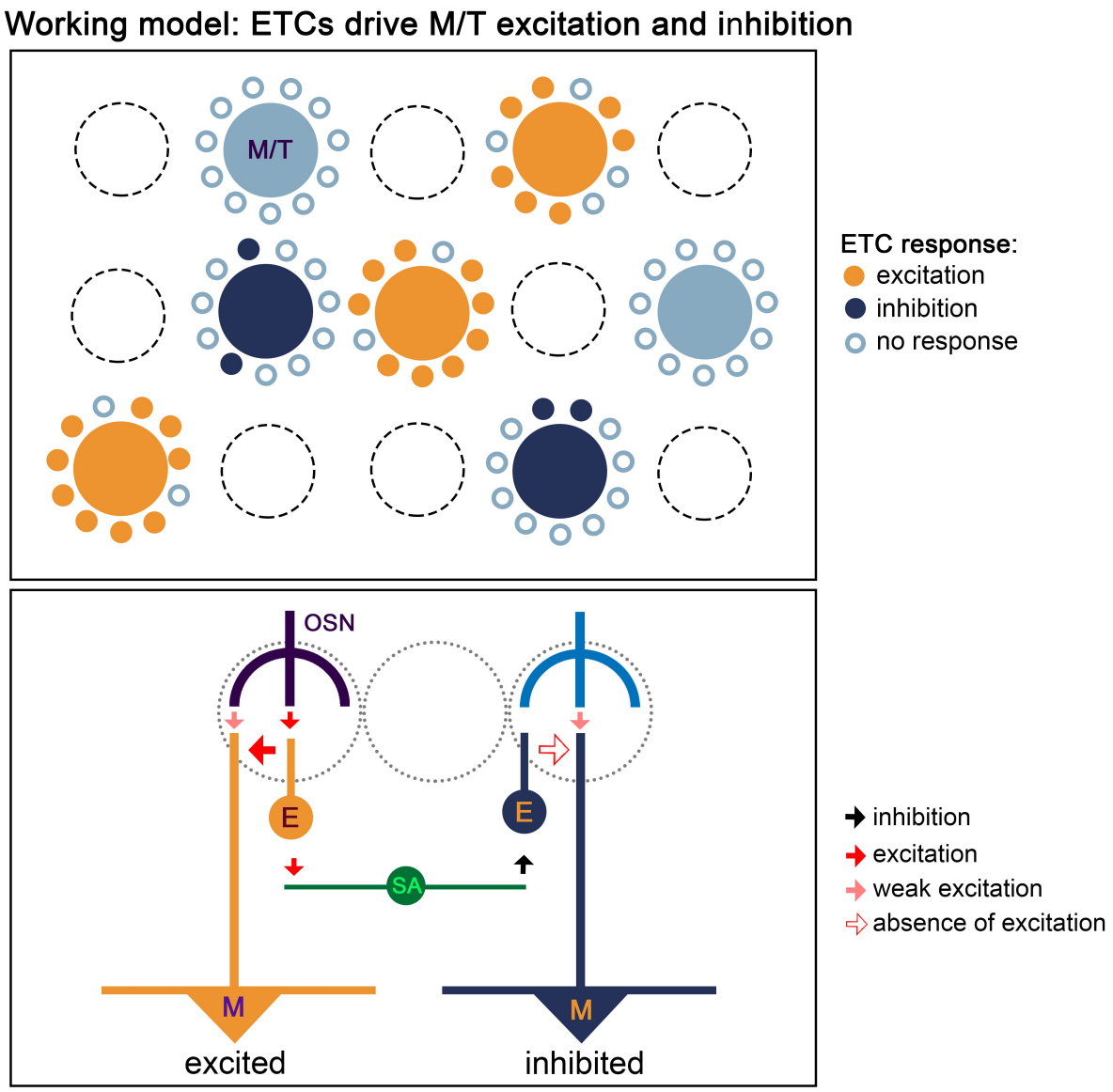

Figure 14. Working model of current study. ETCs drive M/T cell excitation and inhibition *in vivo*. **Up:** Three main hypotheses are proposed based on experimental observations: (1) when excited (orange), the majority of homotypic ETCs act as cell ensembles and evoke M/T cell excitation; (2) when suppressed (dark blue), only very few ETCs can drive for M/T cell inhibition; (3) if ETCs show no odor-evoked response (grey), M/T cells will not respond. **Down:** Possible mechanism of ETC activation and suppression. OSN input drives ETC excitation which excites mitral (M) cell (red arrow). ETC excitation could also excite a short axon (SA) cell which in turn inhibits a heterotypic ETC (black arrow). Absence of excitatory drive in this ETC (hollow arrow) causes suppression of MC. ETC (and thus MC) excitation is therefore a direct OSN effect while inhibition represents an indirect effect exerted from nearby glomerular networks. M/T: Mitral and tufted cells.

To conclude, the present data fills an important gap in understanding ETC physiology and more generally odor processing *in vivo*. Of particular importance are the findings that (1) ETC responses are sparse, (2) ETC activity can be inhibited and (3) ETCs seem to act as homotypic cell ensembles when excited. However, as the analysis is still under progress many questions

remain unsolved. Most importantly, the question as to whether ETCs really drive M/T output *in vivo* needs to be addressed functionally. The experimental paradigm to achieve this would imply to specifically inhibit ETC activation while recording odor-evoked responses in M/T cells. This could be achieved by virus injection of Cre-dependent inhibitory DREADD (hm4Di) into the RMS of young ND6^{Cre}/tdTom/GCaMP6s mice. Interestingly, previous studies have reported specific lentiviral serotypes with high tropism towards ETCs (Adam et al., 2014) allowing for high specificity of DREADD-mediated inhibition. If this hypothesis proves to be true, M/T cells would display decreased odor-responses upon ETC inhibition.

REFERENCES

Ache BW, Young JM. 2005. Olfaction: diverse species, conserved principles. Neuron 48:417–30.

Adam Y, Livneh Y, Miyamichi K, Groysman M, Luo L, Mizrahi A. 2014. Functional transformations of odor inputs in the mouse olfactory bulb. Front Neural Circuits 8:1–17.

Agarwal A, Dibaj P, Kassmann CM, Goebbels S, Nave KA, Schwab MH. 2012. In vivo imaging and noninvasive ablation of pyramidal neurons in adult NEX-CreERT2 mice. Cereb Cortex 22:1473–1486.

Altman J. 1962. Are new neurons formed in the brains of adult mammals? Science 135:1127–8.

Altman J. 1969. Autoradiographic and histological studies of postnatal neurogenesis. IV. Cell proliferation and migration in the anterior forebrain, with special reference to persisting neurogenesis in the olfactory bulb. J Comp Neurol 137:433–457.

Altman J, Chorover SL. 1963. Autoradiographic Investigation of the Distribution and Utilization of Intraventricularly Injected Adenine-3h, Uracil-3h and Thymidine-3h in the Brains of Cats. J Physiol 169:770–9.

Altman J, Das GD. 1965. Autoradiographic and histological evidence of postnatal hippocampal neurogenesis in rats. J Comp Neurol 124:319–35.

Altman J, Das GD. 1966. Autoradiographic and histological studies of postnatal neurogenesis. I. A longitudinal investigation of the kinetics, migration and transformation of cells incorporating tritiated thymidine in neonate rats, with special reference to postnatal neurogenesis. J Comp Neurol 126:337–89.

Alvarez-Buylla a., Kohwi M, Nguyen TM, Merkle FT. 2008. The heterogeneity of adult neural stem cells and the emerging complexity of their niche. Cold Spring Harb Symp Quant Biol 73:357–365.

Alvarez-Buylla A, Lim DA. 2004. For the long run: Maintaining germinal niches in the adult brain. Neuron 41:683–686.

Angelova A, Tiveron M-C, Cremer H, Beclin C, Angelova A, Tiveron M-C, Cremer H, Beclin C. 2018. Neuronal Subtype Generation During Postnatal Olfactory Bulb Neurogenesis. J Exp Neurosci 12.

Antal M, Eyre M, Finklea B, Nusser Z. 2006. External tufted cells in the main olfactory bulb form two distinct subpopulations. Eur J Neurosci 24:1124–1136.

Araneda RC, Kini AD, Firestein S. 2000. The molecular receptive range of an odorant receptor. Nat Neurosci 3:1248–55.

Aungst JL, Heyward PM, Puche a C, Karnup S V, Hayar A, Szabo G, Shipley MT. 2003. Centre-surround inhibition among olfactory bulb glomeruli. Nature 426:623–629.

Axel R. 1995. The molecular logic of smell. Sci Am 273:154–9.

Azim K, Hurtado-Chong A, Fischer B, Kumar N, Zweifel S, Taylor V, Raineteau O. 2015. Transcriptional hallmarks of heterogeneous neural stem cell niches of the subventricular zone. Stem Cells 33:2232–2242.

Baker H. 1990. Unilateral, neonatal olfactory deprivation alters tyrosine hydroxylase expression but not aromatic amino acid decarboxylase or GABA immunoreactivity. Neuroscience 36:761–71.

Baker H, Morel K, Stone DM, Maruniak JA. 1993. Adult naris closure profoundly reduces tyrosine hydroxylase expression in mouse olfactory bulb. Brain Res 614:109–116.

Baker NE, Brown NL. 2018. All in the family: proneural bHLH genes and neuronal diversity. Development 145:dev159426.

Banerjee A, Marbach F, Anselmi F, Gupta P, Li B, Albeanu DF, Banerjee A, Marbach F, Anselmi F, Koh MS, Davis MB, Garcia da Silva P, Delevich K, Oyibo HK, Gupta P, Li B, Albeanu DF. 2015. An Interglomerular Circuit Gates Glomerular Output and

Implements Gain Control in the Mouse Olfactory Bulb. Neuron 87:193–207.
Barlow HB. 1961. Possible Principles Underlying the Transformations of Sensory Messages. Sens Commun:216–234.
Bastien-Dionne PO, David LS, Parent A, Saghatelyan A. 2010. Role of sensory activity on chemospecific populations of interneurons in the adult olfactory bulb. J Comp Neurol 518:1847–1861.
Batista-Brito R, Close J, Machold R, Fishell G. 2008. The Distinct Temporal Origins of Olfactory Bulb Interneuron Subtypes. J Neurosci 28:3966–3975.
Belluscio L, Lodovichi C, Feinstein P. 2002. Odorant receptors instruct functional circuitry in the mouse olfactory bulb. 419:296–300.
Blanchart A, De Carlos JA, López-Mascaraque L. 2006. Time frame of mitral cell development in the mice olfactory bulb. J Comp Neurol 496:529–543.
Bormuth I. 2016. Roles of bHLH Transcription Factors Neurod1, Neurod2 and Neurod6 in Cerebral Cortex Development and Commissure Formation.
Bormuth I, Yan K, Yonemasu T, Gummert M, Zhang M, Wichert S, Grishina O, Pieper A, Zhang W, Goebbels S, Tarabykin V, Nave K-A, Schwab MH. 2013. Neuronal Basic Helix-Loop-Helix Proteins Neurod2/6 Regulate Cortical Commissure Formation before Midline Interactions. J Neurosci 33:641–651.
Bourne JN, Schoppa NE. 2017. Three-dimensional synaptic analyses of mitral cell and external tufted cell dendrites in rat olfactory bulb glomeruli. J Comp Neurol 00:1–18.
Boutin C, Hardt O, de Chevigny A, Coré N, Goebbels S, Seidenfaden R, Bosio A, Cremer H. 2010. NeuroD1 induces terminal neuronal differentiation in olfactory neurogenesis. Proc Natl Acad Sci U S A 107:1201–1206.
Bovetti S, Veyrac A, Peretto P, Fasolo A, de Marchis S. 2009. Olfactory enrichment influences adult neurogenesis modulating GAD67 and plasticity-related molecules expression in newborn cells of the olfactory bulb. PLoS One 4.
Bozza T, McGann JP, Mombaerts P, Wachowiak M. 2004. In vivo imaging of neuronal activity by targeted expression of a genetically encoded probe in the mouse. Neuron 42:9–21.
Brill MS, Ninkovic J, Winpenny E, Hodge RD, Ozen I, Yang R, Lepier A, Gascón S, Erdelyi F, Szabo G, Parras C, Guillemot F, Frotscher M, Berninger B, Hevner RF, Raineteau O, Götz M, Gascon S, Erdelyi F, Szabo G, Parras C, Guillemot F, Frotscher M, Berninger B, Hevner RF, Raineteau O, Gotz M. 2009. Adult generation of glutamatergic olfactory bulb interneurons. Nat Neurosci 12:1524–1533.
Brunjes PC. 1994. Unilateral naris closure and olfactory system development. Brain Res Rev 19:146–160.
Buck L, Axel R. 1991. A novel multigene family may encode odorant receptors: A molecular basis for odor recognition. Cell 65:175–187.
Buck LB. 1996. Information coding in the vertebrate olfactory system. Annu Rev Neurosci 19:517–44.
Buonviso N, Revial M, Jourdan F. 1991. The Proiections of Mitral Cells from Small Local Regions of the Olfactory Bulb : An Anterograde Tracing Study Using PHA-L (Phaseolus vdgaris Leucoagglut in in). 3:493–500.
Burton SD. 2017. Inhibitory circuits of the mammalian main olfactory bulb. J Neurophysiol 84112:jn.00109.2017.
Buzsáki G, Chrobak JJ. 1995. Temporal structure in spatially organized neuronal ensembles: a role for interneuronal networks. Curr Opin Neurobiol 5:504–510.
De Carlos JA, López-Mascaraque L, Valverde F. 1995. The telencephalic vesicles are innervated by olfactory placode-derived cells: a possible mechanism to induce neocortical development. Neuroscience 68:1167–78.
Chen F, Moran JT, Zhang Y, Ates KM, Yu D, Schrader LA, Das PM, Jones FE, Hall BJ.

2016. The transcription factor NeuroD2 coordinates synaptic innervation and cell intrinsic properties to control excitability of cortical pyramidal neurons. J Physiol 594:3729–3744.
de Chevigny A, Coré N, Follert P, Gaudin M, Barbry P, Béclin C, Cremer H. 2012a. miR-7a regulation of Pax6 controls spatial origin of forebrain dopaminergic neurons. Nat Neurosci 15:1120–1126.
de Chevigny A, Core N, Follert P, Wild S, Bosio A, Yoshikawa K, Cremer H, Beclin C. 2012b. Dynamic expression of the pro-dopaminergic transcription factors Pax6 and Dlx2 during postnatal olfactory bulb neurogenesis. Front Cell Neurosci 6:1–8.
Cleland TA. 2010. Early transformations in odor representation. Trends Neurosci 33:130–139.
Cleland TA, Linster C. 2012. On-Center/Inhibitory-Surround Decorrelation via Intraglomerular Inhibition in the Olfactory Bulb Glomerular Layer. Front Integr Neurosci 6:1–10.
Cleland TA, Sethupathy P. 2006. Non-topographical contrast enhancement in the olfactory bulb. BMC Neurosci 7:7.
Cummings DM, Belluscio L. 2010. Continuous Neural Plasticity in the Olfactory Intrabulbar Circuitry. J Neurosci 30:9172–9180.
Dehghani N, Peyrache A, Telenczuk B, Le Van Quyen M, Halgren E, Cash SS, Hatsopoulos NG, Destexhe A. 2016. Dynamic Balance of Excitation and Inhibition in Human and Monkey Neocortex. Sci Rep 6:23176.
Delgado RN, Lim DA. 2017. Maintenance of Positional Identity of Neural Progenitors in the Embryonic and Postnatal Telencephalon. Front Mol Neurosci 10:1–9.
Dhawale AK, Hagiwara A, Bhalla US, Murthy VN, Albeanu DF. 2010. Non-redundant odor coding by sister mitral cells revealed by light addressable glomeruli in the mouse. Nat Neurosci 13:1404–1412.
Doetsch F, García-Verdugo JM, Alvarez-Buylla A. 1997. Cellular composition and three-dimensional organization of the subventricular germinal zone in the adult mammalian brain. J Neurosci 17:5046–61.
Doucette W, Gire DH, Whitesell J, Carmean V, Lucero MT, Restrepo D. 2011. Associative Cortex Features in the First Olfactory Brain Relay Station. Neuron 69:1176–1187.
Doucette W, Restrepo D. 2008. Profound context-dependent plasticity of mitral cell responses in olfactory bulb. PLoS Biol 6:e258.
Economo MN, Hansen KR, Wachowiak M. 2016. Control of Mitral / Tufted Cell Output by Selective Inhibition among Olfactory Bulb Glomeruli. Neuron 91:397–411.
Englund C, Fink A, Charmaine L, Pham D, Ray DAM, Bulfone A, Kowalczyk T, Hevner RF, Lau C, Pham D, Daza RAM, Bulfone A, Kowalczyk T, Hevner RF. 2005. Pax6, Tbr2, and Tbr1 Are Expressed Sequentially by Radial Glia, Intermediate Progenitor Cells, and Postmitotic Neurons in Developing Neocortex. J Neurosci 25:247–251.
Fazel Darbandi S, Robinson Schwartz SE, Qi Q, Catta-Preta R, Pai EL-L, Mandell JD, Everitt A, Rubin A, Krasnoff RA, Katzman S, Tastad D, Nord AS, Willsey AJ, Chen B, State MW, Sohal VS, Rubenstein JLR. 2018. Neonatal Tbr1 Dosage Controls Cortical Layer 6 Connectivity. Neuron.
Fernández ME, Croce S, Boutin C, Cremer H, Raineteau O. 2011. Targeted electroporation of defined lateral ventricular walls: a novel and rapid method to study fate specification during postnatal forebrain neurogenesis. Neural Dev 6:13.
Fiorelli R, Azim K, Fischer B, Raineteau O. 2015. Adding a spatial dimension to postnatal ventricular-subventricular zone neurogenesis. Development 142:2109–2120.
Frazier-Cierpial L, Brunjes PC. 1989. Early postnatal cellular proliferation and survival in the olfactory bulb and rostral migratory stream of normal and unilaterally odor-deprived rats. J Comp Neurol 289:481–492.

Frazier LL, Brunjes PC. 1988. Unilateral odor deprivation: early postnatal changes in olfactory bulb cell density and number. J Comp Neurol 269:355–370.

Fuentealba LC, Rompani SB, Parraguez JI, Obernier K, Romero R, Cepko CL, Alvarez-buylla A, Fuentealba LC, Rompani SB, Parraguez JI, Obernier K, Romero R, Cepko CL, Alvarez-buylla A. 2015. Embryonic Origin of Postnatal Neural Stem Cells Article Embryonic Origin of Postnatal Neural Stem Cells. Cell 161:1644–1655.

Fukunaga I, Berning M, Kollo M, Schmaltz A, Schaefer AT. 2012. Two Distinct Channels of Olfactory Bulb Output. Neuron 75:320–329.

Furutachi S, Miya H, Watanabe T, Kawai H, Yamasaki N, Harada Y, Imayoshi I, Nelson M, Nakayama KI, Hirabayashi Y, Gotoh Y. 2015. Slowly dividing neural progenitors are an embryonic origin of adult neural stem cells. Nat Neurosci 18:657–65.

Gage FH. 2000. Mammalian neural stem cells. Science (80-) 287:1433–1438.

Gage FH. 2002. Neurogenesis in the adult brain. 22:612–3.

Ghosh S, Larson SD, Hefzi H, Marnoy Z, Cutforth T, Dokka K, Baldwin KK. 2011. Sensory maps in the olfactory cortex defined by long-range viral tracing of single neurons. Nature 472:217–222.

Gire DH, Franks KM, Zak JD, Tanaka KF, Whitesell JD, Mulligan AA, Hen R, Schoppa NE. 2012. Mitral Cells in the Olfactory Bulb Are Mainly Excited through a Multistep Signaling Path. J Neurosci 32:2964–2975.

Gire DH, Schoppa NE. 2009. Control of On / Off Glomerular Signaling by a Local GABAergic Microcircuit in the Olfactory Bulb. J Neurosci 29:13454–13464.

Goebbels S, Bormuth I, Bode U, Hermanson O, Schwab MH, Nave K-A. 2006. Genetic targeting of principal neurons in neocortex and hippocampus of NEX-Cre mice. genesis 44:611–621.

Goldberg SJ, Moulton DG. 1987. Olfactory bulb responses telemetered during an odor discrimination task in rats. Exp Neurol 96:430–42.

Götz M, Nakafuku M, Petrik D. 2016. Neurogenesis in the Developing and Adult Brain - Similarities and Key Differences. Cold Spring Harb Perspect Biol:1–23.

Gould E, Tanapat P, McEwen BS, Flügge G, Fuchs E. 1998. Proliferation of granule cell precursors in the dentate gyrus of adult monkeys is diminished by stress. Proc Natl Acad Sci U S A 95:3168–3171.

Grobman M, Dalal T, Lavian H, Shmuel R, Belelovsky K, Xu F, Korngreen A, Haddad R. 2018. A Mirror-Symmetric Excitatory Link Coordinates Odor Maps across Olfactory Bulbs and Enables Odor Perceptual Unity. Neuron 99:800–813.e6.

Grosmaitre X, Santarelli LC, Tan J, Luo M, Ma M. 2007. Dual functions of mammalian olfactory sensory neurons as odor detectors and mechanical sensors. Nat Neurosci 10:348–54.

Gudden B von. 1870. Experimentaluntersuchungen über das peripherische und centrale Nervensystem.

Haberly LB, Price JL. 1978. Association and commissural fiber systems of the olfactory cortex of the rat. I. Systems originating in the piriform cortex and adjacent areas. J Comp Neurol 178:711–740.

Hack M a, Saghatelyan A, de Chevigny A, Pfeifer A, Ashery-Padan R, Lledo P-M, Götz M. 2005. Neuronal fate determinants of adult olfactory bulb neurogenesis. Nat Neurosci 8:865–872.

Hayar A. 2004. Olfactory Bulb Glomeruli: External Tufted Cells Intrinsically Burst at Theta Frequency and Are Entrained by Patterned Olfactory Input. J Neurosci 24:1190–1199.

Hayar A, Karnup S, Ennis M, Shipley MT. 2004. External Tufted Cells: A Major Excitatory Element That Coordinates Glomerular Activity. J Neurosci 24:6676–6685.

Herrera DG, Garcia-verdugo JM, Alvarez-buylla A. 1999. Adult-Derived Neural Precursors Transplanted into Multiple Regions in the Adult Brain. :867–877.

Herrick CJ. 1924. The nucleus olfactorius anterior of the opossum. J Comp Neurol 37:317–359.
Hinds JW. 1968. Autoradiographic study of histogenesis in the mouse olfactory bulb I. Time of origin of neurons and neuroglia. J Comp Neurol 134:287–304.
Hodge RD, Kowalczyk TD, Wolf SA, Encinas JM, Rippey C, Enikolopov G, Kempermann G, Hevner RF. 2008. Intermediate progenitors in adult hippocampal neurogenesis: Tbr2 expression and coordinate regulation of neuronal output. J Neurosci 28:3707–3717.
Huang C, Chan JA, Schuurmans C. 2014. Proneural bHLH Genes in Development and Disease. Curr Top Dev Biol 110:75–127.
Igarashi KM, Ieki N, An M, Yamaguchi Y, Nagayama S, Kobayakawa K, Kobayakawa R, Tanifuji M, Sakano H, Chen WR, Mori K. 2012. Parallel Mitral and Tufted Cell Pathways Route Distinct Odor Information to Different Targets in the Olfactory Cortex. J Neurosci 32:7970–7985.
Ihrie RA, Shah JK, Harwell CC, Levine JH, Guinto CD, Lezameta M, Kriegstein AR, Alvarez-Buylla A. 2011. Persistent sonic hedgehog signaling in adult brain determines neural stem cell positional identity. Neuron 71:250–62.
Imai T, Sakano H, Vosshall LB. 2010. Topographic Mapping — The Olfactory System. Cold Spring Harb Perspect Biol:1–19.
Imamura F, Ayoub AE, Rakic P, Greer C a. 2011. Timing of neurogenesis is a determinant of olfactory circuitry. Nat Neurosci 14:331–337.
Ince-Dunn G, Hall BJ, Hu S-C, Ripley B, Huganir RL, Olson JM, Tapscott SJ, Ghosh A. 2006. Regulation of Thalamocortical Patterning and Synaptic Maturation by NeuroD2. Neuron 49:683–695.
Johnson B, Leon M. 2007. Chemotopic Odorant Coding in a Mammalian Olfactory System. J Comp Neurol 502:275–290.
Jordan R, Fukunaga I, Kollo M, Schaefer AT. 2018. Active Sampling State Dynamically Enhances Olfactory Bulb Odor Representation. Neuron 98:1214–1228.e5.
Kaas JONH. 1997. Topographic Maps are Fundamental to Sensory Processing. 44:107–112.
Kaplan MS, Hinds JW. 1977. Neurogenesis in the adult rat: electron microscopic analysis of light radioautographs. Sci (New York, NY) 197:1092–1094.
Kasowski HJ, Kim H, Greer CA. 1999. Compartmental organization of the olfactory bulb glomerulus. J Comp Neurol 407:261–74.
Kato Y, Kaneko N, Sawada M, Ito K, Arakawa S, Murakami S, Sawamoto K. 2012. A Subtype-Specific Critical Period for Neurogenesis in the Postnatal Development of Mouse Olfactory Glomeruli. PLoS One 7.
Kay JN, Voinescu PE, Chu MW, Sanes JR. 2011. Neurod6 expression defines new retinal amacrine cell subtypes and regulates their fate. Nat Neurosci 14:965–972.
Kelsch W, Mosley CP, Lin CW, Lois C. 2007. Distinct mammalian precursors are committed to generate neurons with defined dendritic projection patterns. PLoS Biol 5:2501–2512.
Khan S, Stott SRW, Chabrat A, Truckenbrodt AM, Spencer-dene B, Nave K-A, Guillemot F, Levesque M, Ang S, Khan XS, Stott XSRW, Chabrat A, Truckenbrodt XAM, Spencer-dene B, Nave XK, Franc X, Levesque XM, Ang S, Khan S, Stott SRW, Chabrat A, Truckenbrodt AM, Spencer-dene B, Nave K-A, Guillemot F, Levesque M, Ang S. 2017. Survival of a Novel Subset of Midbrain Dopaminergic Neurons Projecting to the Lateral Septum Is Dependent on NeuroD Proteins. J Neurosci 37:2305–2316.
Kikuta S, Sato K, Kashiwadani H, Tsunoda K, Yamasoba T, Mori K. 2010. Neurons in the anterior olfactory nucleus pars externa detect right or left localization of odor sources. Proc Natl Acad Sci 107:12363–12368.
Kiyokage E, Pan Y-Z, Shao Z, Kobayashi K, Szabo G, Yanagawa Y, Obata K, Okano H, Toida K, Puche AC, Shipley MT. 2010. Molecular Identity of Periglomerular and Short Axon Cells. J Neurosci 30:1185–1196.

Kohwi M. 2005. Pax6 Is Required for Making Specific Subpopulations of Granule and Periglomerular Neurons in the Olfactory Bulb. J Neurosci 25:6997–7003.
Kohwi M, Petryniak MA, Long JE, Ekker M, Obata K, Yanagawa Y, Rubenstein JLR, Alvarez-Buylla A. 2007. A subpopulation of olfactory bulb GABAergic interneurons is derived from Emx1- and Dlx5/6-expressing progenitors. J Neurosci 27:6878–6891.
Kosaka K, Aika Y, Toida K, Kosaka T. 2001. Structure of intraglomerular dendritic tufts of mitral cells and their contacts with olfactory nerve terminals and calbindin-immunoreactive type 2 periglomerular neurons. J Comp Neurol 440:219–235.
Kosaka K, Heizmann CW, Kosaka T. 1994. Calcium-binding protein parvalbumin-immunoreactive neurons in the rat olfactory bulb. 1. Distribution and structural features in adult rat. Exp brain Res 99:191–204.
Kosaka K, Kosaka T. 2007a. Chemical properties of type 1 and type 2 periglomerular cells in the mouse olfactory bulb are different from those in the rat olfactory bulb. Brain Res 1167:42–55.
Kosaka K, Toida K, Margolis FL, Kosaka T. 1997. Chemically defined neuron groups and their subpopulations in the glomerular layer of the rat main olfactory bulb--II. Prominent differences in the intraglomerular dendritic arborization and their relationship to olfactory nerve terminals. Neuroscience 76:775–86.
Kosaka T, Kosaka K. 2007b. Heterogeneity of nitric oxide synthase-containing neurons in the mouse main olfactory bulb. Neurosci Res 57:165–178.
Kosaka T, Kosaka K. 2011. “Interneurons” in the olfactory bulb revisited. Neurosci Res 69:93–99.
Kriegstein A, Alvarez-Buylla A. 2009. The glial nature of embryonic and adult neural stem cells. Annu Rev Neurosci 32:149–184.
Li J, Liu ZJ, Pan YC, Liu Q, Fu X, Cooper NGF, Li Y, Qiu M, Shi T. 2007. Regulatory module network of basic/helix-loop-helix transcription factors in mouse brain. Genome Biol 8:R244.
Lim DA, Alvarez-Buylla A. 2014. Adult neural stem cells stake their ground. Trends Neurosci 37:563–571.
Lim DA, Alvarez-buylla A, Bulb O, Neurogenesis OB, Lim DA, Alvarez-buylla A. 2016. The Adult Ventricular – Subventricular Zone. Cold Spring Harb Perspect Biol:1–34.
Lin C-H, Stoeck J, Ravanpay AC, Guillemot F, Tapscott SJ, Olson JM. 2004. Regulation of neuroD2 expression in mouse brain. Dev Biol 265:234–45.
Liu S, Puche AC, Shipley MT. 2016. The Interglomerular Circuit Potently Inhibits Olfactory Bulb Output Neurons by Both Direct and Indirect Pathways. J Neurosci 36:9604–9617.
Liu W, Lin L, Shipley MT. 1994. Intrabulbar associational system in the rat olfactory bulb comprises cholecystokinin containing tufted cells that synapse onto the dendrites of GABAergic granule cells. J Comp Neurol 346:541–558.
Lois, C. & Alvarez-Buylla A. 1994. Long-distance neuronal migration in the adult mammalian brain. Science (80-) 264:1145–1148.
Lopez-Garcia C, Molowny A, Garcia-Verdugo JM, Ferrer I. 1988. Delayed postnatal neurogenesis in the cerebral cortex of lizards. Brain Res 471:167–74.
Lopez-Juarez A, Howard J, Ullom K, Howard L, Grande A, Pardo A, Waclaw R, Sun Y-Y, Yang D, Kuan C-Y, Campbell K, Nakafuku M. 2013. Gsx2 controls region-specific activation of neural stem cells and injury-induced neurogenesis in the adult subventricular zone. Genes Dev 27:1272–1287.
Luo M, Katz LC. 2001. Response correlation maps of neurons in the mammalian olfactory bulb. Neuron 32:1165–1179.
Luskin MB. 1993. Restricted proliferation and migration of postnatally generated neurons derived from the forebrain subventricular zone. Neuron 11:173–89.
Macrides F, Schoenfeld TA, Marchand JE, Clancy AN. 1985. Evidence for morphologically,

neurochemically and functionally heterogeneous classes of mitral and tufted cells in the olfactory bulb. Chem Senses 10:175–202.
Malnic B, Gonzalez-Kristeller DC, Gutiyama LM. 2010. Odorant Receptors. CRC Press/Taylor & Francis.
Malnic B, Hirono J, Sato T, Buck LB. 1999. Combinatorial receptor codes for odors. Cell 96:713–23.
Malvaut S, Gribaudo S, Hardy D, David LS, Daroles L, Labrecque S, Lebel-Cormier MA, Chaker Z, Coté D, De Koninck P, Holzenberger M, Trembleau A, Caille I, Saghatelyan A. 2017. CaMKIIα Expression Defines Two Functionally Distinct Populations of Granule Cells Involved in Different Types of Odor Behavior. Curr Biol 27:3315–3329.e6.
Mandairon N, Sacquet J, Jourdan F, Didier A. 2006. Long-term fate and distribution of newborn cells in the adult mouse olfactory bulb: Influences of olfactory deprivation. Neuroscience 141:443–451.
Marks CA, Cheng K, Cummings DM, Belluscio L. 2006. Activity-Dependent Plasticity in the Olfactory Intrabulbar Map. J Neurosci 26:11257–11266.
Matsumoto H, Kobayakawa K, Kobayakawa R, Tashiro T, Mori K, Sakano H, Mori K. 2010. Spatial Arrangement of Glomerular Molecular-Feature Clusters in the Odorant-Receptor Class Domains of the Mouse Olfactory Bulb. J Neurophysiol 103:3490–3500.
McCormick MB, Tamimi RM, Snider L, Asakura A, Bergstrom D, Tapscott SJ. 1996. NeuroD2 and neuroD3: distinct expression patterns and transcriptional activation potentials within the neuroD gene family. Mol Cell Biol 16:5792–800.
McGann JP, Pírez N, Gainey MA, Muratore C, Elias AS, Wachowiak M. 2005. Odorant Representations Are Modulated by Intra- but Not Interglomerular Presynaptic Inhibition of Olfactory Sensory Neurons. Neuron 48:1039–1053.
Merkle FT, Fuentealba LC, Sanders TA, Magno L, Kessaris N, Alvarez-buylla A. 2014. Adult neural stem cells in distinct microdomains generate previously unknown interneuron types. Nat Neurosci 17:207–214.
Merkle FT, Mirzadeh Z, Alvarez-Buylla A. 2007. Mosaic organization of neural stem cells in the adult brain. Science 317:381–384.
Merkle FT, Tramontin AD, García-Verdugo JM, Alvarez-Buylla A. 2004. Radial glia give rise to adult neural stem cells in the subventricular zone. Proc Natl Acad Sci U S A 101:17528–32.
Mirzadeh Z, Merkle FT, Soriano-Navarro M, Garcia-Verdugo JM, Alvarez-Buylla A. 2008. Neural Stem Cells Confer Unique Pinwheel Architecture to the Ventricular Surface in Neurogenic Regions of the Adult Brain. Cell Stem Cell 3:265–278.
Miyamichi K, Amat F, Moussavi F, Wang C, Wickersham I, Wall NR, Taniguchi H, Tasic B, Huang ZJ, He Z, Callaway EM, Horowitz MA, Luo L. 2011. Cortical representations of olfactory input by trans-synaptic tracing. Nature 472:191–199.
Miyamichi K, Serizawa S, Kimura HM, Sakano H. 2005. Continuous and overlapping expression domains of odorant receptor genes in the olfactory epithelium determine the dorsal/ventral positioning of glomeruli in the olfactory bulb. J Neurosci 25:3586–92.
Molyneaux BJ, Arlotta P, Menezes JRLL, Macklis JD. 2007. Neuronal subtype specification in the cerebral cortex. Nat Rev Neurosci 8:427–437.
Mombaerts P, Wang F, Dulac C, Chao SK, Nemes A, Mendelsohn M, Edmondson J, Axel R. 1996. Visualizing an olfactory sensory map. Cell 87:675–686.
Mongillo G, Rumpel S, Loewenstein Y. 2018. Inhibitory connectivity defines the realm of excitatory plasticity. Nat Neurosci 21:1463–1470.
Mori K. 2006. Maps of Odorant Molecular Features in the Mammalian Olfactory Bulb. Physiol Rev 86:409–433.
Mori K, Kishi K, Ojima H. 1983. Distribution of dendrites of mitral, displaced mitral, tufted,

and granule cells in the rabbit olfactory bulb. J Comp Neurol 219:339–355.
Mori K, Nagao H, Yoshihara Y. 1999. The olfactory bulb: Coding and processing of odor molecule information. Science (80-) 286:711–715.
Morin X, Jaouen F, Durbec P. 2007. Control of planar divisions by the G-protein regulator LGN maintains progenitors in the chick neuroepithelium. Nat Neurosci 10:1440–8.
Murphy GJ, Darcy DP, Isaacson JS. 2005. Intraglomerular inhibition: signaling mechanisms of an olfactory microcircuit. Nat Neurosci 8:354–364.
Murphy GJ, Glickfeld LL, Balsen Z, Isaacson JS. 2004. Sensory Neuron Signaling to the Brain: Properties of Transmitter Release from Olfactory Nerve Terminals. J Neurosci 24:3023–3030.
Nagayama S, Enerva A, Fletcher ML, Masurkar A V, Igarashi KM, Mori K, Chen WR. 2010. Differential axonal projection of mitral and tufted cells in the mouse main olfactory system. Front Neural Circuits 4.
Nagayama S, Homma R, Imamura F. 2014. Neuronal organization of olfactory bulb circuits. Front Neural Circuits 8:1–19.
Najac M, Diez AS, Kumar XA, Benito N, Charpak S, Jan XDD Saint, Sanz Diez A, Kumar A, Benito N, Charpak S, De Saint Jan D. 2015. Intraglomerular Lateral Inhibition Promotes Spike Timing Variability in Principal Neurons of the Olfactory Bulb. J Neurosci 35:4319–4331.
Najac M, De Saint Jan D, Reguero L, Grandes P, Charpak S. 2011. Monosynaptic and Polysynaptic Feed-Forward Inputs to Mitral Cells from Olfactory Sensory Neurons. J Neurosci 31:8722–8729.
Najbauer J, Leon M. 1995. Olfactory experience modulates apoptosis in the developing olfactory bulb. Brain Res 674:245–251.
Nunez-Parra A, Li A, Restrepo D. 2014. Coding odor identity and odor value in awake rodents. 1st ed. Elsevier B.V.
Olson JM, Asakura A, Snider L, Hawkes R, Strand A, Stoeck J, Hallahan A, Pritchard J, Tapscott SJ. 2001. NeuroD2 is necessary for development and survival of central nervous system neurons. Dev Biol 234:174–87.
Orona E, Scott JW, Rainer EC. 1983. Different granule cell populations innervate superficial and deep regions of the external plexiform layer in rat olfactory bulb. J Comp Neurol 217:227–37.
Paredes MF, Sorrells SF, Garcia-Verdugo JM, Alvarez-Buylla A. 2016. Brain size and limits to adult neurogenesis: Brain Size and Limits to Adult Neurogenesis. J Comp Neurol 524:646–664.
Parrish-Aungst S, Shipley MT, Erdelyi F, Szabo G, Puche AC. 2007. Quantitative analysis of neuronal diversity in the mouse olfactory bulb. J Comp Neurol 501:825–836.
Paton JA, Nottebohm FN. 1984. Neurons generated in the adult brain are recruited into functional circuits. Science 225:1046–8.
Patterson MA, Lagier S, Carleton A. 2013. Odor representations in the olfactory bulb evolve after the first breath and persist as an odor afterimage. Proc Natl Acad Sci 110:E3340–E3349.
Petreanu L, Alvarez-Buylla A. 2002. Maturation and death of adult-born olfactory bulb granule neurons: role of olfaction. J Neurosci 22:6106–13.
Pfisterer U, Khodosevich K. 2017. Neuronal survival in the brain: Neuron type-specific mechanisms. Cell Death Dis 8:e2643-14.
Philpot BD, Lim JHAEH, Brunjes PC. 1997. Activity-dependent regulation of calcium-binding proteins in the developing rat olfactory bulb. J Comp Neurol 387:12–26.
Pinching a J, Powell TP. 1971a. The neuron types of the glomerular layer of the olfactory bulb. J Cell Sci 9:305–345.
Pinching AJ, Powell TPS. 1971b. the Neuropil of the Glomeruli of the Olfactory Bulb. J Cell

Sci 9:347.
Platel J-CC, Dupuis A, Boisseau S, Villaz M, Albrieux M, Brocard J. 2007. Synchrony of spontaneous calcium activity in mouse neocortex before synaptogenesis. Eur J Neurosci 25:920–928.
Price JL, Powell TP. 1970. The morphology of the granule cells of the olfactory bulb. J Cell Sci 7:91–123.
Puelles L, Kuwana E, Puelles E, Bulfone A, Shimamura K, Keleher J, Smiga S, Rubenstein JL. 2000. Pallial and subpallial derivatives in the embryonic chick and mouse telencephalon, traced by the expression of the genes Dlx-2, Emx-1, Nkx-2.1, Pax-6, and Tbr-1. J Comp Neurol 424:409–438.
Ramón y Cajal S. 1928. Degeneration and regeneration of the nervous system. (May RM, editor.). New York: Oxford University Press.
Ressler KJ, Sullivan SL, Buck LB. 1993. A zonal organization of odorant receptor gene expression in the olfactory epithelium. Cell 73:597–609.
Ressler KJ, Sullivan SL, Buck LB. 1994. Information coding in the olfactory system: evidence for a stereotyped and highly organized epitope map in the olfactory bulb. Cell 79:1245–55.
Reyher CKH, Schwerdtfeger WK, Baumgarten HG. 1988. Interbulbar axonal collateralization and morphology of anterior olfactory nucleus neurons in the rat. Brain Res Bull 20:549–566.
Rochefort C, Gheusi G, Vincent J-D, Lledo P-M. 2002. Enriched odor exposure increases the number of newborn neurons in the adult olfactory bulb and improves odor memory. J Neurosci 22:2679–2689.
Roux L, Buzsáki G. 2015. Tasks for inhibitory interneurons in intact brain circuits. Neuropharmacology 88:10–23.
Roybon L, Deierborg T, Brundin P, Li JY. 2009. Involvement of Ngn2, Tbr and NeuroD proteins during postnatal olfactory bulb neurogenesis. Eur J Neurosci 29:232–243.
Roybon L, Mastracci TL, Li J, Stott SRW, Leiter AB, Sussel L, Brundin P, Li JY. 2015. The origin, development and molecular diversity of rodent olfactory bulb glutamatergic neurons distinguished by expression of transcription factor NeuroD1. PLoS One 10:1–21.
Rubin BD, Katz LC. 1999. Optical imaging of odorant representations in the mammalian olfactory bulb. Neuron 23:499–511.
Saghatelyan A, Roux P, Migliore M, Rochefort C, Desmaisons D, Charneau P, Shepherd GM, Lledo PM. 2005. Activity-dependent adjustments of the inhibitory network in the olfactory bulb following early postnatal deprivation. Neuron 46:103–116.
Saiki RK, Gelfand DH, Stoffel S, Scharf SJ, Higuchi R, Horn GT, Mullis KB, Erlich HA. 1988. Primer-directed enzymatic amplification of DNA with a thermostable DNA polymerase. Science 239:487–91.
De Saint Jan D, Hirnet D, Westbrook GL, Charpak S, Jan DD Saint, Hirnet D, Westbrook GL, Charpak S, De Saint Jan D, Hirnet D, Westbrook GL, Charpak S. 2009. External Tufted Cells Drive the Output of Olfactory Bulb Glomeruli. J Neurosci 29:2043–2052.
Saito H, Chi Q, Zhuang H, Matsunami H, Mainland JD. 2009. Odor coding by a Mammalian receptor repertoire. Sci Signal 2:ra9.
Sawada M, Kaneko N, Inada H, Wake H, Kato Y, Yanagawa Y, Kobayashi K, Nemoto T, Nabekura J, Sawamoto K. 2011. Sensory Input Regulates Spatial and Subtype-Specific Patterns of Neuronal Turnover in the Adult Olfactory Bulb. J Neurosci 31:11587–11596.
Schaefer AT, Margrie TW. 2007. Spatiotemporal representations in the olfactory system. Trends Neurosci 30:92–100.
Schoenfeld TA, Macrides F, Mlckides F, Macrides F, Mlckides F. 1984. Topographic organization of connections between the main olfactory bulb and pars externa of the

anterior olfactory nucleus in the hamster. J Comp Neurol 227:121–135.
Schoenfeld TA, Marchand JE, Macrides F. 1985. Topographic organisation of tufted cells axonal projections in the hamster main OB. J Comp Neurol 518:503–518.
Schwab MH, Druffel-Augustin S, Gass P, Jung M, Klugmann M, Bartholomae A, Rossner MJ, Nave K. 1998. Neuronal basic helix-loop-helix proteins (NEX, neuroD, NDRF): spatiotemporal expression and targeted disruption of the NEX gene in transgenic mice. J Neurosci 18:1408–1418.
Scott JW, Ranier EC, Pemberton JL, Orona E, Mouradian LE. 1985. Pattern of rat olfactory bulb mitral and tufted cell connections to the anterior olfactory nucleus pars externa. J Comp Neurol 242:415–24.
Shao Z, Puche AC, Kiyokage E, Szabo G, Shipley MT. 2009. Two GABAergic Intraglomerular Circuits Differentially Regulate Tonic and Phasic Presynaptic Inhibition of Olfactory Nerve Terminals. J Neurophysiol 101:1988–2001.
Shepherd GM ed. 2004. The Synaptic Organization of the Brain. Oxford University Press.
Shihabuddin LS, Horner PJ, Ray J, Gage FH. 2000. Adult spinal cord stem cells generate neurons after transplantation in the adult dentate gyrus. J Neurosci 20:8727–35.
Shusterman R, Smear MC, Koulakov AA, Rinberg D. 2011. Precise olfactory responses tile the sniff cycle. Nat Neurosci 14:1039–1044.
Sosulski DL, Lissitsyna Bloom M, Cutforth T, Axel R, Datta SR. 2011. Distinct representations of olfactory information in different cortical centres. Nature 472:213–219.
Spassky N. 2005. Adult Ependymal Cells Are Postmitotic and Are Derived from Radial Glial Cells during Embryogenesis. J Neurosci 25:10–18.
Spitzer NC. 2017. Neurotransmitter Switching in the Developing and Adult Brain. Annu Rev Neurosci 40:annurev-neuro-072116-031204.
Spors H, Grinvald A. 2002. Spatio-temporal dynamics of odor representations in the mammalian olfactory bulb. Neuron 34:301–15.
Spors H, Wachowiak M, Cohen LB, Friedrich RW. 2006. Temporal dynamics and latency patterns of receptor neuron input to the olfactory bulb. J Neurosci 26:1247–59.
Stenman J, Toresson H, Campbell K. 2003. Identification of two distinct progenitor populations in the lateral ganglionic eminence: implications for striatal and olfactory bulb neurogenesis. J Neurosci 23:167–74.
Storace DA, Cohen LB. 2017. Measuring the olfactory bulb input-output transformation reveals a contribution to the perception of odorant concentration invariance. Nat Commun 8:1–10.
Takahashi H, Ogawa Y, Yoshihara S -i., Asahina R, Kinoshita M, Kitano T, Kitsuki M, Tatsumi K, Okuda M, Tatsumi K, Wanaka A, Hirai H, Stern PL, Tsuboi A. 2016. A Subtype of Olfactory Bulb Interneurons Is Required for Odor Detection and Discrimination Behaviors. J Neurosci 36:8210–8227.
Tan J, Savigner AA, Ma M, Luo M. 2010. Odor Information Processing by the Olfactory Bulb Analyzed in Gene-Targeted Mice. Neuron 65:912–926.
Tatti R, Bhaukaurally K, Gschwend O, Seal RP, Edwards RH, Rodriguez I, Carleton A. 2014. A population of glomerular glutamatergic neurons controls sensory information transfer in the mouse olfactory bulb. Nat Commun 5:3791.
Tavakoli A, Schmaltz A, Schwarz D, Margrie TW, Schaefer AT, Kollo M. 2018. Quantitative association of anatomical and functional classes of olfactory bulb neurons. J Neurosci:0303-18.
Thivierge J, Marcus GF. 2007. The topographic brain : from neural connectivity to cognition.
Tiveron M-C, Beclin C, Murgan S, Wild S, Angelova A, Marc J, Coré N, de Chevigny A, Herrera E, Bosio A, Bertrand V, Cremer H. 2017. Zic-proteins are repressors of dopaminergic forebrain fate in mice and *C. elegans*. J Neurosci.

Tobin VA, Hashimoto H, Wacker DW, Takayanagi Y, Langnaese K, Caquineau C, Noack J, Landgraf R, Onaka T, Leng G, Meddle SL, Engelmann M, Ludwig M. 2010. An intrinsic vasopressin system in the olfactory bulb is involved in social recognition. Nature 464:413–417.

Toida K, Kosaka K, Aika Y, Kosaka T. 2000. Chemically defined neuron groups and their subpopulations in the glomerular layer of the rat main olfactory bulb--IV. Intraglomerular synapses of tyrosine hydroxylase-immunoreactive neurons. Neuroscience 101:11–7.

Toida K, Kosaka K, Heizmann CW, Kosaka T. 1998. Chemically defined neuron groups and their subpopulations in the glomerular layer of the rat main olfactory bulb: III. Structural features of calbindin D28K-immunoreactive neurons. J Comp Neurol 392:179–98.

Toresson H, Campbell K. 2001. A role for Gsh1 in the developing striatum and olfactory bulb of Gsh2 mutant mice. Development 128.

Uchida N, Mainen ZF. 2003. Speed and accuracy of olfactory discrimination in the rat. Nat Neurosci 6:1224–1229.

Uchida N, Poo C, Haddad R. 2014. Coding and Transformations in the Olfactory System. Annu Rev Neurosci 37:363–385.

Vassar R, Chao SK, Sitcheran R, Nuñez JM, Vosshall LB, Axel R. 1994. Topographic organization of sensory projections to the olfactory bulb. Cell 79:981–91.

Vassar R, Ngai J, Axel R. 1993. Spatial segregation of odorant receptor expression in the mammalian olfactory epithelium. Cell 74:309–18.

Verhagen J V, Wesson DW, Netoff TI, White JA, Wachowiak M. 2007. Sniffing controls an adaptive filter of sensory input to the olfactory bulb. Nat Neurosci 10:631–639.

Vincis R, Lagier S, Van De Ville D, Rodriguez I, Carleton A. 2015. Sensory-Evoked Intrinsic Imaging Signals in the Olfactory Bulb Are Independent of Neurovascular Coupling. Cell Rep 12:313–325.

Vučinić D, Cohen LB, Kosmidis EK. 2006. Interglomerular Center-Surround Inhibition Shapes Odorant-Evoked Input to the Mouse Olfactory Bulb In Vivo. J Neurophysiol 95:1881–1887.

Wachowiak M, Cohen LB. 2001. Representation of odorants by receptor neuron input to the mouse olfactory bulb. Neuron 32:723–735.

Wachowiak M, Economo MN, Díaz-Quesada M, Brunert D, Wesson DW, White JA, Rothermel M. 2013. Optical dissection of odor information processing in vivo using GCaMPs expressed in specified cell types of the olfactory bulb. J Neurosci 158:5285–8300.

Wachowiak M, Shipley MT. 2006. Coding and synaptic processing of sensory information in the glomerular layer of the olfactory bulb. Semin Cell Dev Biol 17:411–423.

Waclaw RR, Allen ZJ, Bell SM, Erdélyi F, Szabó G, Potter SS, Campbell K. 2006. The zinc finger transcription factor Sp8 regulates the generation and diversity of olfactory bulb interneurons. Neuron 49:503–516.

Weinandy F, Ninkovic J, Götz M. 2011. Restrictions in time and space - new insights into generation of specific neuronal subtypes in the adult mammalian brain. Eur J Neurosci 33:1045–1054.

Wesson DW, Carey RM, Verhagen J V, Wachowiak M. 2008. Rapid Encoding and Perception of Novel Odors in the Rat. PLoS Biol 6:e82.

Wichterle H, Garcia-Verdugo JM, Herrera DG, Alvarez-Buylla a. 1999. Young neurons from medial ganglionic eminence disperse in adult and embryonic brain. Nat Neurosci 2:461–466.

Wilke SA, Hall BJ, Antonios JK, DeNardo LA, Otto S, Yuan B, Chen F, Robbins EM, Tiglio K, Williams ME, Qiu Z, Biederer T, Ghosh A. 2012. NeuroD2 regulates the development of hippocampal mossy fiber synapses. Neural Dev 7:9.

Winpenny E, Lebel-Potter M, Fernandez ME, Brill MS, Götz M, Guillemot F, Raineteau O. 2011. Sequential generation of olfactory bulb glutamatergic neurons by Neurog2-expressing precursor cells. Neural Dev 6:12.

Wu S-X, Goebbels S, Nakamura KK, Nakamura KK, Kometani K, Minato N, Kaneko T, Nave K-A, Tamamaki N. 2005. Pyramidal neurons of upper cortical layers generated by NEX-positive progenitor cells in the subventricular zone. Proc Natl Acad Sci U S A 102:17172–7.

Xiong W, Chen WR. 2002. Dynamic gating of spike propagation in the mitral cell lateral dendrites. Neuron 34:115–26.

Yamada Y, Bhaukaurally K, Madarász TJ, Pouget A, Rodriguez I, Carleton A. 2017. Context- and Output Layer-Dependent Long-Term Ensemble Plasticity in a Sensory Circuit. Neuron 93:1198–1212.e5.

Yamaguchi M, Mori K. 2005. Critical period for sensory experience-dependent survival of newly generated granule cells in the adult mouse olfactory bulb. Proc Natl Acad Sci U S A 102:9697–9702.

Yan Z, Tan J, Qin C, Lu Y, Ding C, Luo M. 2008. Precise Circuitry Links Bilaterally Symmetric Olfactory Maps. Neuron 58:613–624.

Yokoi M, Mori K, Nakanishi S. 1995. Refinement of odor molecule tuning by dendrodendritic synaptic inhibition in the olfactory bulb. Proc Natl Acad Sci U S A 92:3371–5.

Young KM, Fogarty M, Kessaris N, Richardson WD. 2007. Subventricular zone stem cells are heterogeneous with respect to their embryonic origins and neurogenic fates in the adult olfactory bulb. J Neurosci 27:8286–8296.

APPENDIX I

Zic-Proteins Are Repressors of Dopaminergic Forebrain Fate in Mice and *C. elegans*

Marie-Catherine Tiveron*, Christophe Beclin*, Sabrina Murgan*, Stefan Wild, **Alexandra Angelova**, Julie Marc, Nathalie Coré, Antoine de Chevigny, Eloisa Herrera, Andreas Bosio, Vincent Bertrand and Harold Cremer, 2017, *Journal of Neuroscience*

In this paper our team demonstrates that Zic proteins are *de novo* expressed in the dorsal (cortical) V-SVZ progenitor population that generates calretinin-positive neurons for the OB. In functional experiments we show that Zic1/2 proteins are sufficient to induce calretinin fate while suppressing dopaminergic fate in the dorsal lineage.

My contribution to this paper consisted in assistance with quantifications and immunohistochemical protocols. In particular, my expertise with difficult antibody stainings helped to set up a low-fixation protocol that would allow visualizing the faint Zic staining in the dorsal V-SVZ.

Development/Plasticity/Repair

Zic-Proteins Are Repressors of Dopaminergic Forebrain Fate in Mice and *C. elegans*

Marie-Catherine Tiveron,[1]* Christophe Beclin,[1]* Sabrina Murgan,[1]* Stefan Wild,[2] Alexandra Angelova,[1] Julie Marc,[1] Nathalie Coré,[1] Antoine de Chevigny,[1] Eloisa Herrera,[3] Andreas Bosio,[2] Vincent Bertrand,[1]† and Harold Cremer[1]†

[1]Aix Marseille Univ, CNRS, IBDM, 13009 Marseille, France, [2]Miltenyi Biotec GmbH, 51429 Bergisch-Gladbach, Germany, and [3]Instituto de Neurosciencias de Alicante, CSIC-UMH, Alicante 03550, Spain

In the postnatal forebrain regionalized neural stem cells along the ventricular walls produce olfactory bulb (OB) interneurons with varying neurotransmitter phenotypes and positions. To understand the molecular basis of this region-specific variability we analyzed gene expression in the postnatal dorsal and lateral lineages in mice of both sexes from stem cells to neurons. We show that both lineages maintain transcription factor signatures of their embryonic site of origin, the pallium and subpallium. However, additional factors, including Zic1 and Zic2, are postnatally expressed in the dorsal stem cell compartment and maintained in the lineage that generates calretinin-positive GABAergic neurons for the OB. Functionally, we show that Zic1 and Zic2 induce the generation of calretinin-positive neurons while suppressing dopaminergic fate in the postnatal dorsal lineage. We investigated the evolutionary conservation of the dopaminergic repressor function of Zic proteins and show that it is already present in *C. elegans*.

Key words: **neural stem cells; olfactory bulb; transcription factor**

Significance Statement

The vertebrate brain generates thousands of different neuron types. In this work we investigate the molecular mechanisms underlying this variability. Using a genomics approach we identify the transcription factor signatures of defined neural stem cells and neuron populations. Based thereon we show that two related transcription factors, Zic1 and Zic2, are essential to control the balance between two defined neuron types in the postnatal brain. We show that this mechanism is conserved in evolutionary very distant species.

Introduction

A key question in developmental neurobiology concerns the molecular mechanisms that control the specification of stem cells to produce neurons with defined neurotransmitter phenotype, positions, and connectivity. Combinatorial expression of transcription factors, highly controlled in space and time, has been shown to underlie the determination events that lead to neuronal diversity in the developing embryo (Guillemot, 2007). Moreover, in defined regions of the mammalian brain neurogenesis continues into postnatal and adult stages, making the control of stem cell determination a lifelong requirement.

Postnatal neurogenesis is particularly prominent in the olfactory system of rodents, where neuronal stem cells in ventricular and subventricular zone (V/SVZ) lining the walls of the lateral ventricles generate continuously new interneurons for the olfactory bulb (OB; Alvarez-Buylla and Garcia-Verdugo, 2002; Alvarez-Buylla et al., 2008). After migration via the rostral migratory stream (RMS) these precursors differentiate into OB periglomerular cells (PGCs) or granule cells (GCs) and use GABA, dopamine, and glutamate as their neurotransmitters. The heterogeneity of neuron types in the OB is based on the existence of predetermined neural stem cells organized in subregions of the postnatal ventricular walls (Merkle et al., 2007, 2014). Recent work indicated that this regionalization of the postnatal and adult stem cell

Received Dec. 20, 2016; revised Sept. 7, 2017; accepted Sept. 15, 2017.

Author contributions: M.-C.T., C.B., S.M., S.W., N.C., A.B., V.B., and H.C. designed research; M.-C.T., C.B., S.M., A.A., J.M., N.C., and A.d.C. performed research; S.W., E.H., and A.B. contributed unpublished reagents/analytic tools; M.-C.T., C.B., S.M., S.W., A.A., N.C., V.B., and H.C. analyzed data; M.-C.T., C.B., V.B., and H.C. wrote the paper.

This work was supported by the Agence National pour la Recherche (ANR), Fondation de France (FDF), and France Parkinson to H.C., the Fondation pour la Recherche sur le Cerveau (FRC) to H.C. and V.B., the European Commission MSC Program (IAPP Dopanew) to H.C. and A.B., the CNRS ATIP program to V.B.; work in the laboratory of E.H. is supported by the following Grants: Prometeo 2012-005, BFU2010-16563, and ERC2011-StG201001109. We thank P. Follert for help with microdissection, L. Miranda for technical assistance, C. Couillault for help with the *C. elegans* injections, Aude Barani from the Regional Flow Cytometry Platform for Microbiology (PRECYM) of the Mediterranean Institute of Oceanography (MIO) for FACS, R. Segal for ZIC-specific antibody, the France-BioImaging/PICsL infrastructure (ANR-10-INSB-04-01) and IBDM animal facilities, and the Caenorhabditis Genetics Center, M. Barr, J. Dent, and S. Alper for *C. elegans* strains and plasmids.

The authors declare no competing financial interests.

*M.-C.T., C.B., and S.M. contributed equally to this work.

†V.B. and H.C. are senior co-authors.

Correspondence should be addressed to Dr. Harold Cremer, Aix-Marseille University, CNRS, IBDM, UMR 7288, Marseille 13009, France. E-mail: harold.cremer@univ-amu.fr.

DOI:10.1523/JNEUROSCI.3888-16.2017

 0270-6474/17/3710611-13$15.00/0

pools is already established during early time points of embryonic forebrain development, starting at E11.5, when subpopulations of embryonic progenitor cells in the developing cortex, striatum, and septum are set aside to be reactivated for OB neurogenesis after birth (Fuentealba et al., 2015).

These observations suggest that developmental mechanisms that are used to generate defined type of neurons in the embryo are maintained and needed for the specification of neuronal phenotype in the postnatal OB. In agreement with this idea, glutamatergic neurons for the embryonic cortex are generated in the dorsal telencephalon (Hevner et al., 2006), a region that gives rise to the postnatal dorsal V/SVZ which later generates the glutamatergic interneurons for the OB (Anderson et al., 1997b; Brill et al., 2009; Winpenny et al., 2011). Similarly, GABAergic interneurons destined for the developing cortex are generated by the ganglionic eminences of the subpallium (Anderson et al., 1997a), a region that postnatally generates GABAergic neurons for the OB (Merkle et al., 2007).

However, the precise situation is more complex. For example the dorsal V/SVZ, which in the embryo generates exclusively glutamatergic neurons, produces in the postnatal brain only low numbers of this neurotransmitter type, but predominantly GABAergic and dopaminergic (DA) neurons (Fiorelli et al., 2015). At the molecular level this indicates that additional regulatory mechanisms have to be activated postnatally, inducing this new diversity. Moreover, fate decisions are not confined to the stem cell compartment, since expression of new transcription factor combinations to produce specific neuronal phenotypes can occur at the postmitotic stage (Brill et al., 2008; de Chevigny et al., 2012b). Thus, to understand the regulatory mechanisms that control neuronal diversity we have to investigate molecular determinants in the postnatal neurogenic system in space (in different stem cell compartments), but also in time (from stem cells to neurons).

We performed an *in vivo* screen that allowed following gene expression in the dorsal (cortical) and lateral (striatal) lineages of OB neurogenesis. We show that both lineages maintain transcription factor signatures corresponding to their sites of origin, the pallium and subpallium. Focusing on the dorsal compartment we demonstrate that additional factors are induced, that can account for the *de novo* potential of this stem cell pool. We demonstrate that the zinc-finger transcription factors Zic1 and Zic2 are expressed postnatally in a subset of dorsal stem and progenitor cells where they repress dopaminergic fate and induce the production of calretinin (CR)-positive GABAergic interneurons.

In parallel, we investigated the conservation of the DA repressor function of Zic proteins using the invertebrate *Caenorhabditis elegans*. We demonstrate that the unique *C. elegans* Zic protein REF-2 represses the dopaminergic pathway in the nematode dorsal head, comparable to the situation in vertebrates.

Materials and Methods

Mice. All animals were treated according to protocols approved by the French Ethical Committee. CD1 (RjOrl:SWISS) mice of both sexes (Janvier Laboratories), held under standard conditions, were used for expression pattern analyses and *in vivo* electroporation. *In vivo* functional studies were performed through P1 animal electroporation (Boutin et al., 2008). When only two conditions were tested, one litter (~15 animals) was used. When more than two conditions were tested in parallel in a same experiment, two litters were used.

Plasmids and in vivo *electroporation.* Overexpression experiments: mouse Zic1 cDNA was amplified from total RNA extracted from P1 pups dorsal SVZ tissue. Briefly, RNA was reverse transcribed using Superscript III (ThermoFisher Scientific, 12574-030) and a nested-PCR was performed on the reverse transcription product using PrimeSTAR polymerase (Ozyme, TAKR050Q) and the two couples of primers:

PCR1: Zic1 FW (TCCTGATCTTCCCTCCTTGG) and Zic1 REV (ACGGCGTATATACGTGTGTG)

PCR2: Zic1 FW_SpeI (TCACTAGTTGCAGCCACGATGCTCCTGG) and Zic1 REV_EI (TCGAATTCTAAATAGGGGGTCGGCATGT). PCR product was subsequently subcloned behind the CAG promoter into the pCX-MCS2 vector (Morin et al., 2007), or behind the BLBP promoter (Schmid et al., 2006). The pCAGGS-human Zic2 plasmid was described by García-Frigola et al. (2008). Downregulation experiments: the shZic1 clone, which was subsequently used for the *in vivo* experiments, was selected among a set of 5 shZic1 clones provided by Sigma-Aldrich. For this selection step, Zic1 cDNA was subcloned into the peGFP-C1 vector (Clontech, GenBank: U55763.1) to fuse Zic1 and eGFP proteins. This Zic1-eGFP construct was cotransfected in mycoplasma free HeLa cells together with a Zic1 shRNA and a pCAGGS-tomato expression vector (all 3 plasmids in equal ratio) using Lipofectamin2000 (ThermoFisher Scientific, 11668019) following the manufacturer's instructions. Two days after transfection images in fluorescence (GFP and Tomato) were randomly acquired in all transfected wells. Using ImageJ software GFP and tomato fluorescences were measured on all images and GFP/tomato ratios were used to evaluate the efficiency of each Zic1 shRNA to target the mouse Zic1 sequence. shZic1 targeting the sequence CCAGCGCT GCTTTCAATTCTA was finally chosen as it induced a 95% decrease in GFP fluorescence. The same sequence has been independently identified, selected, and successfully used in another study (Urban et al., 2015). The mouse shZic2 was described by Escalante et al. (2013).

For all *in vivo* functional experiments overexpression vectors and shRNA plasmids were electroporated in P1 pups, as described by Boutin et al. (2008), together with a pCX-eGFP vector (Morin et al., 2007) in a 2:1 molecular ratio to label the electroporated cells. For triple electroporations, a 2:2:1 ratio was applied (1 dose of pCX-eGFP monitor, 2 doses of gain/loss of function vector, and/or empty pCX plasmid).

Microarrays. The design of the microarray analysis performed to determine the time course of genes expression in the dorsal and lateral lineages in the SVZ-RMS-OB postnatal neurogenic system was previously described (de Chevigny et al., 2012b). Briefly, lateral and dorsal SVZ stem cells were *in vivo* electroporated with a pCX-eGFP plasmid. At various time points after electroporation tissues of interest were microdissected [SVZ tissues at 8 h post-electroporation (hpe) 1 and 2 d post-electroporation (dpe); RMS tissues at 4 dpe; whole bulb at 7 and 14 dpe] and dissociated by trypsin/DNase digestion. GFP-expressing neuronal cells were subsequently sorted by flow cytometry (MoFlow, Beckman-Coulter). Numbers of FACS isolated cells and experimental repetitions are listed in Table 1. Ten to 15 mice were used per condition.

RNA was extracted, amplified and hybridized (2 colors protocol, each color corresponding to a targeted region, dorsal or lateral wall) on a G4122F Whole Mouse Genome (4 × 44K) Oligo Microarrays (Agilent). Microarray results (referenced in GEO as GSE69693) were analyzed using R software (RRID:SCR_001905) and Limma package (RRID: SCR_010943; Gentleman et al., 2004). Briefly, data were first normalized

Table 1. Cell number and repetitions for microarray analyses

	Electroporation target	GFP + cells per animal	No. of repetitions
8 hpe	Lateral SVZ	150	2
	Dorsal SVZ	250	2
1 dpe	Lateral SVZ	358	3
	Dorsal SVZ	1091	3
2 dpe	Lateral SVZ	1066	2
	Dorsal SVZ	1590	2
4 dpe	Lateral SVZ	903	3
	Dorsal SVZ	213	3
7 dpe	Lateral SVZ	500	3
	Dorsal SVZ	371	3
14 dpe	Lateral SVZ	73	4
	Dorsal SVZ	53	4

using quantile normalization. Differential gene expression was analyzed at each time-point using a moderated *t* test applied on a filtered subset of data. The filtering selected genes for which the average of dorsal/lateral intensity ratio (log2) was >2. A FDR corrected *p* value was then calculated for each gene. A corrected $p < 0.05$ was considered significant.

In Figure 1*C–E* the genes for which the time course of the dorsal/lateral intensity ratios is shown were generally selected based on a significant differential expression for at least one time point (except for Nr4f1/COUP-TF1, which did not match this criterion but showed consistent dorsal predominance).

qRT-PCR. RNAs were extracted using miRNeasy mini kit (Qiagen, 217004). cDNAs were prepared using superscript-III (ThermoFisher Scientific, 12574-030) following manufacturer instructions. QPCRs were performed on a Bio-Rad CFX system using SYBR-GreenER qPCR SuperMix (ThermoFisher Scientific, 11762100). β-Actin was used as reference gene. Primers used for mRNA detection are the following: Beta Actin FORseq_ CTAAGGCCAACCGTGAAAAG and REVseq_ ACCAGAG GCATACAGGGACA; Zic1 FOR seq_ AACCTCAAGATCCACAAAA GGA and REVseq_ CCTCGAACTCGCACTTGAA; Zic2 FORseq_ GATCCACAAAAGAACTCATACAGG and REVseq_ CTTCTTCCTG TCGCTGCTGT; Nurr1 FORseq_ CAGCTCCGATTTCTTAACTCCAG and REVseq_ AGGGGCATTTGGTACAAGCAA.

Sample preparation and immunohistochemistry. Animals were deeply anesthetized with an overdose of xylasin/ketamine then intracardially perfused with 4% paraformaldehyde (w/v; PFA) in PBS. The brain were dissected out and further fixed overnight at 4°C in the same fixative. For light tissue fixation required for Zic immunohistochemistry, animals were first perfused with PBS (10 ml/10 g) then with 4% PFA (10 ml/10 g). Brains were dissected out, further fixed for 1 h. Fifty micrometer floating sections were processed as described previously (Boutin et al., 2010), blocked in PBS supplemented with 0.3% Triton and 5% fetal bovine serum for 1 h at room temperature and incubated at 4°C overnight in the blocking solution supplemented with primary antibody. After washing, sections were incubated for 2 h at room temperature in the blocking solution supplemented with a fluorophore-conjugated secondary antibody. After staining of cell nuclei with Hoechst 33258, sections were mounted onto Superfrost Plus slides with Mowiol.

The primary antibodies we used were designed against pan-Zic (rabbit IgG, 1:1000; generous gift from Rosalind Segal; Borghesani et al., 2002), Zic2 (rabbit IgG, 1: 1000; Brown et al., 2003), GFP (rabbit IgG, 1:1000; ThermoFisher Scientific, Catalog #PA1–28521, RRID:AB_1956473; or chicken IgY, 1:1000; Aves Labs, Catalog #GFP-1010, RRID:AB_2307313), KI67 (mouse IgG_1; BD Biosciences, Catalog #550609, RRID:AB_393778; 1:200), CR (mouse IgG_1, 1:2000; Synaptic Systems, Catalog #214 111C3 RRID:AB_2619906;), and tyrosine hydroxylase (TH; chicken IgY, 1:1000; Aves Labs, Catalog #TYH RRID:AB_10013440). The adapted secondary antibodies were provided by ThermoFisher Scientific.

C. elegans. For *ref-2* ubiquitous overexpression in *C. elegans*, a construct containing the *ref-2* cDNA under the control of a heat shock promoter (Alper and Kenyon, 2002) was injected at 20 ng/μl with 80 ng/μl *hisp::his::mCherry* coinjection marker to generate the *vbaEx113* extrachromosomal array; (*vbaEx113; vtIs1*) embryos or (*vtIs1*) control embryos were then mounted on slides at the two-cell stage, incubated 250 min at 20°C (before the birth of the dopaminergic neurons), and then shifted to 33°C for 30 min and put back to 20°C until analysis at the L1 larval stage.

Quantification and statistics. For mice experiments both sexes were used. Quantification of CR or TH-expressing cells among the GFP electroporated periglomerular neurons at 14 and 21 dpe was assessed on photomicrographs taken on an Apotome M2 microscope (Zeiss). The number of independent experiments, animals, and counted cells is detailed in the figure legends. For the characterization of the dorsally originated periglomerular cells at 21 dpe, the percentage of TH+ and CR+ cells represent the mean value of four independent experiments comprising in total 20 animals (CR) and five independent experiments comprising 26 animals (TH); SEM are given.

For all *in vivo* experiments in mouse, statistically significant differences between groups of animals were assessed by the 2K-permutation test, on pooled experimental repetitions using R software (RRID:SCR_001905). This test is a nonparametric test for comparing two populations of samples in conditions where the normality of distribution cannot be assumed or assessed (May and Hunter, 1993). *C. elegans* experiments were performed on hermaphrodite animals. For Figure 6, statistically significant differences between proportions were assessed by a Fisher's exact test, two-tailed.

Results

Gene expression in the postnatal neurogenic forebrain in space and time

We aimed at comparing gene expression between different postnatal stem cell compartments during the entire neurogenic process in the V/SVZ-RMS-OB system of the mouse. Targeted forebrain electroporation allowed the specific labeling of dorsal (cortical) and lateral (striatal) stem cell pools with GFP (Fig. 1*A*; de Chevigny et al., 2012a,b). After electroporation, a labeled cell cohort passed through the different neurogenic steps to finally differentiate and integrate into the OB (Fig. 1*A*; Boutin et al., 2008). Twenty-one days post-electroporation labeled GFP^+ neurons of dorsal origin were predominantly localized in peripheral layers of the OB, the glomerular layer (GL),and the superficial GC layer (GCL; Fig. 1*A*). In the GL this population comprised 22.1% ± 0.7% TH-expressing dopaminergic neurons and 24.9 ± 1.6% CR-expressing GABAergic neurons. The remaining GFP-positive cells did not express known markers of OB interneuron subtypes, except for a small number of Tbr2-expressing glutamatergic neurons (<2%). Neurons targeted by lateral electroporation were in the OB generally confined to deep layers of the GCL (Fig. 1*A*). Among the laterally electroporated neurons <3% expressed TH or CR. Thus, targeted *in vivo* brain electroporation labeled two different heterogeneous stem cell pools that generated neurons that occupied distinct spatial positions in the OB layers and different relative proportions of dopaminergic and GABAergic neurons.

We compared the gene expression programs in the dorsal and lateral lineages from the radial glia (RG) stage to integrated neurons. Using the postnatal brain electroporation approach we labeled specifically either the dorsal or the lateral walls with GFP and performed FACS to isolate fluorescent cells 8 hpe (representing RG), 1 dpe (mainly representing RG and transit amplifying type C cells), 2 dpe (mainly type C cells and migrating neuroblasts in the SVZ), 4 dpe (tangentially migrating neuroblasts in the RMS), 7 dpe (radially migrating neuroblasts in the OB), and 14 dpe (integrating neurons in the OB; Boutin et al., 2008). Subsequent microarray analyses followed by bioinformatics comparison of the different samples provided a high-resolution matrix of gene expression in the forebrain neurogenic system in space (dorsal versus lateral lineages) and time (from stem cells to neurons; Fig. 1*B*; de Chevigny et al., 2012b). This resource is accessible under GEO reference GSE69693.

Recent work suggested that the postnatal neuronal lineages are specified early in the developing cortical and striatal ventricular walls and maintained in a quiescent state for postnatal use in OB neurogenesis (Fuentealba et al., 2015). We asked whether this spatial relationship is detectable at the molecular level in the postnatal OB neurogenic lineages. Comparison of the expression ratio in the dorsal versus lateral lineages revealed that key transcription factors (TFs) implicated in cortex regionalization, cortical layer specification or glutamatergic differentiation were strongly overrepresented in the dorsally generated postnatal OB lineage (heat map: Fig. 1*C*; space/time diagram: Fig. 1*D*). These factors included Emx1, Emx2, Pax6, Tbr1, Tbr2, NeuroD2, NeuroD6, Neurog2, Lhx2, Tcfap2c, and Bhlhe22 (Bishop et al., 2002;

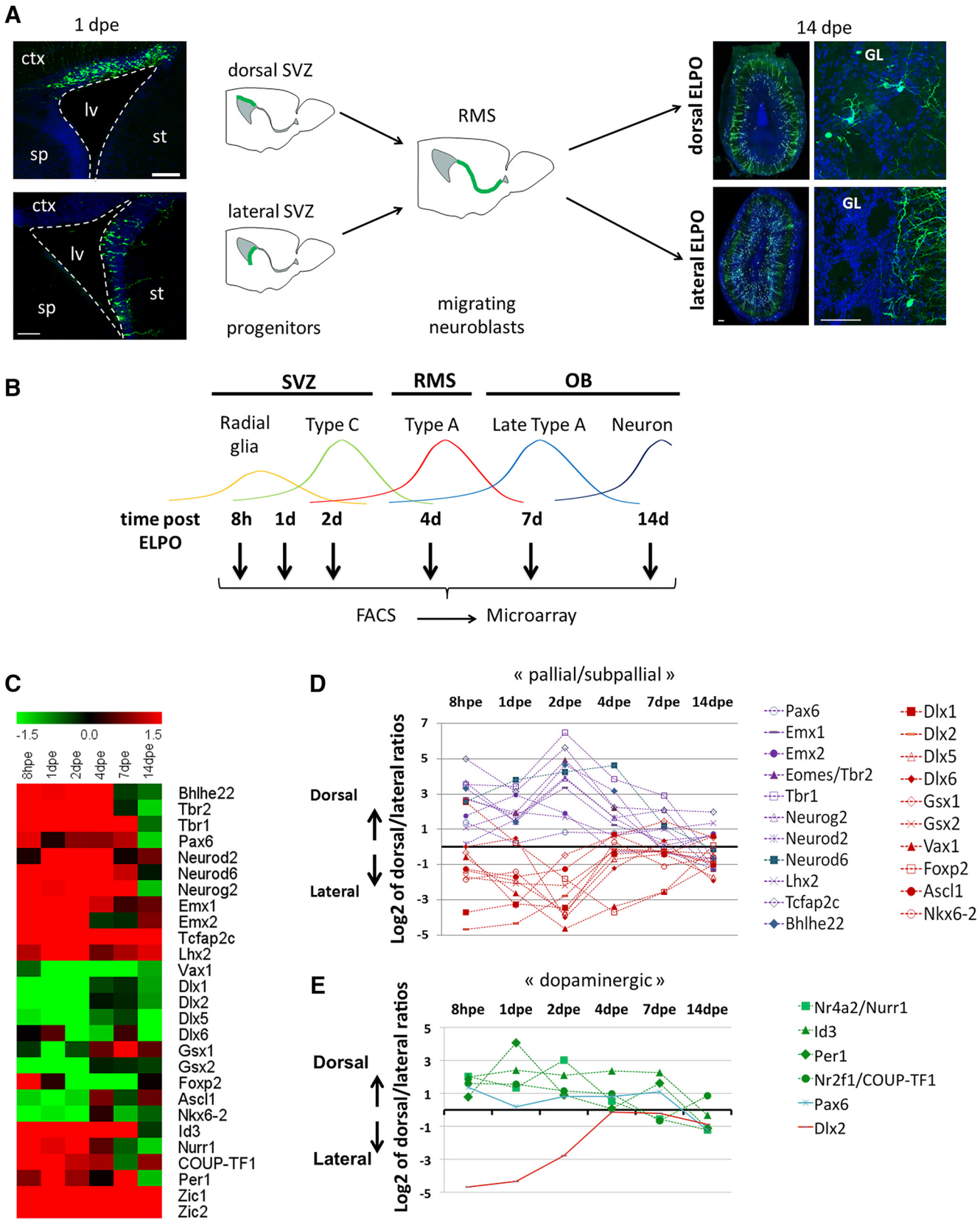

Figure 1. Gene expression analyses in dorsal and lateral neurogenic lineages from stem cells to neurons. ***A***, Schematic representation of the experimental procedure underlying the gene expression screen. V/SVZ was dorsally or laterally transfected by targeted brain electroporation (ELPO). Photomicrographs (left) represent examples for electroporation of the dorsal and lateral ventricular walls at 1dpe. After migration in the RMS GFP-expressing cells segregate into the different layers of the OB. Dorsally electroporated cells integrate after 14 d mainly into peripheral layers while laterally targeted cells remain centrally (right). ***B***, GFP-expressing cells were harvested at 8 hpe, 1 dpe, and 2 dpe from the V/SVZ, at 4 dpe from the RMS and at 7 and 14 dpe from the OB. Colored curves represent the predominant cell type at a given time point. ***C***, Heat map representation of average ratios (log values) for dorsal versus lateral intensities for all genes mentioned in this study. ***D***, Time course of gene expression dorsal/lateral ratios for key factors implicated in telencephalon development. Pallial (blue curves) and subpallial (red curves) (*Figure legend continues.*)

Englund et al., 2005; Britz et al., 2006; Joshi et al., 2008; Pinto et al., 2009; Bormuth et al., 2013; Chou and O'Leary, 2013; Dixit et al., 2014; Zembrzycki et al., 2015). In contrast, factors implicated in regionalization and specification of the subpallium, including Dlx1, Dlx2, Dlx5, Dlx6, Gsx1, Gsx2, Vax1, FoxP2, Ascl1, and Nkx6.2 (Guillemot et al., 1993; Hallonet et al., 1999; Takahashi et al., 2003; Cobos et al., 2006; Sousa et al., 2009; Wang et al., 2010; Pei et al., 2011) were predominant in the laterally generated lineage (Fig. 1*C*,*D*). Thus, molecular signatures of dorsal and lateral OB lineages reflected the cortical or subcortical origin of the respective embryonic precursor pools.

The above results indicate that the same transcriptional programs that control forebrain development in the embryo are maintained and underlie, at least in part, the generation of OB interneurons. However, during corticogenesis the dorsal telencephalon in rodents generates exclusively glutamatergic projection neurons, while in the postnatal and adult brain the cortical stem cell pool generates predominantly dopaminergic and GABAergic neurons, and only very few glutamatergic cells. This suggests that additional mechanisms must be activated in the postnatal stem cell compartments, likely in the form of additional transcription factors, which suppress or override the glutamatergic program and induce these alternative fates.

In line with this notion, we found that the orphan nuclear receptor Nurr1, a regulator of TH (Sakurada et al., 1999), was overrepresented in dorsal progenitors that generate the majority of OB DA neurons (Fig. 1*C*,*E*). Other TF that have been implicated in dopaminergic differentiation in non-midbrain neurons showed also clear dorsal predominance. These included CoupTF1, a regulator of activity-dependent TH expression (Bovetti et al., 2013), Per1, which controls DA neurons implicated in circadian rhythm (Huang et al., 2015), and Id3, which has been implicated in DA neuron maturation in zebrafish (Li et al., 2010). The expression patterns of Pax6 and Dlx2, two postnatal pro-dopaminergic factors (Hack et al., 2005; Kohwi et al., 2005; Brill et al., 2008), also illustrate the evolution of neuronal progenitors that occurs after birth. Pax6, whose expression in the embryonic pallium is confined exclusively to early progenitor stages, becomes permanently expressed in the postnatal dorsal lineage (Fig. 1*E*; de Chevigny et al., 2012b). Dlx2, which in the embryo is expressed in the subpallial stem cell compartment, is postnatally induced during migratory stages in the dorsal/pallial, lineage where it interacts with Pax6 to induce dopaminergic fate (Fig. 1*E*; Brill et al., 2008; de Chevigny et al., 2012b). In contrast, Lmx1a, Lmx1b, and Foxa2, three key factors that cooperatively specify midbrain dopaminergic neurons (Lin et al., 2009; Nakatani et al., 2010), were not detected in our expression studies, underlining that forebrain DA neurons are specified by alternative, forebrain-specific pathways.

Zic1 and Zic2 are repressors of dopaminergic fate in the postnatal forebrain

In the postnatal dorsal lineage we also identified genes that were not so far implicated in cortical neurogenesis or related to dopaminergic fate determination. In particular the zinc-finger transcription factor Zic1 (Ali et al., 2012) was strongly and consistently expressed in the dorsal isolates from the stem cell stage to neurons (Figs. 1*C*, 2*A*,*B*). Zic2 displayed comparable expression dynamics (Figs. 1*C*, 2*A*) at a lower level (Fig. 2*B*), whereas the other members of the Zic-gene family (Zic3–5) showed no significant expression, except for low signal for Zic4 at 14 dpe (Fig. 2*B*). qRT-PCR analyses of microdissected periventricular tissue from neonate (P2) and adult (≥3 months) animals demonstrated that restriction of Zic1 and Zic2 expression to the dorsal compartment was maintained in adult stages (Fig. 2*C*).

We used a pan-Zic antibody (Borghesani et al., 2002) to investigate expression at the protein level. At P2 Zic-immunoreactivity was strongest along the medial wall in agreement with previous observations (Inoue et al., 2007; Merkle et al., 2014; Fig. 2*D*, D_1). In the dorsal aspect Zic-immunoreactivity was also present but at lower levels (Fig. 2*D*, D_2). Expression was absent from the lateral ventricular wall (Fig. 2*D*, D_3). Immunostaining of P2 tissue using a Zic2-specific antibody (Brown et al., 2003) showed a highly comparable pattern to pan-Zic along the ventricular walls (Fig. 2*E*). In the OB, pan-Zic-positive cells were predominantly found in the GL and the superficial GCL (Fig. 2*F*).

We aimed at characterizing the cell types that expressed Zic-protein in the dorsal wall. Zic-protein in this compartment was found in cells with radial glia morphology in agreement with our gene expression data (compare Figs. 3*A*, 1*C*). Moreover, at P2 8.2% of Zic-positive cells in the dorsal V/SVZ were Ki67-positive (Fig. 3*B*). In the RMS, when both dorsal and lateral precursors migrate together toward the OB, only neuroblasts that were labeled by dorsal electroporation showed Zic expression (Fig. 3*C*). After arrival in the GL of the OB, 35.0% of the dorsally labeled neurons expressed Zic-protein (Fig. 3*D*). Less than 1% of these expressed TH (Fig. 3*D*,*E*; Merkle et al., 2014). However, 77.9% of the Zic^+ population expressed CR, therefore representing a subclass of GABAergic neurons (Fig. 3*D*,*F*). Thus, based on the combined use of gene expression data and immunohistochemical analyses we conclude that Zic1 and Zic2 proteins are expressed in a subpopulation of the dorsal neurogenic lineage from stem cells to neurons. In the OB, both proteins are present in the majority of dorsally labeled CR GABAergic interneurons, but absent from labeled TH-expressing cells.

This pattern prompted us to investigate the function of Zic proteins in the regulation of dopaminergic versus CR-GABAergic identity of dorsally generated OB interneurons. We used targeted *in vivo* brain electroporation to introduce a Zic1 expression plasmid based on the constitutively active β-actin promoter (CAGGS-Zic1) into the dorsal stem cell compartment (together with a GFP reporter plasmid). At 14 dpe, when transfected cells arrived in the OB and started their differentiation, the number of CR^+GFP^+ PGC was significantly increased (Fig. 4*A*,*G*). In contrast, shRNA-mediated knockdown of Zic1 (shZic1) induced a significant loss of CR^+GFP^+ interneurons (Fig. 4*B*,*G*). In the next step we investigated the impact of Zic1 alteration on dopaminergic differentiation. Dorsal electroporation of CAGGS-Zic1 induced a significant loss of TH-expressing neurons in the OB at both, 14 dpe and 21 dpe (Fig. 4*C*,*G*). Moreover, Zic1 loss-of-function significantly increased the amount of dopaminergic neurons at 21 dpe (Fig. 4*D*,*G*).

We asked whether Zic1 induced repression of dopaminergic fate could be detected at an earlier stage of neurogenic progression. As mentioned above the nuclear receptor Nurr-1 is a regulator of TH expression and has been implicated in dopaminergic differentiation in OB neurons (Vergaño-Vera et al., 2015). We performed Zic1 gain-of-function via dorsal electroporation of CAGGS-Zic1 and isolated transfected cells from the RMS at 6dpe

←

(*Figure legend continued.*) gene expression signatures are maintained in the postnatal dorsal (cortical) and lateral (striatal) lineages. ***E***, Factors implicated in dopaminergic pathways are predominant in the dorsal lineage. Note the progressive induction of expression of the subpallial gene Dlx2 in the dorsal lineage. ***D***, ***E***, The values plotted in graphs represent for each time point the log2 average of dorsal/lateral intensity value of all different experimental repetitions. ctx, Cortex; lv, lateral ventricle; sp, septum; st, striatum. Scale bars, 150 μm.

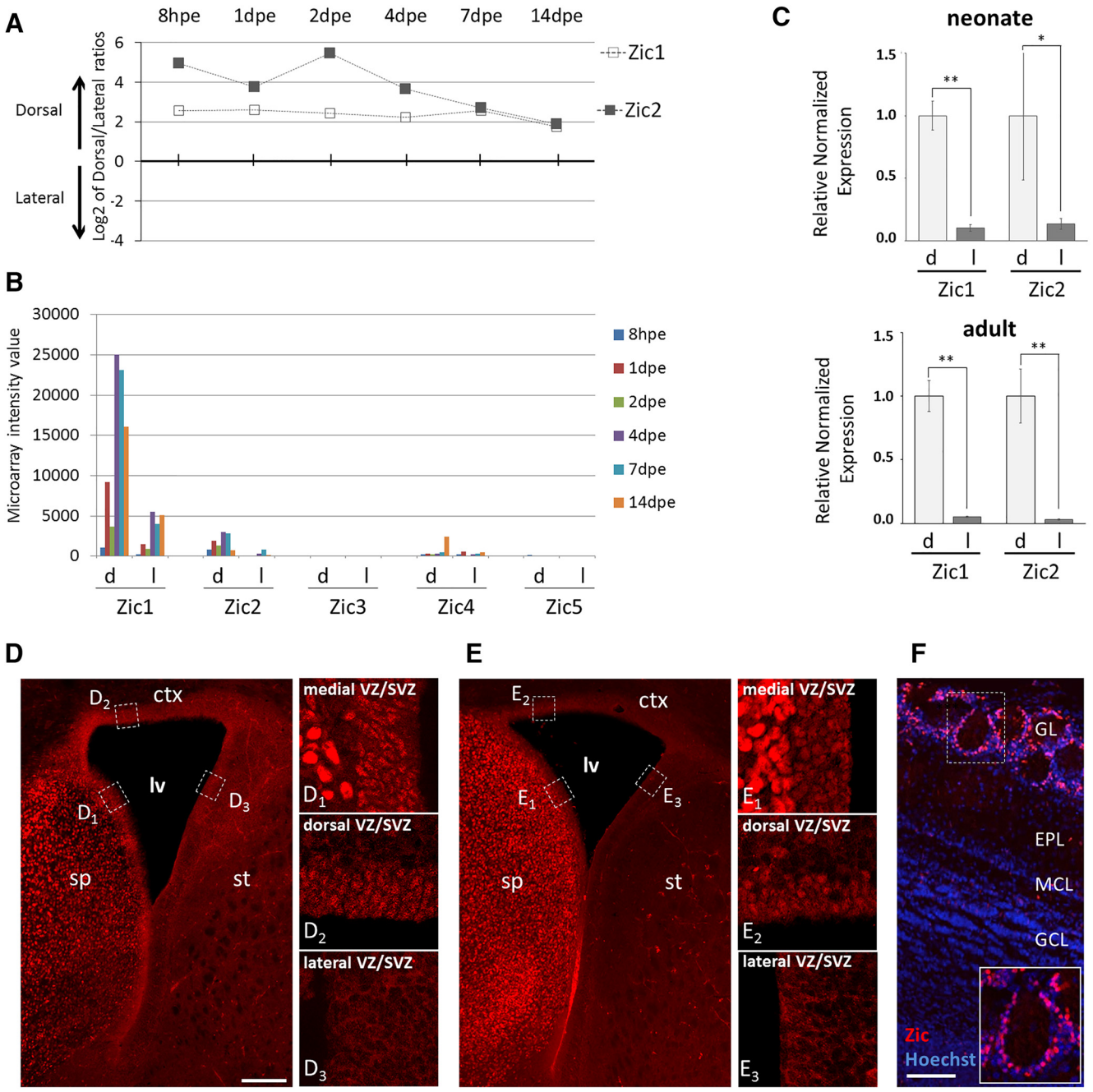

Figure 2. Expression of Zic1 and Zic2 in the mouse forebrain neurogenic system. ***A***, Time course of gene expression ratios for Zic1 and Zic2 showing predominance in the dorsal lineage from stem cells to neurons. The values plotted in graphs represent for each time point the log2 average of dorsal/lateral intensity value of all different experimental repetitions. ***B***, Microarray fluorescence intensity value at different time points of postnatal OB neurogenesis in the dorsal (d) and lateral (l) lineages for all five members of the Zic family. ***C***, qRT-PCR analysis for Zic1 and Zic2 expression in microdissected tissue isolated from neonate and adult brains. This validated the dorsal over lateral predominance of both Zic transcripts in neonates. This predominance is maintained at adult stages. Error bars represent the variation between samples (neonate: $n = 4$, 2 animals/sample, $p_{Zic1} = 0.0102$, $p_{Zic2} = 0.0318$; adult: $n = 5$, 1 animal/sample, $p_{Zic1} = 0.0047$, $p_{Zic2} = 0.0083$). ***D***, ***E***, Immunohistochemistry using anti-pan Zic (***D***) and anti-Zic2 antibody (***E***) on coronal neonate (P2) brain sections. Comparable reactivity for both antibodies is detected in the medial (D_1, E_1) and dorsal (D_2, E_2) stem cell compartment lining the lateral ventricle (lv) but absent from the lateral wall (D_3, E_3). ***F***, Anti pan-Zic immunohistochemistry on a P4 OB section. Strongly pan-Zic-positive cells are abundant in the GL (boxed area) but absent from the inner OB layers. ctx, cortex; sp, septum; st, striatum; EPL, external plexiform layer; MCL: mitral cell layer. Scale bars: ***D***, ***E***, 150 μm for left panel and 60 μm for right panels; ***F***, 300 μm and 200μm in inset. Error bars represent SEM. *$p \leq 0.05$, **$p \leq 0.01$.

by microdissection and FACS. qRT-PCR analyses showed an almost 40% reduction in Nurr1 expression at the mRNA level (Fig. 4*H*; two independent biological replicates). This suggests that an early action of Zic1 underlies repression.

In line with this idea we asked whether transitory expression of Zic1 exclusively at early stages was sufficient to promote the CR at the expense of the TH fate. A fragment of the BLBP promoter has been shown to be strongly and transitorily expressed in RG cells but not in neurons (Schmid et al., 2006). Electroporation of an expression plasmid driving Zic1 under the control of this BLBP promoter increased the generation of CR neurons and decreased the production of TH neurons in the OB GL (Fig. 4*E–G*), comparable to the change observed with the constitutive actin-promoter based construct (Fig. 4*A*,*C*).

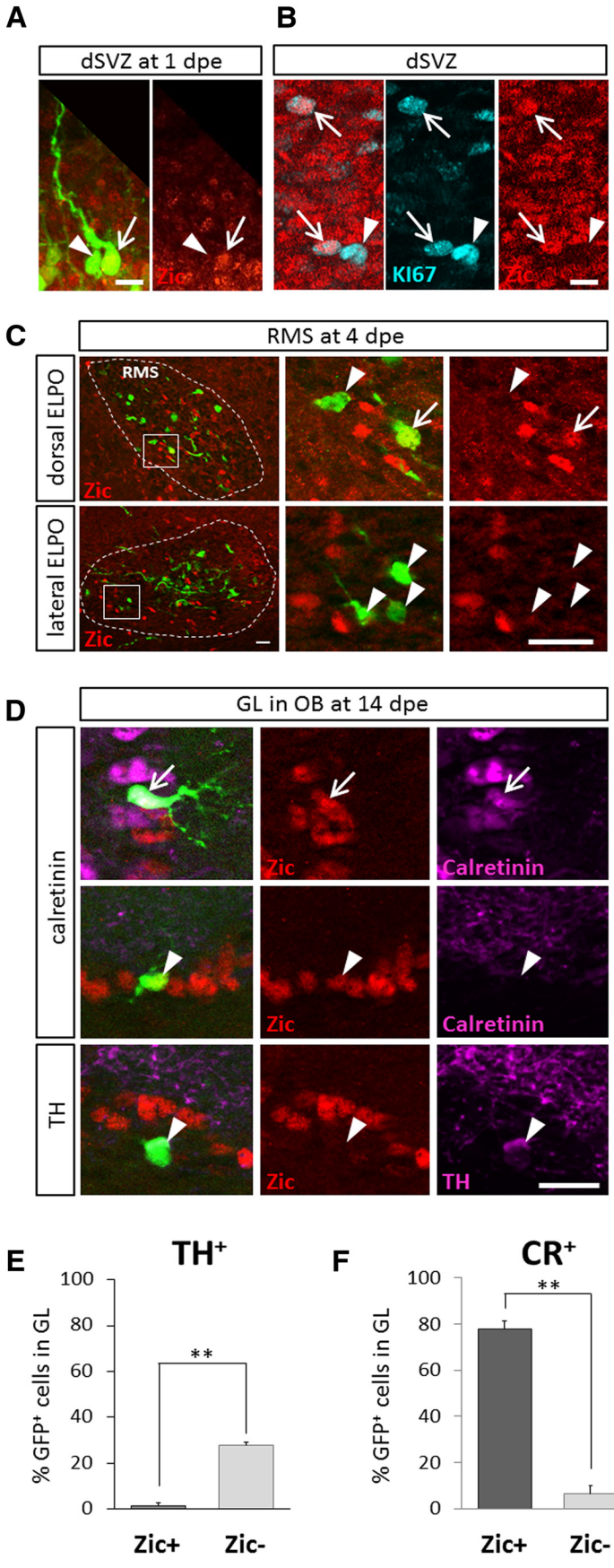

Figure 3. Zic-protein is expressed in the CR-positive GABAergic lineage but absent from dopaminergic neurons. ***A***, ***B***, In the dorsal V/SVZ, Zic protein is expressed in GFP-electroporated radial glia (***A***) at 1 dpe and in KI67$^+$ dividing progenitors (***B***) at P2. ***C***, In the RMS at 4dpe a subpopulation of GFP$^+$ cells showed Zic immunoreactivity after dorsal electroporation. Lateral electroporation did not lead to labeled Zic$^+$ cells in the RMS. ***D***, In the GL of the OB, 14 d after dorsal electroporation the majority of Zic$^+$ PGC coexpressed CR (top lane). However, some Zic$^+$ cells were negative for CR (middle lane) but Zic-immunoreactivity was never found in TH-expressing PGC (bottom lane). ***A–D***, Arrows indicate double- and arrowheads single-labeled cells. ***E***, ***F***, Quantification of TH and CR expression among Zic$^+$ or Zic$^-$ GFP cells of the GL at 21 dpe obtained in two independent experiments. Histograms represent the mean per section calculated over randomly selected sections (TH: $n = 4$, $p = 0.0094$; CR: $n = 5$, $p = 0.0047$; 2–3 sections per animal). Scale bars: **A**, **B**, 15 μm; **C**, **D**, 20 μm. Error bars represent SEM of intersection variations. **$p \leq 0.01$.

Thus, based on the combined use of gain- and loss-of-function approaches we conclude that Zic1 is an early-active neuronal fate determinant that favors generation of CR-GABAergic neurons while inhibiting generation of dopaminergic neurons on the OB.

In the next step we tested whether Zic2 had also a phenotype determining function. Gain-of-function of Zic2 significantly increased the amount of CR-expressing neurons while inhibiting dopaminergic differentiation at 21 dpe (Fig. 5*A*,*B*,*D*). We used a well characterized shRNA targeting Zic2 (Escalante et al., 2013) to investigate the consequences of Zic2 knockdown. However, Zic2 loss-of-function induced an accumulation of transfected cells in the SVZ/RMS with only few cells arriving in the OB precluding the analysis of neuronal phenotype (data not shown).

The gain-of-function results indicated that Zic2 and Zic1 have overlapping functions in CR versus TH fate decisions in PGCs. To demonstrate this parallel roles we performed electroporation experiments, combining the Zic1 knockdown and the Zic2 overexpression vectors. We observed that Zic2 expression significantly reduced the increased TH levels observed after Zic1 knockdown (Fig. 5*C*,*D*). Together these results demonstrate that Zic1 and Zic2 are both capable to induce CR-GABAergic fate while repressing the generation of dopaminergic neurons.

The Zic factor REF-2 represses dopaminergic fate in *C. elegans*

To investigate the evolutionary conservation of Zic proteins as repressors of dopaminergic fate and to circumvent the problem of redundancy between Zic factors in mice we switched to the nematode *C. elegans*. *C. elegans* has only one transcription factor of the Zic family, called REF-2. We have previously observed

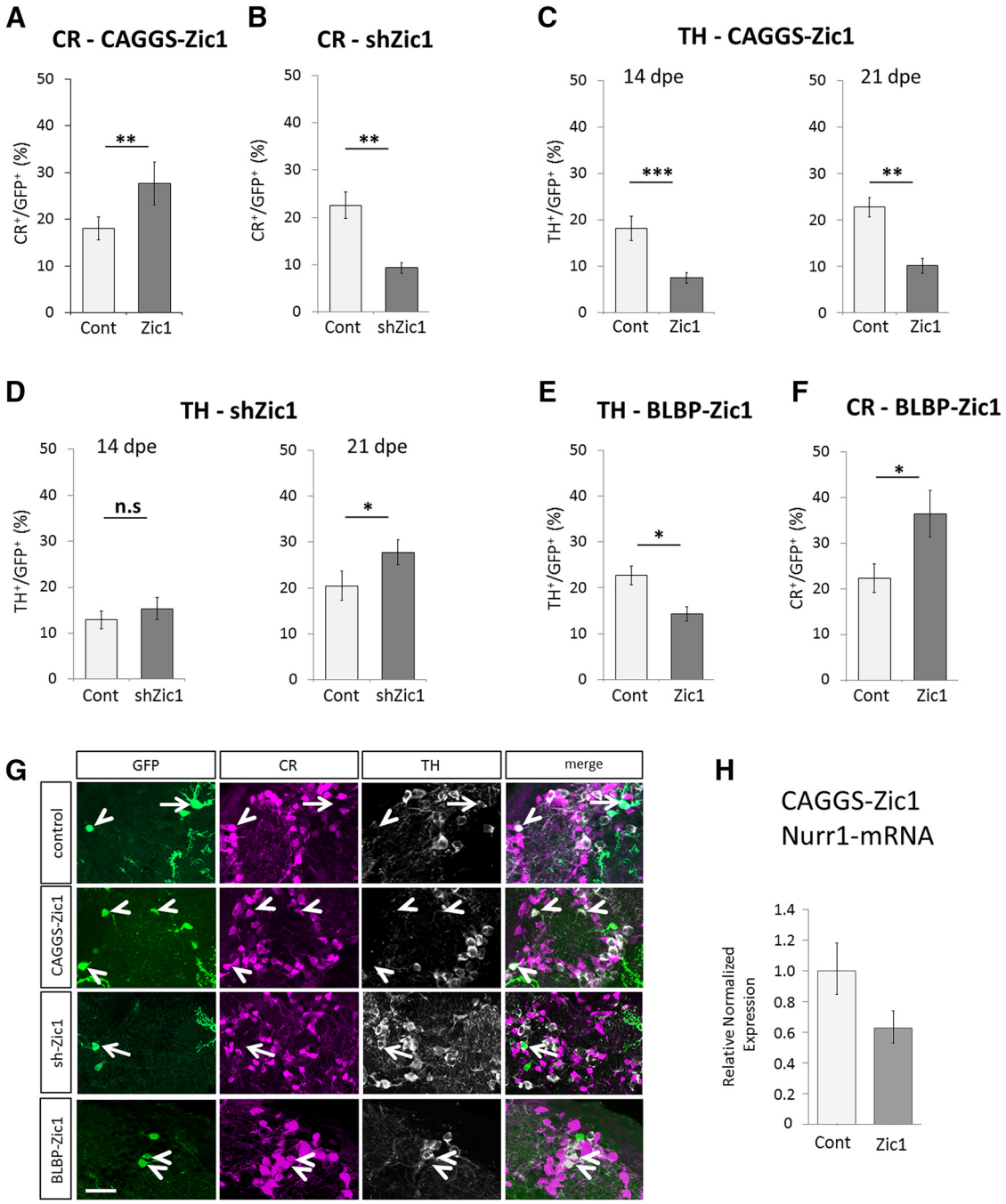

Figure 4. *In vivo* functional analyses of Zic1. ***A***, Zic1 overexpression via *in vivo* brain electroporation increases the amount of CR GABAergic-expressing neurons in the OB at 14 dpe (3 independent experiments; animals: $n_{control} = 17$, $n_{CAGGS\text{-}Zic1} = 17$; cells: $n_{control} = 1432$, $n_{CAGGS\text{-}Zic1} = 907$; $p = 0.0055$). ***B***, shRNA-induced Zic1 knockdown significantly reduces CR neurons in the OB at 14 dpe (2 independent experiments, animals: $n_{control} = 7$, $n_{shZic1} = 8$; cells: $n_{control} = 537$, $n_{shZic1} = 573$; $p = 0.0056$). ***C***, Overexpression of Zic1 in the dorsal compartment decreases dopaminergic neurons at 14 and 21 dpe (14 dpe: 2 independent experiments, animals: $n_{control} = 14$, $n_{CAGGS\text{-}Zic1} = 15$; cells: $n_{control} = 918$, $n_{CAGGS\text{-}Zic1} = 656$, $p = 0.0005$; 21 dpe: 1 experiment, animals: $n_{control} = 6$, $n_{CAGGS\text{-}Zic1} = 5$; cells: $n_{control} = 418$, $n_{CAGGS\text{-}Zic1} = 388$, $p = 0.0077$). ***D***, shRNA-induced knockdown increases dopaminergic neurons in the OB at 21 dpe but not at 14 dpe (14 dpe: 2 experiments, animals: $n_{control} = 11$, $n_{shZic1} = 9$; cells: $n_{control} = 813$, $n_{shZic1} = 459$, $p = 0.4341$; 21 dpe: 1 experiment, animals: $n_{control} = 7$, $n_{shZic1} = 7$; cells: $n_{control} = 330$, $n_{shZic1} = 330$, $p = 0.0351$). ***E***, ***F***, Overexpression of Zic1 under the control of the BLBP promoter reduces TH-expressing neurons in the OB at 21 dpe and increases the amount of CR+ GABAergic neurons (1 experiment, animals: $n_{control} = 6$, $n_{BLBP\text{-}Zic1} = 6$; cells: $n_{control} = 448$, $n_{BLBP\text{-}Zic1} = 392$; p for TH $= 0.0358$; p for CR $= 0.0291$). n.s.: $p > 0.05$, *$p \leq 0.05$, **$p \leq 0.01$, ***$p \leq 0.001$. Error bars represent SEM. ***G***, Representative images of TH and CR-expressing cells among the GFP electroporated GFP$^+$ cells in the GL at 21 dpe for electroporation with the control vector, pCAGGS-Zic1, pU6-shZic1, and pBLBP-Zic1 vectors. ***H***, qRT-PCR analysis of Nurr1 expression performed on mRNA isolated from FACS sorted SVZ cells 6 d after Zic1 overexpression. RNA samples are issued from the dissection of 10 animals. Error bars represent the variation between four technical repetitions. Arrows: CR-expressing GFP$^+$ neurons. Arrowheads: TH-expressing GFP$^+$ neurons. Scale bars, 20 μm.

that, in a null mutant for *ref-2*, the global organization of the nervous system is normal (Bertrand and Hobert, 2009). In addition, although a few neuronal subtypes were lost (for example the AIY cholinergic interneurons), most of the neuronal subtypes tested were unaffected. Dopaminergic neurons were not analyzed in this study.

Dopaminergic neurons are defined by the expression of a battery of terminal differentiation genes required for the synthesis,

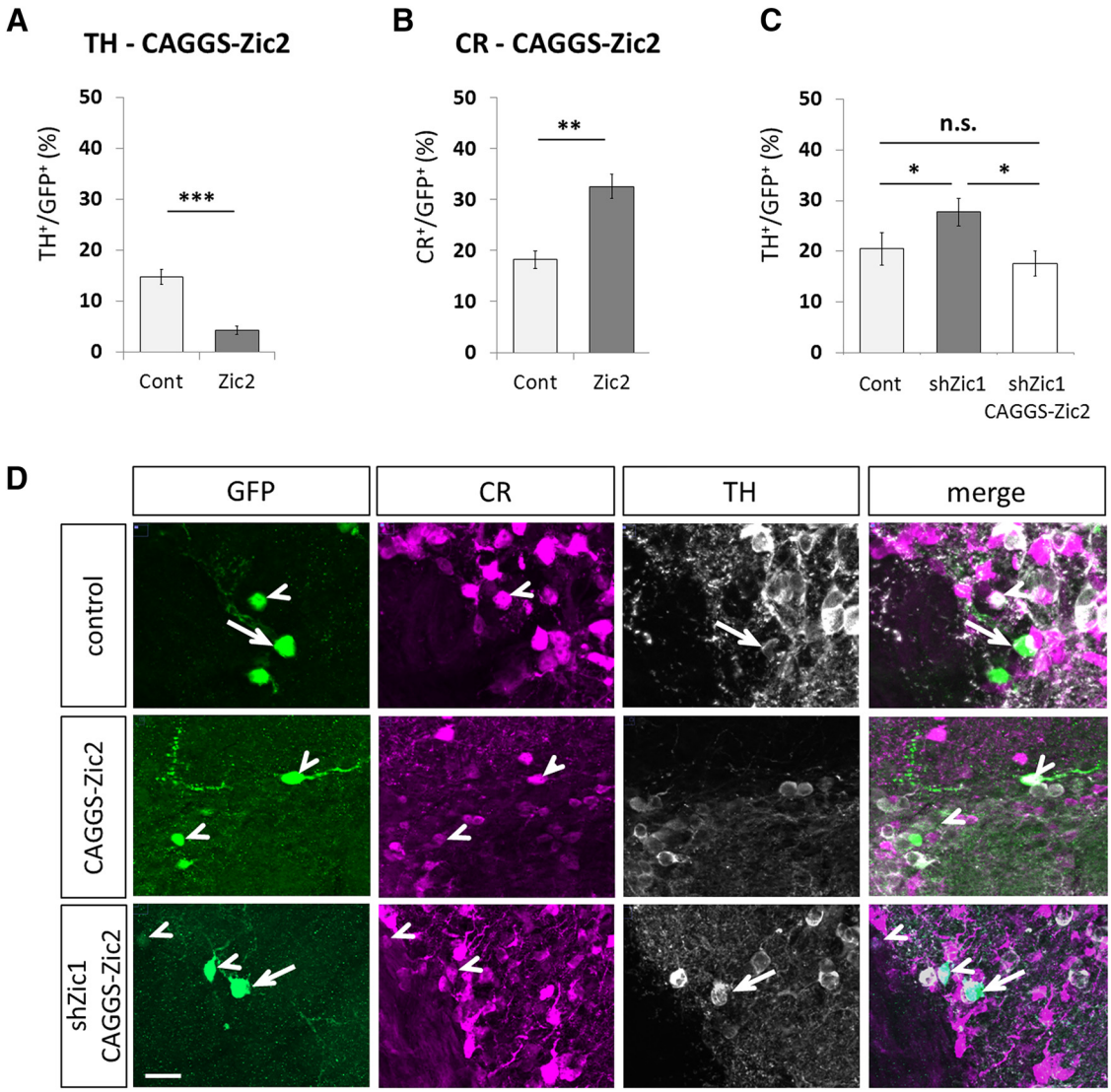

Figure 5. *In vivo* functional analyses of Zic2. ***A***, ***B***, Overexpression of Zic2 by *in vivo* brain electroporation does not significantly change the quantity of CR neurons (***A***) but does not significantly change the quantity of CR neurons (***B***); 1 experiment, animals: $n_{control} = 8$, $n_{CAGGS\text{-}Zic2} = 8$; cells: $n_{control} = 568$, $n_{CAGGS\text{-}Zic2} = 568$; p for CR = 0.00084; p for TH = 0.0023). ***C***, Increase in TH neurons in the OB at 21 dpe after Zic1 knockdown was rescued by overexpression of Zic2 (1 experiment, animals: $n_{control} = 7$, $n_{shZic1} = 7$, $n_{shZic1+CAGGS\text{-}Zic2} = 8$; cells: $n_{control} = 330$, $n_{shZic1} = 330$, $n_{shZic1+CAGGS\text{-}Zic2} = 290$; p value Cont vs shZic1 = 0.0351, p value shZic1 vs shZic1+CAGGS-Zic2 = 0.0127). n.s.: $p > 0.05$, *$p \leq 0.05$, **$p \leq 0.01$, ***$p \leq 0.001$. Error bars represent SEM. ***D***, Representative images of TH and CR-expressing cells among the GFP electroporated GFP$^+$ cells in the GL at 21 dpe, for electroporation with the control vector, pCAGGS-Zic2 vector, and pU6-shZic1 together with pCAGGS-Zic2. Arrows: CR-expressing GFP$^+$ neurons. Arrowheads: TH-expressing GFP$^+$ neurons. Scale bar, 20 μm.

packaging and transport of dopamine. This includes *dat-1* (dopamine transporter), *cat-4* (GTP cyclohydrolase), and *cat-2* (TH). To analyze the role of *ref-2* in dopaminergic neuron specification, we first used a loss-of-function approach. Wild-type *C. elegans* larvae have six dopaminergic neurons in the head (2 ADE neurons and 4 CEP neurons), which are generated during embryogenesis. Importantly, in a null mutant for *ref-2*, one or two additional neurons expressing a dopaminergic marker were observed in the dorsal part of the head (Fig. 6*A*). These neurons expressed the dopaminergic markers *dat-1* and *cat-4*, but not *cat-2* (Fig. 6*A–C*), suggesting that they acquire only a partial dopaminergic fate. In addition, ubiquitous overexpression of *ref-2* during embryogenesis using a heat shock promoter strongly inhibited the formation of dopaminergic neurons in the head (Fig. 6*D*). Thus, like in mice, a Zic protein represses dopaminergic fate in *C. elegans*.

We then investigated the origin of the ectopic "dopaminergic-like" (DA-like) neurons observed in *ref-2* loss of function mutants. As the dopaminergic neuron lineages in the wild-type contain cell death events, we first tested whether the ectopic DA-like neurons in *ref-2* mutants resulted from survival of cells that normally die. When cell death was blocked, using a mutation in the cell death gene *ced-4*, ectopic DA-like neurons were also observed, but in this case they were always located in a distinct, ventral, region of the head. Moreover, the effect of *ref-2* and *ced-4* mutants was additive, with the appearance of ectopic DA-like neurons in both, the dorsal and ventral head regions (Fig. 6*E*), altogether indicating that the appearance of ectopic DA-like neurons observed in *ref-2* mutants was not a result of a reduced cell death.

Next, we investigated whether the appearance of the ectopic DA-like neurons was the result of a conversion of some non-dopaminergic neurons to a dopaminergic fate. The ectopic DA-like neurons observed in *ref-2* mutants are located just posterior to the pairs of cholinergic neurons IL2 dorsal and URA dorsal

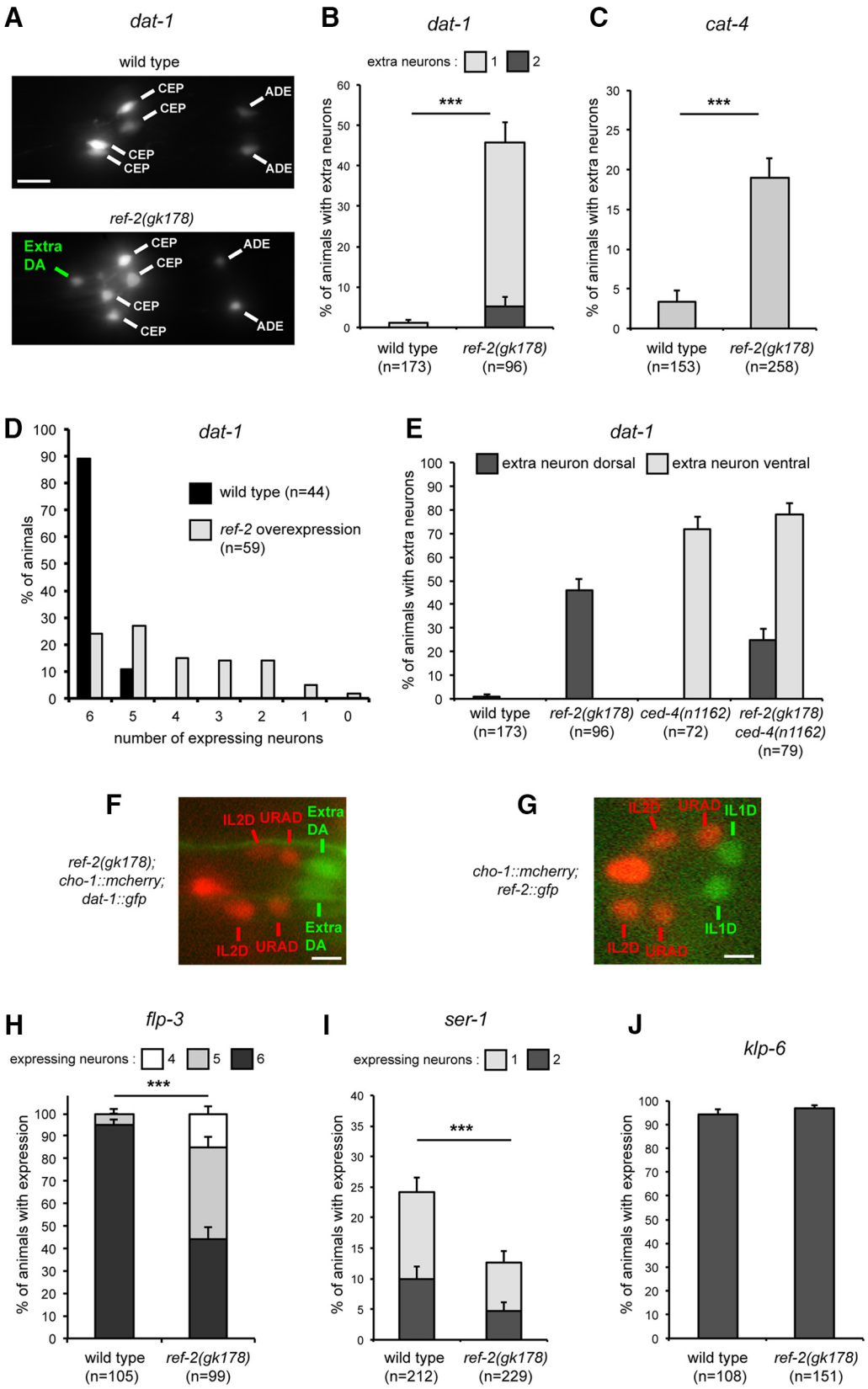

Figure 6. Effect of the *C. elegans* Zic protein REF-2 on dopaminergic fate. ***A***, In the head of wild-type *C. elegans* larvae six dopaminergic neurons are present (4 CEP and 2 ADE), in *ref-2(gk178)* mutants extra dopaminergic neurons are observed (marker of dopaminergic neurons used: *dat-1::gfp* (*vtIs1*); head of L1 larvae, lateral view, anterior is left, dorsal is up). Scale bar, 5 μm. ***B***, Percentage of L1 larvae displaying one or two extra neurons expressing *dat-1::gfp* (n = number of animals, error bars show standard error of proportion; ***$p = 3.9 \times 10^{-21}$, Fisher's exact test). ***C***, Percentage of L1 larvae displaying one extra neuron expressing *cat-4::gfp (otIs225)* in the dorsal region (n = number of animals, error bars show standard error of proportion; *** $p = 1.4 \times 10^{-6}$, Fisher's exact test). ***D***, Percentage of L1 larvae expressing *dat-1::gfp* in 6, 5, . . . , 1, or 0 dopaminergic neurons in absence (black bar) or presence (gray bar) of *ref-2* overexpression (n = number of animals). *ref-2* Overexpression does not block all neuronal differentiation as it does not affect the expression of *klp-6*, a marker of the unrelated neuronal (*Figure legend continues.*)

(Fig. 6*F*). This corresponds to the location, in wild-type animals, of the pairs of glutamatergic neurons IL1 dorsal and URY dorsal. In addition, in *ref-2* mutants, we observed a loss of the URY neuron marker *ser-1* and the IL1 neuron marker *flp-3* (Fig. 6*H*,*I*), whereas the expression of the IL2 neuron marker *klp-6* was unaffected (Fig. 6J). Finally, *ref-2* is expressed in the URY and IL1 lineages but not in the dopaminergic lineages during embryogenesis (Murray et al., 2012), and we observed that during larval and adult stages *ref-2* expression in the head is restricted to only six neurons, corresponding to the six IL1 neurons (2 dorsal, 2 lateral, and 2 ventral; Fig. 6*G* and data not shown). Together, these data suggest that the ectopic DA-like neurons observed in *ref-2* mutants were a result of a cell fate switch of the dorsal IL1 and/or dorsal URY neurons from a non-dopaminergic to a dopaminergic phenotype.

In conclusion, in mice and *C. elegans* a Zic protein represses dopaminergic fate in defined non-dopaminergic neurons.

Discussion

Based on a high-resolution gene expression screen in space and time during postnatal OB neurogenesis we show here that the dorsal and lateral lineages that generate interneurons for the OB during postnatal stages maintain molecular signatures of the embryonic pallium and subpallium. In the postnatal dorsal lineages Zic1 and Zic2 are superposed over the existing program and control neuronal phenotype by repressing dopaminergic fate and favoring the generation of CR GABAergic neurons. This anti-dopaminergic function of Zic-proteins is evolutionary conserved and also present in *C. elegans.*

Our gene expression screen resulted in the first two-dimensional gene-expression matrix that includes the spatial and the temporal components of the postnatal neurogenic system. So far such studies addressed gene expression either in static situations or during individual steps in the temporal sequence that leads to new OB neurons. Pennartz et al. (2004) investigated gene expression in migratory type A cells isolated from the RMS on the basis of PSA-NCAM expression . In another study neuronal precursors and mature neurons from the periglomerular neuron lineage were isolated and analyzed by microarray (Boutin et al., 2010). Other, more recent transcriptomic studies focused on the first steps in the neurogenic process and the switch from silent to activated neural stem cells at the population (Beckervordersandforth et al., 2010; Codega et al., 2014) and at the single cell levels (Llorens-Bobadilla et al., 2015). Only recently, work addressed transcriptomic differences between spatially separated stem cell and progenitor pools (Azim et al., 2015).

Our study provides the first systematic insight into gene expression changes during all steps of the neurogenic sequence, from stem cells in the V/SVZ over amplification and migratory stages to neurons. In addition, at each of these steps we compare two stem cell pools and their lineages that generate different types of OB neurons. This provides a unique resource for the identification of regulators and molecular cascades that control stem cell identity, their activation, and their progression toward functional neurons. Moreover, this resource allows the identification of fate determinants that are active at the stem cell level, but also those that act at the post-stem cell stage. Finally, a major advantage of our electroporation-based approach is that functional studies aiming at determining the *in vivo* function of identified candidates are based on the same technology, and therefore targeting the same cell types and differentiation steps, that we used for the screening process. This is well illustrated by our work on Zic1 and Zic2.

Neuronal diversity in the postnatal OB is based on the existence of predetermined neural stem cells organized in subregions of the postnatal ventricular walls (Merkle and Alvarez-Buylla, 2006; Merkle et al., 2007, 2014). This regionalization is already established during early time points of forebrain development (Fuentealba et al., 2015), when subsets of stem cells appear to be set aside in the cortex, striatum and septum. After birth these cells enter the neurogenic cycle and produce new neurons that migrate into the OB and integrate. Of particular interest in this context is the dorsal aspect of the postnatal neurogenic compartment, which is mainly derived from the developing cortex (Fuentealba et al., 2015). Our lineage studies in this compartment clearly identify a cortical signature with most major players in place, including Pax6, Tbr1/2, Emx1/2, and Ngn1/2. This is in agreement with a cortical descent. Whereas the lateral (striatal) and medial (septal) walls generate exclusively GABAergic neurons, the dorsal aspect shows a high degree of heterogeneity. Although still generating low amounts of glutamatergic neurons, it produces mainly large numbers of GABAergic and dopaminergic neurons. Thus, it can be expected that new combinations of transcription factors occur in this compartment, superposed over the pre-existing cortical program, that allow the acquisition of new phenotypic traits.

One such example is Dlx2, a distal-less homeodomain protein that is expressed in the ventrolateral forebrain, the subpallial ganglionic eminences, and that in the embryo is involved the generation of cortical interneurons (Anderson et al., 1999). However, at postnatal stages Dlx2 is expressed in the dopaminergic lineage of the OB GL, and is interacting with Pax6 to induce this neurotransmitter phenotype (Brill et al., 2008; de Chevigny et al., 2012b). Thus, introduction of a subpallial gene into the pallial lineage is necessary for the appearance of a new neuron type for the postnatal OB.

The situation shows parallels to what we find for Zic-proteins. Like Dlx2, Zic-proteins are expressed in the Pax6-expressing dorsal stem cell compartment and control neuronal fate in OB PGC. Within this population the majority of Zic-positive neurons were of the CR^+ GABAergic phenotype, whereas Zic-proteins were absent from dopaminergic neurons. Our functional work clearly demonstrates that Zic1 and Zic2 are able to repress dopaminergic fate and to induce the second major population derived from the dorsal aspect, GABAergic CR-expressing neurons. We conclude

←

(*Figure legend continued.*) class IL2 (without *ref-2* ectopic expression 20/20 animals express *klp-6::gfp (myIs13*) in the six IL2 neurons; with *ref-2* ectopic expression 25/25 animals express *klp-6::gfp* in the six IL2 neurons). ***E***, Percentage of L1 larvae displaying extra neurons expressing *dat-1::gfp* (*vtIs1*) in the dorsal region (dark gray) or ventral region (light gray; n = number of animals, error bars show standard error of proportion). The effect of *ref-2* and *ced-4* mutations is additive suggesting that the extra neurons expressing *dat-1::gfp* observed in *ref-2* mutants do not come from a loss of cell death. ***F***, The two extra dopaminergic neurons observed in *ref-2(gk178)* mutants (extra DA labeled with *dat-1::gfp*) are located just posterior to the pairs of cholinergic neurons IL2 dorsal (IL2D) and URA dorsal [URAD; labeled with *cho-1::mcherry* (*otIs544*)]. Dorsal view of the head of a L1 larva, anterior is left. Scale bar, 2 μm. ***G***, Expression of *ref-2::gfp* (fosmid translational reporter, *wgIs520*) in the pair of IL1D glutamatergic neurons, located just posterior to the pairs of cholinergic neurons IL2D and URAD [labeled with *cho-1::mcherry* (*otIs544*)]. Dorsal view of the head of a L1 larva, anterior is left. Scale bar, 2 μm. ***H***, Percentage of L1 larvae expressing the IL1 neuron marker *flp-3* (*flp-3::gfp*, *ynIs21*) in 6, 5, or 4 IL1 neurons (n = number of animals, error bars show standard error of proportion; $^{***}p = 1.1 \times 10^{-16}$, Fisher's exact test). ***I***, Percentage of L1 larvae expressing the URYD neuron marker *ser-1* (*ser-1::gfp*, *vuEx172*) in one or both URYD neurons (n = number of animals, error bars show standard error of proportion; $^{***}p = 0.002$, Fisher's exact test). ***J***, Percentage of L1 larvae expressing the IL2 neuron marker *klp-6* (*klp-6::gfp*, *myIs13*) in every IL2 neurons (n = number of animals, error bars show standard error of proportion).

that Zic1 and Zic2 are used in the postnatal dorsal stem cell compartment to induce new phenotypic traits in the form of CR^+ GABAergic PGC, comparable to the introduction of the subpallial factor Dlx2 in the dorsal dopaminergic lineage.

There is a deep phylogenetic conservation of the gene regulatory networks specifying the dopaminergic fate between mice and *C. elegans*. The dopamine biosynthetic pathway in both species is very similar (Flames and Hobert, 2011) and nematode mutants can be rescued by introducing the corresponding human ortholog (Duerr et al., 1999). In addition, dopaminergic neurons in *C. elegans* and in the mouse olfactory bulb express similar combinations of transcription factors, including Ets, Dlx, and Pbx proteins (Flames and Hobert, 2009; Doitsidou et al., 2013). Our finding that Zic proteins function as repressors of dopaminergic fate in worm and mouse represents further support for the deep conservation of the gene regulatory networks specifying this neurotransmitter phenotype. It will be important in the future to characterize the biochemical mechanism by which Zic proteins repress dopaminergic fate in both organisms.

References

Ali RG, Bellchambers HM, Arkell RM (2012) Zinc fingers of the cerebellum (Zic): transcription factors and co-factors. Int J Biochem Cell Biol 44: 2065–2068. CrossRef Medline

Alper S, Kenyon C (2002) The zinc finger protein REF-2 functions with the Hox genes to inhibit cell fusion in the ventral epidermis of *C. elegans*. Development 129:3335–3348. Medline

Alvarez-Buylla A, Garcia-Verdugo JM (2002) Neurogenesis in adult subventricular zone. J Neurosci 22:629–634. Medline

Alvarez-Buylla A, Kohwi M, Nguyen TM, Merkle FT (2008) The heterogeneity of adult neural stem cells and the emerging complexity of their niche. Cold Spring Harb Symp Quant Biol 73:357–365. CrossRef Medline

Anderson DJ, Groves A, Lo L, Ma Q, Rao M, Shah NM, Sommer L (1997a) Cell lineage determination and the control of neuronal identity in the neural crest. Cold Spring Harb Symp Quant Biol 62:493–504. CrossRef Medline

Anderson SA, Qiu M, Bulfone A, Eisenstat DD, Meneses J, Pedersen R, Rubenstein JL (1997b) Mutations of the homeobox genes Dlx-1 and Dlx-2 disrupt the striatal subventricular zone and differentiation of late born striatal neurons. Neuron 19:27–37. CrossRef Medline

Anderson S, Mione M, Yun K, Rubenstein JL (1999) Differential origins of neocortical projection and local circuit neurons: role of Slx genes in neocortical interneuronogenesis. Cereb Cortex 9:646–654. CrossRef Medline

Azim K, Hurtado-Chong A, Fischer B, Kumar N, Zweifel S, Taylor V, Raineteau O (2015) Transcriptional hallmarks of heterogeneous neural stem cell niches of the subventricular zone. Stem Cells 33:2232–2242. CrossRef Medline

Beckervordersandforth R, Tripathi P, Ninkovic J, Bayam E, Lepier A, Stempfhuber B, Kirchhoff F, Hirrlinger J, Haslinger A, Lie DC, Beckers J, Yoder B, Irmler M, Götz M (2010) *In vivo* fate mapping and expression analysis reveals molecular hallmarks of prospectively isolated adult neural stem cells. Cell Stem Cell 7:744–758. CrossRef Medline

Bertrand V, Hobert O (2009) Linking asymmetric cell division to the terminal differentiation program of postmitotic neurons in *C. elegans*. Dev Cell 16:563–575. CrossRef Medline

Bishop KM, Rubenstein JL, O'Leary DD (2002) Distinct actions of Emx1, Emx2, and Pax6 in regulating the specification of areas in the developing neocortex. J Neurosci 22:7627–7638. Medline

Borghesani PR, Peyrin JM, Klein R, Rubin J, Carter AR, Schwartz PM, Luster A, Corfas G, Segal RA (2002) BDNF stimulates migration of cerebellar granule cells. Development 129:1435–1442. Medline

Bormuth I, Yan K, Yonemasu T, Gummert M, Zhang M, Wichert S, Grishina O, Pieper A, Zhang W, Goebbels S, Tarabykin V, Nave KA, Schwab MH (2013) Neuronal basic helix-loop-helix proteins Neurod2/6 regulate cortical commissure formation before midline interactions. J Neurosci 33: 641–651. CrossRef Medline

Boutin C, Diestel S, Desoeuvre A, Tiveron MC, Cremer H (2008) Efficient *in vivo* electroporation of the postnatal rodent forebrain. PLoS One 3:e1883. CrossRef Medline

Boutin C, Hardt O, de Chevigny A, Coré N, Goebbels S, Seidenfaden R, Bosio A, Cremer H (2010) NeuroD1 induces terminal neuronal differentiation in olfactory neurogenesis. Proc Natl Acad Sci U S A 107:1201–1206. CrossRef Medline

Bovetti S, Bonzano S, Garzotto D, Giannelli SG, Iannielli A, Armentano M, Studer M, De Marchis S (2013) COUP-TFI controls activity-dependent tyrosine hydroxylase expression in adult dopaminergic olfactory bulb interneurons. Development 140:4850–4859. CrossRef Medline

Brill MS, Snapyan M, Wohlfrom H, Ninkovic J, Jawerka M, Mastick GS, Ashery-Padan R, Saghatelyan A, Berninger B, Götz M (2008) A Dlx2- and Pax6-dependent transcriptional code for periglomerular neuron specification in the adult olfactory bulb. J Neurosci 28:6439–6452. CrossRef Medline

Brill MS, Ninkovic J, Winpenny E, Hodge RD, Ozen I, Yang R, Lepier A, Gascón S, Erdelyi F, Szabo G, Parras C, Guillemot F, Frotscher M, Berninger B, Hevner RF, Raineteau O, Götz M (2009) Adult generation of glutamatergic olfactory bulb interneurons. Nat Neurosci 12:1524–1533. CrossRef Medline

Britz O, Mattar P, Nguyen L, Langevin LM, Zimmer C, Alam S, Guillemot F, Schuurmans C (2006) A role for proneural genes in the maturation of cortical progenitor cells. Cereb Cortex 16:i138–151. CrossRef Medline

Brown LY, Kottmann AH, Brown S (2003) Immunolocalization of Zic2 expression in the developing mouse forebrain. Gene Expr Patterns 3:361–367. CrossRef Medline

Chou SJ, O'Leary DD (2013) Role for Lhx2 in corticogenesis through regulation of progenitor differentiation. Mol Cell Neurosci 56:1–9. CrossRef Medline

Cobos I, Long JE, Thwin MT, Rubenstein JL (2006) Cellular patterns of transcription factor expression in developing cortical interneurons. Cereb Cortex 16:i82–88. CrossRef Medline

Codega P, Silva-Vargas V, Paul A, Maldonado-Soto AR, Deleo AM, Pastrana E, Doetsch F (2014) Prospective identification and purification of quiescent adult neural stem cells from their *in vivo* niche. Neuron 82:545–559. CrossRef Medline

de Chevigny A, Coré N, Follert P, Gaudin M, Barbry P, Béclin C, Cremer H (2012a) miR-7a regulation of Pax6 controls spatial origin of forebrain dopaminergic neurons. Nat Neurosci 15:1120–1126. CrossRef Medline

de Chevigny A, Core N, Follert P, Wild S, Bosio A, Yoshikawa K, Cremer H, Beclin C (2012b) Dynamic expression of the pro-dopaminergic transcription factors Pax6 and Dlx2 during postnatal olfactory bulb neurogenesis. Front Cell Neurosci 6:6. CrossRef Medline

Dixit R, Wilkinson G, Cancino GI, Shaker T, Adnani L, Li S, Dennis D, Kurrasch D, Chan JA, Olson EC, Kaplan DR, Zimmer C, Schuurmans C (2014) Neurog1 and Neurog2 control two waves of neuronal differentiation in the piriform cortex. J Neurosci 34:539–553. CrossRef Medline

Doitsidou M, Flames N, Topalidou I, Abe N, Felton T, Remesal L, Popovitchenko T, Mann R, Chalfie M, Hobert O (2013) A combinatorial regulatory signature controls terminal differentiation of the dopaminergic nervous system in *C. elegans*. Genes Dev 27:1391–1405. CrossRef Medline

Duerr JS, Frisby DL, Gaskin J, Duke A, Asermely K, Huddleston D, Eiden LE, Rand JB (1999) The cat-1 gene of *Caenorhabditis elegans* encodes a vesicular monoamine transporter required for specific monoamine-dependent behaviors. J Neurosci 19:72–84. Medline

Englund C, Fink A, Lau C, Pham D, Daza RA, Bulfone A, Kowalczyk T, Hevner RF (2005) Pax6, Tbr2, and Tbr1 are expressed sequentially by radial glia, intermediate progenitor cells, and postmitotic neurons in developing neocortex. J Neurosci 25:247–251. CrossRef Medline

Escalante A, Murillo B, Morenilla-Palao C, Klar A, Herrera E (2013) Zic2-dependent axon midline avoidance controls the formation of major ipsilateral tracts in the CNS. Neuron 80:1392–1406. CrossRef Medline

Fiorelli R, Azim K, Fischer B, Raineteau O (2015) Adding a spatial dimension to postnatal ventricular-subventricular zone neurogenesis. Development 142:2109–2120. CrossRef Medline

Flames N, Hobert O (2009) Gene regulatory logic of dopamine neuron differentiation. Nature 458:885–889. CrossRef Medline

Flames N, Hobert O (2011) Transcriptional control of the terminal fate of monoaminergic neurons. Annu Rev Neurosci 34:153–184. CrossRef Medline

Fuentealba LC, Rompani SB, Parraguez JI, Obernier K, Romero R, Cepko CL, Alvarez-Buylla A (2015) Embryonic origin of postnatal neural stem cells. Cell 161:1644–1655. CrossRef Medline

García-Frigola C, Carreres MI, Vegar C, Mason C, Herrera E (2008) Zic2 promotes axonal divergence at the optic chiasm midline by EphB1-

dependent and -independent mechanisms. Development 135:1833–1841. CrossRef Medline

Gentleman RC, Carey VJ, Bates DM, Bolstad B, Dettling M, Dudoit S, Ellis B, Gautier L, Ge Y, Gentry J, Hornik K, Hothorn T, Huber W, Iacus S, Irizarry R, Leisch F, Li C, Maechler M, Rossini AJ, Sawitzki G, et al. (2004) Bioconductor: open software development for computational biology and bioinformatics. Genome Biol 5:R80. CrossRef Medline

Guillemot F (2007) Spatial and temporal specification of neural fates by transcription factor codes. Development 134:3771–3780. CrossRef Medline

Guillemot F, Lo LC, Johnson JE, Auerbach A, Anderson DJ, Joyner AL (1993) Mammalian achaete-scute homolog 1 is required for the early development of olfactory and autonomic neurons. Cell 75:463–476. CrossRef Medline

Hack MA, Saghatelyan A, de Chevigny A, Pfeifer A, Ashery-Padan R, Lledo PM, Götz M (2005) Neuronal fate determinants of adult olfactory bulb neurogenesis. Nat Neurosci 8:865–872. CrossRef Medline

Hallonet M, Hollemann T, Pieler T, Gruss P (1999) Vax1, a novel homeobox-containing gene, directs development of the basal forebrain and visual system. Genes Dev 13:3106–3114. CrossRef Medline

Hevner RF, Hodge RD, Daza RA, Englund C (2006) Transcription factors in glutamatergic neurogenesis: conserved programs in neocortex, cerebellum, and adult hippocampus. Neurosci Res 55:223–233. CrossRef Medline

Huang J, Zhong Z, Wang M, Chen X, Tan Y, Zhang S, He W, He X, Huang G, Lu H, Wu P, Che Y, Yan YL, Postlethwait JH, Chen W, Wang H (2015) Circadian modulation of dopamine levels and dopaminergic neuron development contributes to attention deficiency and hyperactive behavior. J Neurosci 35:2572–2587. CrossRef Medline

Inoue T, Ota M, Ogawa M, Mikoshiba K, Aruga J (2007) Zic1 and Zic3 regulate medial forebrain development through expansion of neuronal progenitors. J Neurosci 27:5461–5473. CrossRef Medline

Joshi PS, Molyneaux BJ, Feng L, Xie X, Macklis JD, Gan L (2008) Bhlhb5 regulates the postmitotic acquisition of area identities in layers II-V of the developing neocortex. Neuron 60:258–272. CrossRef Medline

Kohwi M, Osumi N, Rubenstein JL, Alvarez-Buylla A (2005) Pax6 is required for making specific subpopulations of granule and periglomerular neurons in the olfactory bulb. J Neurosci 25:6997–7003. CrossRef Medline

Li S, Yin M, Liu S, Chen Y, Yin Y, Liu T, Zhou J (2010) Expression of ventral diencephalon-enriched genes in zebrafish. Dev Dyn 239:3368–3379. CrossRef Medline

Lin W, Metzakopian E, Mavromatakis YE, Gao N, Balaskas N, Sasaki H, Briscoe J, Whitsett JA, Goulding M, Kaestner KH, Ang SL (2009) Foxa1 and Foxa2 function both upstream of and cooperatively with Lmx1a and Lmx1b in a feedforward loop promoting mesodiencephalic dopaminergic neuron development. Dev Biol 333:386–396. CrossRef Medline

Llorens-Bobadilla E, Zhao S, Baser A, Saiz-Castro G, Zwadlo K, Martin-Villalba A (2015) Single-cell transcriptomics reveals a population of dormant neural stem cells that become activated upon brain injury. Cell Stem Cell 17:329–340. CrossRef Medline

May RB, Hunter MA (1993) Some advantages of permutation tests. Can Psychol 34:401–407. CrossRef

Merkle FT, Alvarez-Buylla A (2006) Neural stem cells in mammalian development. Curr Opin Cell Biol 18:704–709. CrossRef Medline

Merkle FT, Mirzadeh Z, Alvarez-Buylla A (2007) Mosaic organization of neural stem cells in the adult brain. Science 317:381–384. CrossRef Medline

Merkle FT, Fuentealba LC, Sanders TA, Magno L, Kessaris N, Alvarez-Buylla A (2014) Adult neural stem cells in distinct microdomains generate previously unknown interneuron types. Nat Neurosci 17:207–214. CrossRef Medline

Morin X, Jaouen F, Durbec P (2007) Control of planar divisions by the G-protein regulator LGN maintains progenitors in the chick neuroepithelium. Nat Neurosci 10:1440–1448. CrossRef Medline

Murray JI, Boyle TJ, Preston E, Vafeados D, Mericle B, Weisdepp P, Zhao Z, Bao Z, Boeck M, Waterston RH (2012) Multidimensional regulation of gene expression in the *C. elegans* embryo. Genome Res 22:1282–1294. CrossRef Medline

Nakatani T, Kumai M, Mizuhara E, Minaki Y, Ono Y (2010) Lmx1a and Lmx1b cooperate with Foxa2 to coordinate the specification of dopaminergic neurons and control of floor plate cell differentiation in the developing mesencephalon. Dev Biol 339:101–113. CrossRef Medline

Pei Z, Wang B, Chen G, Nagao M, Nakafuku M, Campbell K (2011) Homeobox genes Gsx1 and Gsx2 differentially regulate telencephalic progenitor maturation. Proc Natl Acad Sci U S A 108:1675–1680. CrossRef Medline

Pennartz S, Belvindrah R, Tomiuk S, Zimmer C, Hofmann K, Conradt M, Bosio A, Cremer H (2004) Purification of neuronal precursors from the adult mouse brain: comprehensive gene expression analysis provides new insights into the control of cell migration, differentiation, and homeostasis. Mol Cell Neurosci 25:692–706. CrossRef Medline

Pinto L, Drechsel D, Schmid MT, Ninkovic J, Irmler M, Brill MS, Restani L, Gianfranceschi L, Cerri C, Weber SN, Tarabykin V, Baer K, Guillemot F, Beckers J, Zecevic N, Dehay C, Caleo M, Schorle H, Götz M (2009) AP2gamma regulates basal progenitor fate in a region- and layer-specific manner in the developing cortex. Nat Neurosci 12:1229–1237. CrossRef Medline

Sakurada K, Ohshima-Sakurada M, Palmer TD, Gage FH (1999) Nurr1, an orphan nuclear receptor, is a transcriptional activator of endogenous tyrosine hydroxylase in neural progenitor cells derived from the adult brain. Development 126:4017–4026. Medline

Schmid RS, Yokota Y, Anton ES (2006) Generation and characterization of brain lipid-binding protein promoter-based transgenic mouse models for the study of radial glia. Glia 53:345–351. CrossRef Medline

Sousa VH, Miyoshi G, Hjerling-Leffler J, Karayannis T, Fishell G (2009) Characterization of Nkx6–2-derived neocortical interneuron lineages. Cereb Cortex 19:i1–10. CrossRef Medline

Takahashi K, Liu FC, Hirokawa K, Takahashi H (2003) Expression of Foxp2, a gene involved in speech and language, in the developing and adult striatum. J Neurosci Res 73:61–72. CrossRef Medline

Urban S, Kobi D, Ennen M, Langer D, Le Gras S, Ye T, Davidson I (2015) A Brn2-Zic1 axis specifies the neuronal fate of retinoic-acid-treated embryonic stem cells. J Cell Sci 128:2303–2318. CrossRef Medline

Vergaño-Vera E, Díaz-Guerra E, Rodríguez-Traver E, Méndez-Gómez HR, Solís Ó, Pignatelli J, Pickel J, Lee SH, Moratalla R, Vicario-Abejón C (2015) Nurr1 blocks the mitogenic effect of FGF-2 and EGF, inducing olfactory bulb neural stem cells to adopt dopaminergic and dopaminergic-GABAergic neuronal phenotypes. Dev Neurobiol 75:823–841. CrossRef Medline

Wang Y, Dye CA, Sohal V, Long JE, Estrada RC, Roztocil T, Lufkin T, Deisseroth K, Baraban SC, Rubenstein JL (2010) Dlx5 and Dlx6 regulate the development of parvalbumin-expressing cortical interneurons. J Neurosci 30:5334–5345. CrossRef Medline

Winpenny E, Lebel-Potter M, Fernandez ME, Brill MS, Götz M, Guillemot F, Raineteau O (2011) Sequential generation of olfactory bulb glutamatergic neurons by Neurog2-expressing precursor cells. Neural Dev 6:12. CrossRef Medline

Zembrzycki A, Perez-Garcia CG, Wang CF, Chou SJ, O'Leary DD (2015) Postmitotic regulation of sensory area patterning in the mammalian neocortex by Lhx2. Proc Natl Acad Sci U S A 112:6736–6741. CrossRef Medline

APPENDIX II

Neuronal Subtype Generation During Postnatal Olfactory Bulb Neurogenesis

Alexandra Angelova, Marie-Catherine Tiveron, Harold Cremer and Christophe Beclin, (2018), *Journal of Experimental Neuroscience*

In this commentary I contextualize a recently published paper from our team (Tiveron et al., 2017, Appendix I). In particular, I emphasize changes in transcription factor signatures that accompany the transition from embryonic to postnatal neurogenesis. Thereafter, I speculate about different mechanisms that could lie at the origin of such changes and the available data that could support such scenarios.

Neuronal Subtype Generation During Postnatal Olfactory Bulb Neurogenesis

Alexandra Angelova, Marie-Catherine Tiveron, Harold Cremer and Christophe Beclin

Aix-Marseille University, CNRS, IBDM, Marseille, France.

Journal of Experimental Neuroscience
Volume 12: 1–4

DOI: 10.1177/1179069518755670

SAGE

ABSTRACT: In the perinatal and adult forebrain, regionalized neural stem cells lining the ventricular walls produce different types of olfactory bulb interneurons. Although these postnatal stem cells are lineage related to their embryonic counterparts that produce, for example, cortical, septal, and striatal neurons, their output at the level of neuronal phenotype changes dramatically. Tiveron et al. investigated the molecular determinants underlying stem cell regionalization and the gene expression changes inducing the shift from embryonic to adult neuron production. High-resolution gene expression analyses of different lineages revealed that the zinc finger proteins, Zic1 and Zic2, are postnatally induced in the dorsal olfactory bulb neuron lineage. Functional studies demonstrated that these factors confer a GABAergic and calretinin-positive phenotype to neural stem cells while repressing dopaminergic fate. Based on these findings, we discuss the molecular mechanisms that allow acquisition of new traits during the transition from embryonic to adult neurogenesis. We focus on the involvement of epigenetic marks and emphasize why the identification of master transcription factors, that instruct the fate of postnatally generated neurons, can help in deciphering the mechanisms driving fate transition from embryonic to adult neuron production.

KEYWORDS: Neural stem cells, olfactory bulb, transcription factor

RECEIVED: December 27, 2017. **ACCEPTED:** January 4, 2018.

TYPE: Commentary

FUNDING: The author(s) disclosed receipt of the following financial support for the research, authorship, and/or publication of this article: H.C. received funding from Agence National pour la Recherche (ANR) and Fondation pour la Recherche sur le Cerveau (FRC).

DECLARATION OF CONFLICTING INTERESTS: The author(s) declared no potential conflicts of interest with respect to the research, authorship, and/or publication of this article.

CORRESPONDING AUTHOR: Harold Cremer, Aix-Marseille University, CNRS, IBDM, UMR 7288, Campus de Luminy, 13009 Marseille, France. Email: harold.cremer@unv-amu.fr

COMMENT ON: Tiveron MC, Beclin C, Murgan S, Wild S, Angelova A, Marc J, Coré N, de Chevigny A, Herrera E, Bosio A, Bertrand V, Cremer H.Zic-proteins are repressors of dopaminergic forebrain fate in mice and C. elegans. Journal of Neuroscience. 2017 Sep 29. pii: 3888-16. doi: 10.1523/JNEUROSCI.3888-16.2017.

New neurons are generated throughout life in two specific regions of the mammalian brain: the hippocampus and the olfactory bulb (OB). In the OB, large numbers of interneurons are permanently issued from stem cells residing in the ventricular/subventricular zone (V/SVZ) lining the forebrain ventricles. From here, they migrate via the rostral migratory stream (RMS) into the OB where they differentiate as interneurons.

These postnatal and adult generated interneurons exhibit considerable phenotypic diversity at several levels. First, they are heterogeneous at the neurotransmitter level. Indeed, it has been shown that neurons using exclusively GABA, neurons that use both GABA and dopamine, and also very few glutamatergic neurons are generated and integrated. Second, they show varying final locations in the OB. Although most OB interneurons remain in the deep positioned granule cell layer, a substantial fraction integrates in the superficial glomerular layer. Finally, adult-born neurons show a wide spectrum of morphologies, projection patterns, and targets.[1]

Lineage studies demonstrated that the diversity of OB interneurons is closely tied to their spatial origin in the stem cell compartment. For example, interneurons generated by progenitors of the dorsal part of the V/SVZ will predominantly integrate in the superficial layers of the OB and express subtype markers such as calretinin (CR), tyrosine hydroxylase, or the transcription factors (TFs) TBR1/2. In contrast, OB neurons produced along the lateral aspect of the ventricle are purely GABAergic and integrate in deeper layers of the OB. The discovery that neuronal heterogeneity is determined by their site of origin led to the notion that the stem cell niche represents a cellular mosaic in which populations of stem cells in defined dorsoventral and anteroposterior positions are predetermined to produce specific neurons for the OB.[2] This, in turn, implies that molecular determinants, for example, differentially expressed TFs, underlie early fate specification and ultimately neuronal function and connectivity.

Gene Expression in Space and Time

Tiveron et al.[3] set out to systematically identify and functionally characterize such fate determinants based on high-resolution gene expression analyses. Up to now, gene expression analyses performed in the V/SVZ-RMS-OB neurogenic system relied either on microdissection of tissues[4] or on cell sorting based on expression of a limited set of membrane markers[5,6] that define specific differentiation stages. However, in this neurogenic system, such approaches present several limitations. Although the stem cell compartments of the dorsal and lateral lineages are physically separated, these regions harbor progenitors at different differentiation stages (neural stem cells [NSCs], transit amplifying progenitors and migrating neuroblasts). In addition, in the RMS and the OB, both lineages are intermingled and cannot be easily distinguished, let alone isolated.

To overcome these limitations, Tiveron et al. performed a lineage tracing approach based on targeted brain electroporation. Previous work demonstrated that in vivo brain electroporation can be used to transfect DNA-based vectors,[7] or even messenger RNA,[8] into the different stem cell compartments

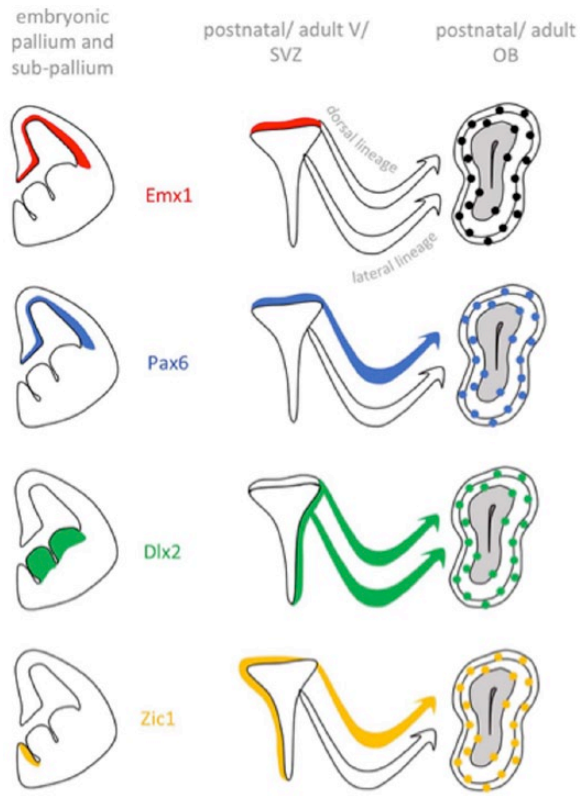

Figure 1. Examples of 4 categories of transcription factors classified based on their respective expression pattern in the embryo versus postnatal dorsal V/SVZ. V/SVZ indicates ventricular/subventricular zone; OB, olfactory bulb.

surrounding the ventricle. Over the following hours and days, relatively homogeneous and timed cohorts of cells pass through the different differentiation stages in the V/SVZ and the RMS to finally integrate as OB interneurons. Using green fluorescent protein expression followed by microdissection, dissociation, and fluorescence-activated cell sorting, the group isolated such cohorts after 8 hours, 1, 2, 4, 7, and 14 days, thus covering the entire neurogenic sequence from stem cells to neurons. This approach was performed in parallel for the dorsal and the lateral neuronal lineage. Subsequent microarray analyses generated a unique high-resolution picture of gene expression in space (dorsal versus lateral stem cells) and in time (from stem cells to neurons).

In a first analytic step, the authors were particularly interested in TFs specifically expressed and regulated in the dorsal lineage because this progenitor pool accounts for most of the interneuron subtype diversity in the OB. Moreover, the dorsal stem cell niche undergoes considerable molecular and structural rearrangements[9] during the transition from embryonic to postnatal neurogenesis and produces remarkably different neuronal subtypes before and after birth: first glutamatergic projection neurons for the developing cortex and later mainly GABA/dopaminergic interneurons for the OB. Therefore, Tiveron et al. compared the expression dynamics of selected candidate factors in the embryo and at postnatal stages.

These analyses led to the description of 4 categories of TFs based on their expression (Figure 1):

First, TFs that are expressed in the embryonic pallium and whose expression pattern and dynamics are maintained after birth in progenitors of the dorsal V/SVZ. This class is, for example, represented by Emx1 and Emx2.

Second, TFs that are expressed in both embryonic and postnatal progenitors but whose expression pattern changes after birth. A striking example of this category is Pax6. Pax6 is transiently expressed during corticogenesis where it controls the generation of glutamatergic projection neurons. However, after birth, most of the dorsal V/SVZ progenitors maintain its expression all along the neurogenic sequence. In this context, Pax6 is indispensable for the generation of dopaminergic OB neurons.[10]

Third, TFs that in the embryo are confined to subpallial NSCs but that start to be expressed in the dorsal lineage after birth. This is the case for the Dlx1/2 TFs, which are expressed in the embryonic ganglionic eminences where they represent major determinants of cortical interneuron fate.[11] At postnatal stages, both TFs are induced during migratory stages in the dorsal lineage.[10] Importantly, it has been demonstrated that Dlx2 interacts with Pax6 to specify dopaminergic interneurons of the OB.[12]

Fourth, TFs that show de novo expression in postnatal NSCs. This is the case for Zic1 and Zic2, which in the embryo are restricted to medial aspects of the ventricular wall. During postnatal and adult stages, Zic1/2 appear in the dorsal stem cell compartment, coincident with the shift of neuron production from glutamatergic projection neurons to GABAergic and dopaminergic interneurons.

Zic Proteins as Molecular Fate Determinants

Based on these results, Tiveron et al. aimed at deciphering the functional implication of Zic1 and Zic2 in the control of neuronal differentiation of dorsal progenitors. Using a pan-Zic antibody,[13] the authors first revealed that Zic proteins are postnatally induced in a mediolateral gradient within the dorsal V/SVZ but are absent from the lateral V/SVZ (Figure 2). By combining electroporation-based lineage tracing with Zic immunostaining, the authors demonstrated that the proteins are expressed in about 50% of all cells in the dorsal stem cell compartment and maintained in migrating neuroblasts and mature neurons. Further analyses with subtype-specific markers revealed that Zic protein is highly expressed in most of the CR-positive OB interneurons but excluded from dopaminergic neurons.[9] Based on this observation, the authors hypothesized that Zic1/2 act as factors promoting the generation of this CR-expressing OB interneuron subtype.

Again, in vivo brain electroporation was used to investigate the validity of this scenario. Indeed, Zic1 or Zic2 overexpression favored the generation of CR-positive interneurons at the expense of dopaminergic neurons. Short hairpin RNA–mediated knockdown led to the opposite effect. Altogether,

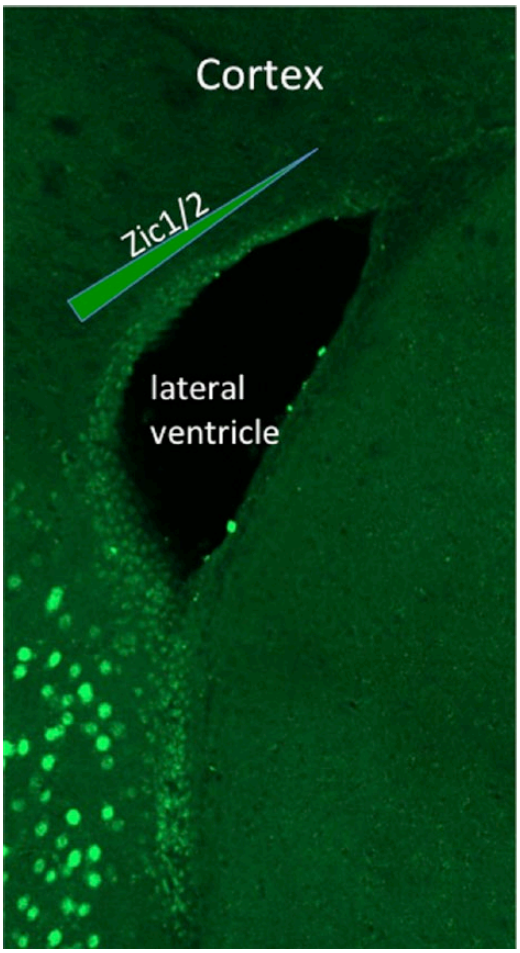

Figure 2. Zic immunostaining of the adult mouse forebrain, showing a mediolateral gradient of Zic1/2 expression in the dorsal wall of the subventricular zone.

these results demonstrated that both Zic proteins act in the postnatal forebrain as inducers of CR expressing neurons while repressing dopaminergic fate. Interestingly, the anti-dopaminergic function of Zic proteins is evolutionary conserved and already present in *Caenorhabditis elegans*.[3]

Intrinsic Determinants versus Extrinsic Cues

One of the most striking features of the V/SVZ-RMS-OB neurogenic system is represented by the radical change in neuronal subtype production by forebrain stem cell compartment that occurs around birth. What underlies the origin of the modifications in the expression pattern of these master TFs? Indeed, expression of some of these factors may be under the control of upstream TFs. However, for genes at the very top of the genetic cascade, the appearance of additional mechanisms seems likely. Work of several teams in the OB neurogenic system pointed to chromatin remodeling factors as important players in the control of fate shifts. For example, the polycomb protein Bmi1 is involved in the maintenance of NSCs,[14] whereas the trithorax-related protein Mll1 drives NSCs into neuronal differentiation. Interestingly, Dlx2 represents the main target of Mll1, which induces histone methylation marks at the Dlx2 locus that are necessary for transcription. Furthermore, the interaction of Mll1 with the Dlx2 locus is crucial for progenitors to give rise to OB interneurons.[15] Based on these data, it is likely that epigenetic events lie at the origin of expression changes of specific TFs which, in turn, lead to the emergence of new traits of V/SVZ progenitors at birth.

At the cellular level, novelty can either occur as an intrinsic program within the cell (cell autonomously) or may originate from extracellular cues (non–cell autonomously). In the V/SVZ-RMS-OB neurogenic system, this point has been addressed in several studies. The presence of a cell-autonomous program was demonstrated in a study where V/SVZ progenitors from distinct subregions were isolated and then re-grafted at different locations within the stem cell niche.[2] The authors observed that the neuronal subtypes generated by these progenitors show fates representing their place of origin rather than the region in which cells were grafted. However, other studies showed that the environment of NSCs also plays a role in neuronal fate determination and that, for example, morphogens regulate adult OB neurogenesis. In particular, the genetic ablation of the Shh pathway in the most ventral V/SVZ progenitors prevented their capacity to generate calbindin positive interneurons in the glomerular layer of the OB.[16] Likewise, the Wnt signaling pathway was shown to control the neurogenic capacity of progenitors located in the dorsal part of the V/SVZ.[17]

Conclusions

During neural development, stem cells pass through successive stages that change the phenotype of the neurons they produce. It is now evident that both intrinsic and extrinsic cues are instructing the NSC niche. Clearly, more experimental work is needed to understand their intricate relationship as players in neuronal fate determination, in general, and specifically the acquisition of novel traits after birth. The identification of new key TFs such as Zic1/2 and a deeper insight into their temporal and spatial expression dynamics will pave the way for the comprehension of the molecular events at the basis of these transformations. Finally, a better understanding of these processes will not only elucidate how novelty is generated by V/SVZ progenitors but will also be relevant to neurodevelopmental processes in general.

Acknowledgements

The authors acknowledge the France-BioImaging/PICsL infrastructure (ANR-10-INSB-04-01) and the IBDM animal facilities.

Author Contributions

AA, MCT, HC and CB wrote the paper. CB provided Images. AA performed artwork.

REFERENCES

1. Lim DA, Alvarez-Buylla A. The adult ventricular-subventricular zone (V-SVZ) and olfactory bulb (OB) neurogenesis. *Cold Spring Harb Perspect Biol*. 2016;8:175–206.
2. Merkle FT, Mirzadeh Z, Alvarez-Buylla A. Mosaic organization of neural stem cells in the adult brain. *Science*. 2007;317:381–384.

3. Tiveron MC, Beclin C, Murgan S, et al. Zic-proteins are repressors of dopaminergic forebrain fate in mice and *C. elegans*. *J Neurosci*. 2017;37:10611–10623.
4. Azim K, Hurtado-Chong A, Fischer B, et al. Transcriptional hallmarks of heterogeneous neural stem cell niches of the subventricular zone. *Stem Cells*. 2015;33:2232–2242.
5. Beckervordersandforth R, Tripathi P, Ninkovic J, et al. In vivo fate mapping and expression analysis reveals molecular hallmarks of prospectively isolated adult neural stem cells. *Cell Stem Cell*. 2010;7:744–758.
6. Khodosevich K, Seeburg PH, Monyer H. Major signaling pathways in migrating neuroblasts. *Front Mol Neurosci*. 2009;2:7.
7. Boutin C, Diestel S, Desoeuvre A, Tiveron MC, Cremer H. Efficient in vivo electroporation of the postnatal rodent forebrain. *PLoS ONE*. 2008;3:e1883.
8. Bugeon S, de Chevigny A, Boutin C, et al. Direct and efficient transfection of mouse neural stem cells and mature neurons by in vivo mRNA electroporation. *Development*. 2017;144:3968–3977.
9. Merkle FT, Fuentealba LC, Sanders TA, Magno L, Kessaris N, Alvarez-Buylla A. Adult neural stem cells in distinct microdomains generate previously unknown interneuron types. *Nat Neurosci*. 2014;17:207–214.
10. de Chevigny A, Core N, Follert P, et al. Dynamic expression of the pro-dopaminergic transcription factors Pax6 and Dlx2 during postnatal olfactory bulb neurogenesis. *Front Cell Neurosci*. 2012;6:6.
11. Anderson SA, Eisenstat DD, Shi L, Rubenstein JL. Interneuron migration from basal forebrain to neocortex: dependence on Dlx genes. *Science*. 1997;278:474–476.
12. Brill MS, Snapyan M, Wohlfrom H, et al. A dlx2- and pax6-dependent transcriptional code for periglomerular neuron specification in the adult olfactory bulb. *J Neurosci*. 2008;28:6439–6452.
13. Borghesani PR, Peyrin JM, Klein R, et al. BDNF stimulates migration of cerebellar granule cells. *Development*. 2002;129:1435–1442.
14. Molofsky AV, Pardal R, Iwashita T, Park IK, Clarke MF, Morrison SJ. Bmi-1 dependence distinguishes neural stem cell self-renewal from progenitor proliferation. *Nature*. 2003;425:962–967.
15. Lim DA, Huang YC, Swigut T, et al. Chromatin remodelling factor Mll1 is essential for neurogenesis from postnatal neural stem cells. *Nature*. 2009;458:529–533.
16. Ihrie RA, Shah JK, Harwell CC, et al. Persistent sonic hedgehog signaling in adult brain determines neural stem cell positional identity. *Neuron*. 2011;71:250–262.
17. Azim K, Fischer B, Hurtado-Chong A, et al. Persistent Wnt/beta-catenin signaling determines dorsalization of the postnatal subventricular zone and neural stem cell specification into oligodendrocytes and glutamatergic neurons. *Stem Cells*. 2014;32:1301–1312.

APPENDIX III

Neuronal integration in the adult olfactory bulb is a non-selective addition process

Jean-Claude Platel, **Alexandra Angelova**, Stephane Bugeon, Jenelle Wallace, Thibault Ganay, Ilona Chudotvorova, Jean-Christophe Deloulme, Christophe Béclin, Marie-Catherine Tiveron, Nathalie Coré[1], Venkatesh N. Murthy , Harold Cremer, 2018, under review in *Nature Neuroscience,*

available in bioRxiv: https://www.biorxiv.org/content/early/2018/03/26/289009

In this paper from our team which is currently under review, we challenge the current concept of a critical period for neuronal survival in the OB. Using chronic two-photon *in vivo* imaging, we show that neuronal death is quasi absent in postnatal and adult-born neurons of the OB. Moreover, using the thymidine analogues BrdU and EdU, we can readily induce neuronal death which could easily explain the result obtained by previous studies interpreted as a critical period. These results bear important implications for the interpretation of numerous studies and the potential to change the current paradigm of adult neurogenesis: to date, continuous generation of OB neurons has been regarded as a neuronal turnover; however, we show that neurons are added, thus contributing to continuous growth of the OB.

My contribution to this work consisted in performing cleared whole brain light-sheet acquisitions of mice at different ages to demonstrate the constant growth of the OB.

Neuronal integration in the adult olfactory bulb is a non-selective addition process

Jean-Claude Platel[1]*, Alexandra Angelova[1], Stephane Bugeon[1], Jenelle Wallace[3], Thibault Ganay[1], Ilona Chudotvorova[1], Jean-Christophe Deloulme[2], Christophe Béclin[1], Marie-Catherine Tiveron[1], Nathalie Coré[1], Venkatesh N. Murthy [3], Harold Cremer[1]

1 Aix-Marseille University, CNRS, IBDM, UMR 7288, Marseille, France

2 Grenoble Institut des Neurosciences, Université Grenoble Alpes

3 Department of Molecular & Cellular Biology, Harvard University, Cambridge, MA 02138, USA

* Correspondence: Jean-Claude Platel (jean-claude.platel@univ-amu.fr)

Abstract:

Adult neurogenesis is considered a competition in which neurons scramble during a critical period for integration and survival. Moreover, newborn neurons are thought to replace preexisting ones that die. Despite a wealth of evidence supporting this model, systematic in vivo observations of the process are still scarce. We used 2-photon in vivo imaging combined with stereological analyses to study neuronal integration and survival in the olfactory bulb (OB). We show that cell-loss in the OB occurs only at low levels. Neuronal death resembling a critical period was induced by standard doses of BrdU or EdU, but disappeared when low doses of EdU were used, demonstrating toxicity. Finally, we demonstrate that the OB grows throughout life. This shows that

neuronal selection during OB-neurogenesis does not occur during integration and argues against the existence of a critical period. Moreover, the OB is not a "turnover" system but shows lifelong neuronal addition.

Introduction

Neurogenesis continues after birth in the hippocampus and olfactory bulb of rodents. During OB neurogenesis predetermined stem cell population along the walls of forebrain ventricles generate neuronal precursors that migrate via the rostral migratory stream (RMS) into the center of the OB. After their radial migration into the principal target layers, the granule cell (GCL) and glomerular layers (GL), cells integrate into the preexisting circuitry and function as interneurons using GABA and dopamine as their principal neurotransmitters (Whitman and Greer, 2007).

The currently available information indicates that OB neurogenesis is based on two key principles: First, neuronal integration in the adult is a competitive process, during which large numbers of newly arriving neurons compete for integration into the circuitry and ultimately survival. This competition is thought to occur during a defined critical window of 2-8 weeks after arrival and leads to the apoptotic elimination of about half of the initial population (Bergami and Berninger, 2012; Lledo et al., 2006; Mandairon et al., 2006; Petreanu and Alvarez-Buylla, 2002; Winner et al., 2002; Yamaguchi and Mori, 2005). Second, the OB represents a turnover system, in which newly integrating cells replace preexisting ones, leading to a relatively stable total number of neurons in the target layers (Bergami and Berninger, 2012; Imayoshi et al., 2008; Lledo et al., 2006).

These two concepts are to a large extend based on lineage tracing experiments using thymidine analogs like bromodeoxyuridine (BrdU) or 3H-thymidine to label the DNA of dividing cells, (Mandairon et al., 2006; Petreanu and Alvarez-Buylla, 2002; Winner et al., 2002; Yamaguchi and Mori, 2005). A common observation in such experiments is a loss of

labeled cells during the first few weeks after their arrival in the bulb, which led to the postulation of a selection mechanism allowing the remodeling of specific OB circuits during a critical window for survival (Petreanu and Alvarez-Buylla, 2002). Alternatively, genetic approaches using CRE-inducible markers layers (Imayoshi et al., 2008) have been performed and demonstrated an accumulation of adult born neurons in the OB over time. In agreement with the turnover model this has been interpreted as a replacement of older neurons that died (Imayoshi et al., 2008). Only recently more direct approaches based on 2-photon in vivo imaging allowed studying OB neurons directly in the living animal (Mizrahi et al., 2006; Sailor et al., 2016; Wallace et al., 2017). Interestingly, long-term observation of either juxtaglomerular neurons in general (Mizrahi et al., 2006), or more specifically of dopaminergic neurons, demonstrated an increase in these populations over time (Adam and Mizrahi, 2011). While at first sight this finding contradicts a pure replacement model, it was interpreted as a change in the interneuron subtype composition of the OB (Adam and Mizrahi, 2011).

Thus, while the available data is still mostly indirect and fragmentary, the elegant model based on selection and replacement appears justified. However, to doubtlessly validate this model and to really understand the adult neurogenic process, all populations of integrating neurons have to be observed in the living animal from their arrival in the OB throughout the critical window until their disappearance.

Here we combined genetic birthdating and lineage tracing with long term in vivo microscopy to follow timed cohorts of postnatal and adult born neurons from their arrival in the OB for up to six months. Quantitative analyses demonstrate that neuronal loss during the critical period and at later stages is rare in all observed populations. We demonstrate that classically used doses of the tracers BrdU and 5-ethynyl-2'-deoxyuridine (EdU) induce cell loss resembling a critical window, but that this toxicity disappears when low doses of EdU are used. Finally, we show that neuronal addition merely than replacement occurs in the adult OB, leading to permanent growth of the structure.

Results

Long term in vivo imaging of postnatal and adult born OB neurons

We used 2-photon imaging to directly study the integration and survival of perinatal and adult born OB neurons at high spatial and temporal resolution in the living animal. We first focused on the perinatal period, when most OB interneurons are generated (Batista-Brito et al., 2008). Postnatal in vivo brain electroporation of the dorsal ventricular zone targets stem cell populations that generate neurons for the superficial layers of the OB (Fig 1a,b (de Chevigny et al., 2012b), which can be reliably reached by two-photon microscopy (Adam and Mizrahi, 2011). We used this dorsal targeting approach to introduce a CRE-expression plasmid into R26-RFP reporter mice (Fig 1a). Three weeks later, OB labeled neurons comprised a mixed population of 6% tyrosine hydroxylase expressing dopaminergic neurons, 12% calretinin positive purely GABAergic neurons, 22% other PGN (Fig 1b) and 60% mostly superficially positioned granule cells (GC).

An adaptation of the reinforced thin skull method allowed for frequent and long term imaging of awake mice while perturbing the physiology of the OB only minimally (Drew et al., 2010). In agreement with previous observations (Xu et al., 2007), there was no detectable astroglia reaction or accumulation of microglia after thinning and window implantation (Fig S1).

Three weeks after electroporation, when skull growth was sufficiently advanced, thin-skull preparation was performed and neurons in the glomerular layer (GL; Fig 1d-g) and the granule cell layer (GCL, Fig S2) were imaged in awake animals at high resolution over the following weeks and months. All analyzed neurons were individually identified in Z-stacks (Supplementary Video 1) based on relative position and morphology. Neurons were numbered and revisited weekly during the critical period (Fig 1d-f; Supplementary Video 1; Fig S3a,b). After identification of the first cohort, smaller numbers of additional neurons appeared permanently in the observation window as a consequence of ongoing

neurogenesis in the stem cell compartment (arrowheads in Fig 1d, 5wpi). These were numbered and followed like the first cohort. Neurons in the observation field showed stable relative positions over time (Fig 1d), however, in some cases minor positional adjustment were observed that could be followed over subsequent imaging sessions (Fig 1d,f). Generally, resolution was sufficient to observe even minor changes in dendritic organization of neurons over time (see neuron no. 7 in Fig 1d,f).

Cell death during the critical period: perinatal born neurons

Based on this direct and systematic imaging approach, we first focused on perinatally born neurons during the proposed critical period, thus until 8 weeks after their generation at the ventricles (Mandairon et al., 2006). Neurons that were present during the first observation time point (3 weeks after electroporation of the respective stem cells) were followed over the next 5 weeks. Among 755 periglomerular neurons (PGN) in 11 mice only 5.1% were lost over the proposed critical period (Fig 2a, see circles for lost cells no. 14 and 17 in Fig 1d,g). The percentage of lost neurons was very similar between individual animals and was independent of the density of labeled cells in the observation window (between 18 and 100 neurons; Fig 2a).

Next, we investigated newborn granule cells (GCs) in the underlying GCL in 6 mice with particularly high-quality and stable window preparations (Fig S2). Out of 178 RFP positive neurons observed between 3 and 8 weeks after their birth not a single cell disappeared over the subsequent imaging sessions (Fig 2b). We conclude that perinatally generated OB interneurons in both, the GL and the GCL are rarely eliminated during the proposed critical period.

Cell death during the critical period: adult born neurons

We then investigated the stability of adult born neurons during the critical period. First, we focused on PGN that can be reliably imaged after thin skull preparation. As in vivo electroporation is inefficient in adult mice we crossed the Rosa-RFP line with Nestin Cre-

ER^{T2} mice (Lagace et al., 2007) and induced a heterogeneous cohort of labeled newborn neurons by tamoxifen injection at 2 months of age (Ninkovic et al., 2007) (Fig S4 a,b). One week after induction virtually all RFP positive cells in the RMS and about 30% in the OB layers expressed the immature neuron marker doublecortin (Fig S4c,d). Reinforced thin skull preparation was routinely performed at 1-week post induction (wpi). Weekly observations of individually identified PGN in the GL were performed as described above (Supplementary Video 2, Fig S3c,d). Analyses of 538 periglomerular neurons of the first cohort in 8 animals showed that only 1.5% disappeared over the 7-weeks period after their first identification (Fig. 2c).

Finally, we investigated the survival of adult born granule neurons during the integration phase. To access this deeply positioned and densely packed cell population we used a cranial window preparation combined with injection of a tomato-expressing lentivirus into the RMS (Fig. 3a; Wallace et al., 2017). Tracing of 48 adult-born GCs in 19 field of views from 3 mice (Fig. 3b) allowed the identification of only a single cell that disappeared (Fig. 3c) during the 7 weeks observation period. Thus, under physiological conditions cell loss in adult born OB neurons during the proposed critical period was almost absent, comparable to the findings for perinatally born neurons.

Next we asked if neuron loss could be detected in non-physiological situations. It has been shown that olfactory sensory deprivation induces additional cell death in adult born OB neurons (Mandairon et al., 2006; Saghatelyan et al., 2005; Yamaguchi and Mori, 2005). To investigate if increased cell death could be observed in our imaging paradigm we performed naris closure in adult Nestin Cre-ER^{T2}/Rosa-RFP mice one week after tamoxifen induction (Fig 4a). Analysis of RFP positive PGN over the following 8 weeks revealed a significant increase in cell loss (Fig 4bc; $p=0.03$, 3 animals, 151 cells).

In conclusion, under physiological conditions newly born neurons in the perinatal and adult OB show very little cell loss during the proposed critical period. However, significant cell loss

during this period was found after blocking sensory input, demonstrating that cell death could be detected.

Dose dependent toxicity of thymidine analogues

The above findings were at odds with the existence of a critical period for survival during which, under normal conditions, about half of the adult born neurons are removed from the OB by cell death (Mandairon et al., 2006; Mouret et al., 2008; Petreanu and Alvarez-Buylla, 2002; Winner et al., 2002; Yamaguchi and Mori, 2005). This concept is to a large extent based on tracing of timed cohorts of newborn neurons using the integration of thymidine analogs, most often BrdU, into the DNA of dividing cells. To investigate if these differences were due to our particular experimental conditions we first repeated such pulse chase studies using commonly used doses of BrdU and following established protocols (Mandairon et al., 2006; Mouret et al., 2008; Whitman and Greer, 2007). Indeed, using four i.p. injections of 50 mg/kg BrdU every two hours into adult mice, we found an approximately 40% loss of labeled neurons in the OB between 2 and 6 weeks in the GL as well as in the GCL (Fig 5ab). As in our direct imaging approach we focused on the dorsal aspect of the OB, we investigated if in this region BrdU positive cells showed a different behavior than in the rest of the structure. BrdU+ cell number in the dorsal OB showed the same 40% loss that was found in the entire bulb (Fig.5b). Moreover, the imaging procedure itself did not influence the presence of BrdU positive cells over time, as window preparation followed by weekly imaging did not lead to increased numbers (Fig. S5).

Altogether, these DNA-labeling based findings were in full agreement with previous studies, showing a strong reduction of newborn cells during the critical period (Mandairon et al., 2006; Mouret et al., 2008; Petreanu and Alvarez-Buylla, 2002; Whitman and Greer, 2007; Winner et al., 2002; Yamaguchi and Mori, 2005). However, they strongly contradicted our *in vivo* observations showing very little cell loss. As suggested before (Lehner et al., 2011), we considered the possibility that incorporation of modified nucleotides impacted on neuronal survival in the OB and developed an approach to test this hypothesis.

To allow immunohistological BrdU detection, tissue samples have to be subjected to strong denaturing conditions that break the complementary base-pairing of DNA, a prerequisite for efficient BrdU antibody binding. Such treatment invariably leads to sample degradation and negatively impacts on staining intensity (Salic and Mitchison, 2008). In concert with limitations due to antibody penetration this imposes the use of relatively high concentrations of BrdU, generally several injections of 50 to 200 mg/kg of body weight i.p., for reliable detection (Brown et al., 2003; Mandairon et al., 2006; Mouret et al., 2008; Petreanu and Alvarez-Buylla, 2002; Whitman and Greer, 2007; Winner et al., 2002). In contrast, EdU labeling of DNA is based on a click-reaction with fluorescent azides (Rostovtsev et al., 2002; Salic and Mitchison, 2008; Tornoe et al., 2002) that have much higher diffusion rates in tissue than antibodies. Moreover, the staining reaction can be can be repeated several times to increase signal strengths and DNA denaturation is dispensable, altogether allowing the use of considerably lower concentrations of EdU in comparison to BrdU (Salic and Mitchison, 2008). Based on this increased sensitivity, we asked if the concentration of altered nucleotides in the DNA impacts on cell survival of new neurons in the OB.

Four injections of 50 mg/kg EdU in two month old mice led to an about 40% loss of labeled cells in the GL and the GCL of the OB between 2 and 6 weeks, highly comparable to the results based on BrdU (Fig 5c,e). Importantly, four injection of 1 or 5 mg/kg EdU under the same conditions led to the detection of slightly lower amounts of newly generated cells in the OB layers after 2 weeks (Fig. 5de). However, under these conditions the decrease in cell numbers between 2 and 6 weeks was not detectable anymore, both in the GL and the GCL (Fig. 5e). As it has been suggested that deep and superficial GCs are differentially susceptible to replacement (Imayoshi et al., 2008) we investigated the impact of low and high doses of EdU on both sub-layers. However, deep and superficial GCs showed the same behavior, cell loss at high EdU dose and survival at 5 mg/kg, as the entire GCL (Fig. 5f). Altogether, these results lead to the conclusion that loss of labeled cells in the OB during the critical period is correlated with the concentration of modified nucleotides in the DNA of newborn OB neurons (Fig. 5g).

Programmed cell death has been suggested to underlie the removal of integrating neurons from the OB during the critical window (Yokoyama, Neuron 2011). We used cleaved Caspase 3 (CC3) immunohistochemistry to investigate the overall extend of apoptosis in the OB and the impact of high and low doses of EdU on the process. Stereological analyses of immunostained tissues detected consistently low numbers of CC3 positive cells in the OB layers (363 +/- 34 cells mm3 n=15; thus about 940 CC3+ cells/GCL) in overall agreement with previous work (770 cells/GCL; Yamaguchi and Mori, PNAS 2005). However, among the 10803 analyzed EdU positive OB neurons only 26 showed co-labeling for CC3. Application of 5mg/kg or 50 mg/kg EdU had no impact on the percentage of double stained cells, indicating that thymidine induced toxicity did not pass via the apoptotic pathway (Fig. 5i).

Next, we investigated the distribution of total CC3 positive cells in the RMS and the OB layers. Interestingly, density of CC3 positive cells was several times higher in the RMS than in the GCL and the GL (Fig. 5j). This is in good agreement with previous data (Biebl, Cooper et al., Neurosci. Letters 2000) and suggests that cell death in the system occurs predominantly at the precursor level.

In conclusion, the above results, showing that lineage tracing by high doses of thymidine analogues is associated with artificial cell loss in the OB, point to considerable toxicity of such DNA modifying agents. Moreover, the finding that at low EdU doses cell loss in the OB during the proposed critical period is non-detectable represents independent confirmation of our in vivo imaging based findings.

Neuronal addition in the OB

The OB is considered to be a turnover system in which new neurons replace older ones, leading to a relatively stable size of the structure (Imayoshi et al., 2008; Petreanu and Alvarez-Buylla, 2002). In such a scenario cell loss has to be expected. As we did not observe considerable cell death during the proposed critical period, we asked if neurons disappear at

later stages. Continuous long-term observations of perinatally generated PGN and GC provided no evidence for sustained cell loss after the initial 8 weeks time window (Fig 6a,b). The same stability of the labeled population was evident when adult generated PGN were observed for up to 24 weeks after their generation (Fig. 6c). Moreover, as CRE-induced recombination in Nestin-CRE-ERT2 mice occurs often at the stem cell level (Imayoshi et al., 2008), recombined stem cells continue neurogenesis. In agreement, additional adult born neurons permanently appeared in the observation window (Fig 6d), leading to a more than doubling of the neuron population of adult generated PGN over an observation period of six months (Fig. 6e).

How does the OB deal with this permanent addition of neurons in the absence of considerable cell loss? Two potential consequences can be imagined: Either the OB grows in size or the cell density in the different layers increases over time. Currently, information about these parameters in the adult rodent OB is based on measurements of serial sections and the available data are fragmentary and in part contradictory (Hinds and McNelly, 1977; Imayoshi et al., 2008; Mirich et al., 2002 ; Petreanu and Alvarez-Buylla, 2002; Pomeroy et al., 1990; Richard et al., 2010).

First, we asked if a volume increase in the OB could be detected directly in the living brain during *in vivo* imaging experiments. We found that over time slightly larger image frames were necessary to accommodate the same group of neurons in our Z-maximum projections of the GCL and GL (Fig 1d; Fig S2b). Using this systematic imaging, we developed an approach to quantify local changes in OB volume over time based on measuring distance between individually identified neurons. Indeed, volumetric analysis of inter-neuronal space between groups of four neurons in X, Y, Z (thus an irregular pyramid) demonstrated that distance between neurons increased steadily between 2 and 5 months (Fig 7a,b, 4 animals), strongly indicating continuous OB growth.

Next, we used light sheet microscopy on CUBIC-treated (Susaki et al., 2014) transparent brains to investigate the structure and volume of the adult mouse OB in its integrity.

Volumetric analysis based on 3D reconstructions of CUBIC treated OBs (Fig 7c,d and Supplementary Video 3) revealed a steady increase in OB size leading to a significant 44% enlargement of the structure from 2 to 12 months (Fig 7d,e). This volume increase affected equally the granule and the glomerular layers (Fig 7f) in the absence of obvious changes in layer repartition (Fig S6a). During the same interval total forebrain volume was unchanged (Fig. 7g).

Next, we investigated the evolution of cell density in the more homogeneous granule cell layer using transparent brain tissues. To count all cells in the GCL we stained nuclei with the fluorescent marker TOPRO3. Quantification revealed that the density of nuclei was highly stable at all observed time points (Fig 7 h,i) while the density of astrocytes decreased and microglia density was stable (Fig. S6b,c).

Thus, both in vivo brain imaging and light sheet microscopy of fixed tissue demonstrate that the mouse OB grows significantly during adult life in the absence of detectable changes in cell density. This is in strong support of the permanent addition of new neurons to a stable preexisting circuitry in the absence of substantial cell death.

Discussion

Our work combining long term in vivo observations, pulse chase experiments and 3D morphometric analyses, leads to three main conclusions:

First, the level of neuronal cell death among perinatal and adult born OB interneurons is very low. Second, the adult OB is not a homeostatic, but a developing and growing brain structure. Third, classical lineage tracing approaches based on thymidine analogs are associated with unwanted side effects and have to be interpreted with care.

Using a non-invasive long-term imaging approach combined with lineage tracing approaches using low concentrations of the thymidine analogue EdU, we were unable to detect

considerable cell loss among postnatal and adult generated neurons during their integration phase in the OB. These findings are not compatible with the existence of a critical period during which only a subset of newborn neurons is selected for survival while about the same amount dies by apoptosis.

The predominant evidence that led to the postulation of a critical period is based on the use of thymidine analogues, generally BrdU or 3H-dT, that incorporate into the nuclear DNA during the S-phase of the cell cycle (Petreanu and Alvarez-Buylla, 2002; Winner et al., 2002).

However, both BrdU and 3H-dT are toxic (Breunig et al., 2007; Ehmann et al., 1975; Kolb et al., 1999; Kuwagata et al., 2007; Nowakowski and Hayes, 2000; Sekerkova et al., 2004; Taupin, 2007) and studies in both rodents (Lehner et al., 2011; Webster et al., 1973) and primates (Duque and Rakic, 2011) pointed to unwanted, and hard to interpret, long term effects associated to their use. Accordingly, warnings concerning the interpretation of such data have been issued (Costandi, 2011; Lehner et al., 2011).

In agreement with the existing literature we observed massive loss of newborn neurons in the OB during the critical period when standard doses (4x50 mg/kg) of BrdU or EdU were used for tracing. Interestingly, in the presence of considerably lower concentrations of EdU (4x1 mg/kg) neurogenesis was still obvious but cell loss during the critical period was not detectable anymore. This finding is in perfect agreement with our in vivo observations, in which we find almost no neuronal death during the critical period. Thus, death of newborn neurons during the critical period appears to be tightly linked to the concentration of thymidine analogues used for their detection.

Only one in vivo imaging study, focusing on dendrite plasticity of OB GCs, addressed the question of GC survival as a sub-aspect (Sailor et al., 2016). While the reported 22% loss during the critical period exceeds our observation, it is in overall agreement with the conclusion that cell death during this phase is far below the expected 50%.

These results lead to the conclusion that a selection step in which an overproduced precursor population is matched to the needs of the target structure, does not occur during synaptic integration in the OB. While this observation is unexpected it is not completely isolated. For example, in Bax-KO mice, in which apoptotic cell death is blocked, the general structure and size of the OB neuron layers are indistinguishable (Kim et al., 2007). However, Bax-mutants show a strong disorganization and accumulation of neuronal precursors in the RMS, pointing to the possibility that neuronal selection occurs more at the level of recruitment from the RMS than at the level of integration in the target layers. Such a scenario of "early selection" is also supported by the observation that the density of apoptotic cells is much higher in the RMS than in the OB proper (Biebl et al., 2000). However, other scenarios, like an impact of altered migration on survival in the OB, cannot be excluded.

Alternatively, integration or death of OB interneurons might be intrinsically encoded. It has been shown that in developing cortical interneurons neuronal survival is largely independent of signals from the local environment but that about 40% of the total population is predestined to undergo Bax-dependent apoptosis (Southwell et al., 2012). In such a scenario cell death would be expected to occur already in the SVZ/RMS.

Our results demonstrate that neuronal death is a rare event not only during the postulated critical selection period, but at all observed time points. However, the permanent arrival of new neurons in the absence of considerable cell removal is not compatible with the current idea that the OB represents a turnover system of constant size (Bergami and Berninger, 2012; Imayoshi et al., 2008). Growth has to be expected, and our in vivo imaging and light sheet microscopy studies clearly demonstrate a 40% volume increase during the first year of adulthood in the absence of detectable changes in cell density. Indeed, growth of the adult OB in mice has been observed in other studies, although considerable variation and dependence on genetic background have been reported (Mirich et al., 2002; Richard et al., 2010). Other studies did not find considerable differences in total OB size or specific sublayers (Imayoshi et al., 2008; Petreanu and Alvarez-Buylla, 2002; Pomeroy et al., 1990).

What could be the reason underlying these contradictory findings? Past approaches were based on the 2D analysis of a subset of tissue sections and the extrapolation of the total volume based thereon. However, the OB is not a simple radial symmetric globule, but a complex multi-layered structure that shows huge variations along the rostro-caudal and dorso-ventral axes (see Supplementary Video 3). Measuring a limited amount of tissue sections may not sufficiently consider longitudinal growths and intra-bulbar variations.

Light sheet microscopy is suited to overcome many of these limitations as the OB is imaged and measured in its entirety. Extrapolations can be avoided and the selection of comparable levels for layer analyses is simple and reliable. Increases in OB lengths are directly obvious and do not have to be deduced from varying numbers of sections that can be generated from a given bulb. As a consequence inter-animal variations are minor and growth of the structure becomes evident. Independently from the light-sheet approach we show that during in vivo long-term observations constantly larger frames are needed to accommodate the same group of cells and that the distance of individually identified neurons measurably increases. The latter finding is in full agreement with the finding that the distance between specific glomeruli increases with age of the animal (Richard et al., 2010). Altogether, these data clearly demonstrate growth of the mouse OB during the entire first year of the animal's life.

In conclusion, we show here that neuronal cell death is rare in the OB and that neuronal addition, but not replacement, is the outcome of adult neurogenesis. Genetic fate mapping studies (Ninkovic et al., 2007) and also direct observation of the TH positive neuron population (Adam and Mizrahi, 2011) already pointed towards an increase in specific neuronal subsets in the adult OB. We show that neuronal addition is a general phenomenon that affects perinatally and adult generated neurons, leading to substantial growth of the OB throughout life. Thus, OB neurogenesis appears to reflect ongoing brain development rather than homeostasis.

How many neurons are added to the adult OB? Our data, based on measurements of cell density and volume of the structure, allows to estimate that between 2 and 6 months about

8000 cells/day are added to the growing OB. Interestingly, using a genetic approach, Imayoshi et al found that 6 months after tamoxifen induction, labeled neurons represent 41.2 % of the total population (1 500 000, thus 620 000 new neurons). Considering 60-70% recombination efficiency at the stem cell level (Imayoshi et al., 2008) this leads to a number of almost 6000 new cells that are added per day. Thus, our direct measurements and the genetic approach render highly comparable results in terms of the number of neurons that integrate in the adult OB. However, these numbers are substantially lower than estimates based on thymidine analogue labeling (Petreanu and Alvarez-Buylla, 2002) and future experiments will be needed to address this discrepancy.

Our work leaves of course other open questions. For example, it has been shown that olfactory enrichment and learning increases the survival of newborn neurons in the OB. Neurons are "saved" from dying apoptotic death (Mouret et al., 2008; Rochefort et al., 2002; Sultan et al., 2010). But how can neurons be saved when death is extremely rare in first place? Repeating in vivo observations and low-dose EdU studies in the context of olfactory stimulation and learning will help to clarify these matters.

Finally, neuronal selection at the level of integration has been proposed to underlie adult hippocampal neurogenesis and also cortical development (Bergami and Berninger, 2012; Buss et al., 2006). Despite the difficulty to perform in vivo long-term observations in deep brain regions or at embryonic/early postnatal stages, our findings oblige to revisit these structures to clarify the general impact of cell competition during neuronal integration.

Acknowledgements

The authors thank Andrea Erni for critical reading of the manuscript, Brice Detailleur for technical help on the 2 photon microscope. We are particularly grateful to the local PiCSL-FBI core facility (IBDM, AMU-Marseille) supported by the French National Research Agency through the « Investments for the Future" program (France-BioImaging, ANR-10-INBS-04) as

well as the IBDM animal facilities. We thank Francois Michel from INMED for help with light sheet microscopy. This work was supported by Agence National pour la Recherche (grant ANR- 13-BSV4-0013), Fondation pour la Recherche Médicale (FRM) grants ING20150532361, FDT20160435597 to HC and FTD20170437248 to AA, Fondation de France (FDF) grant FDF70959 to HC.

Adam, Y., and Mizrahi, A. (2011). Long-term imaging reveals dynamic changes in the neuronal composition of the glomerular layer. J Neurosci *31*, 7967-7973.
Batista-Brito, R., Close, J., Machold, R., and Fishell, G. (2008). The distinct temporal origins of olfactory bulb interneuron subtypes. J Neurosci *28*, 3966-3975.
Bergami, M., and Berninger, B. (2012). A fight for survival: the challenges faced by a newborn neuron integrating in the adult hippocampus. Dev Neurobiol *72*, 1016-1031.
Biebl, M., Cooper, C.M., Winkler, J., and Kuhn, H.G. (2000). Analysis of neurogenesis and programmed cell death reveals a self-renewing capacity in the adult rat brain. Neurosci Lett *291*, 17-20.
Boutin, C., Diestel, S., Desoeuvre, A., Tiveron, M.C., and Cremer, H. (2008). Efficient in vivo electroporation of the postnatal rodent forebrain. PLoS One *3*, e1883.
Breunig, J.J., Arellano, J.I., Macklis, J.D., and Rakic, P. (2007). Everything that glitters isn't gold: a critical review of postnatal neural precursor analyses. Cell Stem Cell *1*, 612-627.
Brown, J., Cooper-Kuhn, C.M., Kempermann, G., Van Praag, H., Winkler, J., Gage, F.H., and Kuhn, H.G. (2003). Enriched environment and physical activity stimulate hippocampal but not olfactory bulb neurogenesis. Eur J Neurosci *17*, 2042-2046.
Buss, R.R., Sun, W., and Oppenheim, R.W. (2006). Adaptive roles of programmed cell death during nervous system development. Annu Rev Neurosci *29*, 1-35.
Costandi, M. (2011). Warning on neural technique. Nature.
Cummings, D.M., Henning, H.E., and Brunjes, P.C. (1997). Olfactory bulb recovery after early sensory deprivation. J Neurosci *17*, 7433-7440.
de Chevigny, A., Core, N., Follert, P., Gaudin, M., Barbry, P., Beclin, C., and Cremer, H. (2012a). miR-7a regulation of Pax6 controls spatial origin of forebrain dopaminergic neurons. Nat Neurosci *15*, 1120-1126.
de Chevigny, A., Core, N., Follert, P., Wild, S., Bosio, A., Yoshikawa, K., Cremer, H., and Beclin, C. (2012b). Dynamic expression of the pro-dopaminergic transcription factors Pax6 and Dlx2 during postnatal olfactory bulb neurogenesis. Front Cell Neurosci *6*, 6.
Drew, P.J., Shih, A.Y., Driscoll, J.D., Knutsen, P.M., Blinder, P., Davalos, D., Akassoglou, K., Tsai, P.S., and Kleinfeld, D. (2010). Chronic optical access through a polished and reinforced thinned skull. Nat Methods *7*, 981-984.
Duque, A., and Rakic, P. (2011). Different effects of bromodeoxyuridine and [3H]thymidine incorporation into DNA on cell proliferation, position, and fate. J Neurosci *31*, 15205-15217.
Ehmann, U.K., Williams, J.R., Nagle, W.A., Brown, J.A., Belli, J.A., and Lett, J.T. (1975). Perturbations in cell cycle progression from radioactive DNA precursors. Nature *258*, 633-636.

Hinds, J.W., and McNelly, N.A. (1977). Aging of the rat olfactory bulb: growth and atrophy of constituent layers and changes in size and number of mitral cells. J Comp Neurol *72*, 345-367.
Imayoshi, I., Sakamoto, M., Ohtsuka, T., Takao, K., Miyakawa, T., Yamaguchi, M., Mori, K., Ikeda, T., Itohara, S., and Kageyama, R. (2008). Roles of continuous neurogenesis in the structural and functional integrity of the adult forebrain. Nat Neurosci *11*, 1153-1161.
Kim, W.R., Kim, Y., Eun, B., Park, O.H., Kim, H., Kim, K., Park, C.H., Vinsant, S., Oppenheim, R.W., and Sun, W. (2007). Impaired migration in the rostral migratory stream but spared olfactory function after the elimination of programmed cell death in Bax knock-out mice. J Neurosci *27*, 14392-14403.
Kolb, B., Pedersen, B., Ballermann, M., Gibb, R., and Whishaw, I.Q. (1999). Embryonic and postnatal injections of bromodeoxyuridine produce age-dependent morphological and behavioral abnormalities. J Neurosci *19*, 2337-2346.
Kuwagata, M., Ogawa, T., Nagata, T., and Shioda, S. (2007). The evaluation of early embryonic neurogenesis after exposure to the genotoxic agent 5-bromo-2'-deoxyuridine in mice. Neurotoxicology *28*, 780-789.
Lagace, D.C., Whitman, M.C., Noonan, M.A., Ables, J.L., DeCarolis, N.A., Arguello, A.A., Donovan, M.H., Fischer, S.J., Farnbauch, L.A., Beech, R.D.*, et al.* (2007). Dynamic contribution of nestin-expressing stem cells to adult neurogenesis. J Neurosci *27*, 12623-12629.
Lehner, B., Sandner, B., Marschallinger, J., Lehner, C., Furtner, T., Couillard-Despres, S., Rivera, F.J., Brockhoff, G., Bauer, H.C., Weidner, N.*, et al.* (2011). The dark side of BrdU in neural stem cell biology: detrimental effects on cell cycle, differentiation and survival. Cell Tissue Res *345*, 313-328.
Lledo, P.M., Alonso, M., and Grubb, M.S. (2006). Adult neurogenesis and functional plasticity in neuronal circuits. Nat Rev Neurosci *7*, 179-193.
Madisen, L., Zwingman, T.A., Sunkin, S.M., Oh, S.W., Zariwala, H.A., Gu, H., Ng, L.L., Palmiter, R.D., Hawrylycz, M.J., Jones, A.R.*, et al.* (2010). A robust and high-throughput Cre reporting and characterization system for the whole mouse brain. Nat Neurosci *13*, 133-140.
Mandairon, N., Sacquet, J., Jourdan, F., and Didier, A. (2006). Long-term fate and distribution of newborn cells in the adult mouse olfactory bulb: Influences of olfactory deprivation. Neuroscience *141*, 443-451.
Mirich, J.M., Williams, N.C., Berlau, D.J., and Brunjes, P.C. (2002). Comparative study of aging in the mouse olfactory bulb. J Comp Neurol *454*, 361-372.
Mizrahi, A., Lu, J., Irving, R., Feng, G., and Katz, L.C. (2006). In vivo imaging of juxtaglomerular neuron turnover in the mouse olfactory bulb. Proc Natl Acad Sci U S A *103*, 1912-1917.
Mouret, A., Gheusi, G., Gabellec, M.M., de Chaumont, F., Olivo-Marin, J.C., and Lledo, P.M. (2008). Learning and survival of newly generated neurons: when time matters. J Neurosci *28*, 11511-11516.
Ninkovic, J., Mori, T., and Gotz, M. (2007). Distinct modes of neuron addition in adult mouse neurogenesis. J Neurosci *27*, 10906-10911.
Nowakowski, R.S., and Hayes, N.L. (2000). New neurons: extraordinary evidence or extraordinary conclusion? Science *288*, 771.
Petreanu, L., and Alvarez-Buylla, A. (2002). Maturation and death of adult-born olfactory bulb granule neurons: role of olfaction. J Neurosci *22*, 6106-6113.
Platel, J.C., Dave, K.A., Gordon, V., Lacar, B., Rubio, M.E., and Bordey, A. (2010). NMDA receptors activated by subventricular zone astrocytic glutamate are critical for neuroblast survival prior to entering a synaptic network. Neuron *65*, 859-872.

Pomeroy, S.L., LaMantia, A.S., and Purves, D. (1990). Postnatal construction of neural circuitry in the mouse olfactory bulb. J Neurosci *10*, 1952-1966.
Richard, M.B., Taylor, S.R., and Greer, C.A. (2010). Age-induced disruption of selective olfactory bulb synaptic circuits. Proc Natl Acad Sci U S A *107*, 15613-15618.
Rochefort, C., Gheusi, G., Vincent, J.D., and Lledo, P.M. (2002). Enriched odor exposure increases the number of newborn neurons in the adult olfactory bulb and improves odor memory. J Neurosci *22*, 2679-2689.
Rostovtsev, V.V., Green, L.G., Fokin, V.V., and Sharpless, K.B. (2002). A stepwise huisgen cycloaddition process: copper(I)-catalyzed regioselective "ligation" of azides and terminal alkynes. Angew Chem Int Ed Engl *41*, 2596-2599.
Saghatelyan, A., Roux, P., Migliore, M., Rochefort, C., Desmaisons, D., Charneau, P., Shepherd, G.M., and Lledo, P.M. (2005). Activity-dependent adjustments of the inhibitory network in the olfactory bulb following early postnatal deprivation. Neuron *46*, 103-116.
Sailor, K.A., Valley, M.T., Wiechert, M.T., Riecke, H., Sun, G.J., Adams, W., Dennis, J.C., Sharafi, S., Ming, G.L., Song, H.*, et al.* (2016). Persistent Structural Plasticity Optimizes Sensory Information Processing in the Olfactory Bulb. Neuron *91*, 384-396.
Salic, A., and Mitchison, T.J. (2008). A chemical method for fast and sensitive detection of DNA synthesis in vivo. Proc Natl Acad Sci U S A *105*, 2415-2420.
Schindelin, J., Arganda-Carreras, I., Frise, E., Kaynig, V., Longair, M., Pietzsch, T., Preibisch, S., Rueden, C., Saalfeld, S., Schmid, B.*, et al.* (2012). Fiji: an open-source platform for biological-image analysis. Nat Methods *9*, 676-682.
Sekerkova, G., Ilijic, E., and Mugnaini, E. (2004). Bromodeoxyuridine administered during neurogenesis of the projection neurons causes cerebellar defects in rat. J Comp Neurol *470*, 221-239.
Southwell, D.G., Paredes, M.F., Galvao, R.P., Jones, D.L., Froemke, R.C., Sebe, J.Y., Alfaro-Cervello, C., Tang, Y., Garcia-Verdugo, J.M., Rubenstein, J.L.*, et al.* (2012). Intrinsically determined cell death of developing cortical interneurons. Nature *491*, 109-113.
Sultan, S., Mandairon, N., Kermen, F., Garcia, S., Sacquet, J., and Didier, A. (2010). Learning-dependent neurogenesis in the olfactory bulb determines long-term olfactory memory. FASEB J *24*, 2355-2363.
Susaki, E.A., Tainaka, K., Perrin, D., Kishino, F., Tawara, T., Watanabe, T.M., Yokoyama, C., Onoe, H., Eguchi, M., Yamaguchi, S.*, et al.* (2014). Whole-brain imaging with single-cell resolution using chemical cocktails and computational analysis. Cell *157*, 726-739.
Taupin, P. (2007). BrdU immunohistochemistry for studying adult neurogenesis: paradigms, pitfalls, limitations, and validation. Brain Res Rev *53*, 198-214.
Tiveron, M.C., Beurrier, C., Ceni, C., Andriambao, N., Combes, A., Koehl, M., Maurice, N., Gatti, E., Abrous, D.N., Kerkerian-Le Goff, L.*, et al.* (2016). LAMP5 Fine-Tunes GABAergic Synaptic Transmission in Defined Circuits of the Mouse Brain. PLoS One *11*, e0157052.
Tornoe, C.W., Christensen, C., and Meldal, M. (2002). Peptidotriazoles on solid phase: [1,2,3]-triazoles by regiospecific copper(i)-catalyzed 1,3-dipolar cycloadditions of terminal alkynes to azides. The Journal of organic chemistry *67*, 3057-3064.
Wallace, J.L., Wienisch, M., and Murthy, V.N. (2017). Development and Refinement of Functional Properties of Adult-Born Neurons. Neuron *96*, 883-896 e887.
Webster, W., Shimada, M., and Langman, J. (1973). Effect of fluorodeoxyuridine, colcemid, and bromodeoxyuridine on developing neocortex of the mouse. Am J Anat *137*, 67-85.
Whitman, M.C., and Greer, C.A. (2007). Adult-generated neurons exhibit diverse developmental fates. Dev Neurobiol *67*, 1079-1093.

Winner, B., Cooper-Kuhn, C.M., Aigner, R., Winkler, J., and Kuhn, H.G. (2002). Long-term survival and cell death of newly generated neurons in the adult rat olfactory bulb. Eur J Neurosci *16*, 1681-1689.
Xu, H.T., Pan, F., Yang, G., and Gan, W.B. (2007). Choice of cranial window type for in vivo imaging affects dendritic spine turnover in the cortex. Nat Neurosci *10*, 549-551.
Yamaguchi, M., and Mori, K. (2005). Critical period for sensory experience-dependent survival of newly generated granule cells in the adult mouse olfactory bulb. Proc Natl Acad Sci U S A *102*, 9697-9702.

Figures and legends

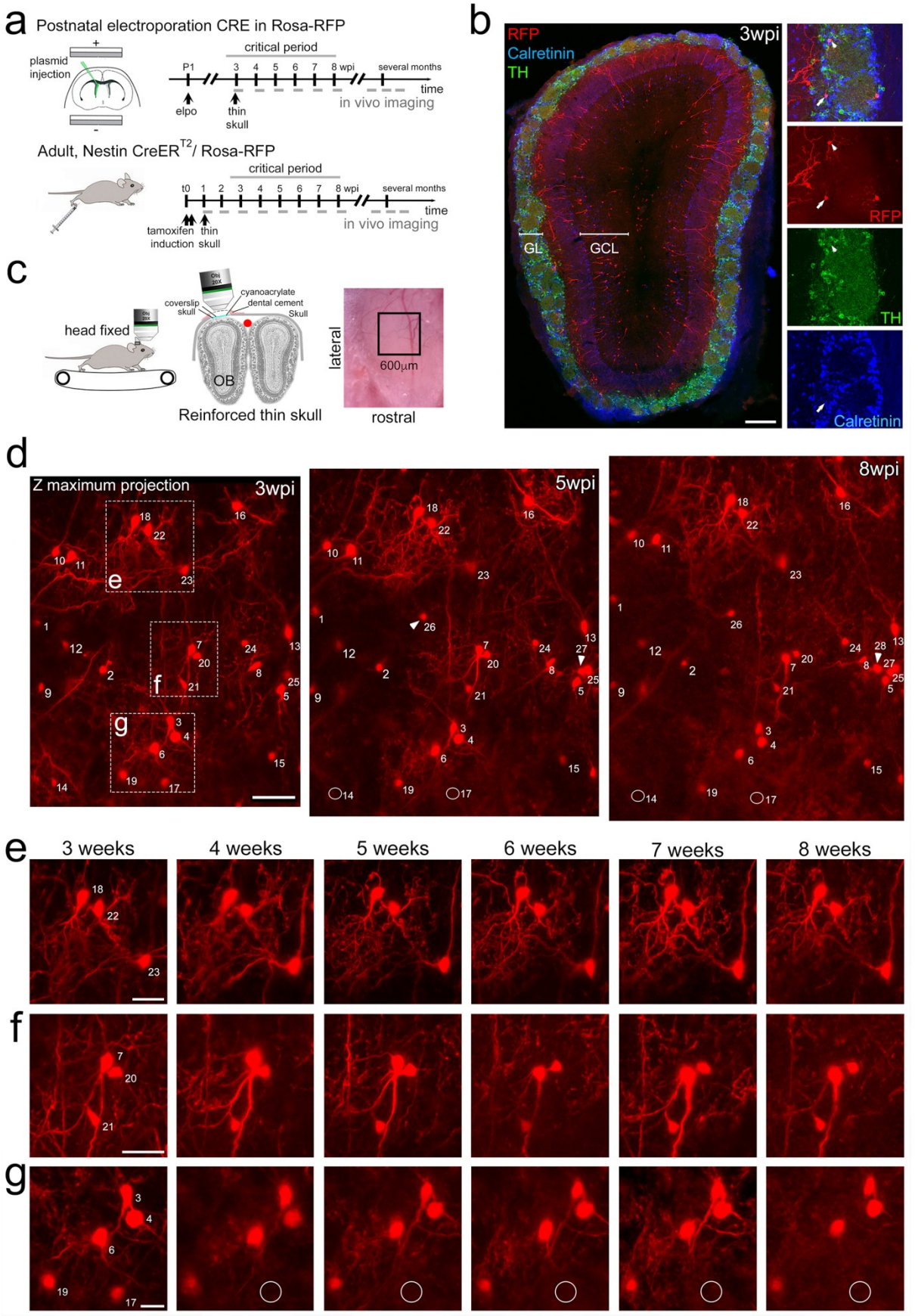

Figure 1: Long-term in vivo imaging in the OB

a. Induction protocols and imaging timeline. In perinatal animals a CRE-expression plasmid was introduced in the dorsal neural stem cell compartment of Rosa-RFP mice using postnatal electroporation. To label neurons in adults, Nestin-CreERT2 animals were bred to Rosa-RFP mice and induced with tamoxifen at 2 months of age. Thin skull preparation was routinely performed one-week post induction. A weekly imaging scheme was implemented over the critical period and up to 5 months. **b**. Postnatal in vivo brain electroporation at P1-P4 leads at 3 wpi to the appearance of various interneuron types, including TH and CR expressing subtypes, in the superficial GCL and the GL layers of the OB. **c.** In vivo microscopy setup. Mice were imaged with the head fixed to the two-photon microscope. Animals could move on a treadmill but rarely did so during imaging sessions. Thin skull preparation allowed high-resolution imaging on a weekly basis. **d**. Example of an image Z-stack showing 25 individually identified neurons from 3, 5, and 8 weeks after CRE electroporation. Note that neurons 14 and 17 are lost (circles) while several neurons are added (arrowheads). **e,f,g.** High resolution images of weekly observations of three groups of neurons highlighted in d. Cell substructures, dendrites and minor cell displacements can be followed over time. Scale bar: 200 μm in b, 50 μm in d, 30 μm in e,f, g.

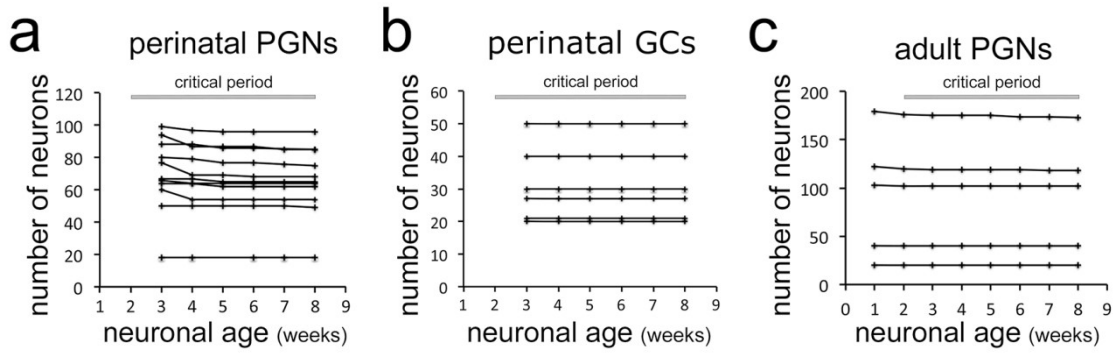

Figure 2: Stability of neuron populations in the OB in vivo

a. Tracing of perinatally induced timed neuron first cohorts (755 neurons) in 11 mice from 3 to 8 wpi. **b**. Tracing of perinatally induced first cohorts of granule cells (178 cells in 6 mice) during the proposed critical period. **c.** Tracing of the first cohort of periglomerular neurons in 8 adult animals (538 neurons) after induction with tamoxifen injection at two months.

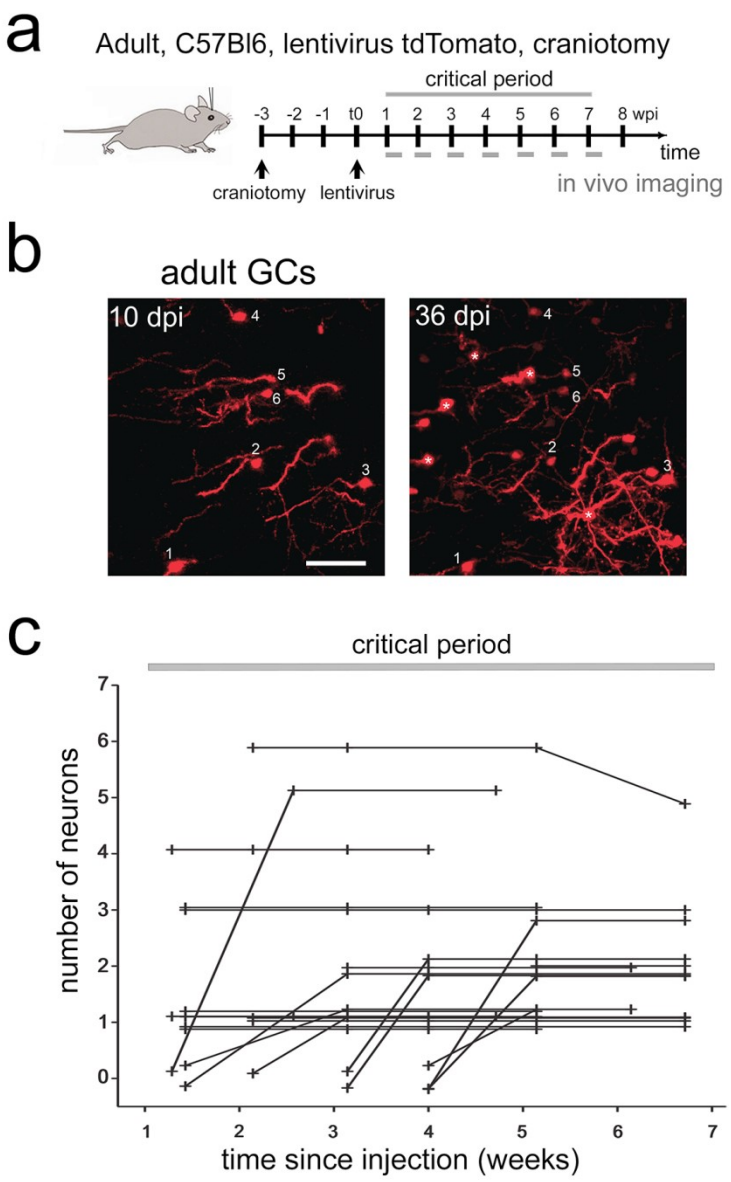

Figure 3: Adult-born granule cells stability in the OB in vivo

a. Labeling protocols and imaging timeline. To label granule neurons in adults, C57Bl6 animals were injected with a tomato lentivirus in the RMS. A craniotomy was performed 3 weeks before lentivirus injection. A weekly imaging scheme was implemented over the critical period.

b. Example field of view (maximum intensity projection of volume with depth 90 µm) showing cells that were tracked between 10 and 36 days post injection (dpi). * indicates a newcomer that appeared after the first day of imaging and was subsequently stable at 36 dpi. Scale bar 50 µm. **c.** Tracing of adult-born granule cells (48 neurons) in 3 mice from 19 field of views

from 1 to 7 weeks post injection in the RMS. Lines beginning at zero indicate new cells that appeared in the field of view and were subsequently tracked.

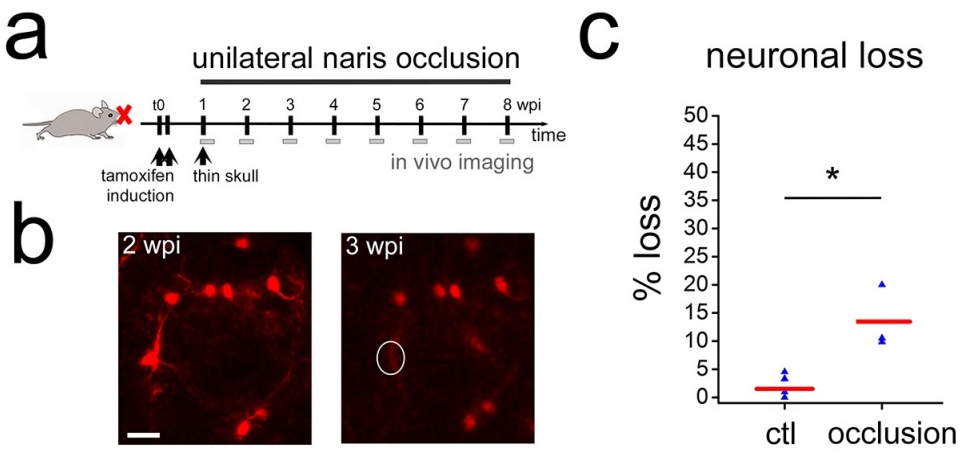

Figure 4: Sensory deprivation in the OB lead to neuronal death

a. Timeline for sensory deprivation experiment. Naris occlusion and thin skull preparation were performed one week after induction of RFP positive neurons in adult mice. **b.** Two weeks after occlusion neurons with complex morphologies were lost in the OB. **c.** Quantification of neuron loss in control and occluded OBs over 8 weeks. Scale bar: 20 µm in b.

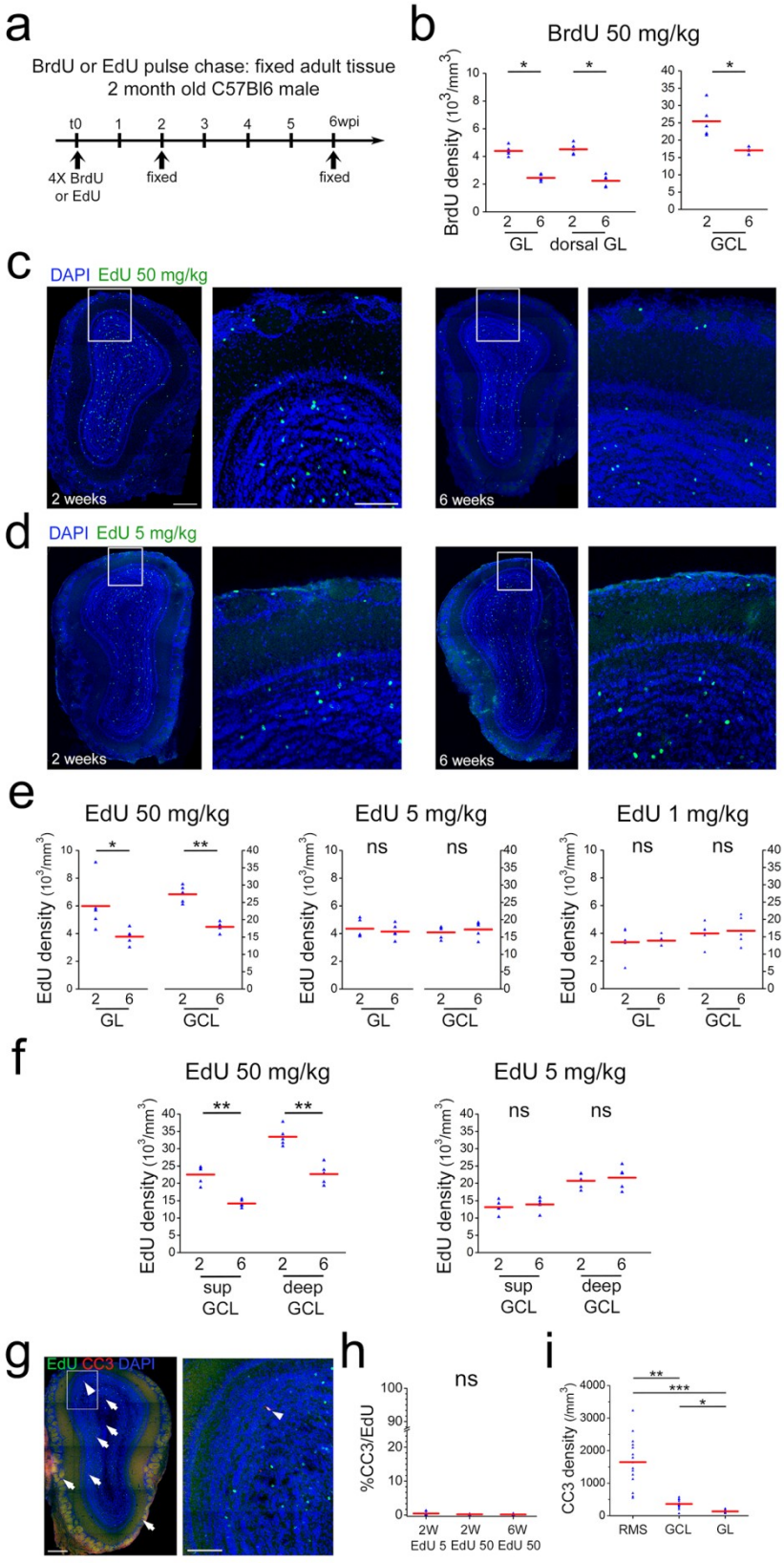

Figure 5: Neuronal survival after thymidine analog pulse chase

a. Timeline of BrdU or EdU pulse chase experiment. Four BrdU/EdU injections at different concentrations were performed in adult mice. Animals were sacrificed 2 and 6 wpi, respectively. **b**. BrdU cell density in GL, dorsal GL and GCL between 2 and 6 weeks after injection. **c.** Example of immunohistochemical staining of a coronal OB section 2 and 6 weeks after 4x50 mg/kg EdU injection. **d.** Example of immunohistochemical staining of coronal OB sections 2 and 6 weeks after 4x5 mg/kg EdU injection. **e**. EdU cell density in GL and GCL between 2 and 6 weeks after 4x50 mg/kg edU, 4x5 mg/kg edU and 4x1 mg/kg EdU injection, respectively. Note the strong cell loss at 50mg/kg of EdU between 2 and 6 weeks and the absence of cell loss at 4X5 and 4x1 mg/kg EdU. **f.** EdU cell density in superficial and deep GCL between 2 and 6 weeks after 4x50 mg/kg edU and 4x5 mg/kg edU injection, respectively. Note that for EdU 50kg both layers show a similar cell loss between 2 and 6 weeks while this cell loss is absent in both layers at 5 mg/kg. **g.** Example of immunohistochemical staining of a coronal OB section for EdU at 50mg/kg (green) and cleaved Caspase 3 (red) **h.** Increased concentrations of EdU do not augment the number of EdU/cleaved Caspase3 co-labeled cells. **i.** Cleaved Caspase 3 density is more than 4 times higher in the RMS that in the GCL or GL layers. Scale bar: 300 μm in left panel in c, 100 μm in middle panel in c, 300 and 100 μm in g.

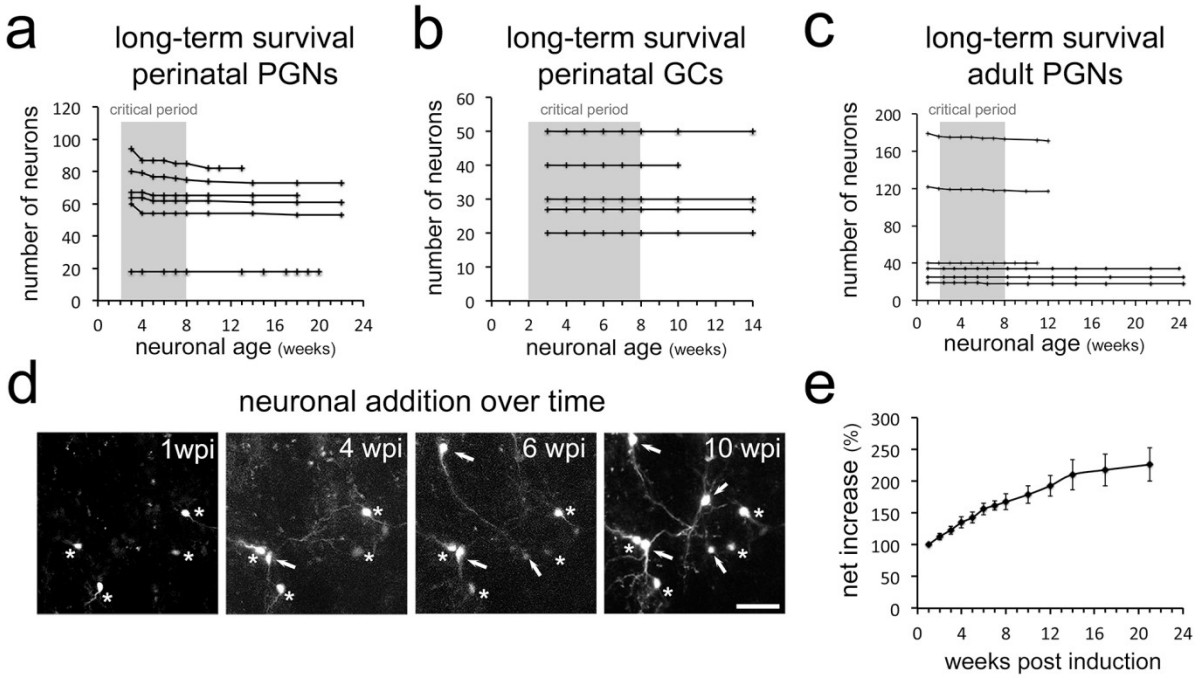

Figure 6: Long-term survival of neuron populations and neuronal addition in vivo

Absence of cell loss in **a.** perinatal PGNs, **b.** perinatal GCs and **c.** adult born PGNs in long-term in vivo observations. **d.** Additional RFP expressing neurons appear constantly in the observation window. **e.** Net increase in all newborn periglomerular neurons in adult Nestin Cre-ERT2 mice over time. Scale bar in 40 µm in d.

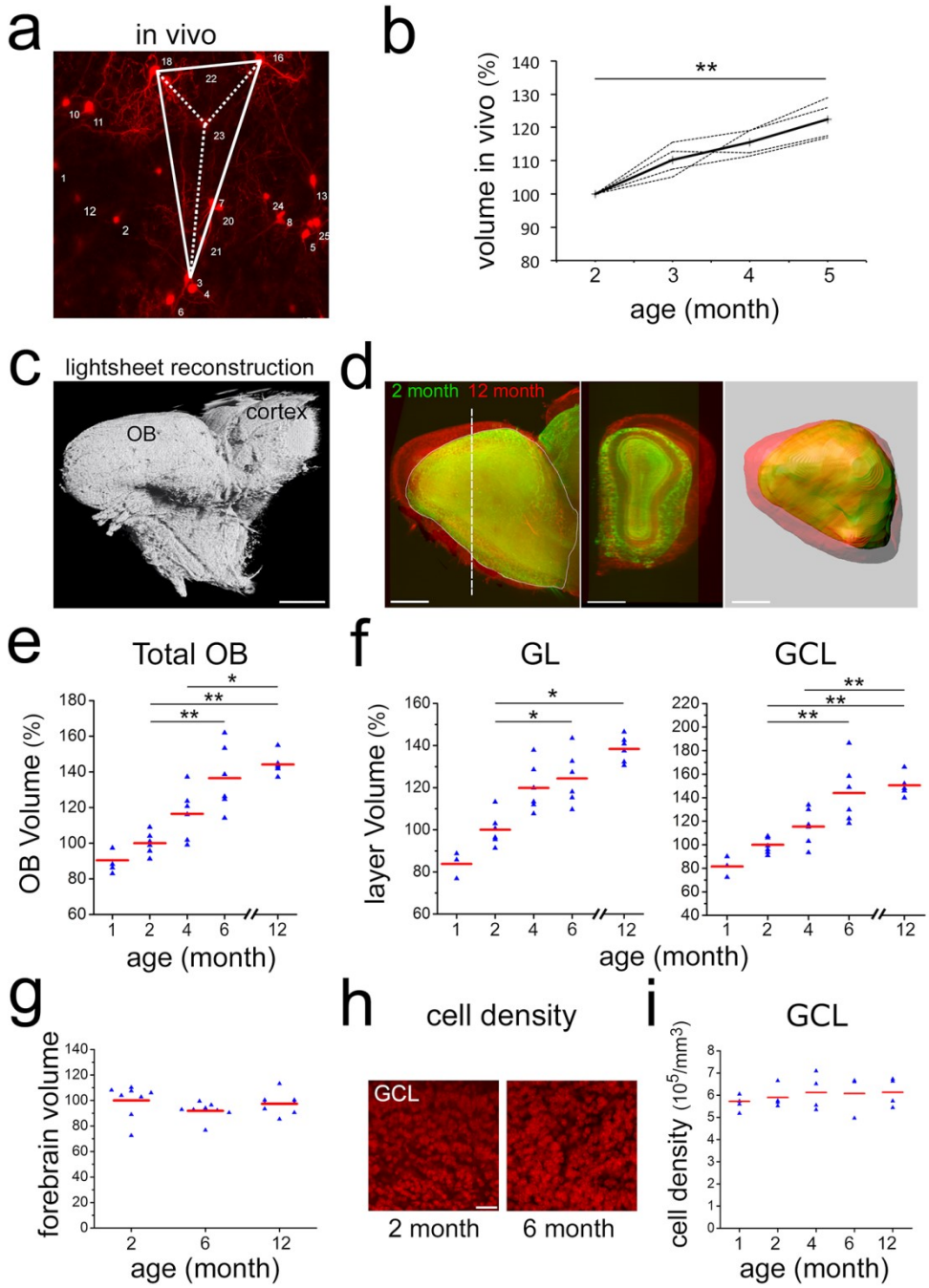

Figure 7: Neuronal addition and growth of the OB

a. Example of volumetric analysis of inter-neuronal space between individually identified neurons in vivo (groups of four neurons in X,Y,Z; thus an irregular pyramid). **b.** Quantification inter-neuronal space shows that distances between identified neurons increase in adult animals. **c.** Reconstruction of an adult OB and part of the cortex based on 3-D light sheet imaging. **d.** Comparison of 2- and 12-month old OBs reconstructed from lightsheet images. **e**. Quantification of volume increase in OBs from 1-12 months, normalized to 2 months. **f.** Quantification of volume increase in OB sublayers from 1-12 months, normalized to 2

months. Volume increase affects both, the GL and the GCL. **g.** Quantification of the volume of the forebrain at 2, 6 and 12 months, normalized to 2 months. Forebrain size over time does not change. **h.** Examples of GCL cell density based on TOPRO-3 nuclear staining in whole, cleared OBs of 2 and 6 month old mice. **i.** Quantification of cell density from 1 to 12 months. Cell density is constant over the observation period. Scale bar: 800 µm in a,b. 40 µm in f, 50 µm in h.

Materials and Methods

Animals

All mice were treated according to protocols approved by the French Ethical Committee (#5223-2016042717181477v2). Mice were group housed in regular cages under standard conditions, with up to 5 mice per cage on a 12-h light–dark cycle. 2 months old C57Bl6 males were used for BrdU and edU pulse chase experiments. Rosa-RFP mice (Ai14, Rosa26-CAG-tdTomato(Madisen et al., 2010)) were obtained from the Jackson laboratory and used on a mixed C57Bl6/CD1 background. For lightsheet experiments, 1, 2, 4,6 and 12 months old male C57Bl6 were obtained from Janvier labs. Nestin-CreERT2 mice were obtained from Amelia Eisch (Lagace et al., 2007) and crossed with Rosa-RFP mice. Male and female Nestin-CreER^{T2} X rosa-RFP mice were used between 2 and 3 month old at the time of surgery.

In vivo labeling of neurons

In vivo electroporation was performed as previously described(Boutin et al., 2008). Briefly, 1-day-old pups were anaesthetized by hypothermia and 1µl of a pCAG-CRE) plasmid(Platel et al., 2010) at 4µg/µl) was injected in the lateral ventricle. Electrical pulses were applied to target the dorsal V-SVZ.

In adult Nestin-CreERT2 X rosa-RFP mice, RFP expression was induced by tamoxifen injection (Sigma-Aldrich; intraperitoneal; dissolved in 10% EtOH/ 90% sunflower oil) at 100mg/kg per day for 2 days.

Surgical preparation

Implantation of an observation window was performed as previously described(Drew et al., 2010) but with minor modifications. Briefly, mice were anaesthetized by intraperitoneal (ip.) injection of ketamine/ xylazine (125/12,5 mg/kg). Dexaméthasone (0.2 mg/kg) and buprenorphine (0.3 mg/mL) were injected subcutaneously and lidocaine was applied locally onto the skull. The pinch withdrawal reflex was monitored throughout the surgery, and additional anesthesia was applied if needed. Carprofen (5 mg/kg) was injected ip. after the surgery. A steel bar was added during this step to allow fixation of the animal to the microscope. The skull overlying the OB was carefully thinned with a sterile scalpel blade until a thickness of 10-20 µm was reached. A thin layer of cyanoacrylate (superglu3, Loctite) was applied and a 3mm round coverslip was apposed and sealed with dental cement (superbond, GACD). A first microscopic observation was performed on these anesthetized mice.

For olfactory sensory deprivation, a silicone tube was inserted (Intramedic; 0,5mm diameter, 3mm long) into one naris and sealed with cyanoacrylate glue (Cummings et al., 1997). Efficiency of occlusion was checked the following day and before each imaging session. At the end of the experiment immunostaining against tyrosine hydroxylase was performed to confirm the efficiency of occlusion.

***In vivo* two-photon imaging**

We used a Zeiss LSM 7MP two-photon microscope modified to allow animal positioning under a 20X water immersion objective (1.0 NA, 1.7mm wd) and coupled to a femtosecond pulsed infrared tunable laser (Mai-Tai, SpectraPhysics). After two-photon excitation, epifluorescence signals were collected and separated by dichroic mirrors and filters on 4 independent non-descanned detectors (NDD). Images were acquired using an excitation wavelength of 950 nm. RFP was first collected between 605-678. In addition, we collected an additional RFP signal between 560-590 that was voluntarily saturated to allow a better identification of subcellular structures like dendrites.

In general, image acquisition lasted about 10 min. Mice could potentially move on a treadmill during imaging, but rarely did so. On consecutive observation, the same field of view was localized based on the geometric motifs of groups of neurons and specific morphological features of individual cells. Between 18 and 179 neurons were imaged initially every week for the first 8 weeks and further imaged at irregular intervals for up to 22 weeks. Images of 606x606 µm were acquired at 0.59 µm/pixel resolution in the xy dimension and 2 µm/frame in the z dimension to a maximal depths of 400 µm.

***in vivo* imaging of adult born GCs**

see Wallace et al. 2017 for cranial window, virus, and imaging. All cells in the present analysis were labeled with the dTomato-GCaMP6s version of the lentivirus.

Analysis:

Z stacks taken with a 1 or 2 µm z-step were used for tracking cells over weeks. Maximum intensity projections were created and annotated manually in ImageJ and cross-referenced with z-stacks to confirm that the dendritic structure and location of a cell allowed unambiguous identification. Each line in 3C represents cells tracked for different lengths of time, and multiple lines may correspond to a single field of view. For example, this imaged field of view corresponds to the two lines representing 3 cells tracked over time, with one line ending at 5 weeks and one ending at 7 weeks (due to the final z stack not extending deep enough to include the first 3 cells). The newcomers arrived at different times, so they have

different lines. For example, some of the cells with asterisks arrived at 3 weeks and others arrived at 4 weeks. Incoming cells not marked with asterisks had cell bodies that either were not fully included within the z stack or we were not able to track them for more than one imaging session and so were not quantified.

Chronic *in vivo* imaging analysis

Quantitative analyses were performed on raw image stacks using FIJI software(Schindelin et al., 2012). All neurons identified on the first image were assigned a number using ImageJ overlay. Based on morphology and relative position each neuron was individually numbered and tracked on the successive weekly images (see fig. S3b,d). After identification of the first cohort, smaller numbers of additional neurons appeared permanently in the observation window as a consequence of ongoing neurogenesis in the stem cell compartment (arrowhead in Fig 1d, 5wpi). These were numbered and followed like the first cohort. Results were summarized in Microsoft Excel. Occasionally neurons located at the border of an image were placed outside of the imaged field in one of the following sessions. These cells were excluded from further analyses. Animals showing an evident degradation of the imaging window were excluded from further imaging sessions.

For the analyses of the distance between neurons (fig. 7ab), we measured over time the volume between 4 neurons (3 neurons in the same plane and another neuron in a different plane) using FIJI. We measured 2 pyramids per animal in 4 animals from 2 to 5 months

Brdu and EdU pulse chase experiments

BrdU (Sigma) was injected ip. 4 times at 50mg/kg body weight every 2 hours. EdU (Sigma) was injected 4 times at 1, 5 or 50 mg/kg body weight every 2 hours. Staining was performed as described previously (de Chevigny et al., 2012a). For the dose of 1mg/kg of edu, the labeling protocol was repeated to increase the intensity of the staining. This was not necessary for the dose of 5mg/kg. Optical images were taken either using a fluorescence microscope (Axioplan2, ApoTome system, Zeiss, Germany) or a laser confocal scanning microscope (LSM880, Zeiss, Germany). BrdU/EdU positive cells in the glomerular layer or granule cell layer of 3 to 5 slices from 5 animals were counted in around 20 μm section using FIJI software and Imaris software.

Light sheet microscopy

For brain transparization, we followed the Cubic protocol (Susaki et al., 2014). Briefly, brains where incubated in Cubic1 solution for 10 days at 37°C using gentle agitation. After clearing, brains were incubated for 1 day in the red nuclear dye TOPRO3 (1/1000) in PBS, 0.01%

Tween 20, 0.01% sodium Azide at 37°C. The brains were then re-incubated for 3 hours in Cubic1 solution and subsequently placed in Cubic2 solution for 2 days at 37°C. Timing of all steps was carefully monitored.

We used a lightsheet Z1 microscope (Zeiss) with a 5x/0.16NA objective to image the transparized OB and UltraMicroscope II (LaVision BioTec) with LWDO 2x/0.14NA for whole brain imaging. OB layers were easily distinguishable using the nuclear staining of the TOPRO3. The OB was imaged every 5.9 µm in Z with a xy pixel dimension of 2.5 µm and the whole brain with 30 µm steps in Z and a xy resolution of 3.03 µm, respectively. We used Imaris software (Bitplane, Germany) for reconstruction of the total volume based on the nuclear TOPRO3 staining. To determine total forebrain size we measured the entire volume from the caudal end on the OB to the caudal end of the neocortex. All measurements were normalized to the mean obtained on 2 month old brains.

Measurement of cell density

We measured cell density in the granule cell layer by imaging the same transparized brain with the 2-photon microscope used for *in vivo* imaging to obtain a better resolution. We acquired Z stacks of 200 µm with 2µm resolution in Z and 0.3 µm in xy in the central part of the OB. These images were first de-noised in Fiji using a 3D mean filter. Then the volumetric density of nuclei was quantified using *Imaris* software: We use the cell detection module to detect nuclei in the granule cell layer. We used 4 µm as a seed point value to split the connected objects.

Immunohistochemistry

Stainings were done on 50 µm floating vibratome sections as described before (Tiveron et al., 2016). Primary antibodies: GFP (rabbit IgG, Life technologies,1 1:1000 or chicken Ig, AVES, 1:1000), Calretinin (mouse IgG1, Synaptic Systems; 1:2000), Tyrosine Hydroxylase (chicken Ig, AVES; 1:1000), IBA1 (life technologies, 1:500), GFAP (life technologies, 1:500). Secondary antibodies were purchased from Life Technologies. Before mounting, cell nuclei were stained with Hoechst 33258 or TOPRO3. Optical images were taken either using a fluorescence microscope (Axioplan2, ApoTome system, Zeiss, Germany) or a laser confocal scanning microscope (LSM880, Zeiss, Germany).

Statistical analyses

All data are presented as mean ± s.e.m. Statistical comparisons were performed using Matlab software (Mathworks) or R. In box plot representation, center line,represent the median; box limits, upper and lower quartiles; whiskers, outliers). All statistical tests were

two-tailed. Threshold for significance was set at p=0.05. For occlusion experiments (Fig 2g) we used a Wilcoxon Rank-sum test (p=0,0357). For Brdu and Edu pulse chase experiment, (Fig 3), we used a Wilcoxon Rank-sum test ((* 0,05, ** 0,01, *** 0,001). For quantification of the volume of the OB and the volume of the layer we used a wilcoxon ranksum test for each comparison (6 comparison) and adjusted the p-value threshold for multiple comparison using Bonferroni (* 0,0083, ** 0,00167, *** 0,000167). For the quantification of the increase of size during in vivo imaging experiments, (Fig 5i) we used a Friedman rank sum test followed with a post hoc test in the Matlab software (between 2 and 4 month p=0,0928, between 2 and 5 month p=0,0097).

Supplementary Materials

Fig S1 – S7

Supplementary Video S1-S3

a

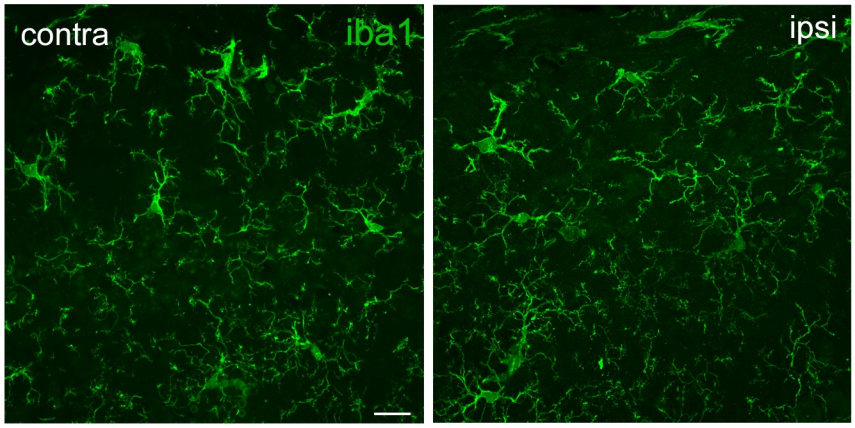

microglia, 1 day post surgery, fixed brain

b

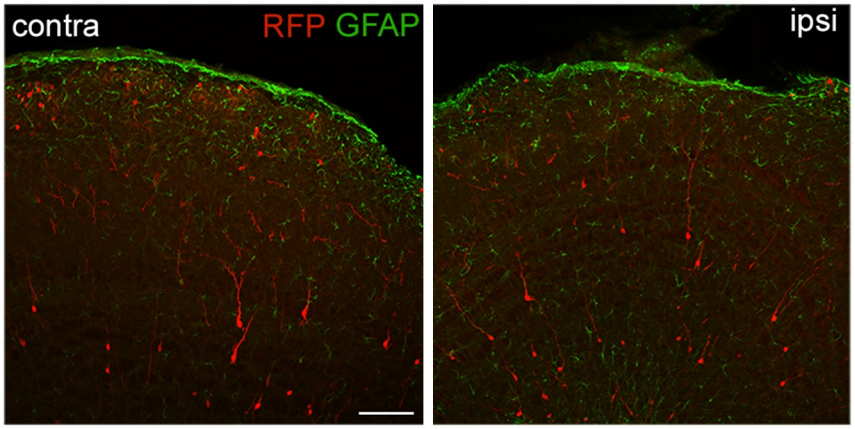

astrocytes, 1 week post surgery, fixed brain

c

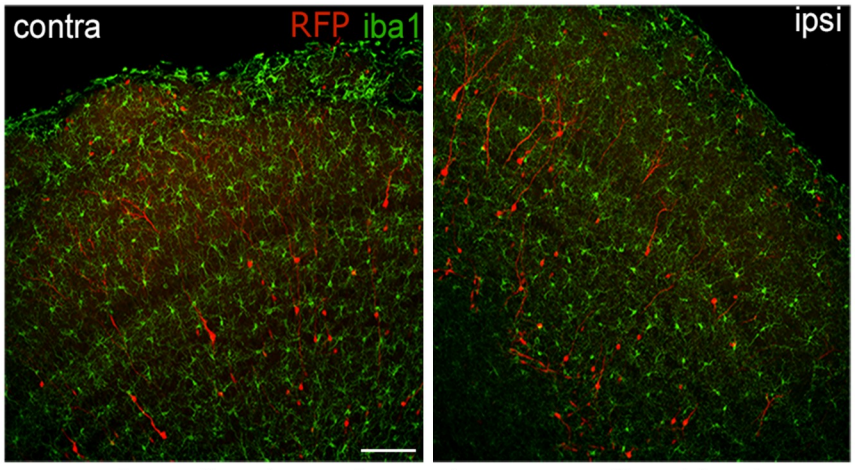

microglia, 1 week post surgery, fixed brain

Supplementary Fig. 1

a. Immunostaining for the microglial marker iba1 demonstrates the absence of a detectable microglia reaction at 1-day post surgery.

b. Comparison of GFAP staining in the OB. Control and window carrying OB are indistinguishable at 1-week post surgery.

c. Immunostaining for the microglial marker iba1 demonstrates the absence of a detectable microglia reaction at 1-week post surgery. Scale bar: 10 μm in a, 50 μm in b,c.

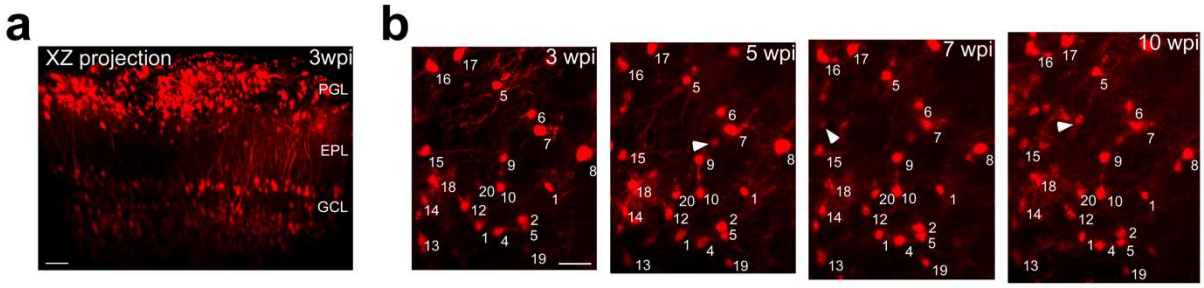

Supplementary Fig. 2

A. XZ projection of the OB showing that the PGL, EPL and the superficial GCL can be reached through a thin skull preparation. b. Example of Z-projection identifying individual granule neurons between 3 and 10 weeks post induction in perinatal mice. The first cohort is numbered. Additional neurons of later cohorts appeared in the observation window over successive imaging sessions (arrowheads). Scale bar: 50 µm in a, 30 µm b.

a

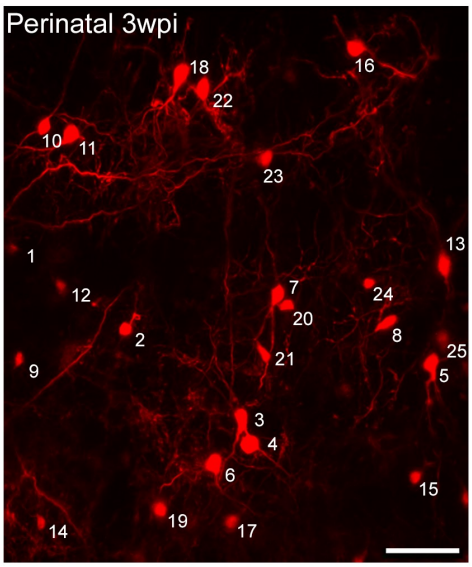

b

cell number	3wpi	4wpi	5wpi	6wpi	7wpi	8wpi
1	x	x	x	x	x	x
2	x	x	x	x	x	x
3	x	x	x	x	x	x
4	x	x	x	x	x	x
5	x	x	x	x	x	x
6	x	x	x	x	x	x
7	x	x	x	x	x	x
8	x	x	x	x	x	x
9	x	x	x	x	x	x
10	x	x	x	x	x	x
11	x	x	x	x	x	x
12	x	x	x	x	x	x
13	x	x	x	x	x	x
14	x	x	LOST	LOST	LOST	LOST
15	x	x	x	x	x	x
16	x	x	x	x	x	x
17	x	LOST	LOST	LOST	LOST	LOST
18	x	x	x	x	x	x
19	x	x	x	x	x	x
20	x	x	x	x	x	x
21	x	x	x	x	x	x
22	x	x	x	x	x	x
23	x	x	x	x	x	x
24	x	x	x	x	x	x
25	x	x	x	x	x	x
26	-	-	x	x	x	x
27	-	-	x	x	x	x
28	-	-	-	x	x	x

c

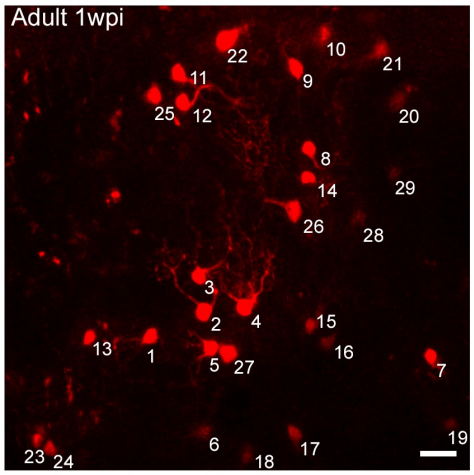

d

cell number	3wpi	4wpi	5wpi	6wpi	7wpi	8wpi
1	x	x	x	x	x	x
2	x	x	x	x	x	x
3	x	x	x	x	x	x
4	x	x	x	x	x	x
5	x	x	x	x	x	x
6	x	x	x	x	x	x
7	x	x	x	x	x	x
8	x	x	x	x	x	x
9	x	x	x	x	x	x
10	x	x	x	x	x	x
11	x	x	x	x	x	x
12	x	x	x	x	x	x
13	x	x	x	x	x	x
14	x	x	x	x	x	x
15	x	x	x	x	x	x
16	x	x	x	x	x	x
17	x	x	x	x	x	x
18	x	x	x	x	x	x
19	x	x	x	x	x	x
20	x	x	x	x	x	x
21	x	x	x	x	x	x
22	x	x	x	x	x	x
23	x	x	x	x	x	x
24	x	x	x	x	x	x
25	x	x	x	x	x	x
26	x	x	x	x	x	x
27	x	x	x	x	x	x
28	x	x	x	x	x	x
29	x	x	x	x	x	x
30	-	x	x	x	x	x
31	-	-	-	x	x	x

Supplementary Fig. 3

Image and table exemplifying how perinatally (a,b) and adult (c,d) generated neurons were scored over the critical period (for a,b compare also Fig. 1d). Scale bar: 50 µm in a, 20 µm b.

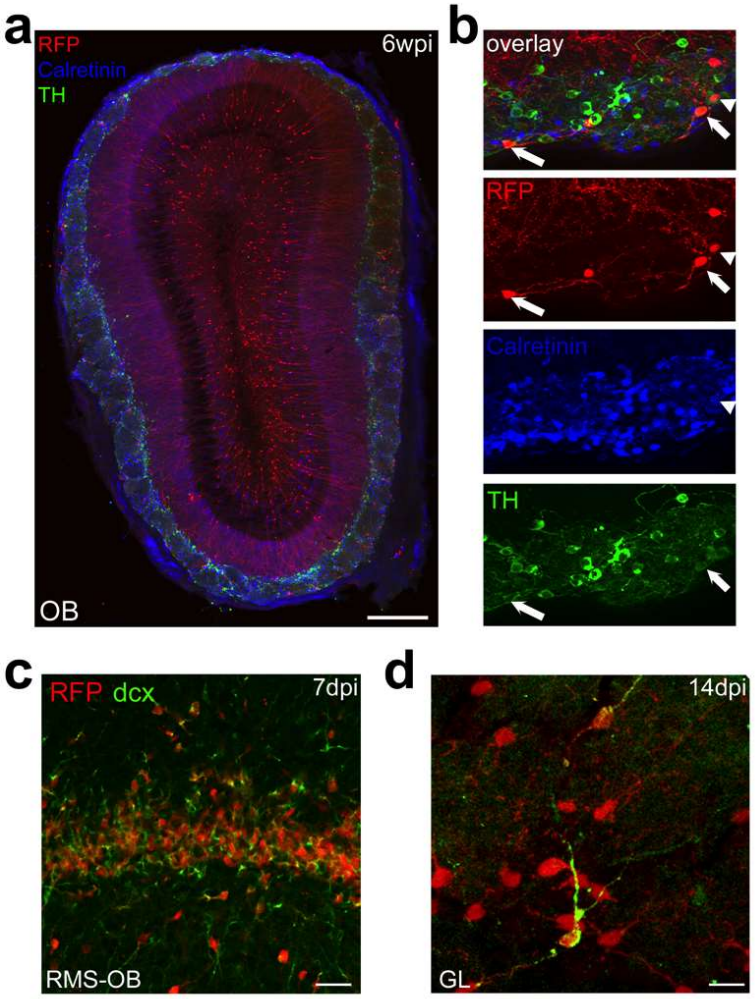

Supplementary Fig. 4

a, b. Coronal section through the OB of an adult Nestin-Cre-ERT2/Rosa-RFP mouse 6 weeks after tamoxifen injection at 2 months of age stained for the OB neuron subtype markers TH and Calretinin.

c, d. Seven days post induction (dpi) large amounts of OB neurons in the OB express the immature neuronal marker doublecortin (dcx). At 14 dpi individual cells in the GCL still express dcx. Scale bar: 300 µm in a, 30 µm in c, 10 µm in d.

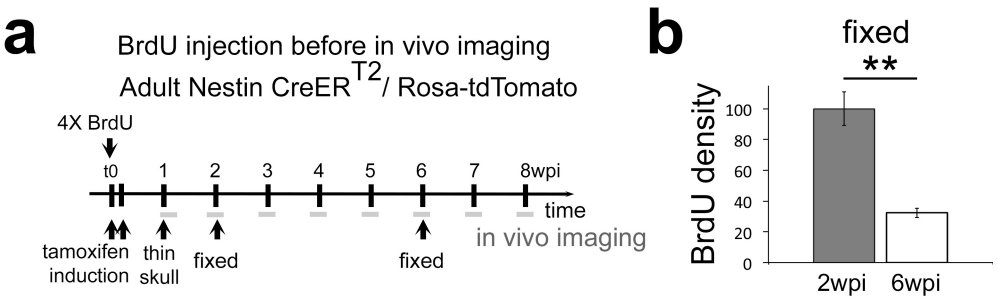

Supplementary Fig. 5

a. Experimental design and timeline for BrdU injection combined with thin-skull surgery and imaging. b. Surgery and regular imaging have no positive impact on BrdU cell survival in the OB.

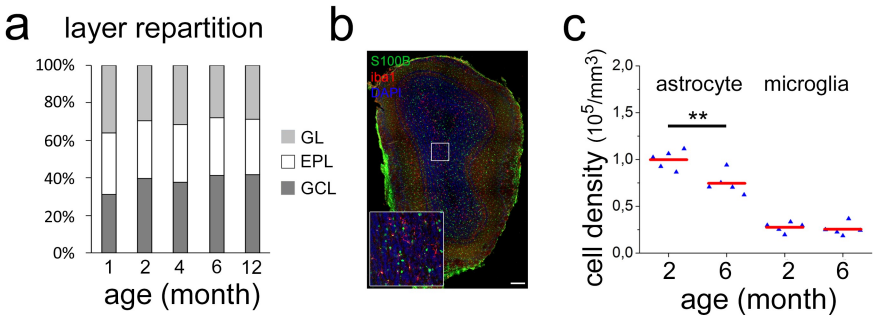

Supplementary Fig. 6

a. Repartition of OB layers (GL, EPL, GCL) with increasing age. Although the volume of all layers increases with time their ratio remains constant.

b. Coronal section through the OB of a 6 month old C57Bl6 stained for the astrocytic marker S100b, the microglial marker iba1 and the nucleus with DAPI.

c. Quantification of astrocytic and microglial density between 2 and 6 months. Astrocyte density is significantly decreased (p=0,006) while microglia density is constant. Scale bar: 200 µm in b

Supplementary Video 1

Example of a Z-stack showing perinatally born neurons in the GL. This stack was the basis for the projection presented in Fig. 1d.

Supplementary Video 2

Example of a Z-stack showning adult born neurons in the GL. This stack was the basis for the projection presented in Extended Data Fig. 3d.

Supplementary Video 3

3D representation of an adult OB based on light sheet microscopy.